PNC ZJ222 82-16(1)Tr

NOT FOR PUBLICATION

本資料は　年　月　日付けで登録区分、
変更する。
[技術情報室]

分 謄

SODIUM SPRAY COMBUSTION TEST

—Part1: Sodium Spray Combustion Test—

December, 1982

MITSUBISHI HEAVY INDUSTRIES, LTD.

under contract from

Power Reactor and Nuclear Fuel Development Corporation

This document is not intended for publication.

No public reference should be mabe to it without prior written consent of

本資料は、核燃料サイクル開発機構の開発業務を進めるために作成されたものです。
したがって、その利用は限られた範囲としており、その取扱には十分な注意を払ってください。 この資料の全部または一部を複写・複製・転載あるいは引用する場合、特別の許可を必要としますので、下記にお問い合わせください。

〒319-1184 茨城県那珂郡東海村大字村松4番地49
核燃料サイクル開発機構
技術展開部 技術協力課

Inquiries about copyright and reproduction should be addressed to:
Technical Cooperation Section,
Technology Management Division,
Japan Nuclear Cycle Development Institute
4-49 Muramatsu, Tokai-mura, Naka-gun, Ibaraki, 319-1184
Japan

© 核燃料サイクル開発機構 (Japan Nuclear Cycle Development Institute)

Ⓦ

登録区分
変更表示

NOT FOR PUBLICATION
PNC Z J222 82-16 (1) Tr
December, 1982

Sodium Spray Combustion Test*

- Part 1; Sodium Spray Fire Experiment -

Takabumi Nakahara**, Tamotsu Sano**
Sabuo Ueda***, Takayuki Imazu***
Mitsuo Tamaki***, Kazuaki Nemoto****
(Translated by H. Tanabe)

Abstract

In the safety design of the sodium cooled fast breeder reactor Monju, an unlikely event of a large sodium leakage accident must be considered in the design. Therefore the behavior of sodium combustion must be understood in full details.

This test program dealt with sodium spray combustion in both the primary and secondary cells. Experimental studies were performed using the sodium combustion facility with a volume of 21 m^3.

---

* Work performed under contracts between Power Reactor and Nuclear Fuel Development Corporation and Mitsubishi Heavy Industries, Ltd.

** Combustion and Heat Transfer Research Laboratory, Takasago Technical Institute, Mitsubishi Heavy Industries, Ltd.

*** Third Experiment Section, Takasago Technical Institute, Mitsubishi Heavy Industries, Ltd.

**** Advanced Nuclear Plant Engineering Department, Kobe Shipyard Engine Works, Mitsubishi Heavy Industries, Ltd.

In these experiments, sodium spray at about 530°C with a mean volume droplet diameter of about 1 mm was discharged from the full-cone spray nozzle in the ceiling of the test vessel. As test parameters, the initial humidity and oxygen concentration were selected. The experiments named TASP were carried out successfully, and valid data were obtained for the validation of the analytical code such as the time-dependent concentrations of gas and sodium aerosols in sodium spray combustion, which were the main purposes of this test program.

Summaries of the results obtained are as follows:

(1) Concerning the effect of gas concentration on the response of temperature and pressure, the TASP experiments showed that humidity caused insnignificant effects but rather oxygen concentration was the predominant factor.

(2) The comparison between the experiment and calculations concerning the gas pressure response showed that the calculation based on the heat and mass transfer model of the Ranz-Marshall equation agreed well with the experimental data.

(3) Experimental results are as follows relating to the effect of the initial humidity on the hydrogen generation during the sodium spray combustion:

   (a) In the absence of oxygen, hydrogen is generated to the maximum possible stoichiometrical hydrogen concentration.
   (b) In the presence of oxygen under the primary cell condition (2 $\sim$ 3% oxygen), the amount of generated hydrogen was lower than the maximum stoichiometrical value. This result implies that humidity adsorption by sodium oxide aerosols plays an important role.
   (c) Under the air-filled condition, no hydrogen generation was observed.

(4) Several kinds of valid and quantitative data were obtained concerning the sodium aerosol behavior. For example, the decay characteristics of aerosol concentration, deposition rate to the wall, settling rate on the floor and aerosol particle diameter distribution were measured successfully.

Results obtained in this test program will be applied to the design estimation of Monju. Moreover, spray combustion tests in a large vessel are necessary in the near future for a more prototypical simulation.

CONTENTS

1. FOREWORD

In the safety design of the sodium cooled fast breeder reactor Monju, an unlikely event of a large sodium leakage accident must be taken into consideration. Therefore, the behavior of sodium combustion must be understood in full detail.

There are several items for study regarding the prototype FBR Monju such as the basic design conditions of the cell and liners, considerations of structural integrity, gas concentration change and aerosol behavior.

In order to determine the basic design conditions, it is necessary to know the transient temperature and pressure changes during a sodium leak. Hence, the analysis codes for pool combustion (eg. SOFIRE [1][2]) and spray combustion (eg. SPRAY code[3]) have been developed to determine the basic design conditions.

Concerning the analysis codes it is extremely important to verify these against test data. The sodium tests were conducted in a test vessel with a volume of 21 m^3 for the sodium pool combustion, to compare the test data with the analysis code.

On the other hand small-scale sodium tests were conducted using a vessel of approximately 2 m^3 for spray combustion. Since there have been no large-scale tests regarding spray fire so far, the spray tests were also conducted using the larger vessel of 21 m^3 for more realistic code verification. The concentration change of gas ingredients and the aerosol behavior during the spray combustion were also obtained, which would be useful to understand problems in the actual plant.

2. TEST ITEMS AND PURPOSE OF TEST

It is extremely difficult to directly observe droplet distribution and spray conditions from the sodium spray combustion test. Therefore, a water simulation test was conducted prior to the sodium test. That is, there are two test phases:

(1) Water simulation test
(2) Sodium spray combustion test

The following are the objectives for both tests.

2.1 Purpose of Water Simulation Test

The water simulation test was conducted with the following purpose.

- o Provide the basic data regarding the sodium test, which cannot be observed visually, by determining the flow conditions and droplet size distribution.

2.2 Purpose of Sodium Combustion Test

The sodium combustion test was conducted with the following purpose.

(1) Obtain data for verification of the spray combustion analysis code.
(2) Obtain the information on the various phenomena occurring in spray combustion, such as the generation of hydrogen gas and the change of aerosol concentration under a high moisture concentration.

3. TEST EQUIPMENT AND TESTING METHOD

3.1 Water Simulation Test Equipment and Testing Method

3.1.1 Outline of Test Equipment

The vessel used in the water simulation test is shown in Fig. 3.1. Because the aim is to obtain the basic data for the sodium spray combustion test as previously explained, the following arrangements are made to the equipment.

(a) The shapes and dimensions of the catch pan are the same as those of the sodium combustion test to obtain the data during the pool combustion following the spray combustion.

(b) The distance between the sodium spray nozzle and the catch pan is the same as that in the sodium combustion test, to correlate the size of the suspended droplets.

(c) The capacity of the pipe section from the valve just upstream of the nozzle to the nozzle is chosen the same as that in the sodium combustion to clarify the transient immediately after the beginning and the end of spraying.

Besides, this equipment comprises a blockout curtain, collimator, etc. to observe the other aspects of the spray.

3.1.2 Testing Method

The following were measured or observed during the steady spraying.

(1) Spray pressure

(2) Spray flow rate

(3) Spray observation

The spray dispersion angle, envelope, etc. are recorded by photographing.

(4) Droplet diameter distribution:

It is calculated after sampling by collection method.

(5) Dispersed mass is measured by collection method.

The flow aspects immediately after opening and closing the spray valve are also observed. In addition, the following quantities were measured in the tests where catch pans were installed at the bottom of the vessel.

(6) Dispersed mass in the catch pans: The mass of accumulated water in each catch pan was measured after spraying for a certain period.

3.1.3 Test Conditions

(1) Selection of spray nozzle;

As the verification of the analysis code was the main objective, it was necessary to select a most suitable nozzle for this purpose. Therefore, investigations of existing documents and a preliminary calculation by analysis codes were conducted. Several types of nozzles were manufactured by way of trial and tested, and two types of nozzles were selected. The following are the main specifications of the selected nozzles and reasons for the selection.

(a) Spray nozzle type: full-cone nozzle.

As the model of the SPRAY[3] code is similar to the full-cone nozzle, it was appropriate to select the same type of nozzles. Another reason is that standard one for which plenty of experimental data have already obtained was thought to be better.

(b) Mean droplet diameter: The desired value of the mean volume diameter is approximately 1 mm ϕ.

The height of the test vessel is approximately 3 m; if the falling droplets reach the floor surface without sufficient reaction, it may cause difficulty because of the ensuing pool fire, and this will be incompatible with the capability of the analysis code. According to the report of the single droplet fall out test [5] conducted by AI in USA, the ignition of a droplet is dependent upon the droplet size. The smaller the size, the quicker the ignition. (See Fig. 3.2) For this reason a smaller droplet size is appropriate to generate a sufficient reaction in a vessel of limited height. On the other hand, however, if the droplet is too small it could cause an excessive increase in pressure in the vessel, which might exceed the maximum operational pressure. In addition there was a limit on the droplet size range which standard nozzles could produce. From the consideration of all the investigation including a preliminary analysis using the analysis code, it was concluded that approximately 1 mm ϕ was the most suitable droplet size.

(c) Spray dispersion angle: The aim was approximately 30°.

Spray nozzles with three types of dispersion angles (15°, 30° and 55°) were prepared and the nozzle with a dispersion angle of 30° was finally chosen, because this angle was the closest to the angle of 28° used in the CRBRP sodium spray combustion analysis conducted in USA.

(d) Spray discharge rate: approximately 50 ℓ/min

Standard leak rates in this test vessel were in the range of 10 ∿ 100 ℓ/min in consideration of the scale factor with Monju chambers. Then 50 ℓ/min was chosen as the average of that range. This leak rate was confirmed to be suitable in the preliminary analysis.

(e) Spray pressure: less than 1.9 kg/cm^2.

In the sodium test equipment sodium was stored in the high temperature tank in the upper section, then pressure was applied to the sodium to cause spray ejection. Therefore, the maximum operational pressure of the high temperature tank, 1.9 Kg/cm^2, is the upper limit of the spray pressure in the test.

The following values are references during the planning of the sodium spray combustion test, though they were not directly related to the selection of nozzles.

(f) Spray period: approximately 1 min.

An excessively short spray period will cause difficulty for the varification of the code. On the other hand if the spray period is too long, the pressure would increase too much, producing a large quantity of sodium which

must be disposed after the test. For this reason and from the results of the preliminary analysis with the computer code, this spray period was provisionally determined. However, it could be adjusted slightly depending on the pressure response in the test.

(g) Total amount of sprayed sodium: approximately 50 ℓ.

As the sodium was to be sprayed at 50 ℓ/min for one minute, it was set at approximately 50 ℓ. Table 3.1 shows examples of available sodium spray combustion tests, including overseas tests. As seen from this list, the total amount of sprayed sodium in our test was quite large compared with the vessel capacity, so it could be considered a sufficiently conservative test regarding thermal load.

The spray nozzles which were finally selected are shown in Fig. 3.3. Hereafter the upper nozzle in Fig. 3.3 is called the B nozzle, and the lower nozzle is called the D nozzle.

(2) The conditions of the water simulation test are as follows:

(a) Flow rate: $\sim$ 50 ℓ/min.
(b) Spray pressure: $\sim$ 2 kg/cm^{2}g

3.2 Sodium Spray Combustion Test Facility and Testing Method

3.2.1 Outline of Test Facility

(1) Test vessel

This test vessel was used in the sodium pool combustion test, therefore see Reference (2) for details.

Figs. 3.4 and 3.5 show the schematic and photo of this test vessel, respectively, and Fig. 3.4 also includes the major dimensions the device.

In this sodium spray combustion test the following points were improved.

(a) The installation of a moisture control system

(b) The measurement of the gas composition and the installation of the monitor system.

(c) The measurement of the sodium aerosols and the installation of the monitor system.

(d) The improvement of a discharge piping system;

To reduce the piping inner capacity, the 4 inch piping at the lower stream of the discharge valve was altered to 1 inch.

(e) The installation of thermal insulation layer in the bottom section of the test cell:

The thermal insulation layer was installed under the thin steel liner as shown in Fig. 3.4 to minimize the heat dissipation during the pool combustion because it occurs after spray discharge.

(f) Alteration of the catch pan structure:

"Separated catch pan" method was adopted as shown in Fig. 3.4 in order to lessen the trouble of the waste diposal after the test.

(2) Test system

Fig. 3.6 shows the flow sheet of the test facility. The test facility is divided into three systems.

(a) Sodium system; A system which ejects the sodium by applying pressure to the high temperature tank, also the sodium drainage system.

(b) System of control and measurement of gas concentration; a system which controls the oxygen and moisture concentrations, measures the compositions of sampled gas, and monitors continuously.

(c) Aerosol system; A system which monitors the aerosol by leading it in a closed loop through a sampling tube. To reduce the aerosol adhesion to the sampling tube wall it is heated up to approximately 300°C. Not only the gas introduction method with the sampling tube, but the airlock type sampling system is also adopted as explained later.

3.2.2 Testing Method

(1) Measuring items and measuring method.

Table 3.2 shows the measurement or monitoring items and also the measuring method. Fig. 3.7 shows the details of the thermocouple locations, while Fig. 3.8 is a schematic of the air lock type aerosol sampler. This method was such that the sampling tube filled with crystal wool was connected to the vessel wall through a ball valve. The aerosol absorbed into the crystal wool was then sampled. This method could increase the measuring accuracy. Also gas was replaced as indicated in the figure so that when the sampling tube was inserted into

the cell, outside air would not enter the cell. This is known as the airlock method. From the aerosol sample, the mass of sodium was determined through the neutralization titration or atomic absorption method, and from the ratio with the integrated quantity of absorbed gas, the concentration was determined.

(2) Test procedure

Table 3.3 summarizes the test procedure.

3.2.3 Test Conditions

Seven cases of the sodium spray combustion tests were conducted in all and Table 3.4 shows the test conditions of each case.

TASP-N1 is the test to check the efficiency of the sensible heat, and the effect of the primary system atmosphere is the object of TASP-N2 through N5, while that of the secondary system atmosphere is that of TASP-A1 and A2. They are special features which regards the moisture concentration as a variable parameter. In addition only TASP-N5 used the D nozzle which produces slightly greater particles than the B nozzle.

4. RESULTS OF WATER SIMULATION TEST

For the selection of a spray nozzle for the sodium test, four different full-cone spray nozzles were tested altogether. As a result, Nozzles B and D were finally selected in the sodium test as shown in Table 3.4. The results of each test are shown below.

(1) Dispersion Angle

Table 4.1 summarizes the spray dispersion angle, which was defined from the height of the nozzle and the radius of dispersion circle which involves 99% of the total discharged mass.

Photographs of typical discharging cases using Nozzles B and D are shown in Figs. 4.1 (1) and (2), respectively.

It is important to define the dispersion angle according to that used in the code. In the SPRAY code, volumes inside and outside of the spray zone are taken into account. Therefore it is considered a sufficient approximation to use the dispersion angle defined at the spraying point and the measured average dispersion angle at each height.

Average dispersion angles are as follows:

- o B nozzle: approximately 40°
- o D nozzle: approximately 30°

(2) Flow Characteristics

Figs. 4.2 (1) and (2) indicate the flow characteristics of nozzles B and D, respectively and Fig. 4.3 indicates the flow rate coefficient of nozzle B which was defined for the nozzle orifice. The coefficient is almost constant within the range of the Reynolds numbers used. This value can be used in the sodium spray test to determine the initial spray pressure.

As this flow rate coefficient was approximately 1, it means that fluid was filling the discharge orifice prior to discharge. Thus, the initial discharge velocity of a sodium droplet can be approximated to the average flow velocity at the nozzle orifice.

(3) Dispersion

Figs. 4.4 (1) and (2) show the dispersion results for nozzles B and D, respectively.

(4) Droplet Size

Figs. 4.5 (1) and (2) show the particle sizes measured 1 m below nozzles B and D, respectively. There are various definitions of the droplet mean diameter according to analytical purposes. The mean volume diameter, mean surface diameter and surface mean diameter are plotted for future use. As it is confirmed that the measured data follows the log-normal distribution function, the relationship between these mean droplet sizes can be determined from following formula:

$$f(\ell n\, d) = \frac{1}{\ell n\, \sigma_G \cdot \sqrt{2\pi}} \exp\left[-\frac{(\ell n\, d - \ell n\, d_G)}{2\ell n^2 \sigma_G}\right] \cdots\cdots\cdots\cdots (4.1)$$

f : log-normal mean distribution function

d : droplet diameter

d_G: geometric mean diameter

σ_G: geometric standard deviation

If the droplet sizes measured were arranged according to the size and their accumulated frequencies were plotted on the logarithmic probalility chart, then the measured values would lie on one straight line.

The standard deviation is expressed as below.

$$\sigma_G = \frac{84.13\%\ \text{diameter}}{50\%\ \text{diameter}} = \frac{50\%\ \text{diameter}}{15.87\%\ \text{diameter}} \quad \cdots\cdots\cdots\cdots (4.2)$$

The average droplet diameters, the standard deviation, etc. were calculated from the following equation. If it totally followed the log-normal distribution, σ_G of the formula (4.2) and σG of the following equation should be the same.

$$\left.\begin{aligned} d_n &= \Sigma(n_i d_i \Delta d_i) / \Sigma(n_i \Delta d_i) \\ d_s &= \{\Sigma(n_i d_i^2 \Delta d_i) / \Sigma(n_i \Delta d_i)\}^{1/2} \\ d_v &= \{\Sigma(n_i d_i^3 \Delta d_i) / \Sigma(n_i \Delta d_i)\}^{1/3} \\ d_M &= \Sigma(n_i d_i^3 \Delta d_i) / \Sigma(n_i \Delta d_i^2) \\ \sigma_G &= \exp(\sqrt{\ell n(d_v / d_s)^2}) \end{aligned}\right\} \quad \cdots\cdots\cdots\cdots\cdots (4.3)$$

d_n : count mean diameter
d_s : mean surface diameter
d_v : mean volume diameter
d_M : surface mean diameter

(5) Water Dispersion in the Catch Pan

Fig. 4.6 shows the water dispersion into the catch pans for nozzles B and D. In the case of nozzle B, approximately 50% of the water was collected in the 4 catch pans in the center. 96% of the water was collected in the 16 catch pans in the center. As the pool combustion will occur in the sodium test, care must be taken so that its dispersion is similar to that of water.

It was observed that the flow had attained a steady state within one second after opening the discharge valve. When the discharge valve was closed, the water remaining between the valve and the nozzle flowed intermittently. The amount of the residual water was very small compared with the total discharge, and it will have no substantial effect on the results.

5. RESULTS OF SODIUM SPRAY COMBUSTION TEST

5.1 General Discription of the Test Results

Figs. 5.1 (1) through (8) show the main results of each test. The conditions for each test are outlined below.

5.1.1 TASP-N1 (Sensible Heat Efficiency Test)

This test was conducted to determine the sensible heat efficiency of sodium. Oxygen concentration was approximately zero and the atmosphere was dry.

(1) Discharge (Fig. 5.1 (1))

In this test, the pressure in the high temperature tank was set to provide a sodium discharge rate of 50 ℓ/min. The nozzle flow rate coefficient used in this test was that obtained in the water simulation test. Fig. 5.1 (1) shows that the desired flow rate of 50 ℓ/min was obtained immediately after the valve opening. As the pressure inside the vessel rose slightly, the flow rate reduced.

(2) Gas pressure and temperature (Figs. 5.1 (2))

Gas temperature and gas pressure increased continuously after the spray discharge commenced and peaked near the completion of the discharge. They then decreased gradually. Maximum pressure was 0.39 kg/cm^{2}g.

(3) Ambient Temperature Distribution (Fig. 5.1 (3) $\sim$ (5))

During the spray test, the ambient temperature, measured radially in the inner tank, varied greatly because the spray zone is located at the tank center. In a vertical direction outside the spray zone there was no great temperature difference. On the other hand however, the temperature varied

greatly in the vertical direction inside the spray zone. The temperature inside the spray zone was a reference value which indicates the intermediate value between the sodium temperature and the surrounding gas temperature. The reason for the lower temperature in the lower part of the tank may be due to two factors. Firstly, the sodium droplets radiated heat to the surroundings as they fell. Secondly, the gas temperature differences in and out of the spray zone caused a convection current within the spray zone. This caused the cooler gas to move toward the lower part of the spray zone, reducing the temperature.

(4) Temperature of the Catch Pan (Fig. 5.1 (6))

Sodium falling into the catch pan causes the pan to heat up. It can be assumed that the temperature of the catch pan approximates the sodium temperature.

As shown in Fig. 5.1 (2), the temperature of the accumulated sodium after completion of discharge was approximately 370°C. If the partial heat loss to the catch pan and its support structure is considered, the temperature of the sodium as it reachs the catch pan is slightly higher. The temperature can be calculated using equation 5.1, ignoring heat loss to the atmosphere during the spray discharge and using the accumulated sodium weight measured in the catch pan.
(See Fig. 5.1 (8)).

$$T_{Na} = \frac{(W_{Na}\, C_{pNa} + W_R\, C_{pR})\, T_{MIX} - W_R\, C_{pR}\, T_R}{W_{Na}\, C_{pNa}} \quad \cdots\cdots\cdots\cdots\cdots \quad (5.1)$$

W : weight (kg)

Cp: specific heat (Kcal/kg°C)

T : temperature (°C)

Subscript

Na: sodium

R : catch pan

MIX: Mixed temperature (Actual measurement of sodium)

$$\begin{cases} W_{Na} = 6.37 \text{ kg} & W_R = 1.27 \text{ kg} \\ C_{PNa} = 0.31 \text{ Kcal/kg°C} & C_{PR} = 0.11 \text{ Kcal/kg°C} \\ T_R = 20°C & T_{MIX} = 370°C \text{ (Refer to Fig. 5.1(2) TE602 data)} \end{cases}$$

When the above values are substituted into equation 5.1, calculation yields:

$$T_{Na} = 395 (°C) \quad \cdots\cdots\cdots\cdots\cdots\cdots\cdots\cdots\cdots\cdots \quad (5.2)$$

This indicates that sodium discharged at 500°C lost approximately 100°C before it reached the catch pan. Also, the pan temperature distribution indicates that the pans which held a greater dispersion quantity had higher temperatures.

(5) Additional Temperatures

The temperatures of the floor liner, the side wall liner, the ceiling liner and the concrete were measured. While these values will be further discussed in part 2 of this report, the results are outlined as follows:

(i) Floor liner and concrete; virtually no change in temperature.

(ii) Side wall and ceiling liner; approximately 5°C temperature increase during the spray discharge.

(6) Gas Concentration Change: Fig. 5.1 (7)

As this is the sensible heat efficiency test, the change in gas concentration was not measured. However, the hydrogen concentration increased to approximately 1500 ∿ 2000 ppm when it was checked after the spray discharge. Gas concentrations will be quoted in moles hereafter unless otherwise specified. Because oxygen concentration was approximately zero, hydrogen gas was generated from the reaction between ambient moisture and the sodium.

There are two reactions between the sodium and moisture:

$$Na + H_2O \rightarrow NaOH + 1/2\,H_2 \quad \cdots\cdots\cdots\cdots\cdots\cdots\cdots\cdots \quad (5.3)$$

$$2Na + H_2O \rightarrow Na_2O + H_2 \quad \cdots\cdots\cdots\cdots\cdots\cdots\cdots\cdots \quad (5.4)$$

Reaction (5.3) occurs easily when there is excess moisture, and reaction (5.4) occurs when the ambient temperature is above the melting point of sodium hydroxide (approximately 320°C) and sodium is in excess.

Therefore, reaction (5.4) should occur in this test. As initial moisture concentration was of the order of 1000 ppm, it can be assumed that the quantity of hydrogen produced during the test was of the same order.

Gas concentrations measured during the test are plotted in Fig. 5.1 (7). It should be noted that the delay in the sample collection time, due to the length of the sampling line, is included in this graph. The delay time for collecting the oxygen sample was approximately 2.5 minutes, for the moisture sample the delay was 5.7 minutes, and for the hydrogen sample the delay was approximately one minute.

(7) Cell Inspection

Although the oxygen concentration was approximately zero during this test, sodium aerosols were generated and was observed to settle on the tank floor and wall. The amount will be discussed in section 5.2. Fig. 5.1 (8) shows the amount of sodium accumulated in each catch pan. The amounts are similar to the dispersed masses obtained in the water test.

5.1.2 TASP-N2 (3% oxygen concentration and low moisture concentration test)

This test was a simulation of the primary cell atmosphere. Moisture concentration was of the order of 1000 ppm.

(1) Discharge: Fig. 5.2 (1)

The discharge in this test was similar to that in TASP-N1. However, the flow rate was reduced more quickly due to a greater increase in gas pressure than in TASP-N1. The discharge time was set to approximately 75 seconds, due to the expected flow rate reduction. The sodium temperature at discharge was approximately 540°C.

(2) Gas Pressure: Fig. 5.2 (2)

The ambient gas pressure was higher than that in TASP-N1. The maximum pressure was 0.7 kg/cm^2g. During TASP-N1, the maximum gas pressure was recorded at the completion of spray discharge. For this test and subsequent tests, TASP N3 - N4 which are discussed later, the peak pressure was observed during the spray discharge.

(3) Ambient Temperature Distribution: Figs. 5.2 (3) ∿ (5)

The higher temperature in this test than in TASP-N1 means that a plenty of reaction heat was generated due to oxidation even though the oxygen concentration was only 3%. Around the spray zone center a higher temperature than that of the supplied sodium was measured just after starting the discharge. It is estimated that as the spray was not yet dispersed, sodium droplets could easily make contact with the surrounding oxygen. In addition, the ambient gas could be easily caught in the spray zone by a shearing effect caused by the falling droplets. These reasons established the conditions for the reaction, and it can be considered a localized effect.

(4) Catch Pan Temperature: Fig. 5.2 (6)

The temperature of the catch pans was again much higher than for TASP-N1. The sodium temperature at the pans was approximately 480°C, using the same method of calculation as previously. This means that the heat loss of the falling droplet is approximately half of that in TASP-N1. This indicates that the reaction heat generated much more.

(5) Additional Temperatures

The side wall liner and ceiling liner temperatures increased by 150°C during the spray discharge, which is, a much larger increase than that measured in TASP-N1. The temperature of the floor liner and concrete did not change significantly.

(6) Gas Concentration: Fig. 5.2 (7)

It was discovered later that a small quantity of sodium was leaking from the discharge valve seat in this test while the moisture concentration was being adjusted. As hydrogen gas was generated, the initial hydrogen concentration increased to approximately 3000 ppm. Therefore when the sodium was discharged, not only the oxygen and moisture concentration, but also the hydrogen concentration was reduced. This indicates that generated hydrogen further reacted somehow. Recombination of hydrogen and oxygen, or transformation to NaH are possible reasons. Recombination with oxygen requires a high temperature while transformation to NaH requires a low temperature. However the reaction speed to generate NaH is very slow. In addition, with the high temperature of the spray combustion, reaction with oxygen is more likely. If the reaction was with oxygen, it is possible that H_2O was first generated through combination of oxygen and hydrogen, then it reacted with sodium producing hydrogen again. However it should be noted that this reaction did not occur.

It is very likely that of Na_2O aerosols may have absorbed the moisture. In this case hydrogen would not generate as indicated below.

$$Na_2O + H_2O \rightarrow 2NaOH \quad \cdots\cdots\cdots\cdots\cdots\cdots\cdots\cdots \quad (5.5)$$

This will be mentioned in paragraph 6.2.

(7) Cell Inspection

While deposition of the sodium aerosols will be discussed later, a large mass of aerosols was observed.

5.1.3 TASP-N3 (3% oxygen concentration and high moisture concentration test)

In this test the oxygen concentration was 2.8% and the moisture concentration was 16,500 ppm. The moisture concentration was set to the saturated level (≒ 15,000 ppm) at the cold temperature (15°C) of the Monju primary cell ambient gas control system, which is the maximum moisture concentration in the actual plant.

(1) Discharge: Fig. 5.3 (1)

Both the sodium discharge flow rate and the gas pressure change were very similar to those in TASP-N1. This means that the moisture concentration does not affect the pressure change. The sodium discharge temperature was 538°C.

(2) Gas Pressure: Fig. 5.3 (2)

The gas pressure change was very similar to that for TASP-N2. Maximum pressure was 0.72 kg/cm^2g.

(3) Ambient Temperature Distribution: Fig. 5.3 (3) ∿ (5)

It did not differ from TASP-N2 so much in ambient temperature. The distribution pattern was very similar to that for TASP-N2.

(4) Catch Pan Temperature: Fig. 5.3 (6)

This temperature was approximately the same as that for TASP-N2.

(5) Gas Concentration Change: Fig. 5.3 (7)

Oxygen and moisture concentration decreased after the sodium discharge. Hydrogen concentration increased to

approximately 2,000 ppm. As the initial moisture concentration was approximately 16,000 ppm, if all the moisture reacted with sodium according to formula 5.4, the hydrogen concentration should have been 16,000 ppm. However, the hydrogen concentration was much lower than that value. As Na_2O aerosol tends to absorb moisture to a large extent as explained previously, it could explain the difference in the hydrogen concentration. It is not clear if the generated hydrogen combined with the oxygen to produce moisture which was absorbed into the aerosol, or if the moisture was in the ambient gas originally and was absorbed into the aerosol. It is possible that both of these cases occurred. It was, however, confirmed that when initial moisture concentration was 16,000 ppm, the increase in hydrogen concentration was less than expected from this test.

(6) Cell Inspection

There was no significant difference in the amount of sodium aerosols deposited, etc. to that for TASP-N2.

5.1.4 TASP-N4 (3% oxygen concentration, ultra-high moisture concentration test)

In this test the oxygen concentration was 3% and the moisture concentration was 23,000 ppm. This moisture level would not be used under normal operating conditions, but the moisture concentration was set similar to the concentration of oxygen to study the result.

(1) Discharge: Fig. 5.4 (1)

As indicated in the graph, the discharge flow rate was very similar to that of TASP-N3. The sodium discharge temperature was approximately 520°C.

(2) Gas Pressure: Fig. 5.4 (2)

The pressure increase was very similar to that for TASP-N3. The maximum gas pressure was 0.62 kg/cm^2g, slightly lower than that for TASP-N3.

(3) Ambient Temperature Distribution: Fig. 5.4 (3) ∿ (5)

The distribution was similar to those for TASP-N2 and TASP-N3.

(4) Catch Pan Temperature: Fig. 5.4 (6)

There was no significant difference to results of TASP-N2 or TASP-N3.

(5) Gas Concentration: Fig. 5.4 (7)

The oxygen concentration reduced from 3% to approximately 1% due to the spray discharge. The hydrogen concentration, similar to the results in TASP-N2 and N3, increased to approximately 10,000 ppm after the spray discharge. This test was performed with extremly high moisture concentration and the initial atmosphere temperature close to the dew-point. The moisture concentration was adjusted so that the dew-point was lower than the vessel liner temperature. However, moisture was condensed in a section of the moisture concentration measuring system outside the cell. This is because the temperature was not measured in that section and may have been lower than the dew-point. For this reason the moisture data could not be used effectively. The sodium spray discharge period was only one minute and the amount of condensation in the narrow tube of the moisture concentration measuring system would be insufficient to affect the spray combustion directly. It was, therefore, disregarded.

Hydrogen concentration was much higher than which was expected after the results of TASP-N3. In TASP-N3, the hydrogen concentration was one tenth of the concentration expected if all the moisture had reacted with sodium. However, in this test it was approximately half of the theoretical maximum concentration. This indicates that the higher the primary moisture concentration the greater the generation ratio of hydrogen. It could be estimated that as the moisture absorption into sodium oxide controls the generation of hydrogen, the generation of sodium oxide and its hydrogen absorption effect would be reduced. So the oxygen concentration is relatively much lower than the moisture concentration compared with that in TASP-N3.

(6) Cell Inspection

There was no significant difference in the aerosol deposition quantity to that for TASP-N3.

5.1.5 TASP-N5 (droplet size effect test)

In TASP-N1 through N4 and TASP-A1 and A2 (discussed later), the B nozzle was used. In this test the D nozzle, which produces a larger droplet size than the B nozzle, was used. The cover gas pressure in the high temperature tank was increased according as the cell pressure increased so that the pressure difference was controlled to provide an approximately constant discharge flow rate. Oxygen concentration was 3% and the moisture concentration was 8,000 ppm in the initial ambient gas.

(1) Discharge: Fig. 5.5 (1)

As the pressure in the cell increased during the spray discharge, the cover gas pressure in the high temperature tank was increased artificially, providing a comparatively stable flow rate of 45 ∿ 50 ℓ/min. The discharge duration was approximately 59 seconds and the temperature of the discharged sodium was approximately 520°C.

(2) Gas Pressure: Fig. 5.5 (2)

It was noted that the gas pressure became approximately constant just before the completion of spray discharge in the TASP test series, including this case. This means that the heat generation due to the spray combustion balanced with the heat loss to the surroundings, such as the liner. Therefore the peak pressure coincides with this constant pressure level, and this level will be greatly affected by the extent of the heat loss to the surroundings. On the other hand, the pressure increase following commencement of the spray discharge was greatly affected by the spray combustion. The effect of the sensible heat transfer, and the effect of the heat radiated to the surroundings was comparatively small.

The maximum pressure in this test was approximately 0.62 kg/cm^{2}g, similar to that in TASP-N4. A comparison of the maximum pressures shows that the difference between the B and D nozzles which affect their droplet diameters has a small effect on the gas pressure. However, it can be explained by the way that effect of the heat loss to the surrounding was so strong, as explained previously, that the effect of the difference between the nozzles was not directly observed. The pressure change, from the commencement of discharge until the constant pressure is attained, appears more relevant and therefore should be compared.

Comparing Fig. 5.4 (1) and Fig. 5.5 (1), the pressure increase of the TASP-N5 was definitely slower, even though the discharge flow rate was higher. Hence, it can be concluded that the difference caused by changing the droplet diameter was shown in the test data.

(3) Ambient Temperature Distribution: Figs. 5.5 (3) ∿ (5)

Fig. 5.5 (3) shows the temperature distribution 50 seconds after the discharge. Compared with the TASP-N4 temperature distribution inside the spray zone, TASP-N5 indicated slightly higher temperatures. However, gas and liner temperatures outside the spray zone were much lower in TASP-N5. The pressure was approximately constant 50 seconds after the spray commenced; this result must be caused by the difference in pressure transient states prior to the steady states as previously explained. This indicates that size of the droplets also affects the temperature distribution. The more rapid reaction transfers the heat more quickly and raises the temperature more readily. However, as the oxygen concentration in the spray zone is reduced, a corresponding reduction in spray zone temperature is observed.

(4) Catch Pan Temperature: Fig. 5.5 (6)

There was no significant difference in the catch pan temperature from that of TASP-N4.

(5) Gas Concentration: Fig. 5.5 (7)

Reduction in the oxygen concentration was gradual compared to that of TASP-N4. Also the reaction continued even after pool combustion commenced.

Hydrogen concentration increased to approximately 500 ppm. As the initial moisture concentration was approximately 8,000 ppm, the hydrogen concentration should have reached approximately 8,000 ppm if all this moisture reacted with the sodium. However, the measured hydrogen concentration was less than one-tenth of that estimated, which was similar to the result in TASP-N3.

(6) Cell Inspection

There was no significant difference in the deposited amount of aerosols to that in TASP-N3 and N4.

5.1.6 TASP-A1 (21% oxygen concentration, high moisture concentration test)

The TASP-A test series were conducted on the secondary cell ambient gas (ambient air). In TASP-A1 a very humid atmosphere (16,500 ppm) was used, and in TASP-A2 a very dry atmosphere was used.

(1) Discharge: Fig. 5.6 (1)

The pressure in the high temperature tank was fixed for this test. As there was a leak from the discharge valve seat in TASP-N2, as previously described, a manual valve by remote control was installed in series. Because in such tests using the air, reaction was violent and the pressure increased quickly, the flow rate reduced greatly. As the valve was opened manually, the flow rate was small and unstable during the first few seconds. However, a stable flow rate was attained very quickly, then it reduced gradually to an approximately constant flow rate of 25 ℓ/min. This indicates that the heat from the spray combustion and the heat loss to the surrounding liner were balanced then. Fig. 5.6 (7)) shows the aspect of the spray discharge with an 8 mm projector

through the observation window in the ceiling. The photographs show the violent flame reaction and the large quantity of aerosols. Spray discharge was terminated in 18 seconds for safety considerations. The discharged sodium temperature was 512°C.

(2) Gas Pressure: Fig. 5.6 (1)

The gas pressure increased immediately after commencement of the sodium discharge. The discharge flow rate decreased at the same time, then the gas pressure and the flow rate became stable. This indicates the balanced condition between the heat generation from the sodium combustion and the heat loss to the surrounding structure. The maximum pressure was 11.6 kg/cm^2g. The rate of pressure rise at its initial stage is 0.22 $kg/cm^2/sec$ and a time constant is 5.3 seconds. This rate is much greater than that of TASP-N series.

(3) Ambient Temperature Distribution: Figs. 5.6 (2) ∿ (4)

The temperature near the center section should be noted as it exceeded 1,000°C. This value indicates the magnitude of the reaction. Also, the gas temperature around center section was higher than that of the surrounding gas, even after completion of the spray discharge. This indicates pool combustion of the accumulated sodium near the center section.

(4) Catch Pan Temperature: Fig. 5.6 (5)

The temperature of the sodium in the catch pans was also high near the center, which was about 650°C after the spray discharge. This value is greater than the initial sodium temperature. Disregarding the pool combustion effect during the spray discharge, the temperature of the sodium in the catch

pans can be calculated using the formula in section 5.1.1., which results in approximately 830°C. However, this value is only the reference value since the pool combustion effect is large.

The catch pan temperature increased gradually after the completion of spray due to the pool combustion. During the pool combustion, the temperature of the peripheral area of the pans increased more than that of the central area. This may be because the thermocouples were installed on the bottom of the pans. The thermocouples were more affected in the peripheral area as they were closer to the surface combustion due to a smaller amount of accumulated sodium.

(5) Temperatures at Additional Points

The temperature of the ceiling liner increaced to a maximum of 70°C, which was higher than that in the TASP-N series. The side wall temperature also increased to the range of 50 to 60°C. However, no clear change occurred at the temperatures of the floor liner and concrete.

(6) Gas Concentration Change; Fig. 5.6 (6)

Even in this atmosphere of high humidity, hydrogen generation was insignificant. This could be explained by the high combustion temperature due to the high oxygen concentration. Even though hydrogen was generated in the reaction between moisture and sodium, it subsequently recombined with the oxygen.

The oxygen concentration was approximately 18% after the spray discharge. This may be due to the short spray discharge period.

The moisture concentration was approximately 2,000 ppm 50 minutes after the commencement of the spray, and it reduced throughout the spray and pool combustion periods.

The carbon dioxide content was sampled before the test, and 12 minutes, 40 minutes and 100 minutes after the sodium spray. It was comfirmed that the carbon dioxide concentration in each sample was less than 300 ppm, that is, a normal atmospheric concentration.

(7) Cell Inspection

Aerosol deposition was much greater than that in the TASP-N series. The aerosols accumulated to the height of 2 - 5 mm in the catch pans. The result is quantitatively discussed in section 5.2.

5.1.7 TASP-A2 (21% oxygen concentration, ultra-low moisture concentration test)

The air of an extremely low moisture was achieved artificially by mixing dry oxygen gas with dry sodium gas. The oxygen concentration prior to spray discharge was 20.4% and the moisture concentration was 410 ppm.

(1) Discharge: Fig. 5.7 (1)

The discharge period was set to approximately 57 seconds, much longer than that of TASP-A1.

Similar to the TASP-A1 results, the discharge flow rate reduced as the gas pressure increased. It reached a constant value of 22 ℓ/min approximately 20 seconds after a commencement of discharge. The discharged sodium temperature was 512°C.

(2) Gas Pressure: Fig. 5.7 (2)

The gas pressure at the constant level was 1.25 kg/cm^2g, which was also the maximum pressure. Considering the difference in initial conditions such as temperature, pressure there was no significant difference to the TASP-A1 results.

(3) Ambient Temperature: Fig. 5.7 (3) ∿ (5)

Temperatures at some parts in the central section exceeded 1000°C as in TASP-A1. The hottest area was around the middle height of the vessel 10 seconds after the sodium discharge commenced. However, when the sodium began to form pools, the hottest area moved to a lower part of the vessel. This is due to the sodium pool combustion.

The maximum temperature of the ambient gas was 1200°C or more.

(4) Catch Pan Temperature: Fig. 5.7 (6)

Some trends noticed in TASP-A1 were much more obvious. The catch pan temperature during the pool combustion was highest a little further from the center.

(5) Temperatures at Additional Points

The temperature of the ceiling liner increased to 100°C as the test duration was longer than TASP-A1.

(6) Gas Concentration Changes: Fig. 5.7 (7)

Oxygen concentration reduced to approximately 12% at the completion of the spray. After that the oxygen concentration reduced gradually due to the pool compustion.

(7) Cell Inspection

This test showed the largest aerosol deposition among all the tests. The accumulation on the floor was 5 ∿ 10 mm deep. Fig. 5.7 (8) shows an inside view of the test cell.

5.2 Measured Results Concerning Aerosols

This section discusses the aerosol deposition results of each test.

5.2.1 Aerosol Concentration Changes inside the Test Vessel

The masses of the sodium aerosols were obtained from those in the air-lock aerosol sampler using the neutralization titration method or the atomic absorption method. Figs. 5.8 (1) ∿ (3) show typical examples of the aerosol concentration changes using the above methods.

Using such a sampling method, errors appear easily because the results are obtained through several processes, and the sampling cannot be done so frequently.

An optical aerosol densitometer also used in this test will allow a reasonable measurement when used together with the above-mentioned sampling analyses. Fig. 5.8 (2) shows the results from the aerosol densitometer. From this figure the following are observed:

(1) The aerosol concentration reduced rapidly in the first hour, then the rate of reduction slowed. The main reason for this is the settling of the aerosols on the vessel floor. Since larger particles fall more rapidly, only smaller particles would remain after a certain period. Other factors include the coagulation of particles by collision and the deposition of aerosols on the vessel wall. These factors should be considered in analysis codes.

(2) The aerosol concentration was highest in the atmospheric air, and became lower in the order of the 3% oxygen concentration test, the 0% oxygen concentration tests. This result is qualitatively reasonable. While the aerosol concentrations were in the above order, the reduction of the concentration was remarkable in each case, as previously mentioned. The aerosol concentration in the atmospheric air test became similar to that in the 3% oxygen concentration test after one hour.

It can be assumed that the higher the earosol concentration, the greater the reduction rate, since the collision and coagulation of aerosol particles are frequent.

(3) Aerosol concentrations at the completion of the spray discharge estimated by extrapolation of Fig. 5.8 are roughly in the following order. These match the orders of maximum aerosol concentrations calculated from the settling and deposition, as explained in section 6.3.

3% oxygen concentration test: the order of 10 g/m^3

Atmospheric test: the order of 100 g/m^3

(4) As indicated in Fig. 5.8 (2), revised aerosol concentration data was obtained. This data will be very effective for future tests. The optical aerosol densitometer did not operate during the primary stage of TASP-A series tests because the aerosol concentration was too high. It was found later that the instrument utilizing side dispersion phenomemon cannot be applied under the condition of high aerosol concentration. However, this problem can be solved by improving the aerosol dilution adjustment method.

5.2.2 Measured Amount of Settled Aerosols

As explained in section 3.2.2, two methods were used to measure the amount of aerosols settled: measured total amount of settled aerosols at the completion of the test, and periodically measured amount of the settled aerosols throughout the test.

(1) Total aerosol settled

The samplers were covered during the spray discharge to prevent the entry of sodium droplets. At the completion of the spray discharge they were uncovered from a distance and measurement continued to the completion of the test.

Fig. 5.9 shows a comparison of the results of the TASP-N series and TASP-A series. The following can be seen from the figure:

(a) There is no great difference between the moisture concentration in the TASP-N3 test and that in the TASP-N4 test.

(b) TASP-A2 has a greater amount of settled aerosols than TASP-A1. The main reason for this may be the longer spray discharge duration of TASP-A2, indicating that the aerosols were largely generated during the spray discharge.

(c) TASP-A series have much larger aerosol amounts than TASP-N series, which indicates that aerosol generation is greater in the atmospheric air environment.

(d) The settled aerosol distribution data was measured radially in the vessel. However, as the distribution pattern is unstable, no trend could be established. It would be appropriate to state that there is no radial distribution in the aerosol generation.

(2) Settling Change with Time

An airlock-type measuring device was inserted into the vessel to obtain the information of aerosol settleing change with time. Typical results of the TASP-N series and the TASP-A series are shown in Fig. 5.10. The following can be seen from this figure:

(a) The amount of aerosol settling reduced greatly as time elasped. This is consistant with what is expected from the aerosol concentration measurement.

(b) TASP-A series using the air as an atmospheric gas has a greater settling. TASP-A2 data has a greater settling than TASP-A1 data. Such a relation is consistent with the result from the total amount of the aerosol settling.

5.2.3 Measured Results of Aerosol Deposition on the Wall

Concerning the aerosol deposition on the wall, both the total amount and its change with time are obtained.

(1) Measurement of the total deposition

Fig. 5.11 (1) shows the amount of aerosol deposition. Also Fig. 5.11 (2) shows the ratio of the total amount of aerosol deposition on wall to floor settling in TASP-N3, N4, N5, A1, and A2.

(a) There is no trend in the deposition per unit area in the vertical direction. It can be concluded that the deposition distribution per unit area in the vertical direction is nearly constant considering errors of the sampling, analysis, etc.

(b) The TASP-N1 test, which has very low oxygen concentration, has the smallest amount of deposition. TASP-N2, N3 and N4 tests had 3% oxygen concentration and showed greater deposition. TASP-N4, conducted in atmospheric air, had the greatest amount of deposition. This result is considered quantitatively appropriate.

(c) TASP-N2 had a smaller amount of deposition than TASP-N3. TASP-N4 had the greatest amount of deposition from the comparison among these three tests. This result may relate to the initial moisture concentration, that is, the greater the concentration, the smaller the deposition quantity. The reason for this relation is unknown at this moment. There are no great differences in the ambient gas condition in these three cases, such as aerosol concentration and temperature distribution. Therefore, it may result from a difference in the physical property of the aerosol.

It is explained later that the main factor for the deposition on the wall could be thermo-phoresis. As seen in formula 6.25 in section 6.3, the greater the heat conduction of the aerosol particles, the slower the thermophoresis speed. One possible reason why the thermophoresis speed was slower was that in the high moisture concentration test the aerosol, which was sodium oxide, could easily change to NaOH, and the thermal conductivity of NaOH is much greater than that of sodium oxide. To clarify this tendency the change in the chemical composition of the aerosol must be studied in the future.

(d) The TASP-A2 data indicated a greater amount of aerosol deposition compared to TASP-A1. The moisture concentration in these test cases varied greately, but oxygen was far in excess of the moisture. Therefore, it is difficult to expect that the moisture affected the amount of aerosol deposition. More likely it relates to the difference in the spray discharge period as explained previously. Because the TASP-A2 aerosol concentration in the ambient gas was greater, it is appropriate to assume that the difference was due to the amount of the deposition. However, as indicated in Fig. 5.11 (2) the quantity ratio of the wall deposition to the floor settling is similar in TASP-A1 and A2. Also the ratio in TASP-A1 and A2 is less than that of TASP-N5. This may be because the test conducted in the atmospheric air generated more settling aerosol.

(2) Deposition Change with Time

For this measurement, an airlock-type deposition measurement device was installed to allow insertion into the vessel at any time during the test.

Fig. 5.12 shows a change of the aerosol deposition flux on the side wall with time while Fig. 5.13 shows the change of the aerosol deposition flux on the ceiling. Some significant points from the figure are:

(a) All the test cases indicate a rapid reduction in the aerosol deposition flux. This means that the majority of the aerosol was deposited in the initial period.

(b) In TASP-A series conducted in the atmospheric air, the deposition flux is ten times or more higher than in TASP-N series, during initial periods.

(c) The deposition flux on the wall becomes smaller in the order, TASP-N2, N3, N4, which agrees with the trend of the total deposition measurement. TASP-N4 had a lower aerosol deposition flux on the ceiling than TASP-N3, as expected.

(d) TASP-N2 had a higher deposition flux than TASP-A1, which agreed with the total deposition measurement.

(e) Difference in the amount of deposition between the side wall and ceiling can be considered insignificant.

5.2.4 Measured Results of Aerosol Particle Size Distribution

A cascade impactor, which has been used for normal aerosol measurement for a long time, is an effective device for the measurement of sodium aerosol (6) (7). In this test, the Andersen 3371 model was used to obtain aerosol size distribution. As is well known, a fundamental principle of the cascade impactor is the inertia collision separation method using multistaged perforated collection plates.

This impactor consists of 8 stages. When the gas containing aerosols is taken into this impactor at a constant flow rate, the aerosol particles will be collected according to their sizes as the collision velocity increases when it reaches to the lower stage. The following equation is used to calculate the 50% effective cut diameter of the aerosol particles which are collected at each stage.

$$D_{P50} = \sqrt{\frac{18\mu\phi N\pi D_C^3}{4CQ\rho_p}} \quad \cdots\cdots\cdots\cdots\cdots\cdots\cdots\cdots\cdots\cdots\cdots\cdots\cdots\cdots\cdots\cdots \quad (5.6)$$

D_{P50} : 50% effective cut diameter of aerosol particle (cm)

μ	: coefficient of viscosity	(Poise)
ϕ	: inertial parameter	(-)
N	: number of holes per one stage of jet plate	(holes)
D_C	: jet plate hole diameter	(cm)
C	: Cunningham correction value $(= 1 + \frac{2A\lambda}{D_P})$	(-)
λ	: mean free path of gas molecule	(cm)
A	: constant determined by the type of gas	(-)
Q	: gas induction flow rate	(cm^3/sec)
ρ_p	: density of aerosol particles	(g/cm^3)

For example, the mean free path of a gas molecule, λ, and the constant, A, can be utilized in following equation:

$$\lambda = \frac{\mu'}{0.499P}\sqrt{\frac{\pi RT}{8M}} \quad \cdots\cdots (5.7)$$

$$A = 1.25 + 0.42\exp(-0.87\, D_P/2\lambda) \quad \cdots\cdots (5.8)$$

R	: universal gas constant	(erg/mol/°K)
P	: pressure	(g/cm^2)
T	: absolute temperature	(°K)
M	: molecular weight of gas	(-)
μ'	: viscosity coefficient of gas	($g.sec/cm^2$)

The inertial parameter of this cascade impactor ϕ, is 0.14, and the 50% effective cut diameter can be calculated from the above equations.

Table 5.2 shows the major values on the impacter used for calculations. However, the main concern in using equation (5.6) is what value should be used for the aerosol density ρ_p. Strictly speaking, the chemical composition of the aerosol or photomicrographs of the aerosol should be examined. However, according to studies on the aerosol generated during the sodium pool combustion, the density of 1.0 g/cm^3[6] or 1.32 g/cm^3[7], has been recommended as the particle densities.

In this calculation the aerosol density of 1 g/cm^3 was used. Typical calculational results are plotted on the logarithmic probability charts shown in Figs. 5.14 (1) through (3). There are insufficient data for a statistical discussion, and it is difficult to consider a part of the data as the perfect logarithmic normal distribution function. However, as a whole they are close to the logarthmic normal distribution function. Because of the lack of data, it has to be considered as approximate value. Fig. 5.15 indicates the transition of the geometric standard deviation with time calculated from the typical cases. Also the change of mass median diameter of (i.e. the particle diameter at accumulative frequency of 50%) is shown Fig. 5.16. The following are concluded from the figure.

(a) Mass median diameter has a tendency to reduce the size within the range of 4 to 1 μm as the time elapsed.

(b) There is no clear difference of the mass median diameter change characteristics between the tests conducted in the air and those conducted in the low oxygen concentration.

(c) The geometric standard deviation also tends to reduce with time. TASP-A2 conducted in atmospheric air, where greater amount of aerosol was generated than the other test cases, has a greater standard deviation. The transition in Fig. 5.16 indicates that the phenomenon that the larger the particles, the faster they fall, is more predominant than the collision and coagulation of the aerosol particles. Also the settling of the larger particles on the floor surface and the deposition of the smaller particles on the wall surface may be proceeding concurrently according to the tendency in Fig. 5.15.

(d) In TASP-N4, conducted in the very high moisture concentration, it is very different from the logarithm normal distribution. On the logarithmic probability chart, the curve for the small particle accumulation had a greater slope than the curve for the large particle accumulation as time elasped. This indicates that the reduction in the number of smaller droplets was inactive compared with the deposition of the larger droplets. This coincides quantitatively with the result of the aerosol deposition on the wall in TASP-N4 which was less than the other test cases as indicated in section 5.2.3. This is an interesting subject for future study. There is another example of distribution of sodium aerosol which is different from the log-normal distribution under high moisture concentration in literature (8).

5.3 Other Test Results

5.3.1 Leak Rate from Test Vessel

It becomes an important subject if the aerosol generated from the sodium combustion will leak from the test vessel, or if the aerosol will block the leak holes of each vessel section. Although to study this subject systematically would require further tests, the leakage rate was measured prior to these tests. This result is shown in Table 5.3, and the following can be seen:

(1) With the exception of TASP-N3, N4 and N5, the leak rates after the tests were definitly smaller than the rate before the tests. This indicates the blocking of the leak holes by the aerosols.

(2) In TASP-N3, the leak rate increased slightly; besides in the TASP-N4 and N5, the leak rate approximately doubled. All these tests were conducted in a low oxygen and high moisture concentration. However, the reason for these results is unknown, and will be the subject of future study.

(3) The leak rate never became zero by total blocking by the aerosols. However, this test vessel is so small compared to the actual plant that the reduction of the aerosol concentration was extremely rapid and the period of high aerosol concentration was extremely short, as mentioned in section 5.2. Therefore, these results cannot be applied directly to the actual case.

There was no observed smoke outside the vessel, indicating that no aerosol had leaked to the vessel surroundings.

5.3.2 Test Vessel Inspection Results

After each spray combustion test had been completed and the temperature had dropped, the manhole was opened for inspection, following the CO_2 stabilization process.

As the result of the inspection, no fault was found in the liner wall and other structures in each case. This indicates the integrity of the vessel under the severe conditions of the sodium spray combustion.

6. DISCUSSION

6.1 Sodium Droplet Combustion and Temperature and Pressure Behavior

6.1.1 Correlation of Water and Sodium

To obtain the characteristics of each nozzle, the full-cone nozzles were tested using water. These nozzles were used later in the sodium test. Therefore, it is essential to know how the data obtained in the water should be applied to the sodium. In the detailed evaluation, as each spray nozzle has different characteristics, individual test data with the different liquids are required for each nozzle. In this test the standard centrifugal full-cone nozzles were used and there are a few literatures and reports relating to this type of nozzle. The suitability of these nozzles with sodium was studied from these literatures.

The following formula[9] relates to the centrifugal spray nozzle.

$$\bar{D}_p \propto d_0^{1.35} \cdot G^{-1.0} \cdot \sigma^{0.62} \cdot \eta^{0.26} \quad \cdots\cdots\cdots\cdots\cdots\cdots \quad (6.1)$$

D_p	: reference droplet diameter	(m)
d_o	: nozzle orifice diameter	(m)
G	: flow rate	(kg/sec)
σ	: surface tension	(kg/m)
η	: coefficient of viscosity	(kg.sec/m^2)

As shown in Table 6.1, the value of the viscosity coefficient of sodium at 530°C is approximately 1/4.4 of that for water at normal temperature. Also the surface tension of the sodium is approximately twice as much as that for water.

The exponents of the surface tension and viscosity coefficient slightly depend on the nozzles used. However, by applying formula 6.1 the sodium D_p is approximately 0.8 time as large as that of water when same nozzle is used at the same flow rate. Therefore, the difference in aerosol size between water and sodium could be comparatively small.

According to formula 6.1, the surface tension is the most influencing factor on the particle size among the physical properties included in formula 6.1, so the Weber number, related surface tension should be applied for data arrangement.

$$We = \gamma u^2 d_0 / \sigma g \quad \cdots\cdots\cdots\cdots\cdots\cdots\cdots\cdots\cdots\cdots \quad (6.2)$$

γ : specific weight of fluid (kg/m^3)
u : mean velocity of flow through the nozzle orifice (m/sec)
g : acceleration of gravity (m/sec^2)

Fig. 6.1 shows the relationship between the Weber number and the mean particle diameter for the nozzle used in this test. The range of the Weber numbers for the TASP series is also shown in the same figure. Considering that the ranges of the Weber numbers are not much different between the water tests and sodium tests and that the mean particle size is approximately constant in the measuring range, it is assumed that the values such as mean particle diameter obtained in the water test are applicable to the sodium test with a good approximation.

The test result of literature (10), where the distribution of the sodium diameter was measured using centrifugal spray nozzles, also indicates that the particle size distribution for water is similar to that for sodium if there are no great differences in the Weber numbers.

Besides, the spray dispersion data obtained from the water test can also be applied to the sodium test as the dispersion of the water on the catch pans was similar to that of sodium, as described in the section 5.1.1.

The following mean diameters will be used to in calculations hereafter under the condition of the discharge pressures close to the target values.

B nozzle : mean volume diameter = 0.8 mm,
mean surface diameter = 0.7 mm

D nozzle : mean vlolume diameter = 1.5 mm,
mean surface diameter = 1.3 mm

6.1.2 Parametric Survey for Sodium Droplet Combustion

(1) Basic Equations

SPRAY code[3] of AI Co. is well-known for sodium spray combustion analysis. In this code the following Ranz-Marshall formula, which has been used for the analysis of oil droplet combustion, is applied for heat and mass transfer.

$$Nu = 2 + 0.6\,Re^{1/2}\,Pr^{1/3} \quad \cdots\cdots (6.3)$$

$$Sh = 2 + 0.6\,Re^{1/2}\,Sc^{1/3} \quad \cdots\cdots (6.4)$$

Nu	: Nusselt number ($=\frac{\alpha d}{\lambda}$)	(-)
Re	: Reynolds number ($=\frac{u d}{\nu}$)	(-)
Pr	: Prandtl number	(-)
Sh	: Sherwood number ($=\frac{k d}{D}$)	(-)
Sc	: Schmidt number ($=\frac{\nu}{D}$)	(-)
α	: heat transfer coefficient around droplet	(kcal/m^{2}h°C)
d	: droplet diameter	(m)
u	: relaltive fall velocity of droplet	(m/h)
k	: mass transfer coefficient	(m/h)
D	: diffusion coefficient	(m^2/h)
ν	: kinematic viscosity of gas	(m^2/h)
λ	: thermal conductivity of gas	(kcal/mh°C)

In this analysis, the mole fluxes of all constituents are considered in the transport term, the first term on the right-hand side of the formula (6.6) of the Fick's equation. If the quantity of moisture is too great to be disregarded, compared to that of oxygen it is important not to neglect the corresponding term. Further detail is described in literature (11).

(a) Fick's equation on flame inner surface

$$N_{Na} = Y_{Na}(N_{Na} + N_N) - CD_{Na}\frac{dY_{Na}}{dr} \quad \cdots\cdots\cdots\cdots (6.5)$$

(b) Fick's equation on flame outer surface

$$N_i = Y_i(N_O + N_H + N_N) - \frac{Sh_i}{2} CD_i \frac{dY_i}{dr}\,(i = H, O)$$

$$\cdots\cdots\cdots\cdots\cdots\cdots\cdots\cdots\cdots\cdots (6.6)$$

where

N	: mole flux	(kmol/m^2h)
Y	: molarity	(-)
C	: molarity of gas	(kmol/m^3)
r	: radial length	(m)

Subcript ; Na : sodium
O : oxygen
H : hydrogen
N : nitrogen

(c) Mass conservation law

The following formula is established by the conservation law of each constituent.

$$\frac{d}{dr}(r^2 N_i) = 0 \quad \cdots\cdots (6.7)$$

(i = Na, H, O)

(d) Boundary condition

$$r = r_A \quad ; \quad N_N = 0 \ ,$$
$$r = r_B \quad ; \quad N_j = 0 \quad \cdots\cdots (6.8)$$

r_A : Sodium droplet radius (m)
r_B : flame radius (m)

(e) Solution on inner flame surface

The mole flux for sodium N_{Na} can be solved on the inner flame surface as follows:

$$N_{Na} = CD_{Na} \frac{1/r^2}{1/r_A - 1/r_B} \ell n \frac{P}{P - P_{Na,A}} \quad \cdots\cdots\cdots\cdots (6.9)$$

where

P : total pressure of system

$P_{Na,A}$: partial vapor pressure of sodium at $r = r_A$ (kg/cm^2)

Mole flow rate of the sodium vapor W_{Na} (kmol/h) can be written as follows:

$$W_{Na} = 4\pi r_A^2 N_{Na,A} = \frac{4\pi r_A \cdot r_B}{r_B - r_A} CD_{Na} \ell n \frac{P}{P - P_{Na,A}} \quad \cdots\cdots\cdots\cdots\cdots (6.10)$$

$P_{Na,A}$ has the following relationship to the saturated sodium vapor pressure P_{sat}.

$$P_{Na,A} = P_{sat} \quad \cdots\cdots\cdots\cdots\cdots\cdots\cdots\cdots\cdots\cdots (6.11)$$

Although in the previously mentioned SPRAY code, $P_{Na,A}$ was adjusted so that it would have a slightly lower value than P_{sat}, formula (6.11) was used here instead.

(f) Solution on the outer flame surface;

Mole flux of oxygen and moisture, W_O (kmol/h) and W_H (kmol/h), on the outer flame surface can be solved using the above formula as follows:

$$Wi = -4\pi Cj \quad \cdots\cdots\cdots\cdots\cdots\cdots\cdots\cdots\cdots\cdots (6.12)$$

$$C_i = \frac{Y_{i,c}\,(C_H + C_O)}{1 - \exp\left\{\dfrac{C_H + C_O}{\dfrac{Sh}{2} C D_i\, r_B}\right\}} \qquad \cdots\cdots\cdots\cdots\cdots\cdots \quad (6.13)$$

where

$Y_{i,c}$: mole concentration at infinity

(g) Reaction mole ratio

The following reactions are assumed here:

$$\begin{cases} Na + \frac{1}{4} O_2 \rightarrow \frac{1}{2} Na_2O \\ Na + \frac{1}{2} H_2O \rightarrow \frac{1}{2} Na_2O + \frac{1}{2} H_2 \\ \frac{1}{2} H_2 + \frac{1}{4} O_2 \rightarrow \frac{1}{2} H_2O \\ \frac{1}{2} H_2O + \frac{1}{2} Na_2O \rightarrow NaOH \end{cases} \qquad \cdots\cdots\cdots\cdots\cdots\cdots \quad (6.14)$$

The reason for the assumption of these reaction was the expected water absorption by the sodium oxide aerosol.

From the assumed reaction above, the following relations are established for the mole flow of each composition.

$$\begin{cases} W_O = (W_O)_1 + (W_O)_2 = -4\pi C_O \\ (W_{Na})_O = 4\,(W_O)_1 \\ (W_{Na})_H = 2W_H = -8\pi C_H \\ (W_O)_2 = \frac{1}{2} W_H = -2\pi C_H \end{cases} \qquad \cdots\cdots\cdots\cdots\cdots\cdots \quad (6.15)$$

where

$(W_O)_1$: oxygen mole flow of reaction ($Na + \frac{1}{4}O_2 \rightarrow \frac{1}{2}Na_2O$) (kmol/h)

$(W_O)_2$: oxygen mole flow of reaction ($\frac{1}{2}H_2 + \frac{1}{4}O_2 \rightarrow \frac{1}{2}H_2O$) (kmol/h)

$(W_{Na})_O$: sodium mole flow of reaction ($Na + \frac{1}{4}O_2 \rightarrow \frac{1}{2}Na_2O$) (kmol/h)

$(W_{Na})_H$: sodium mole flow of reaction ($Na + \frac{1}{2}H_2O \rightarrow \frac{1}{2}Na_2O + \frac{1}{2}H_2$) (kmol/h)

The last formula of (6.15) indicates that the mole number of O_2 reacting with H_2 generated from the second reaction in (6.14), is 1/2 of the mole number of H_2O which reacts with Na.

The total sodium mole flux W_{Na} is written as follows, using equations in (6.15):

$$\begin{aligned} W_{Na} &= (W_{Na})_O + (W_{Na})_H \\ &= 4\,(W_O)_1 + 2W_H \\ &= 4\,(W_O - (W_O)_2) + 2\,W_H \\ &= 4\,(W_O - \tfrac{1}{2}W_H) + 2\,W_H \\ &= 4\,W_O \end{aligned} \qquad \cdots\cdots\cdots\cdots\cdots\cdots \quad (6.16)$$

If the reaction $Na + \frac{1}{2}O_2 \rightarrow \frac{1}{2}Na_2O_2$ occurs, W_{Na} becomes:

$$W_{Na} = 2\,W_O + W_H \qquad \cdots\cdots\cdots\cdots\cdots\cdots\cdots\cdots \quad (6.16)'$$

(h) Flame Radius r_B:

In the case of formula (6.16) the flame radius is expressed as follows:

$$\frac{1}{r_B} = \frac{1}{r_A} + \frac{C D_{Na} \ell_n \left\{ \dfrac{P}{P - P_{Na,A}} \right\}}{4 C_O} \qquad \cdots\cdots\cdots\cdots\cdots\cdots \quad (6.17)$$

W_{Na}, W_O, W_H, r_B can be obtained by combining the above basic equations.

(2) Parametric survey

By establishing a value for W_{Na} from the above equations, the combustion rate of the sodium droplets can be determined.

In this consideration, the following values are held constant:

- o Sodium temperature = 530°C
- o Ambient gas temperature = 30°C
- o System inner pressure = 760 mmHg

(a) Effect of droplet falling velocity;

Fig. 6.2 (1) shows the results of the calculation. The effect of the droplet falling velocity is very large, and the greater the droplet velocity, the greater the combustion rate. However, in the actual case, if the initial velocity of the droplet was very high, the period in which the droplet remains in the space becomes short, so it cannot be simplified. Furthermore, if the vessel is high enough for the droplets to reach their terminal velocity, the initial droplet velocity has no great effect.

In the TASP tests, the range of initial droplet velocity is 6 ∿ 17 m/sec, and the height of the vessel is approximately 3 m. The terminal velocities for the droplet mean volume diameter of 0.8 mm from the B nozzle, and 1.5 mm from the D nozzle, are shown below. If the initial velocity of the droplet is zero, the falling velocities of the droplet 3 m below the nozzle are also shown below. The atmospheric gas was assumed to be stationary.

B nozzle : o Terminal velocity = 15.8 m/sec
o If the initial velocity = 0,
the velocity 3 m below the nozzle is
6.5 m/sec.

D nozzle : o Terminal velocity = 55.4 m/sec
o If the initial velocity = 0,
the velocity 3 m below the nozzle is
7.3 m/sec.

As shown in the above figures, the chamber height of 3 m in this test is not sufficient to allow the droplet to reach the terminal velocity.

However, as explained later in paragraph 6.1.4.1, the initial velocity of the droplet of this system does not affect the peak of the gas pressure greatly, thus, the effect of the initial droplet velocity seems to be small.

(b) Effect of droplet diameter; refer to Fig. 6.2.(1)

It is clear that the effect of the droplet diameter is extremely large. However, as the droplet diameter becomes larger, the reduction in the combustion rate slows down; in other words, the smaller the particle size, the greater the effect of the droplet diameter on the combustion rate.

(c) Effect of oxygen concentration; refer to Fig. 6.2 (2)

The combustion rate is directly proportional to the oxygen concentration.

(d) Effect of moisture concentration; refer to Fig. 6.3 (1) and (2)

If the reaction in (6.14) was assumed, not all the diffused oxygen (W_O) to the sodium droplets would react

with the sodium. A portion of $(W_o)_2$ would be used in the recombining reaction with H_2 generated from the reaction of Na and H_2O.

This $(W_o)_2$ is one half of the moisture mole flow W_H necessary for the reaction with Na. It may be assumed that if there is high humidity, the sodium combustion rate is far greater than if only oxygen was present because Na and H_2O will react. However, the sodium combustion rate does not increase in practice because some portion of the oxygen is spent to the reaction with hydrogen instead of sodium.

Fig. 6.3 (1) shows the humidity effect on the sodium combution rate by reaction (6.14). From this figure, it is clear that the combustion rate does not increase greatly even in the high moisture concentration.

Literature (11) assumes a reaction model in which the recombination of the oxygen and generated hydrogen is not taken into account. This reaction is shown in the following formula:

$$\begin{cases} Na + \frac{1}{4}O_2 \rightarrow \frac{1}{2}Na_2O \\ Na + \frac{1}{2}H_2O \rightarrow \frac{1}{2}Na_2O + \frac{1}{2}H_2 \end{cases} \quad \cdots\cdots\cdots\cdots\cdots\cdots \quad (6.18)$$

The results using the above formula are shown in Fig. 6.3 (2). If this reaction is assumed, the Na combustion rate increases very much in a high moisture concentration. However, this tendency is pronounced only in a low oxygen concentration. If this reaction occurs in a high oxygen concentration, the effect of the moisture concentration on the combustion rate is very small.

For the above reasons it is guessed that humidity does not affect the sodium combustion rate greatly in a high oxygen concentration, regardless of the reaction modeling, and that it does not affect the sodium combustion rate greatly in a low oxygen concentration. If the bonding of H_2 and O_2 or the aerosol moisture absorption is assumed.

Also it is obvious that the combustion rate during the spray combustion is generally far greater than during the pool combustion.

6.1.3 Outline of Analytical Model

To compare the test data with analysis a droplet motion model and a existing pool combustion model are introduced in addition to the basic combustion model of the previous paragraph. The outline of this analytical model is explained:

(1) Characteristics of the Model

In this model, the basic formulas described in section 6.1.2 are used for the spray combustion and heat transfer. Besides, the basic formulas in the SPRAY code[2] of AI is used for the natural convection, and those for the pool combustion are derived from the SOFIRE-II code. Their characteristics are as follows:

(a) This model was designed to fit this testing procedure where sodium would be accumulated in the catch pan. This enables the consideration of the pool and spray combustion together.

(b) The model allows a various parametric survey such as the selections of droplet mean diameter definitions, chemical reaction equations and basic combustion equations.

(c) Transients at the commencement and completion of the spray discharge are included in the model, so the spray does not immediately spread over the whole space at zero hour. It is effective for a high cell.

(2) Assumption and condition on calculation.

The following assumptions are used:

(a) The model uses spherical droplets which have a sigle diameter. The mean droplet diameter and the combustion heat transfer are to be separately applied as input.

(b) The motion of the droplet will follow the Stokes formula. However, the initial velocity should be variable.

(c) The heat and mass transfer to the surroundings from a droplet should follow the basic formulas in section 6.1.2.

(d) The model in the SPRAY code will be used for natural convection of the gas.

(e) SOFIRE-II model will be used for the heat transfer at the sodium pool surface.

(f) The structure should have the catch pans on the floor surface.

(g) The equations in section 6.1.2 should be used; however, it can be selected depending on the input.

(h) Fig. 6.4 should be applied as the heat transfer path. The wall surface heat transfer coefficient during the spray discharge is derived from the SPRAY code, and that after completion of the spray is from SOFIRE II.

(3) Calculation method

The heat and mass transfer and droplet and gas motion shown in Fig. 6.3 are calculated explicitly, and at each time interval a quasi-stationary state is assumed.

Table 6.2 shows the flow chart of the calculation.

6.1.4 Comparision between Test Data and Analysis

Experimental data are compared with the analytical result using the model explained previously.

6.1.4.1 Comparision with TASP-N5 Data

In TASP-N5 the pressure in the high temperature tank was adjustable so that the discharge flow rate was made constant. The D nozzle was used and the mean droplet diameter was as indicated in section 4.

The following three cases were conducted for the analysis, in which the Na_2O generation equation was used.

Case 1

(1) Combustion model;
The model indicated in paragraph 6.1.2

(2) Particle size;
Mean particle mass diameter of 1.5 mm was used for the droplet motion volume, and mean surface diameter of 1.3 mm was used for heat and mass transfer.

(3) Initial falling velocity;
The initial velocity calculated from the nozzle orifice diameter was used. (Approx. 6 m/sec)

Case 2 (Supplementary case)

(1) Combustion model:
same as case 1

(2) Particle size:
same as case 1

(3) Initial falling velocity;
0 m/sec

Case 3 (Supplementary case)

(1) Combustion model:
same as case 1

(2) Particle size:
Mean volume diameter (Approx. 2.5 mm) was used for both the droplet motion and heat and mass transfer.

(3) Initial velocity:
same as case 1

A comparision between the test data and the calculational results of above cases, is shown for the gas pressure in Fig. 6.5.
The following are the results of the comparison:

(1) The gas pressure in case 1 is in the best agreement with the measured value.

(2) The gas pressure of the case 2 was unexpectedly close to the result of the case 1. The reason for this could be that as the sodium discharge with a small velocity has a low mass heat transfer rate as mentioned in 6.1.3. and it has a longer residence time on the other hand they will cancel each other.

(3) When the larger particles were descharged as in case 3, the gas pressure reduced greatly. This clearly indicates that the gas pressure is very sensitive to the droplet diameter.

6.1.4.2 Comparision with TASP-N2 Data

TASP-N2 was conducted under low oxygen concentration and used the B nozzle. The change of the discharge flow rate with time was taken into account. Since a fixed value must be used for the initial velocity, the mean flow velocity was used. As explained previously, the difference in the initial velocity was comparatively small.

The following points were considered:

(1) Combustion model:

The model is explained in section 6.1.2.

(2) Particle size:

For the droplet motion the mean mass diameter (0.8 mm), and for the mass transfer the mean volume diameter (0.7 mm) were used.

(3) Initial velocity: 11.6 m/sec

Fig. 6.6 shows the comparison between the calaculated value and the test value for the gas pressure.

- The rise rate and the peak of the pressure are similar. The pressure peak is almost flat. At the beginning of the pressure increase, the heat loss to the wall has a small effect. However, when the pressure becomes constant due to heat balance, the heat transfer to the wall greatly affects the stationary peak pressure. In this case the evaluation of the heat transfer is appropriate.

In this example, the calculational value of the sodium pool combustion rate was approximately 1/100 that of the spray combustion rate. Therefore, the effect of the pool combustion on the gas pressure was unexpectedly small in this test geometry.

6.1.4.3 Comparision with TASP-A2 Data

TASP-A2 was conducted in the atmospheric air using the B nozzle. The flow rate and the initial velocity were the same as paragraph 6.1.4.2. Na_2O generation reaction was assumed in the analysis.
Calculation was completed using the following values:

(1) Combustion model: The model is indicated in paragraph 6.1.2

(2) Particle size: Same as the case in section 6.1.4.2

(3) Initial velocity: 8.3 m/sec.

Fig. 6.7 shows the comparison of the calculated gas pressure with the test data.

Fig. 6.8 shows the temperature distribution of case 1, 15 seconds after the spray. From these figures the following are compared:

(1) The rise rate and the peak pressure are very similar between the test and analysis. However, in the test the pressure is constant after it reaches the maximum value until the spray discharge is completed. The calculated value decreases faster. Therefore, the evaluation of the heat loss to the liner wall could be a major influencing factor.

(2) The calculated flame temperature is 1000 ∿ 1200°C. This is assumed to be of the correct order since the actual measured value is an intermediate between the sodium temperature and the flame temperature.

In this model, while the sodium temperature was not high, the flame length was very short. In this case the reaction heat is used first for heating first the sodium droplets, then released as sensible heat to the ambient gas. However, after the sodium temperature does increase substantially and so the flame length gets longer, the reaction heat is split into two portions. One is released to the ambient gas from the flame and the other is transferred to the sodium droplets from the combustion. As the result of the present analysis, these two amounts of heat dissipation were approximately equal. This means that approximately half of the reaction heat was transfered to the ambient gas as sensible heat.

6.1.5 Conditions of Spray Ignition

The combustion rate of single droplet was examined by considering the mass transfer only in Section 6.1.2. In the actual case the motion of the droplet and the heat transfer should be included. AI conducted a test to study the ignition of a single falling droplet. (refer to Fig. 3.2) Input data similar to AI's were given to the above model to study the ignition behavior. Literature (12) includes a similar analysis; however, the simplified assumptions that all reaction heat is absorbed into the sodium droplets and that there is no heat interaction between the droplets and the ambient gas resulted in a conclusion that the ignition temperature is equal to the sodium boiling temperature. However, it could be too rough to disregard the transfer of sensible heat from the

droplets to the ambient gas. In this section the study was based on the assumption that the actual ignition temperature would be much lower than the boiling point.

Fig. 6.9 shows the temperature distribution in the falling direction of particle, which coresponds to the particle temperature change with time. In the test conducted by AI, the height of droplet ignition in each case was measured. It can be seen from this figure that the sodium temperature was approximately 600°C when the ignition commenced.

In literature (13), tests showed that when the temperature exceeded 600°C in the sodium pool combustion, oxide disappeared from the sodium surface. This indicates that the sodium had vaporized and ignited at 600°C. It is said that for the pool combustion, the oxide settling could affect the ignition. However, it is not clear what kind of process could remove the oxide from the falling droplets.

6.2 Gas composition Change

In the TASP test series, the moisture concentration was changed to examine the effect on the generation of hydrogen gas.

(1) Background

As an extreme example of the hydrogen generation during sodium combustion, Fig. 6.10 shows gas concentration changes measured in the F-1 test[14] conducted by HEDL in U.S.A.

As this is a sodium pool combustion test in a concrete catch pan, a large amount of hydrogen is generated by the reaction between sodium and concrete. If there is a comparatively high oxygen

concentration, hydrogen concentration will not increase due to recombination of hydrogen with oxygen. After the oxygen had been used up, hydrogen was generated. It confirms the thesis that "hydrogen will not be generated until the oxygen is consumed." However, in the spray combustion this is not proved experimentally, and the sodium droplets can come into contact with moisture much easier than in the case of the pool combustion. Therefore, the following are required for the generation of hydrogen gas in the spray combution.

(a) Proof that hydrogen gas will not be generated if there is a sufficiently high concentration of the oxygen.

(b) An experimental understanding of the hydrogen generation by a certain initial moisture in a low oxygen concentration.

(c) An experimental understanding of the hydrogen generation by the reaction of the initial moisture with sodium in a zero concentration. The above items were examined in this series of tests.

(2) Study of test results

From the test results, the following can be said regarding the above-mentioned items.

(a) In the comparatively high oxygen concentration, that is, in the atmospheric air hydrogen was not generated, even in a high moisture concentration, as seen in TASP-A1.

(b) In the low oxygen concentration, as seen in TASP-N3, the amount of hydrogen generated is approximately 1/10 of the amount stoichiometrically expected, even in the maximum moisture concentration (approx. 15,000 ppm) of the primary system of the actual plant. As seen in TASP-N4, when the moisture concentration increases further, the amount of hydrogen generated approaches the expected amount.

(c) During sodium spray combustion with no oxygen, as seen in TASP-N1, the amount of hydrogen generated is as much as expected.

(d) The highter the initial moisture concentration and the lower the initial oxygen concentration, the more hydrogen will be generated. As indicated in Fig. 6.11, when the ratio of initial moisture concentration to oxygen concentration was more than 0.1, hydrogen was generated in the TASP experiment.

As described in section 5.1, the main reason for the results could be that the Na_2O aerosol or Na_2O_2 aerosol absorbed the moisture to produce NaOH. The equilibrium H_2O pressure for the reaction of sodium oxide with moisture is shown in Fig. 6.12; even if the moisture concentration is as low as the order of 0.01 ppm at 500°C, the reaction can occur in the equilibrium state. The reaction speed is generally fast, even though it consists of complicated phenomena such as the change of chemical compositions during the reaction [15][16]. For the above reasons, it could be very possible that the aerosol generated in the reaction between oxygen and sodium would absorb the moisture form the atmosphere rapidly.

6.3 Sodium Aerosol Behavior

6.3.1 Maximum Aerosol Concentration

The aerosol released into the surrounding gas during the spray combustion and the following pool combustion is settled on the floor or is deposited on the wall and ceiling eventually. Therefore the total amount of sodium discharged can be estimated from the sum of the deposition and settling quantities. Also, if all the aerosol is transformed to oxide, the actual amount of sodium available for reaction can be calculated.

The ratio of aerosol discharged is defined as follows:

$$\text{Aerosol discharge ratio} = \frac{\text{Sodium amount discharged as aerosol}}{\text{Calculated amount of reacted sodium}} \quad \cdots\cdots(6.9)$$

Table 6.3 shows the calculated amximum aerosol concentration and the aerosol discharge rate.

The data of the settling amount on the floor in the pool combustion test are alos included in the table.

The aerosol discharge rations for both the Na_2O generation reaction and the Na_2O_2 generation reaction are calculated individually and expressed as a range of values. From this table the following can be seen:

(1) TASP-A2 has comparatively long discharge time and has the highest concentration of aerosol. The maximum concentration is 163 g-Na/m^3,

(2) The aerosol discharge ratio is 20 $\sim$ 40% in each case, except when the discharge period is short. This ratio is much greater that for the pool combustion.

6.3.2 Relationship of Aerosol Settling on the Floor with Particle Size

Fig. 5.10 shows the change with time in the aerosol settling flux on the floor. The settling flux reduced greatly as time elapsed. This change can be expressed the following equation:

$$W \propto t^{2.61} \quad \cdots\cdots (6.20)$$

W : settling flux (kg-Na/m^2h)

t : time (h)

The terminal falling velocity Vt for the particles with a diameter of 1 ∿ 10 μm, can be determined using Stokes law on settling.

$$Vt \propto dp^2 \quad \cdots\cdots (6.21)$$

Vt : terminal falling velocity (m/h)

dp : aerosol particle diameter (m)

When the height of the vessel is h, then the time, t_f, for the particles to reach the floor is as follows:

$$t_f = \frac{h}{Vt} \quad \cdots\cdots (6.22)$$

The weight, W_p of a single aerosol particle is proportional to dp^3. The relationship between the aerosol particle weight and the settling flux W is as follows:

$$W = \frac{W}{t_f} \propto dp^5 \quad \cdots\cdots (6.23)$$

If this relationship is applicable to each particle, the trend in the particle size change with time can be estimated from the change in settling flux.

The equation of the particle size change is as follows using equations (6.20) and (6.23).

$$dp = Co\ t^{-\frac{2.61}{5}} = Co\ t^{-0.52} \quad \cdots\cdots (6.24)$$

Fig. 5.16 shows the change in mean volume diameter with time, determined using the cascade impactor. The trend in these results is similar to that using equation (6.24), which reconfirms the close relationship between the transition of the aerosol settling and that of the particle size.

6.3.3 Aerosol Deposition Speed

From the measurement of deposition flux w_d obtained using the air-lock type deposition measurement device, the mass transfer coefficient k of the aerosols can be expressed as the following formula:

$$k = \dot{\omega}_d / C \quad \cdots\cdots\cdots\cdots\cdots\cdots\cdots\cdots\cdots\cdots \quad (6.25)$$

k	: mass transfer coefficient	(m/h)
$\dot{\omega}_d$	: aerosol deposition rate	(kg-Na/m^2h)
C	: aerosol concentration	(kg-Na/m^3)

The k's of the representative test cases are roughly as follows.

- o TASP-N2 k = 0.067 m/h after 0.5 hour
- o TASP-N3 k = 0.046 m/h after 0.5 hour
- o TASP-N4 k = 0.011 m/h after 0.5 hour

The Brownian diffusion can be assumed as the particle size is already known. The k value obtained is extremely small and is 10^{-5} m/h.

The aerosol deposition flux due to thermo-phoresis obtained from the following formula[17]:

$$Kt \fallingdotseq \frac{3\nu}{2T} \cdot \frac{2\lambda g}{2\lambda g + \lambda p} \cdot \frac{dT}{dx} \quad \cdots\cdots\cdots\cdots\cdots\cdots\cdots\cdots \quad (6.26)$$

Kt : deposition flux due to thermo-
phoresis (m/h)

T : temperature (°K)

dT/d/t: temperature gradient at wall (°C/m)

ν : coefficient of gas kinematic viscosity (m^2/h)

λ_g : thermal conductivity of gas (kcal/mh°C)

λ_p : thermal conductivity of aerosol (= 0.65 kcal/mh°C)

The mass transfer coefficient is estimated using the gas temperature of 100°C (=373°K) and the wall temperature of 50°C. If the heat transfer coefficient to the wall surface due to natural convection is assumed 5 kcal/m^2h°C, then the temperature gradient at the boundary layer is approximately dT/dx=9300°C/m.

The Kt value is calculated by substituting each value into formula (6.26)

$$Kt = \frac{3 \times 0.0857}{2 \times 373} \times \frac{2 \times 0.0269}{2 \times 0.0269 + 0.65} \times 9300 = 0.0245 \quad (m/h) \qquad \cdots\cdots (6.27)$$

This result is within the range of the test results (0.0114 ∿ 0.0667). Therefore, the predominant mechanism of the aerosol deposition on the wall may be thermo-phoresis.

7. CONCLUSION

The sodium spray combustion tests were conducted. The sodium of 530°C was sprayed from the full-cone nozzle located in the test vessel ceiling, 3 m above the catch pans. The mean volume diameter of the sodium droplets was approximatly 1 mm. The following are conclusions of the test results.

(1) Temperature and pressure behaviors during the sodium spray combustion.

(a) The initial oxygen concentration was the primary factor of the temperature and pressure behavior while the moisture concentration had little effect.

(b) A violent combustion occurred in the atmospheric air with the test vessel. A thermocouple located in the spray zone indicated a maximum temperature of 1200°C during the combustion.

(2) The following results were obtained from the comparison with the analytical model based on the Ranz-Marshall equation.

(a) The gas pressure agrees well with the actual test data in a low oxygen concentration.

(b) In the atmospheric air, the calculated result agrees well with the test data in the rising of the pressure. However, the behavior of quasi-steady pressure differs slightly. It isassumed that if the amount of heat loss to the wall surface is precisely estimated, the results may be improved.

(c) By comparison with the single falling droplet test conducted by AI in U.S.A., the ignition temperature of the droplet was estimated to be approximately 600°C.

(3) The effect of the moisture concentration on the generation of the hydrogen gas during the sodium spray combustion test.

(a) When the oxygen concentration was zero, a large quantity of hydrogen was generated, which was very similar to the expected result.

(b) When the oxygen concentration in the vessel was 2 ∿ 3%, the hydrogen concentration was lower than expected. This may be caused by the large amount of moisture absorption by the generated aerosol.

(c) The generation of hydrogen was not observed in the test conducted in the atmospheric air even when the moisture concentration was comparatively high.

(4) Extensive consideration was given to the sodium aerosol behavior during the spray combustion. The following are the main points:

(a) Quantitative results were obtained regarding the concentration reduction characteristics. The rate of reduction was extremely high in the first hour due to the low ceiling. These data are avilable for the future consideration of aerosol behavior.

(b) The test result of the aerosol diameter was obtained. There was no significant difference between each test result concerning the mean droplet diameter. The mean droplet diameter was in the range of 1 ∿ 4 μm.

(c) Quantitative results concerning the aerosol settling were obtained. The test conducted in the atmosperic air had a much greater aerosol settling amount than the test conducted with a low oxygen concentration.

(d) With a high moisture concentration in the vessel, the amount of aerosol deposition on the vessel wall was small. The major factor in this aerosol deposition is thermo-phoresis.

(e) The aerosol release ratio and the maximum aerosol concentration estimated from the aerosol settling and deposition data were 20 ∿ 40%, and 163 g/m3 respectively, for the spray combustion test conducted in the atmospheric air. Compared to the sodium pool combustion test conducted previously by opening the manhole of the same test vessel, the spray combustion had a higher maximum aerosol concentration and aerosol release ratio overall.

(5) Other conclusions

(a) Reference data relating to the cell leakage rates before and after the spray combustion were obtained.

(b) Throughout this spray combustion testing, no faults were found in the concrete lined test vessel. This proves that the vessel can maintain its integrity under the severe conditions of the sodium spray combustion.
The test results are expected to effectively reflect on the designs the prototype reactor Monju. Furthermore, it is recommended to obtain sodium spray combustion test data using a larger test vessel.

8. AFTERWORD

As no prototypical test data were available on the sodium spray combustion, information was insufficient for understanding miscellaneous problems of sodium spray combustion and for verifying the analytical codes. From our spray combustion test using the 21 m3 test vessel, temperature and pressure measurements were obtained as well as the effective data relating to the hydrogen generation in high humidity and the characteristics of sodium aerosols. As the temperature and pressure data are detailed in Part 2 of this report, they will be used as a benchmark for future analysis.

We have received much advice and assistance from the personnel in the FBR Developement Projct of Power Reactor and Nuclear Fuel Development Corporation (PNC) to perform these test series. Especially, we appreciate the valuable advice from Mr. Shinya Miyahara through out the stages of the preliminary calculation, planning and evaluation during the actual test.

BIBLIOGRAPHY

(1) P. Beiriger et al.;
"SOFIRE-II User Report," AI. AEC-13055 (1973)

(2) Yagi, Naganuma;
"Primary Containment Structure Integrity Test," PNC SJ222 77-08 (1977),
"Primary Containment Structure Integrity Test II," PNC SJ222 78-01 (1978)

(3) P.R.Shire;
"SPRAY Code User's Report," HEDL-TME 76-94 (1977)

(4) Sagawa et al.;
"Sodium Combustion Test in Sealed Vessel," PNC SJ 202 76-06 (1976)

(5) H.A. Morewitz et al.;
"Experiments on Sodium Fire and Their Aerosols," Nuclear Eng. and Design, Vol 42 (1977)

(6) Kitani et al.;
"Study of Sodium Aerosol Behavior," JAERI-4136 (1970)

(7) J. Wegrazyn et al.; NUREG/CR-099 (1979)

(8) A.R. Sundararajan et al.;
"Effect of Relative Humidity on Growth of Sodium Oxide Aerosols," Journal of Nuclear Science and Technology, Vol 19 (1982)

(9) Chemical Engineering Bulletin (The Third Revision), Maurzen (1968)

(10) Sagawa et al.;
"Sodium Combustion Test in Sealed Vessel (2)," PNC SJ202 77-10 (1977)

(11) S.S. Tsai et al.;
"The Effect of Humidity on The Burning Rate of Sodium Droplet," Transaction, of The ANS, Vol.26 (1977)

(12) S.S. Tsai;
"Surface Oxidation Process Prior to Ignition of a Sodium Droplet," Transaction of The ANS, Vol.27 (1977)

(13) R.N. Newman;
"The Role of Carbon Dioxide in the Combustion of Sodium in Air," Proceedings of LMFBR Safety Meeting Lyon (1982)

(14) R.K.Hillard;
"Summary of HEDL Sodium Fire Tests," IAEA/IWGFR Specialists' Meeting, Cadarache (1978)

(15) W.S. Clough;
"The Behavior in the Atomosphere of the Aerosol from a Sodium Fire," Journal of Nuclear Energy, Vol.25 (1970)

(16) S. Jordan;
"Experimental Result on Sodium Aerosol Transformation and Filtration," PNC SD082 81-02 (1982)

(17) Kanji Takahashi;
"Basic Aerosol Engineering (First Edition)," Yokendo (1972) (in Japanese)

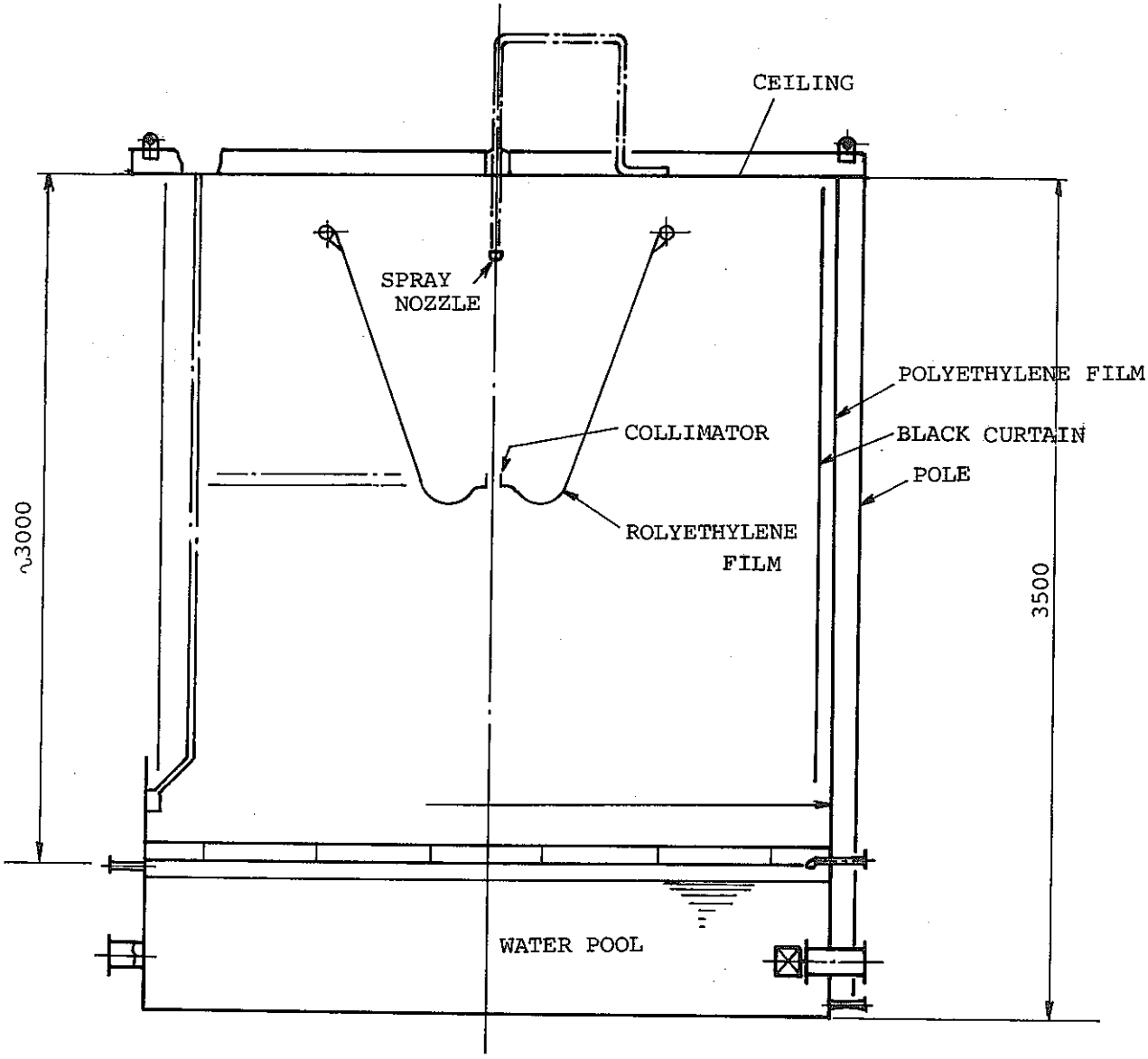

Fig.3.1 Equipment for Water Simulation Test

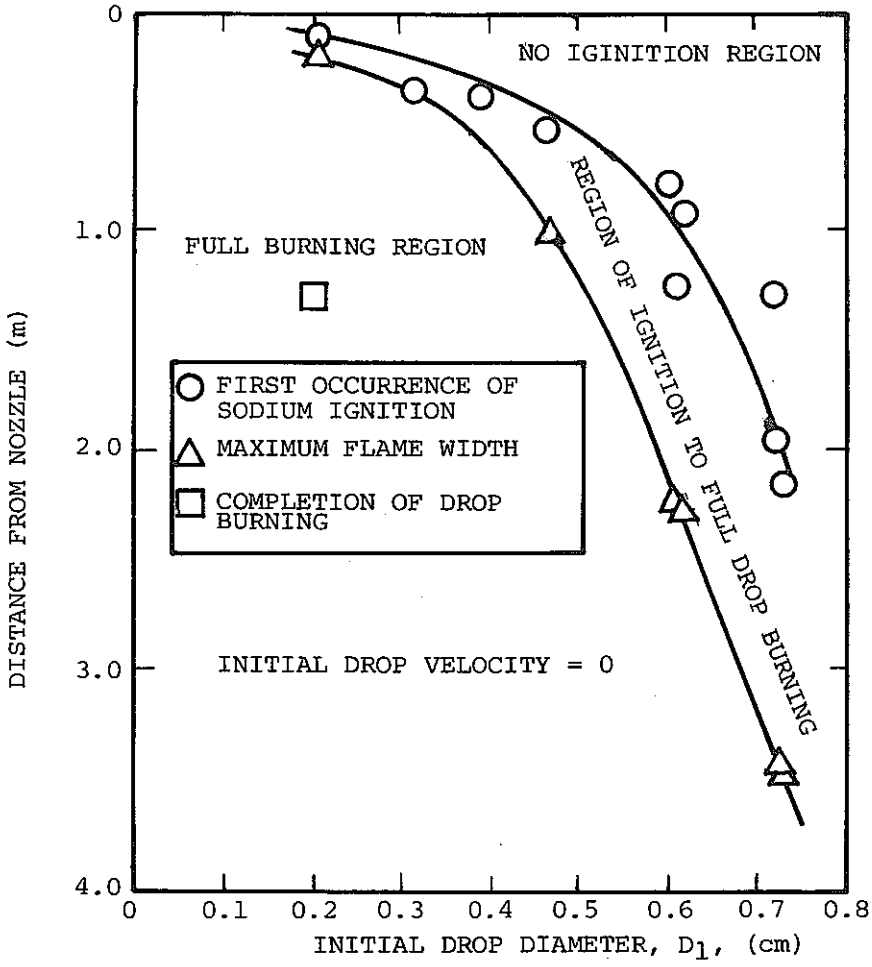

Fig.3.2 Burning Characteristics of Sodium Drops in Air (ref.(5))

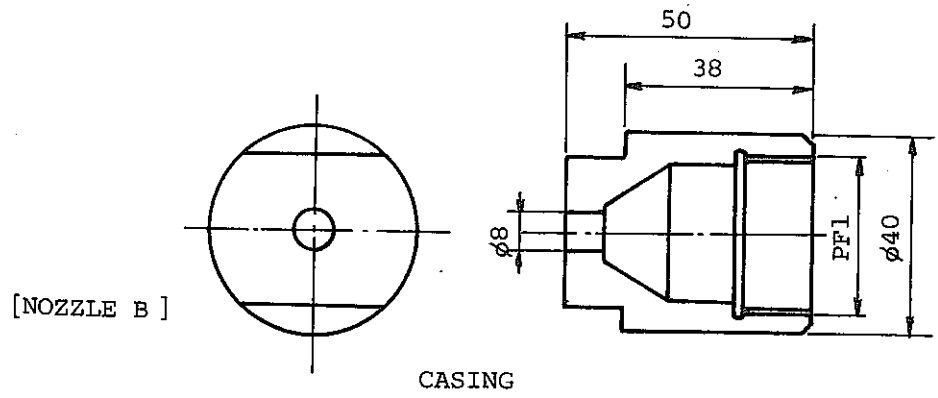

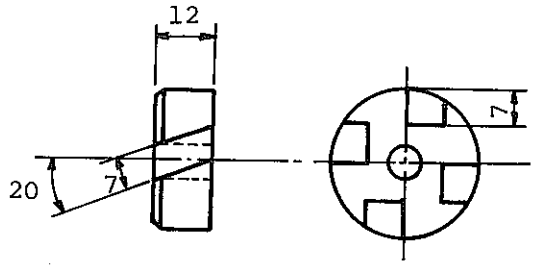

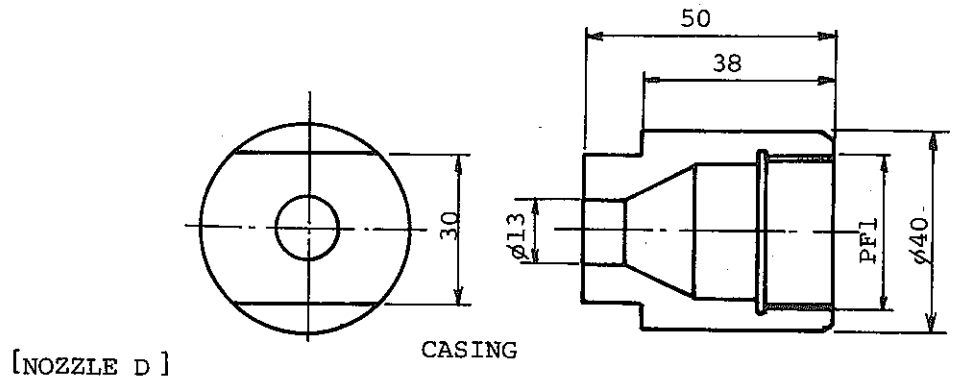

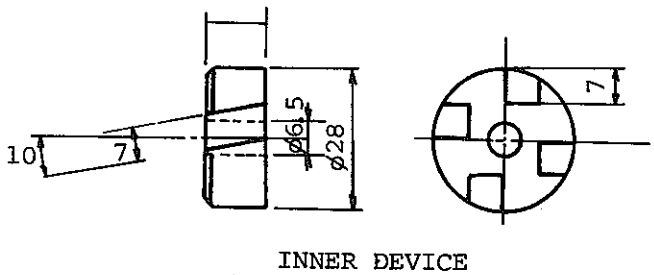

FIG.3.3 Full Corn Spray Nozzle

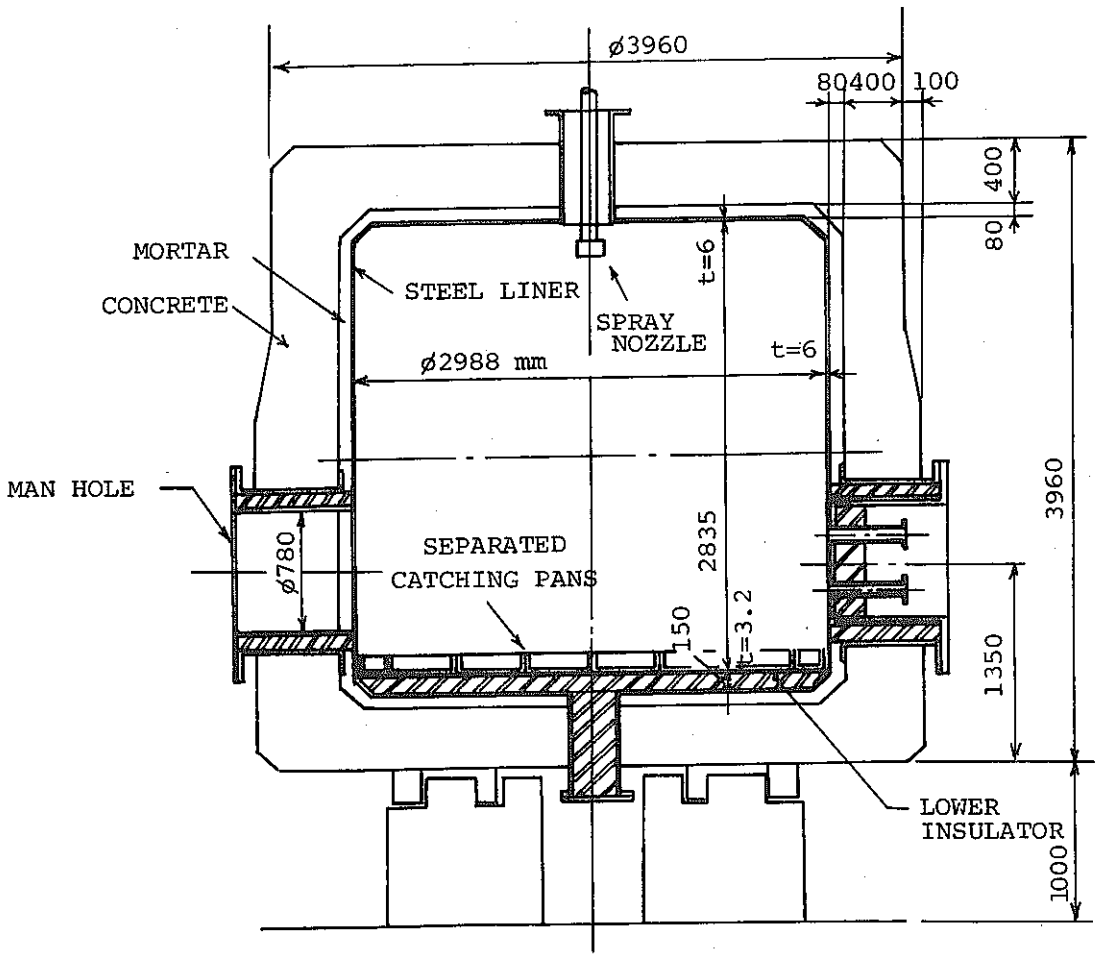

Fig.3.4 Schematic Figure of Test Vessel

DESCRIPTION OF TEST VESSEL

SIZE	:	INNER DIA. = 3 m INNER HIGH. = 3 m
STRUCTURE	:	STEEL LINED CONCRETE STRUCTURE
VOLUME	:	19.9 m^3 (NOT INCLUDING LOWER INSULATOR)
FLOOR AREA	:	ABOUT 7 m^2
WALL AREA	:	ABOUT 26.6 m^2
CEILING AREA	:	ABOUT 7 m^2

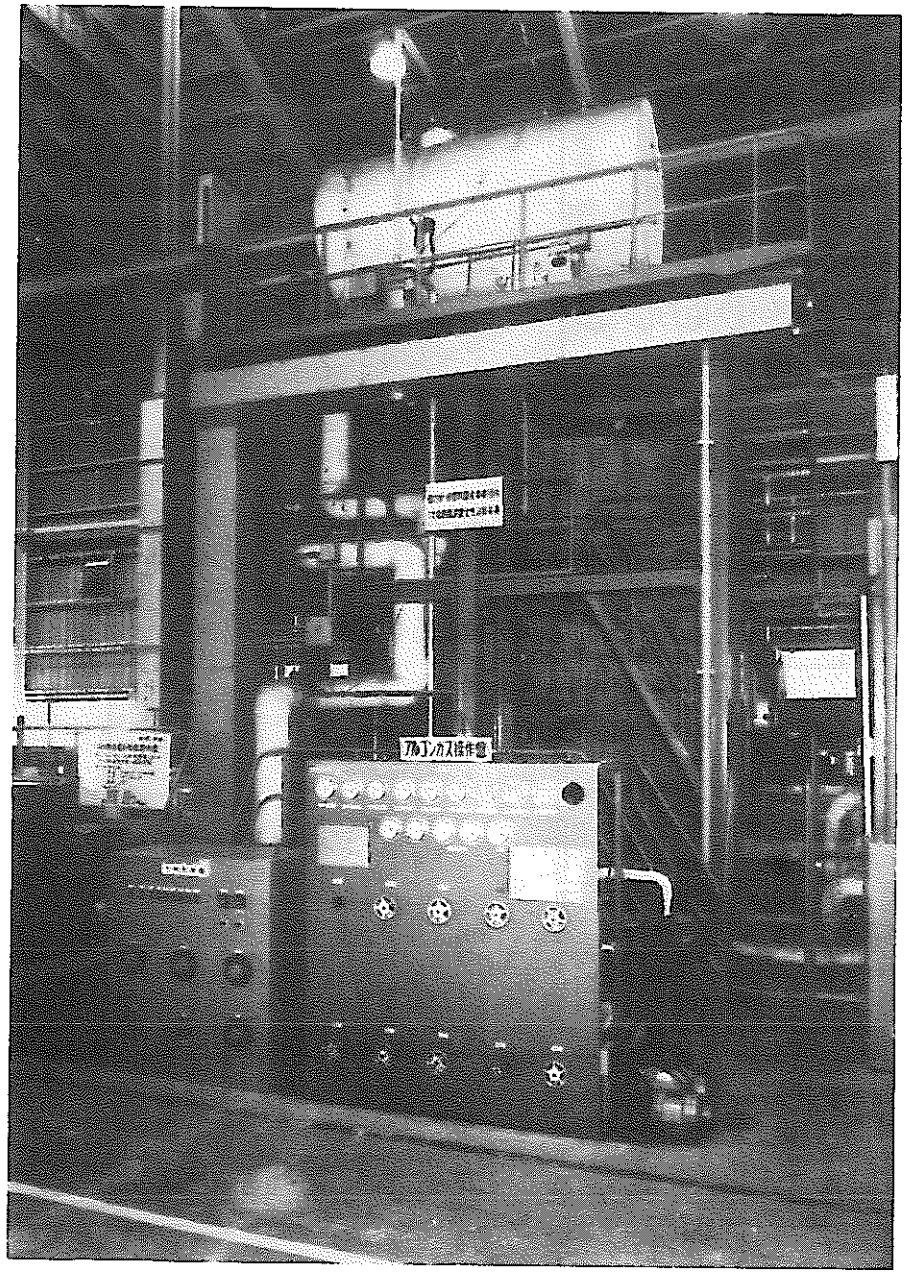

Fig. 3.5 Photograph of Test Vessel

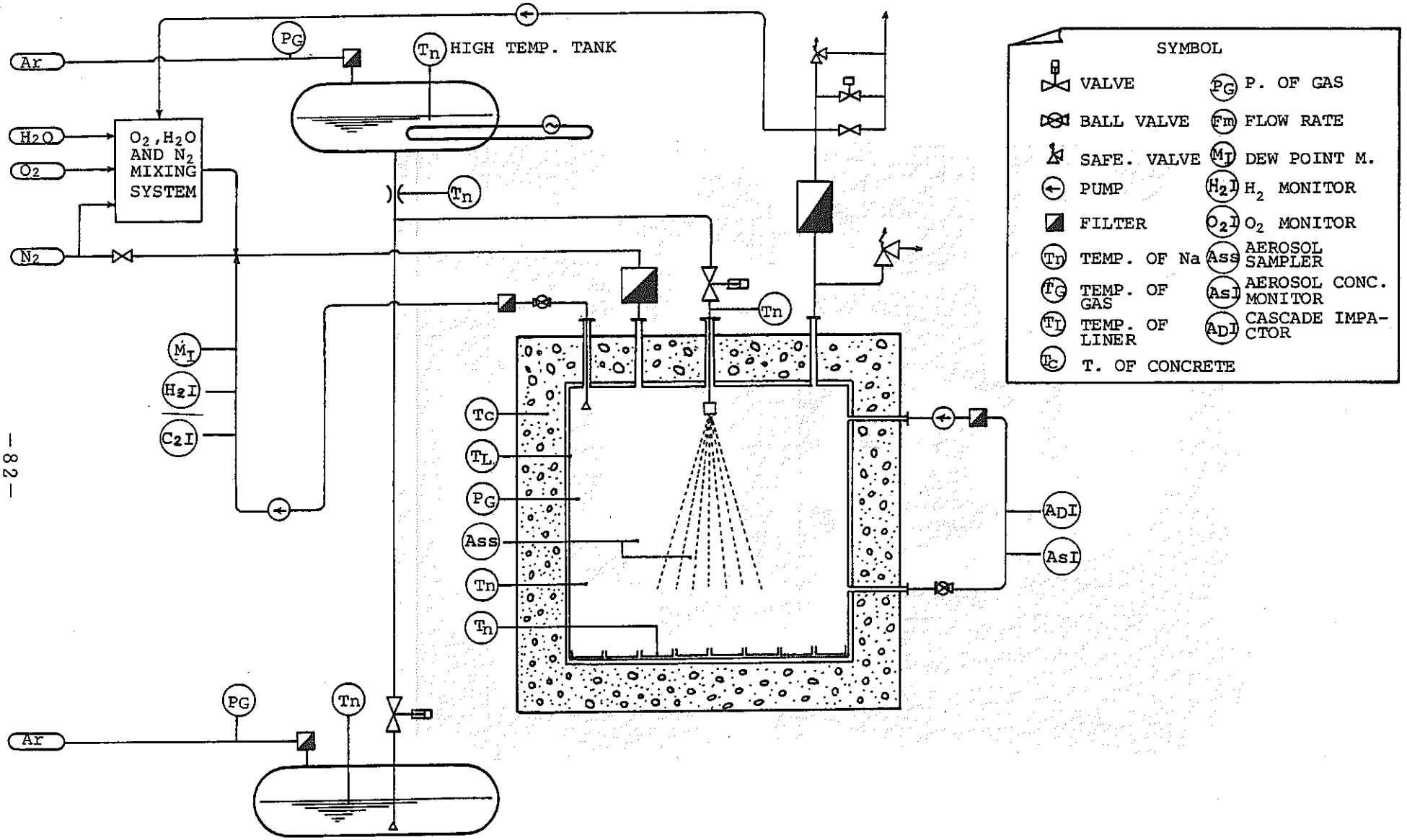

Fig.3.6 Flow Sheet of Test Facility

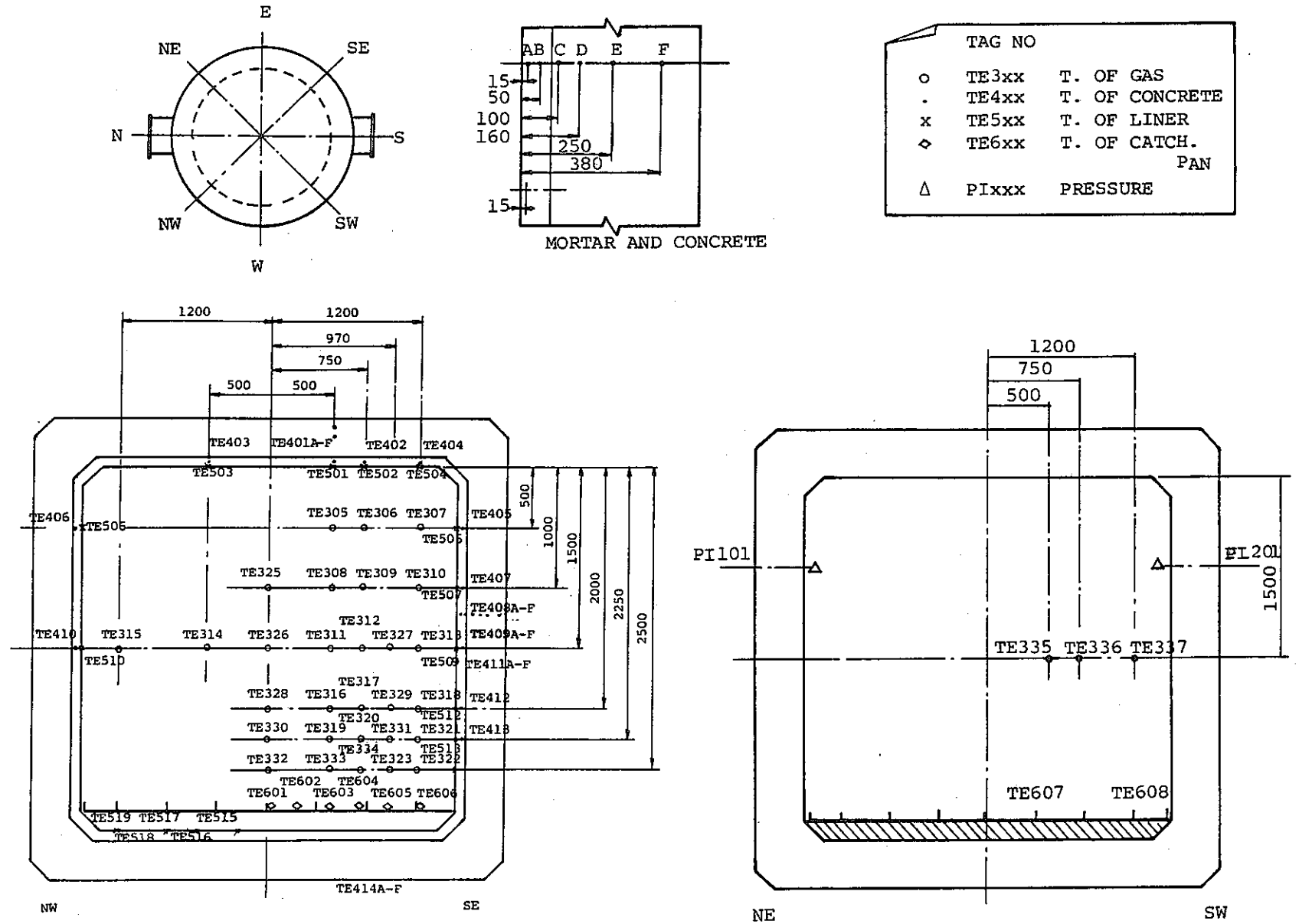

Fig.3.7 Position of Thermo Couple

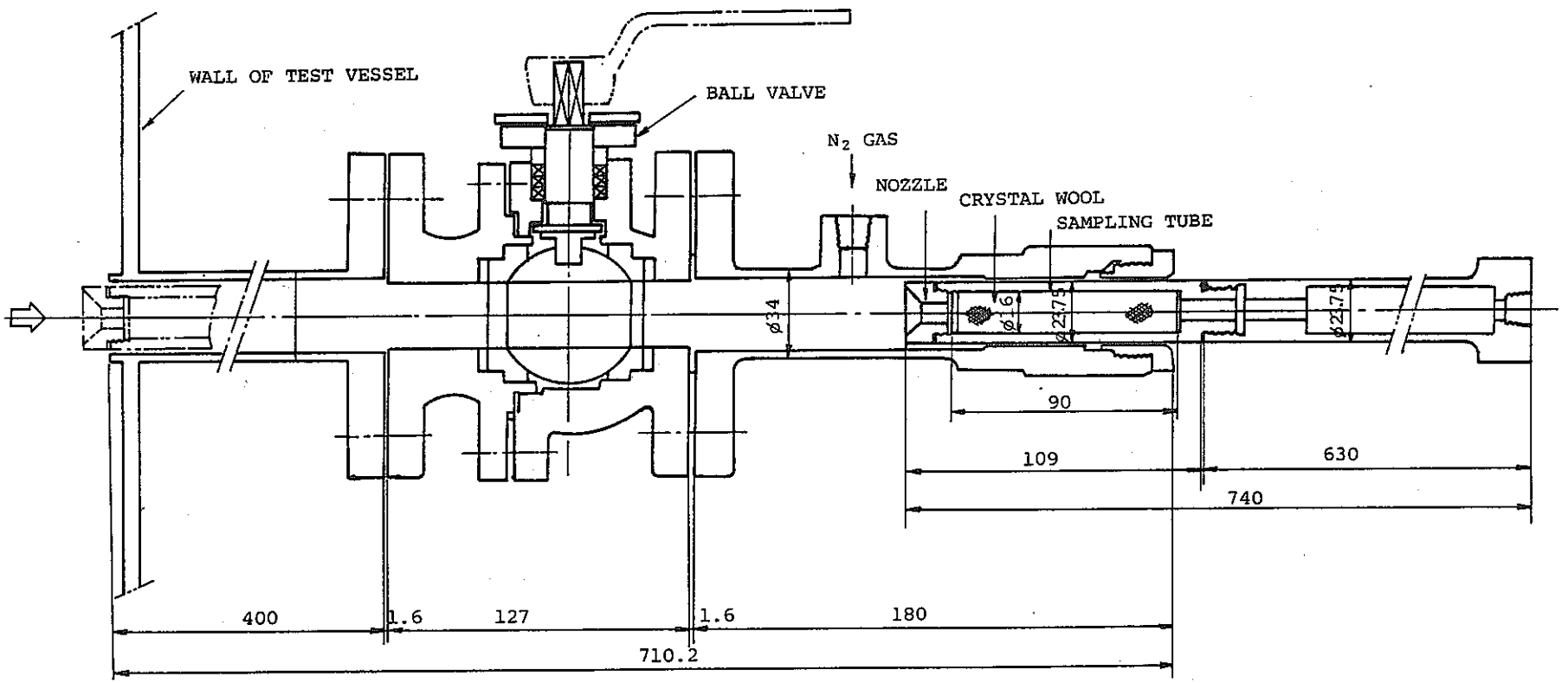

Fig.3.8 Sodium Aerosol Sampler

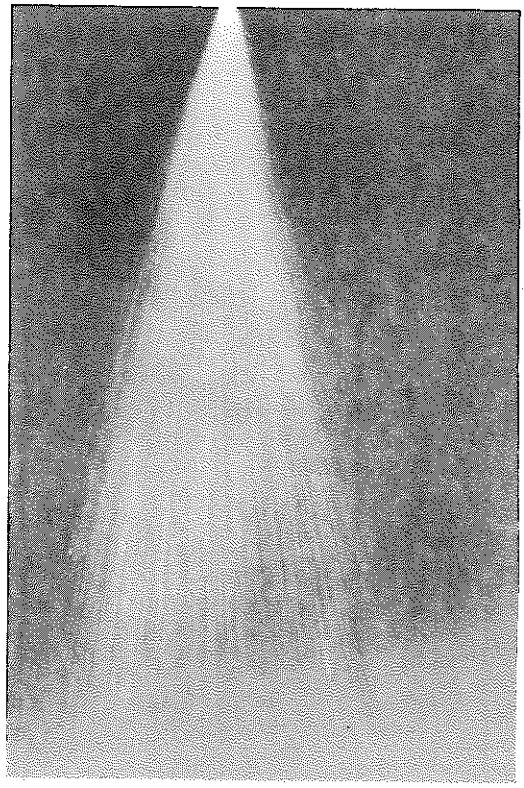

P = 0.5 kg/cm^2

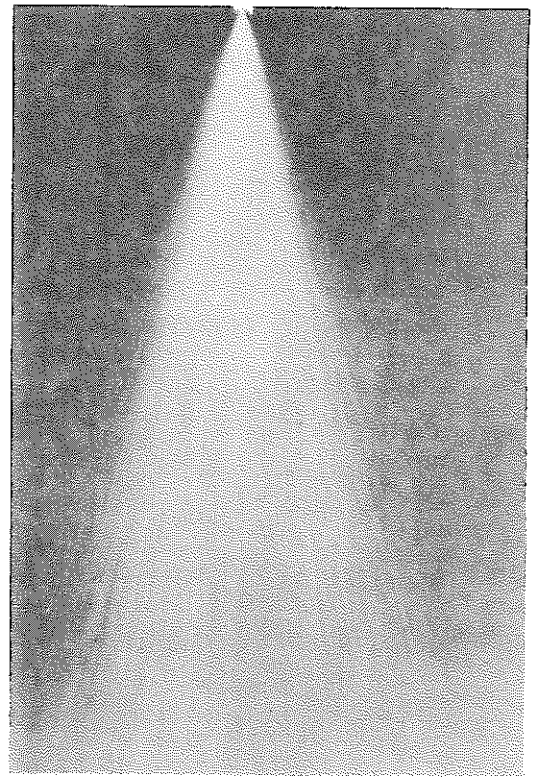

P = 1.0 kg/cm^2

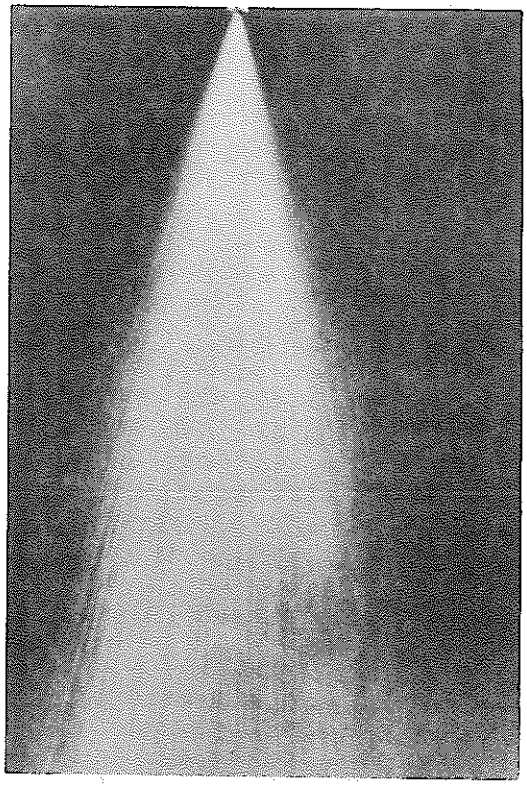

P = 1.5 kg/cm^2

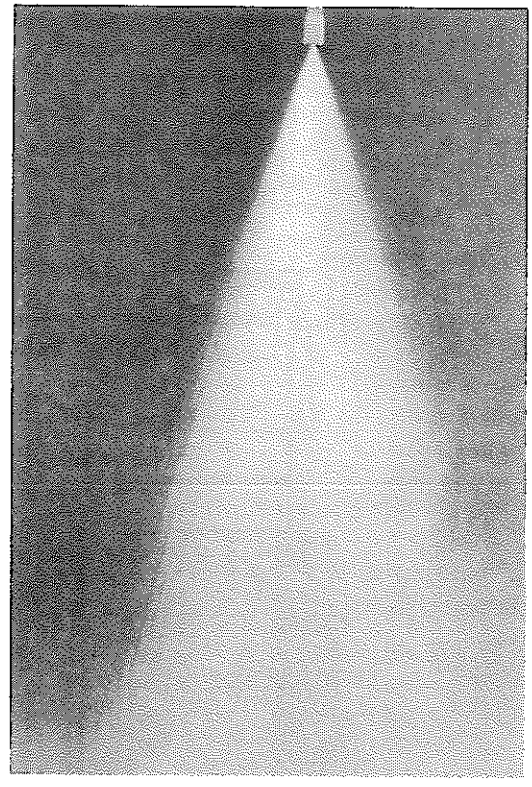

P = 2.0 kg/cm^2

Fig.4.1(1) Photagraph of Spray (B Nozzle)

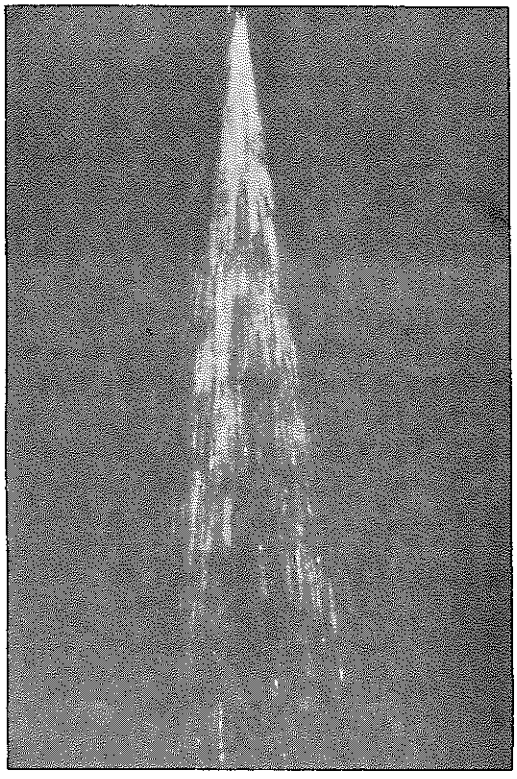

P = 0.2 kg/cm^2

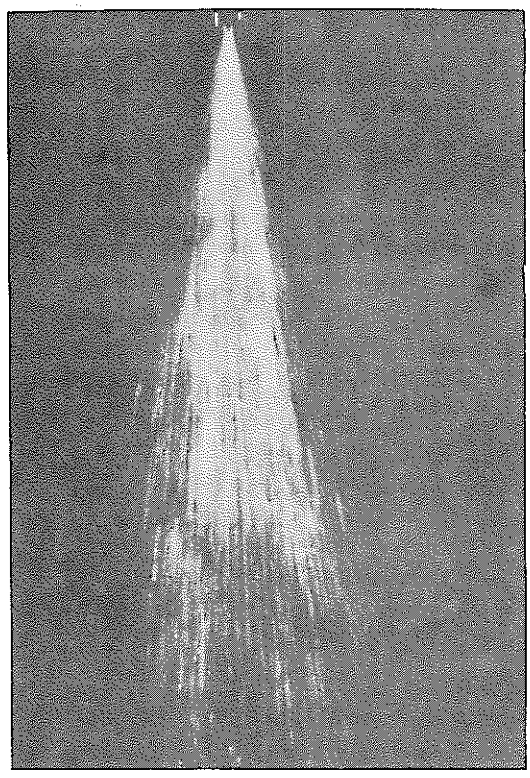

P = 0.3 kg/cm^2

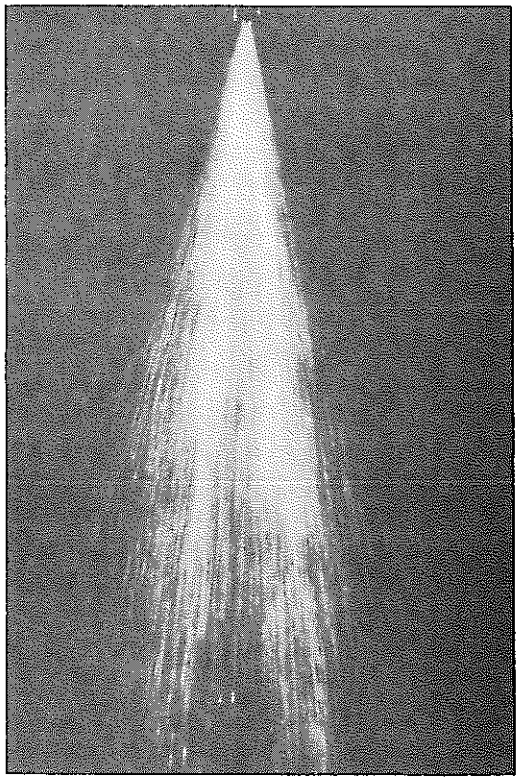

P = 0.4 kg/cm^2

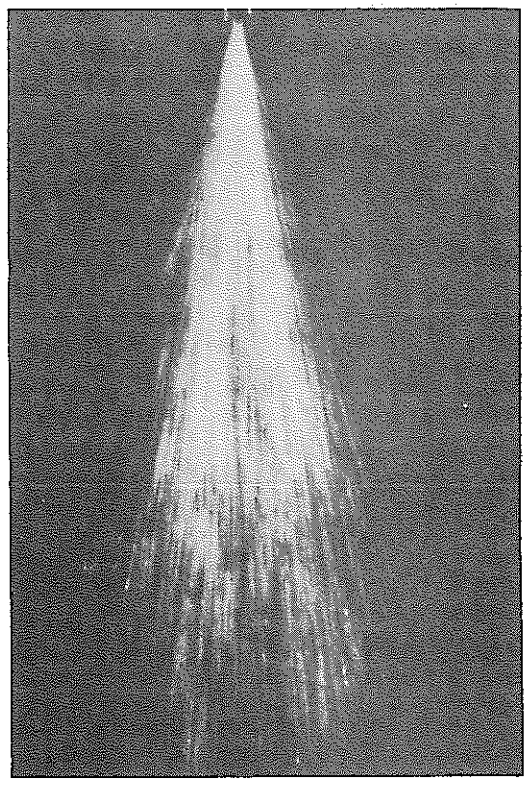

P = 0.5 kg/cm^2

Fig.4.1(2) Photograph of Spray (D Nozzle)

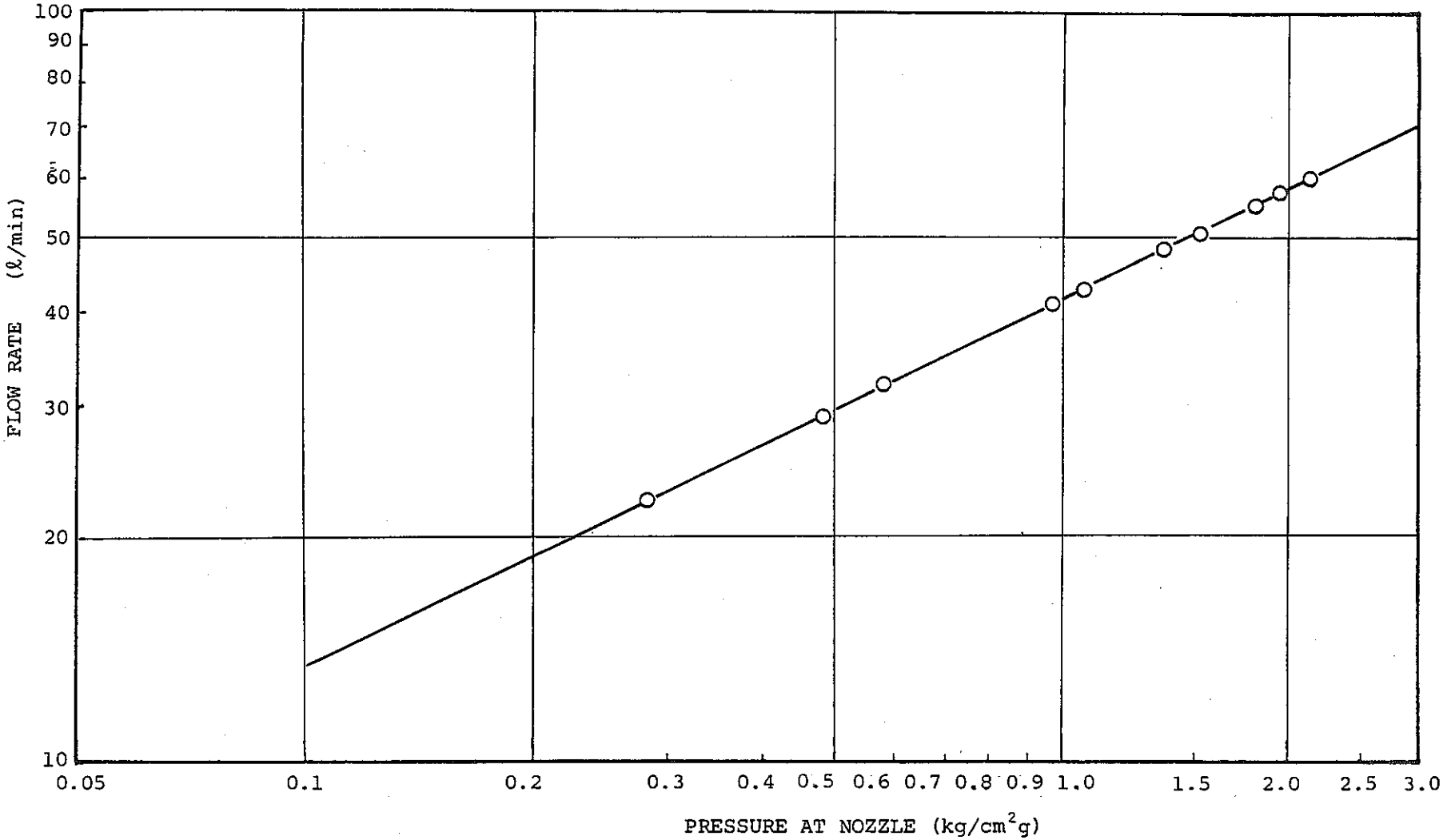

Fig.4.2(1) Flow Characteristics of Spray Nozzle (Nozzle B)

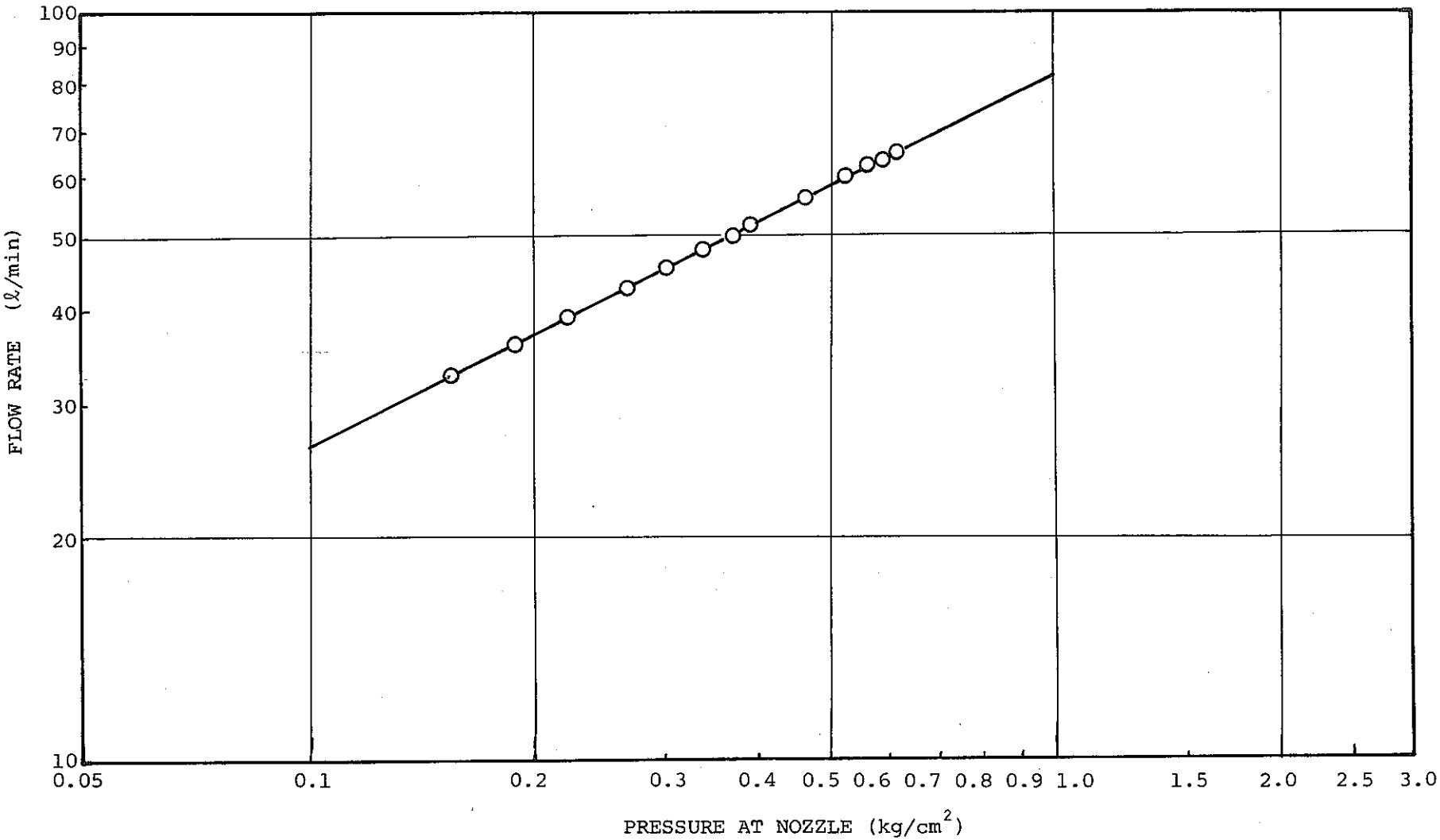

Fig.4.2(2) Flow Characteristics of Spray Nozzle (Nozzle D)

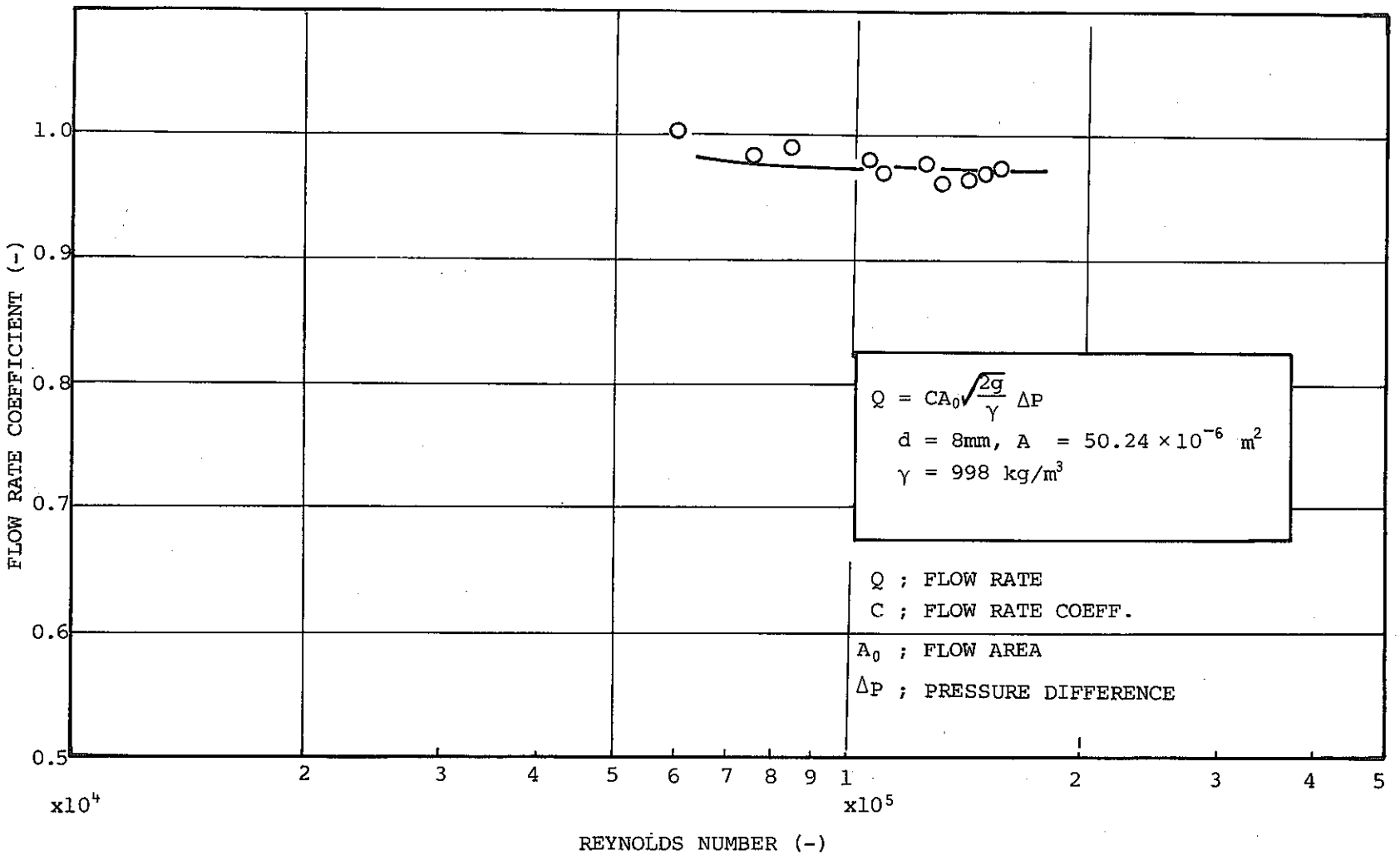

Fig.4.3 Flow Rate Coefficient Versus Reynolds Number (Nozzle B)

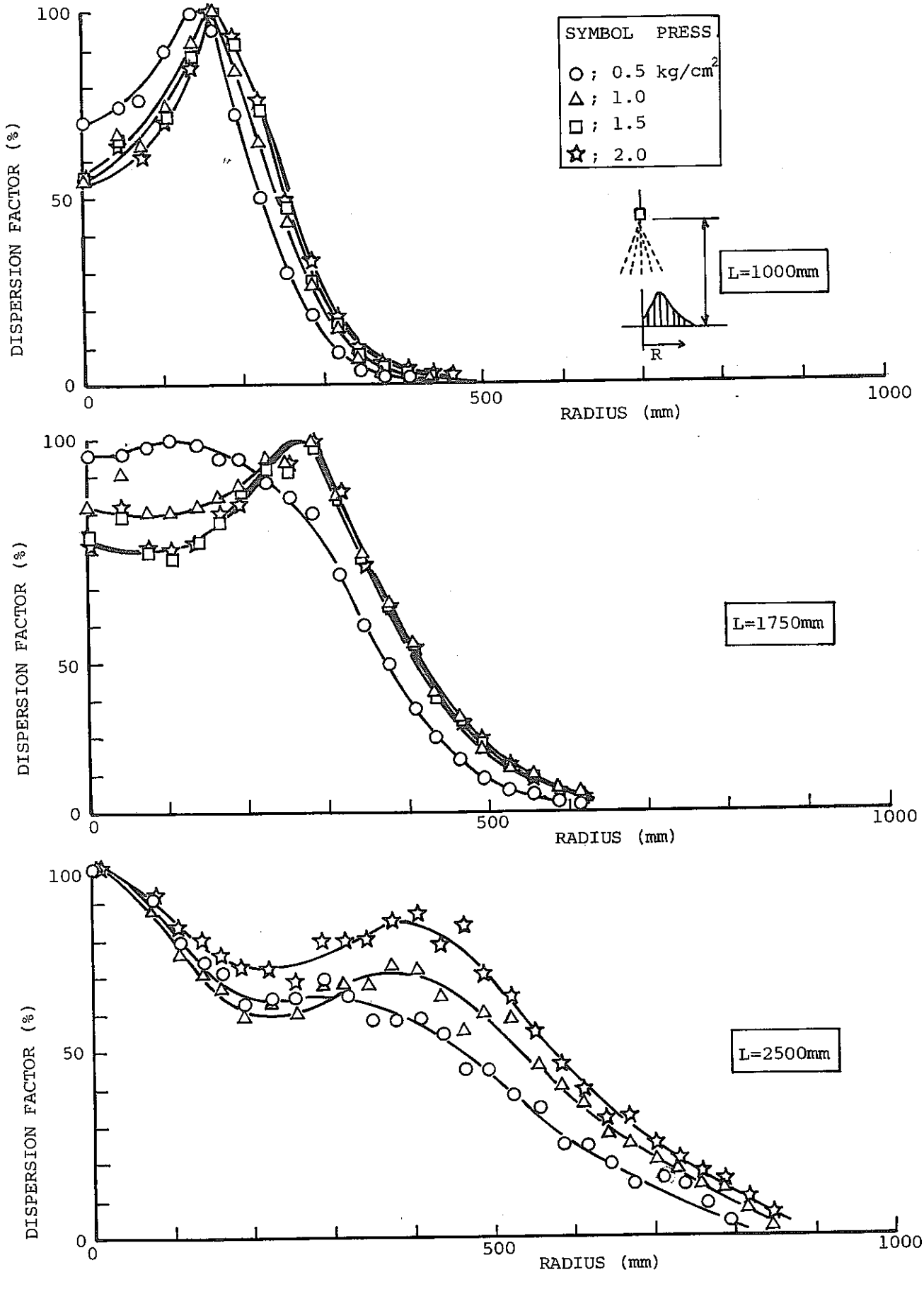

Fig.4.4(1) Dispersion Curve (Nozzle B)

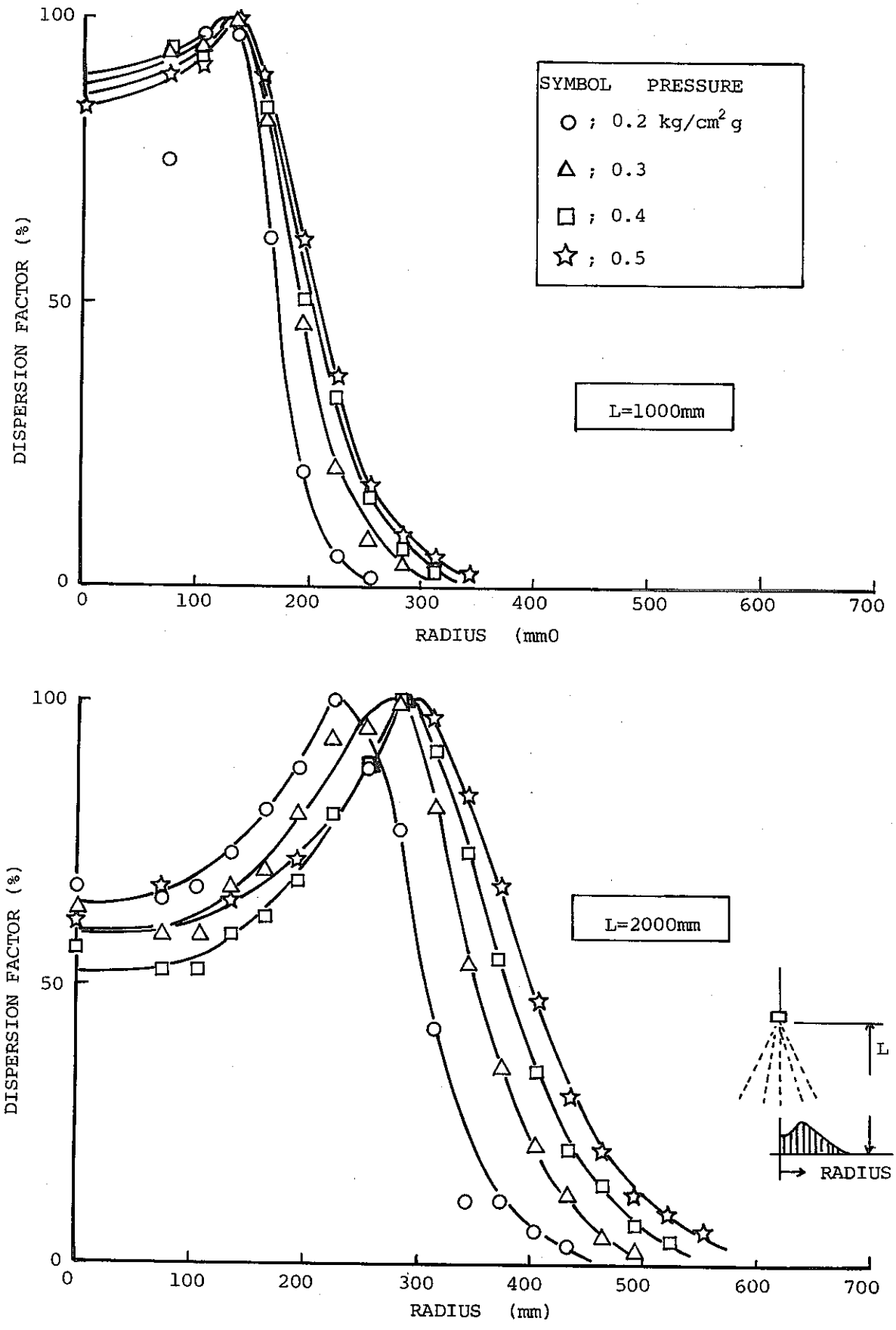

Fig.4.4(2) Dispersion Curve (Nozzle D)

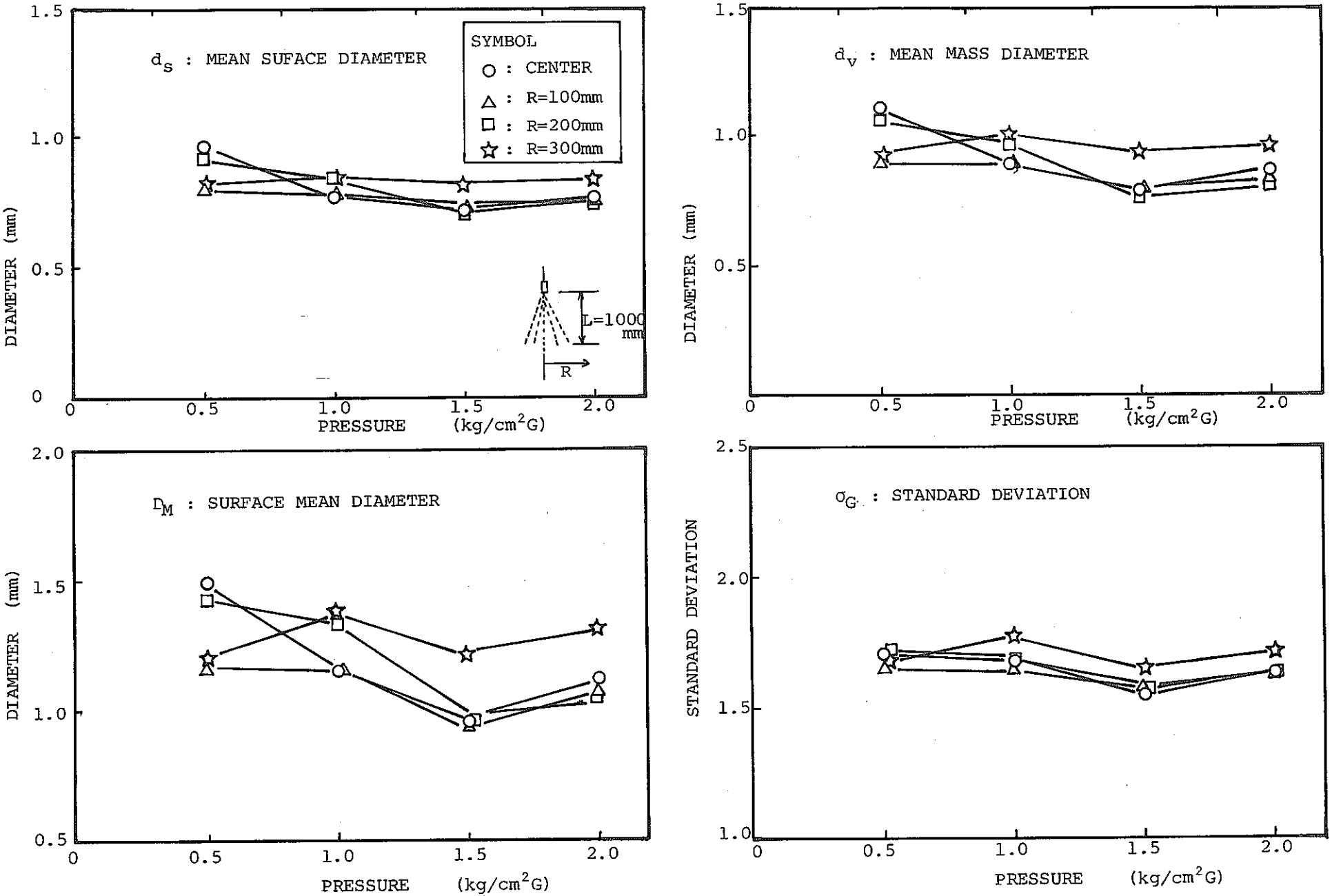

Fig.4.5(1) Mean Diameter and Standard Deviation (Nozzle B)

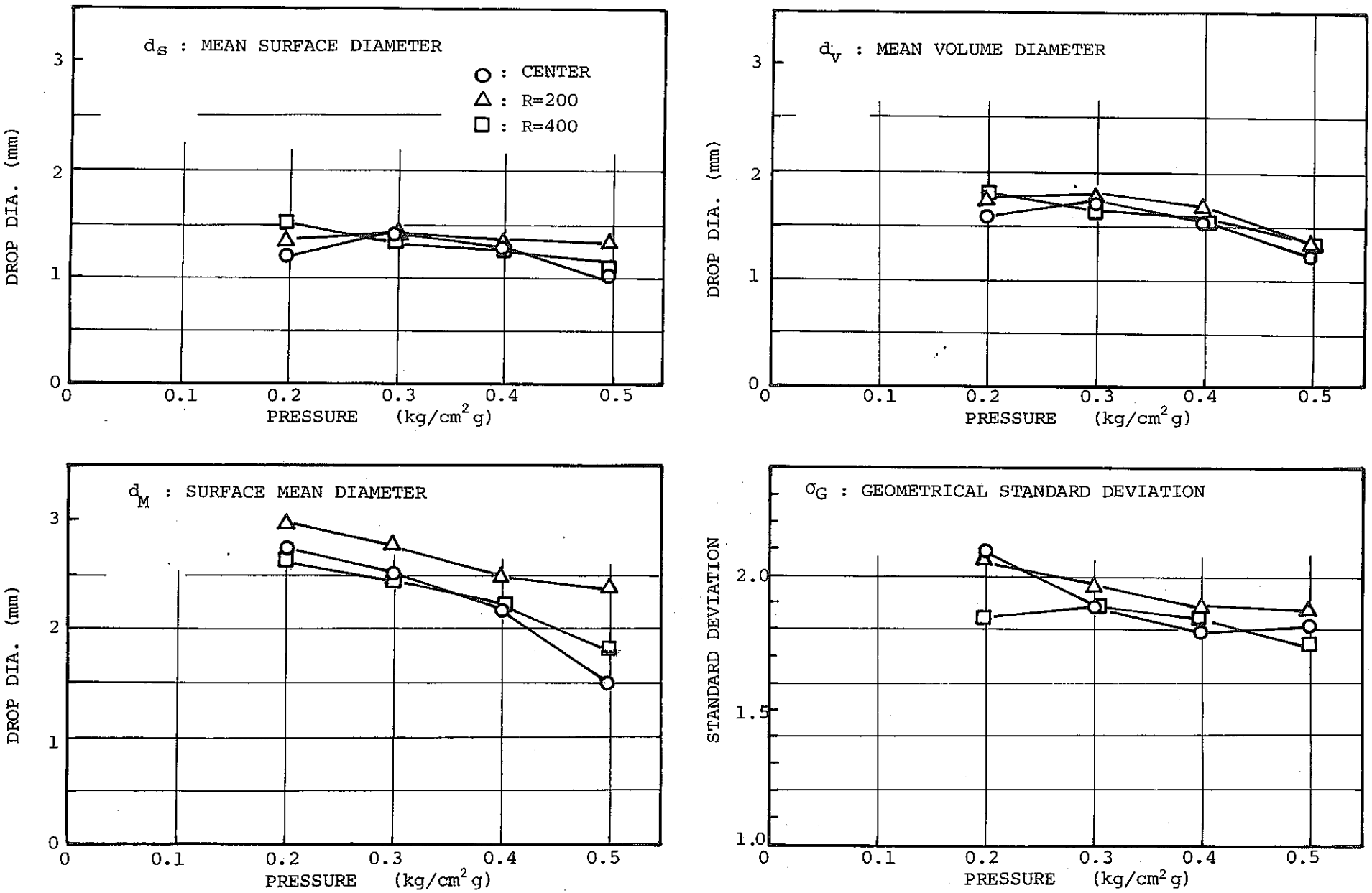

Fig.4.5(2) Mean diameter and Standard Deviation (nozzle D)

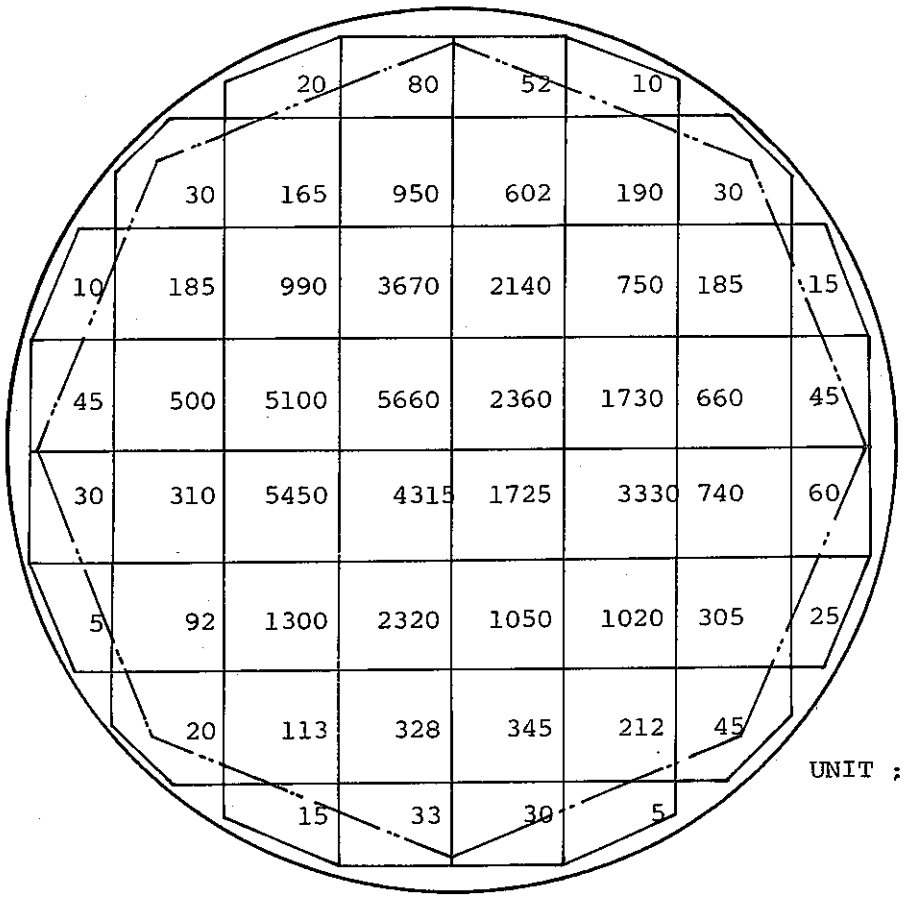

NOZZLE ; D
PRESSURE ; 0.4 kg/cm^{2}g
FLOW RATE ; 52 ℓ/min
DURATION : 1 min

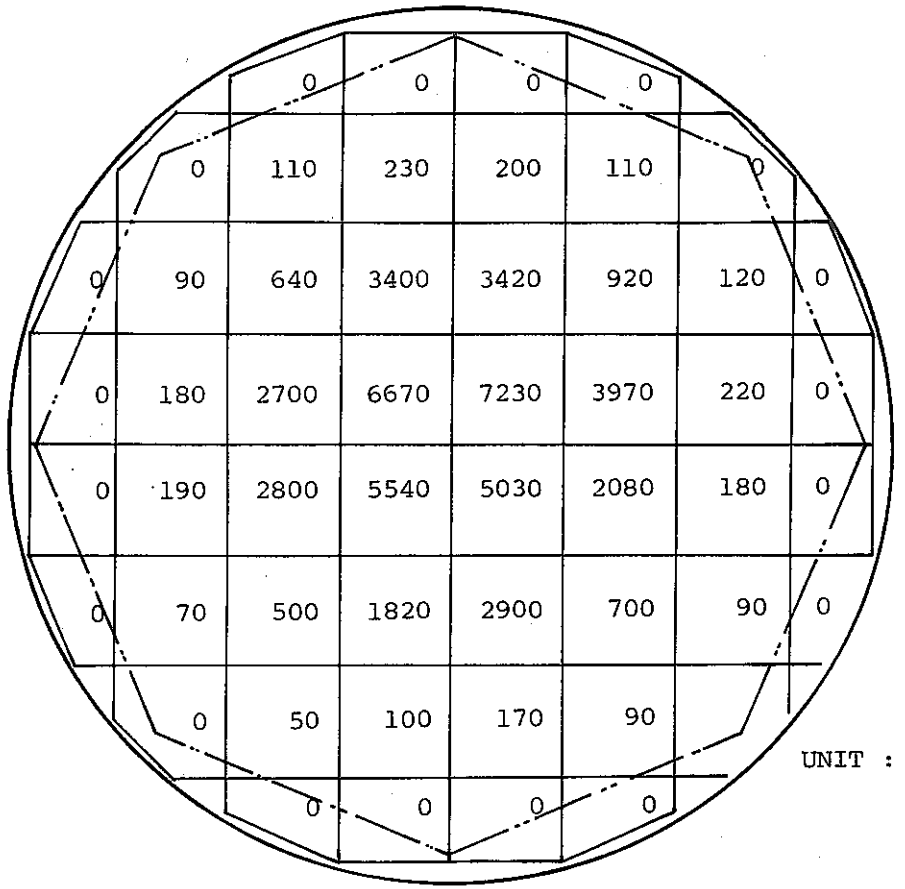

NOZZLE ; B
PRESSURE ; 1.6 kg/cm^{2}g
FLOW RATE ; 52 ℓ/min
DURATION ; 1 min

Fig.4.6 Water Dispersion in The Catching Pan

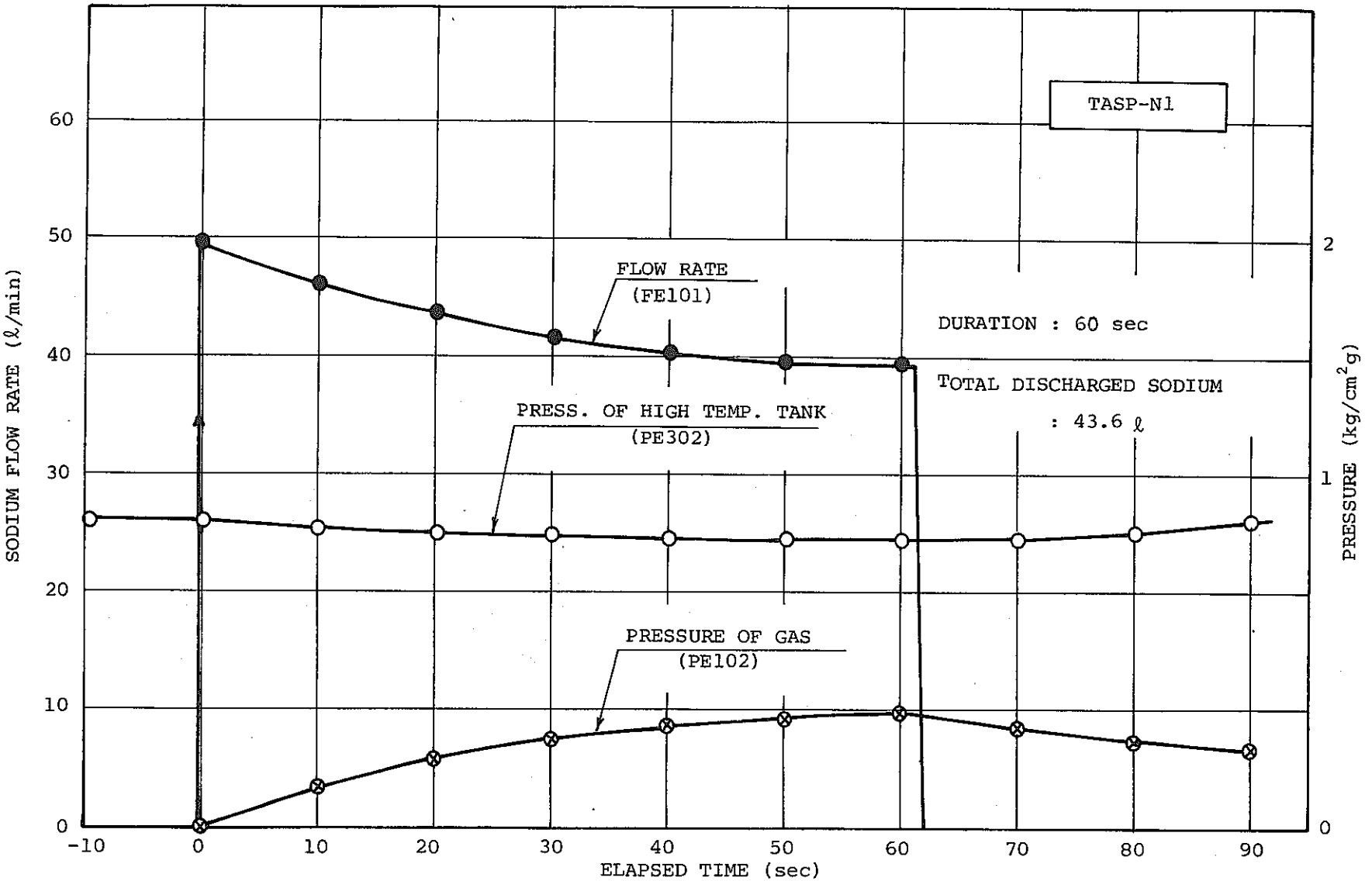

Fig.5.1(1) TASP-N1 Data ; Sodium Discharge Flow Rate

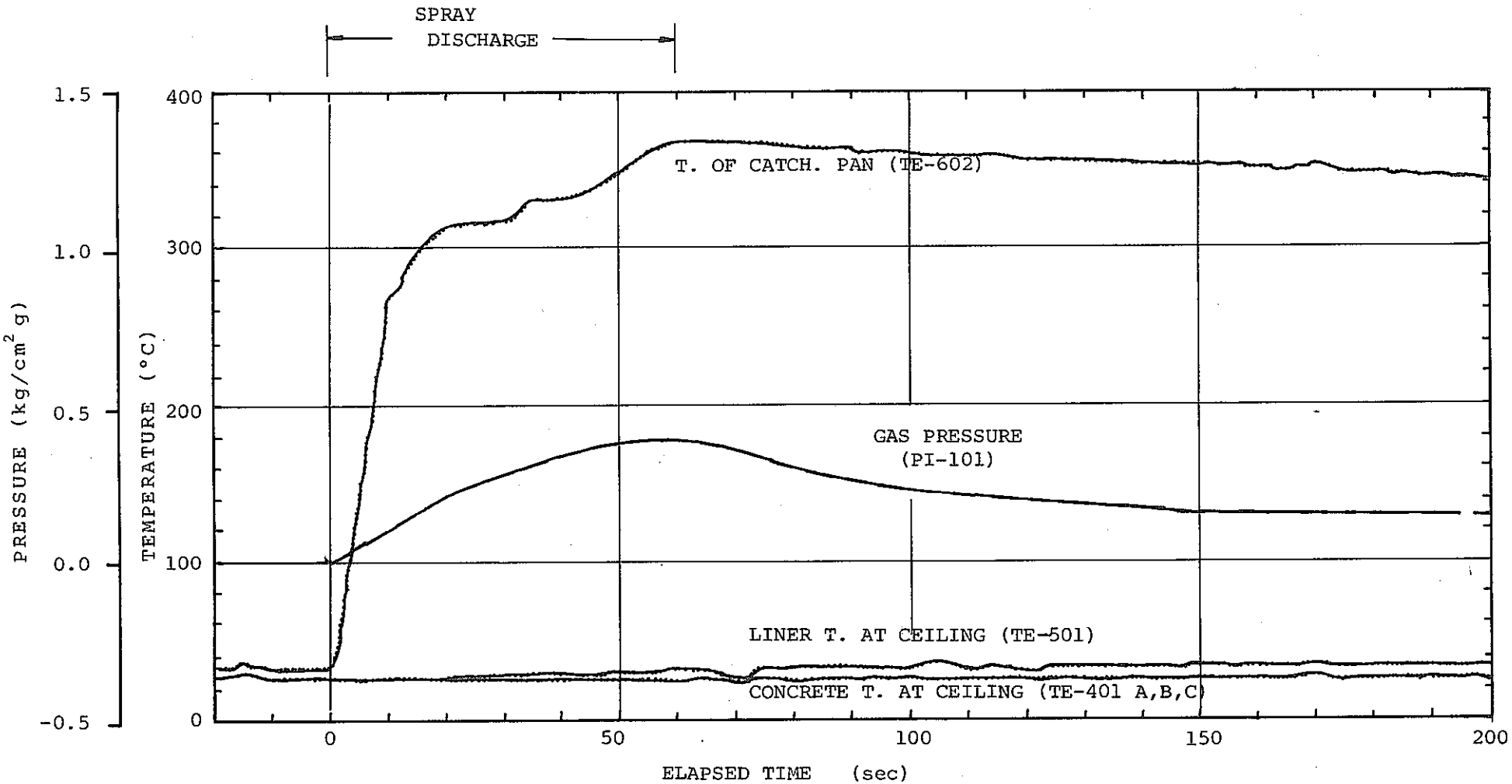

Fwg.5.1(2) TASP-N1 Data ; Pressure and Temperature Response

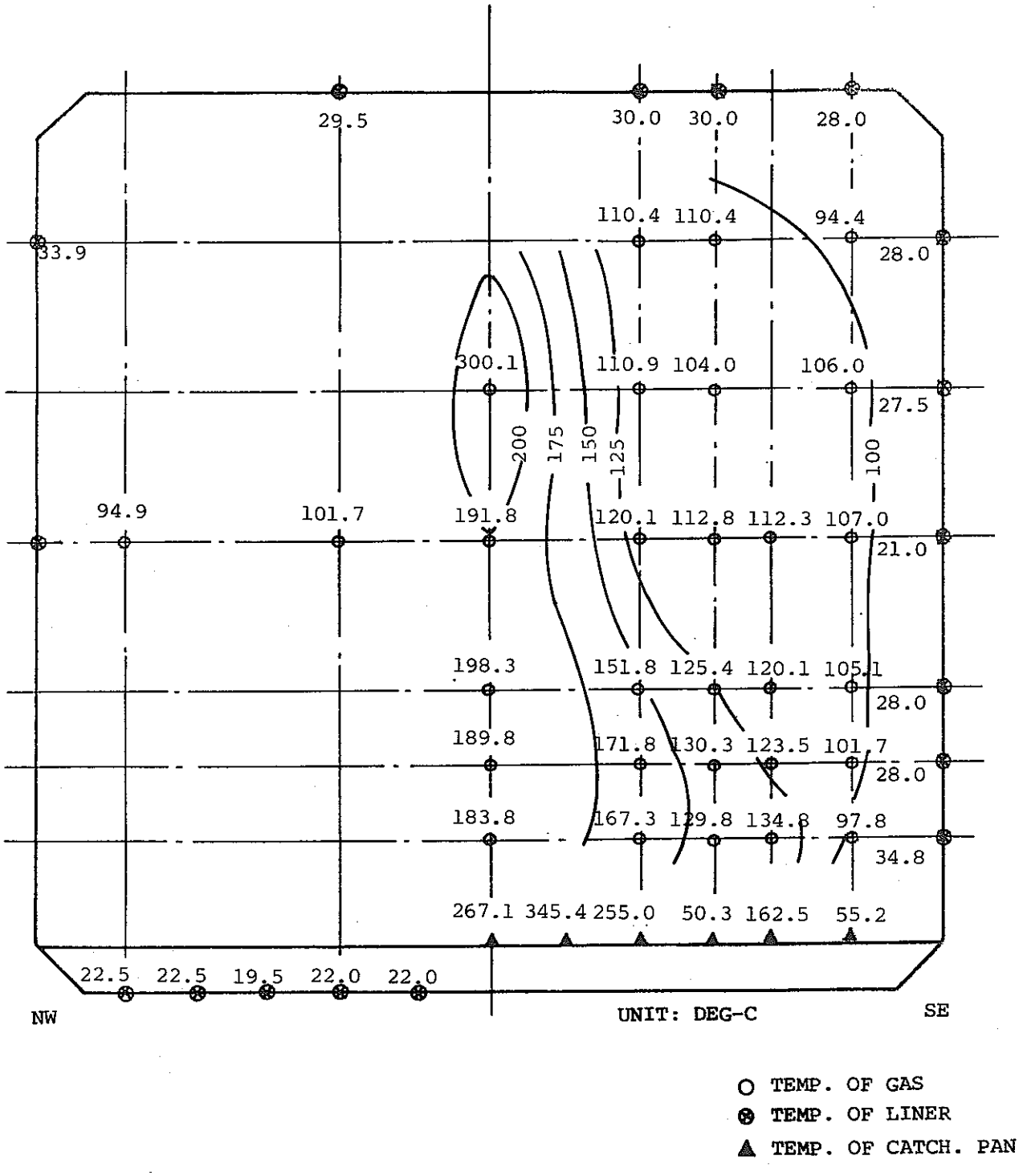

Fig.5.1(3) TASP-N1 Data ; Temperature Distribution

(Elapsed Time = 50 sec)

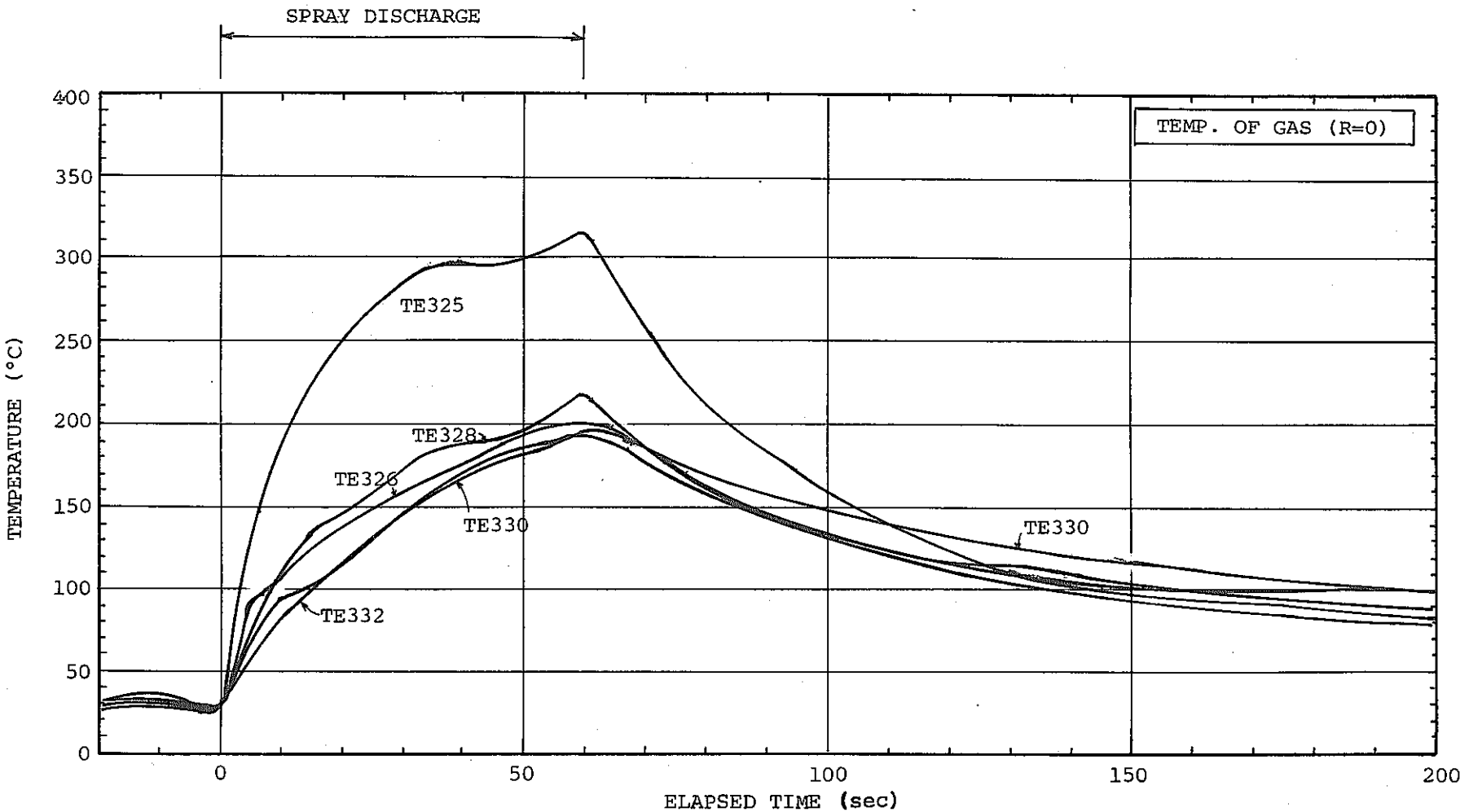

Fig.5.1(4) TASP-N1 Data ; Gas Temperature

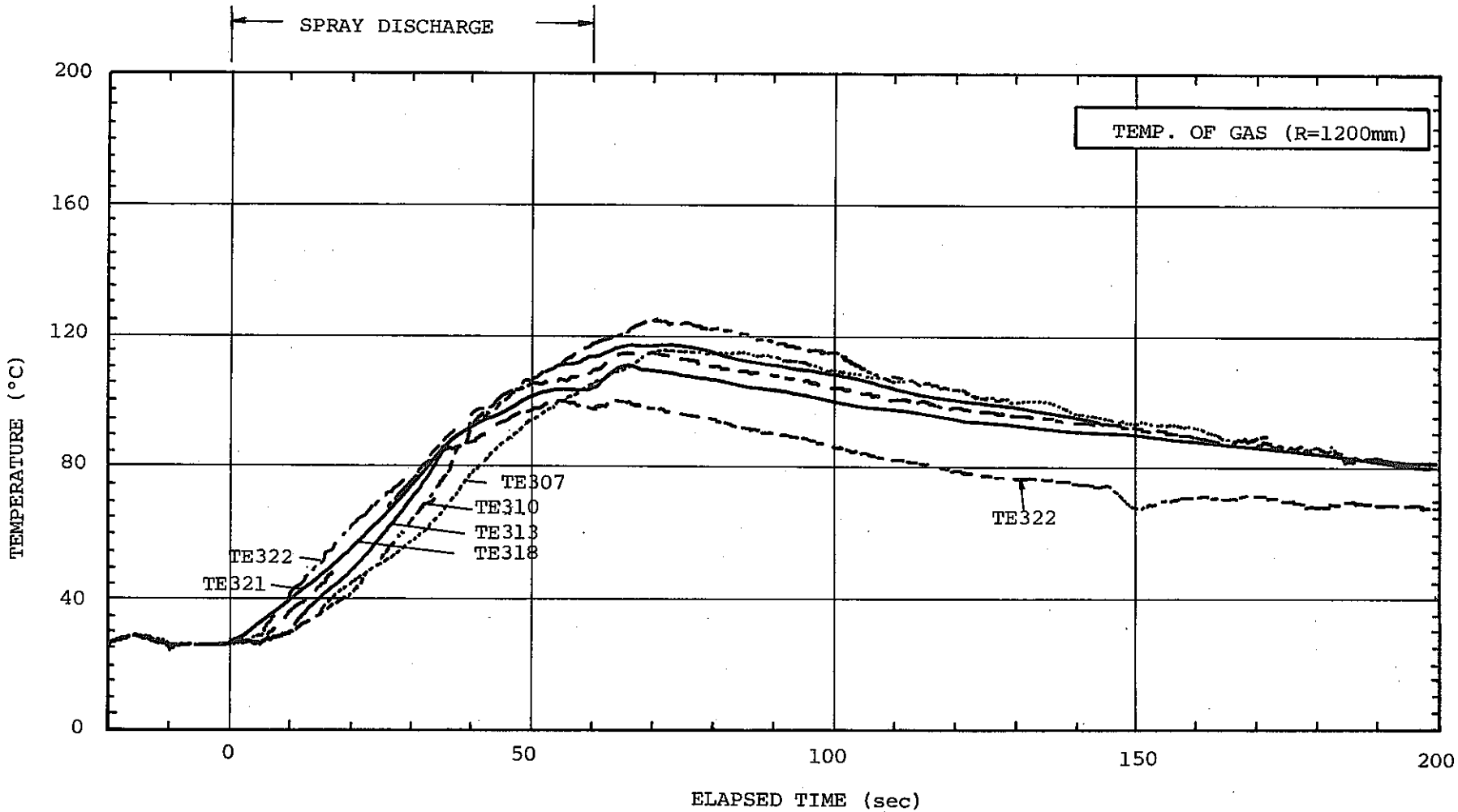

Fig.5.1(5) TASP-N1 Data ; Gas temperature

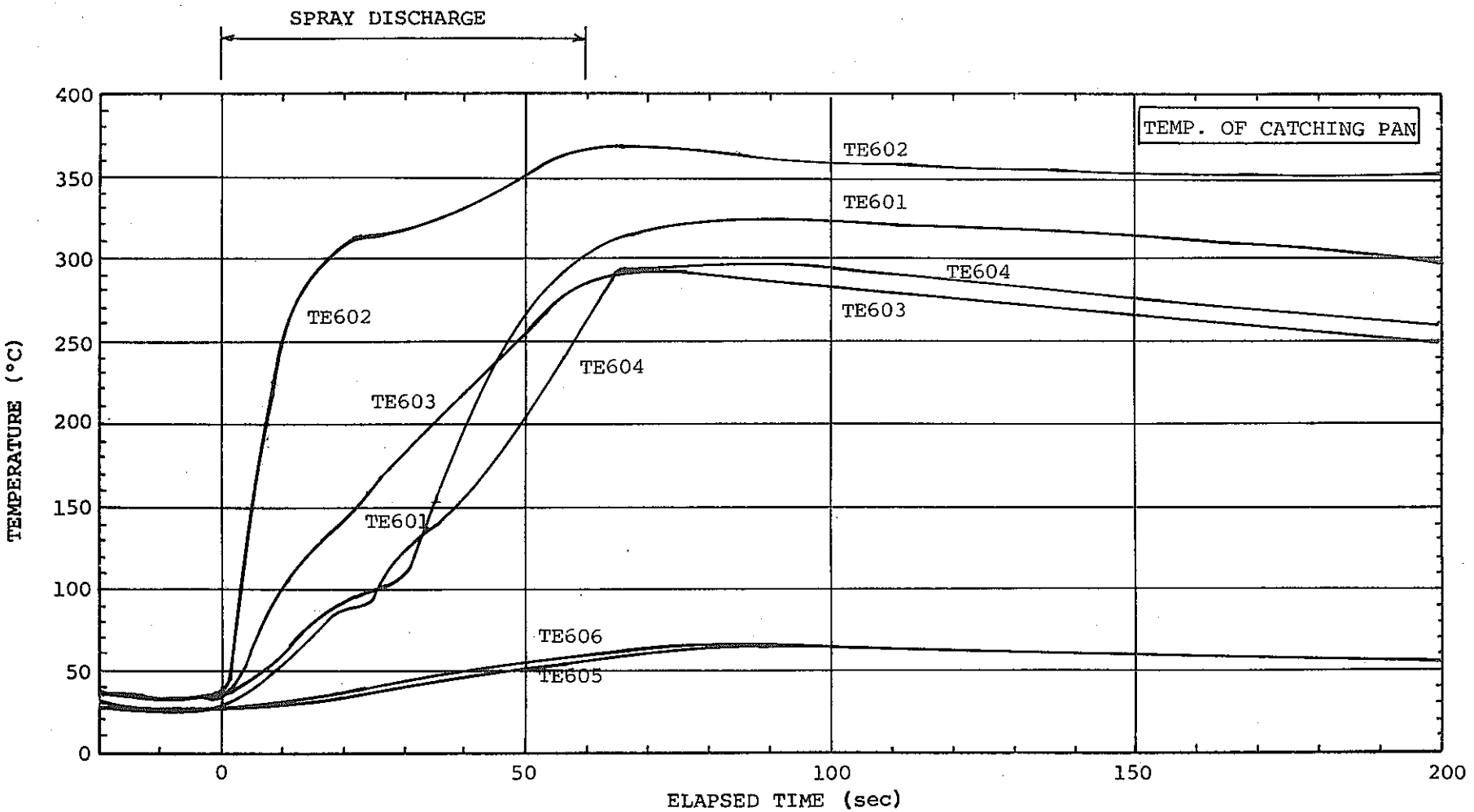

Fig.5.1(6) TASP-N1 Data ; Temperature of Catching Pan

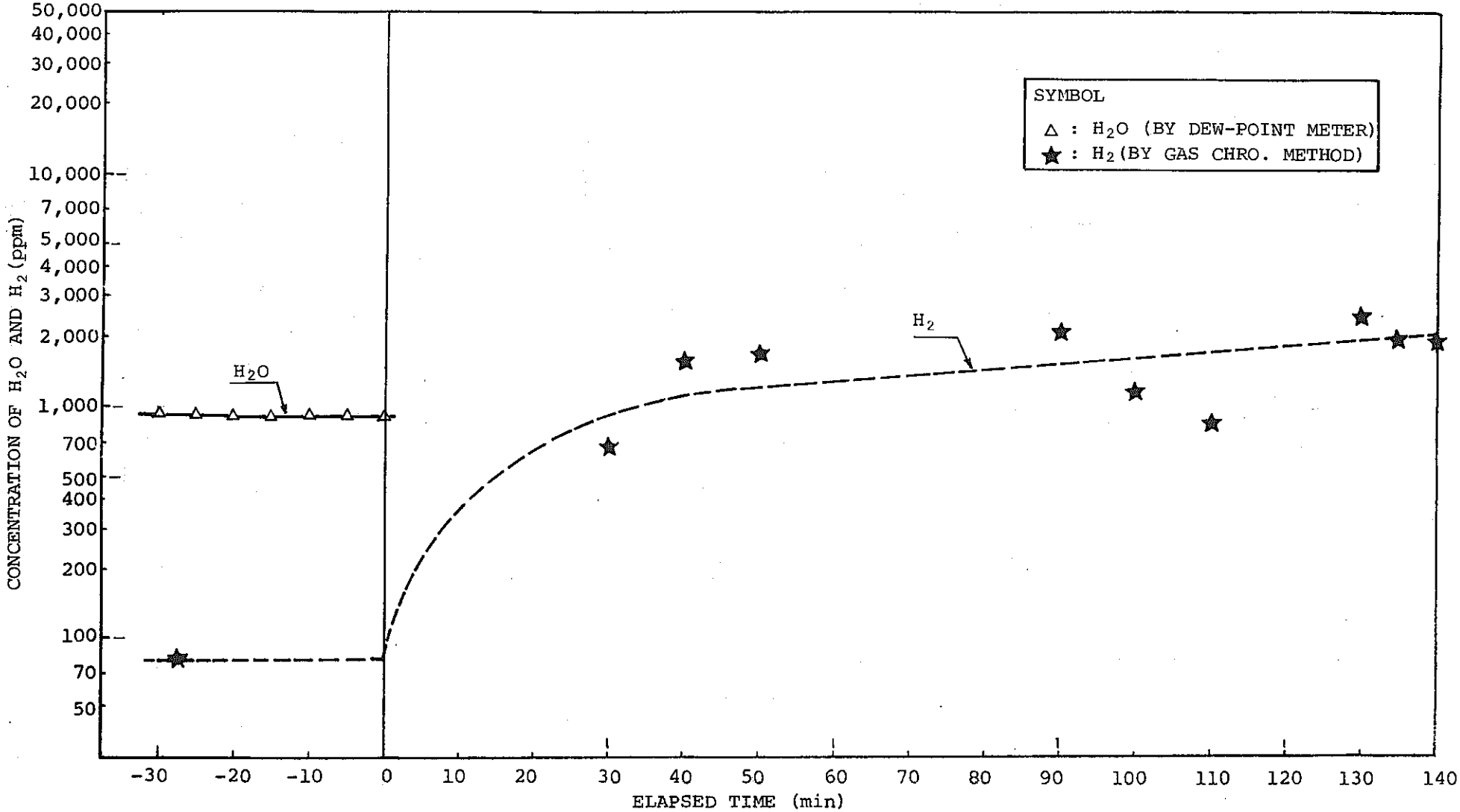

Fig.5.1(7) TASP-N1 Data ; Gas concentration

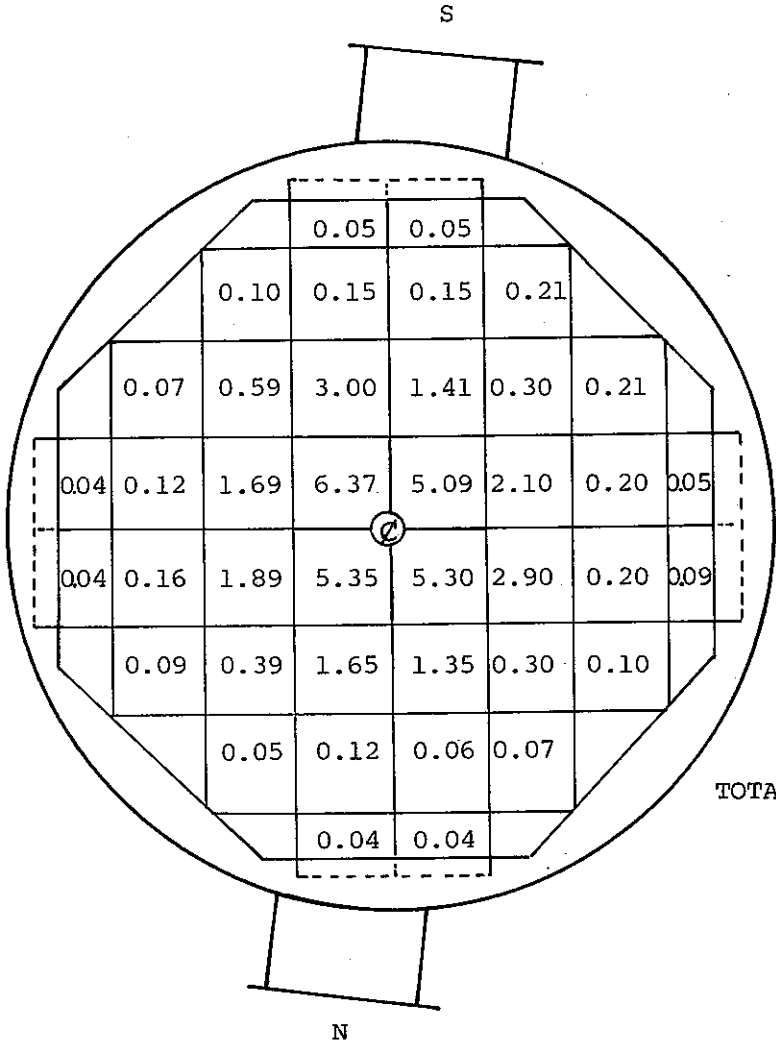

TOTAL WEIGHT : 42.05 kg

Fig.5.1(8) TASP-N1 Data ; Weight of Contents in Catching Pan After Test

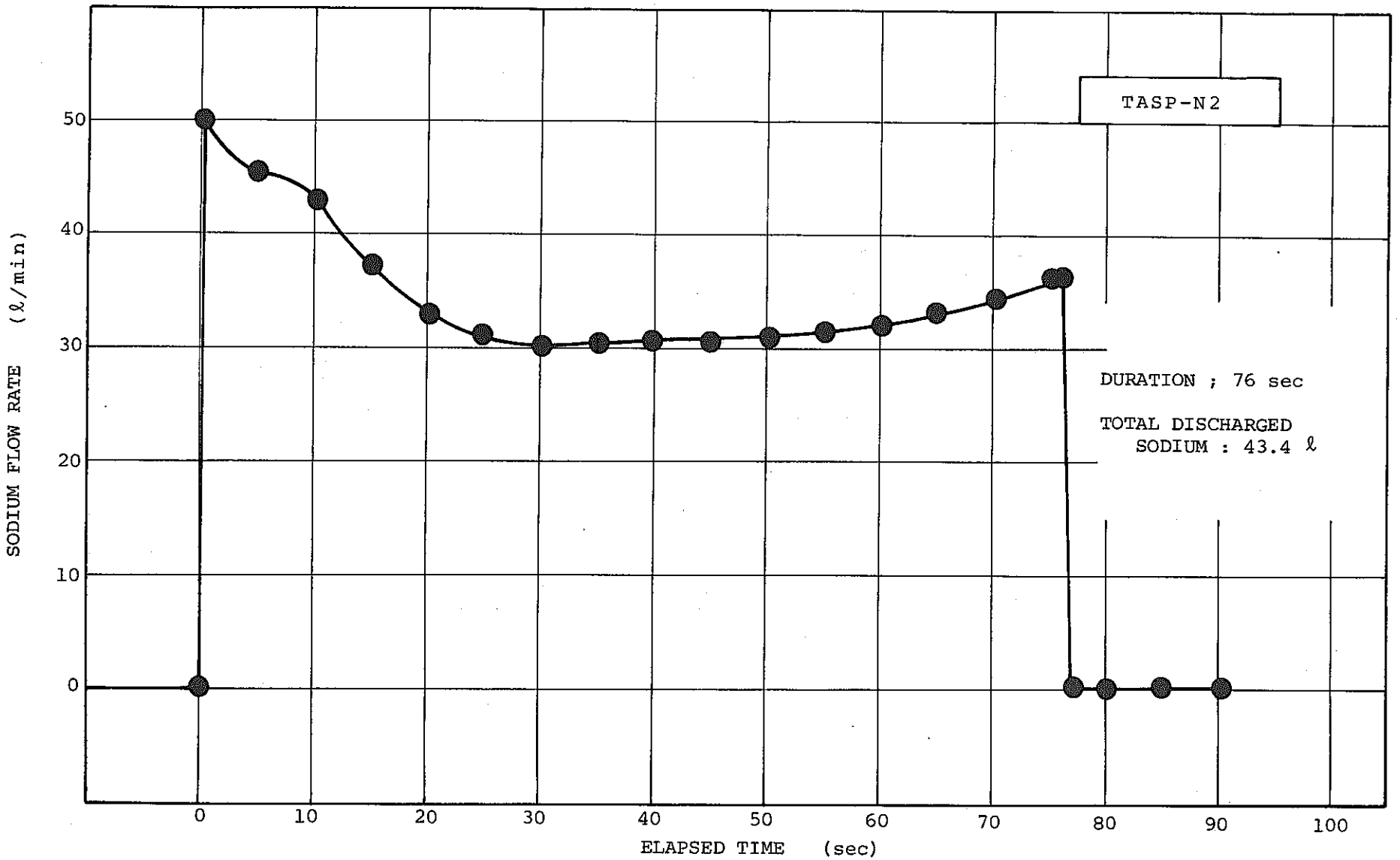

Fig.5.2(1) TASP-N2 Data ; Sodium Discharge Flow Rate

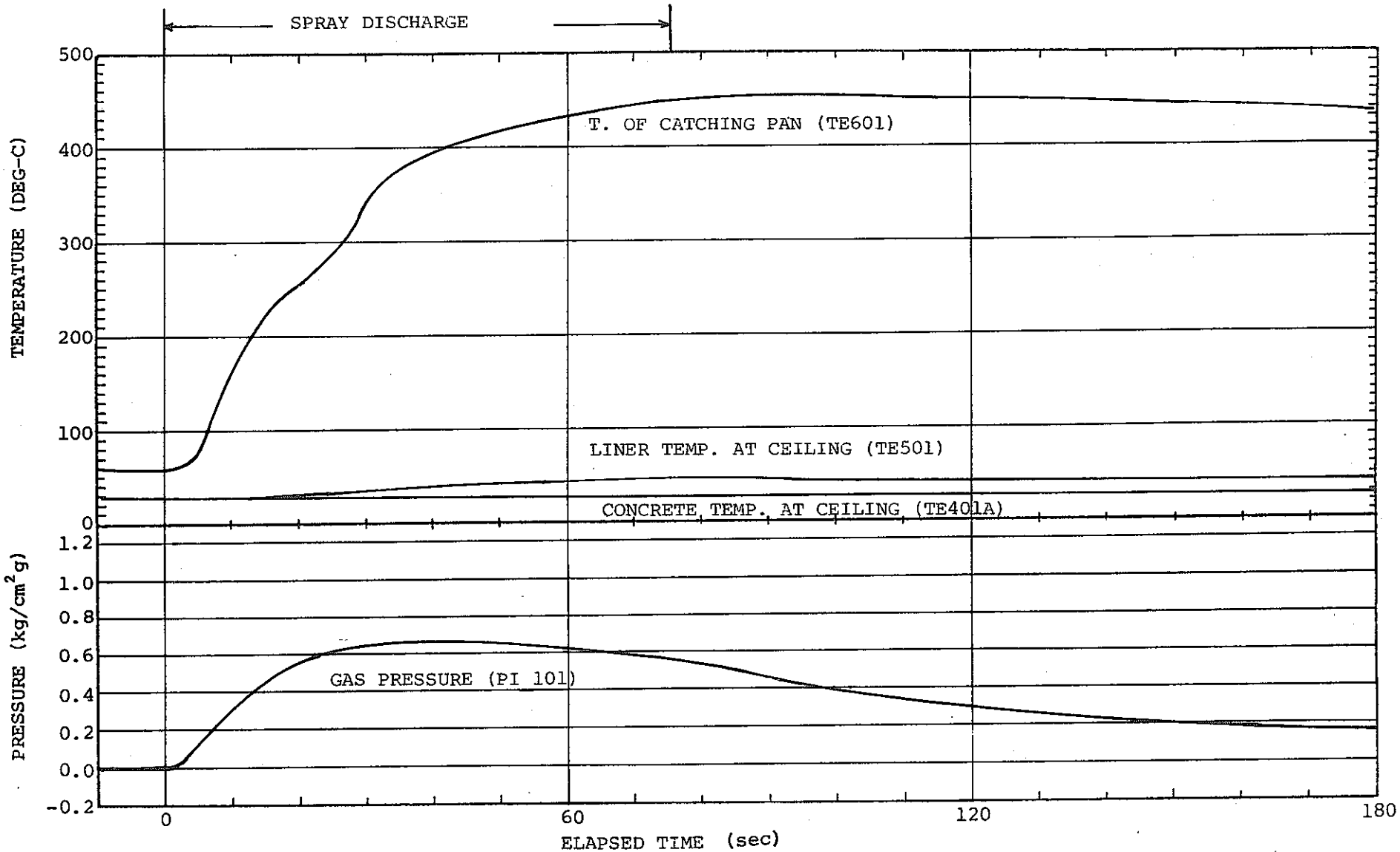

Fig.5.2(2) TASP-N2 Data ; Pressure and Temperature Response

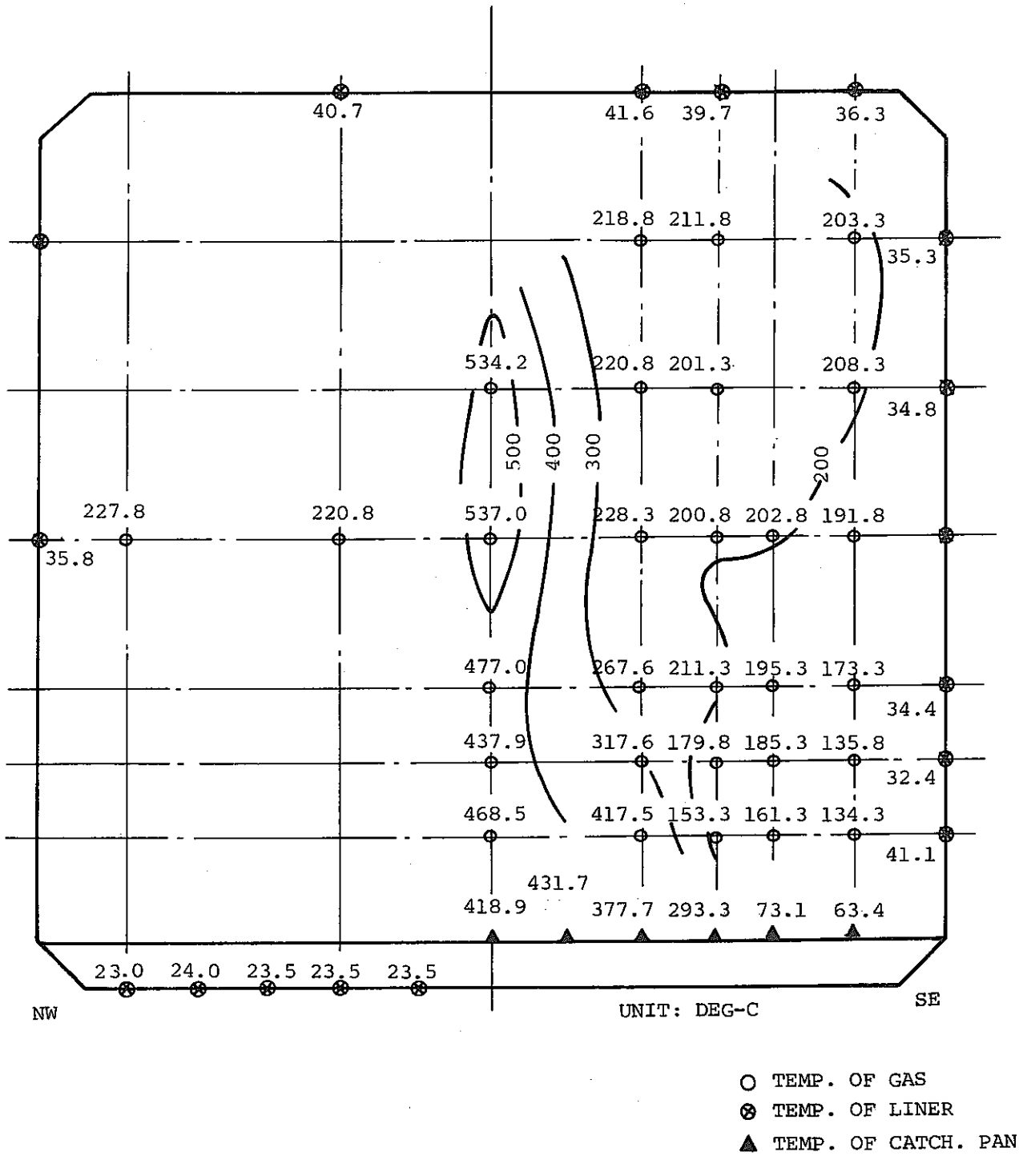

Fig.5.2(3) TASP-N2 Data ; Temperature Distribution

(Elapsed Time = 50 sec)

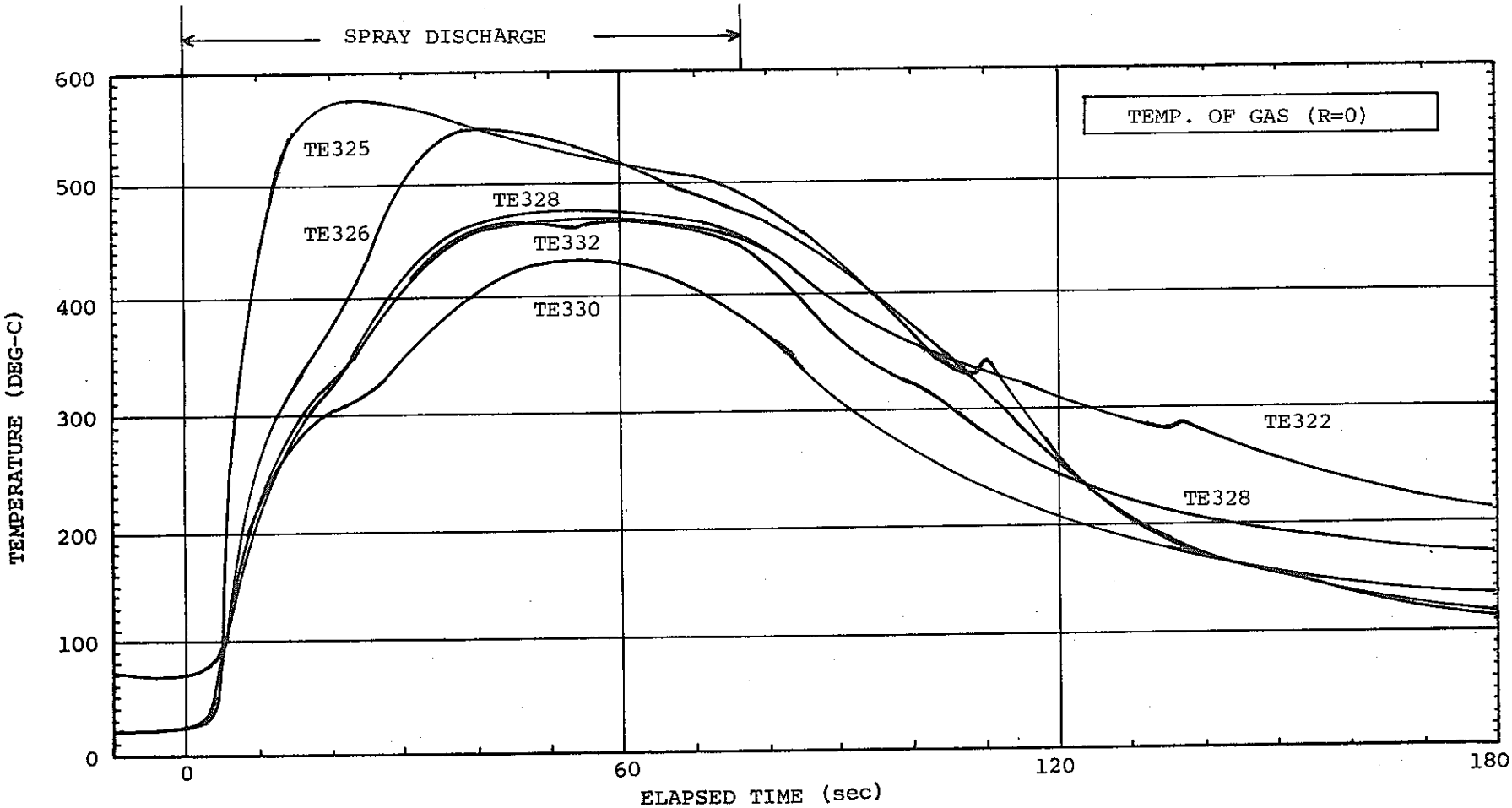

Fig.5.2(4) TASP-N2 Data ; Gas Temperature

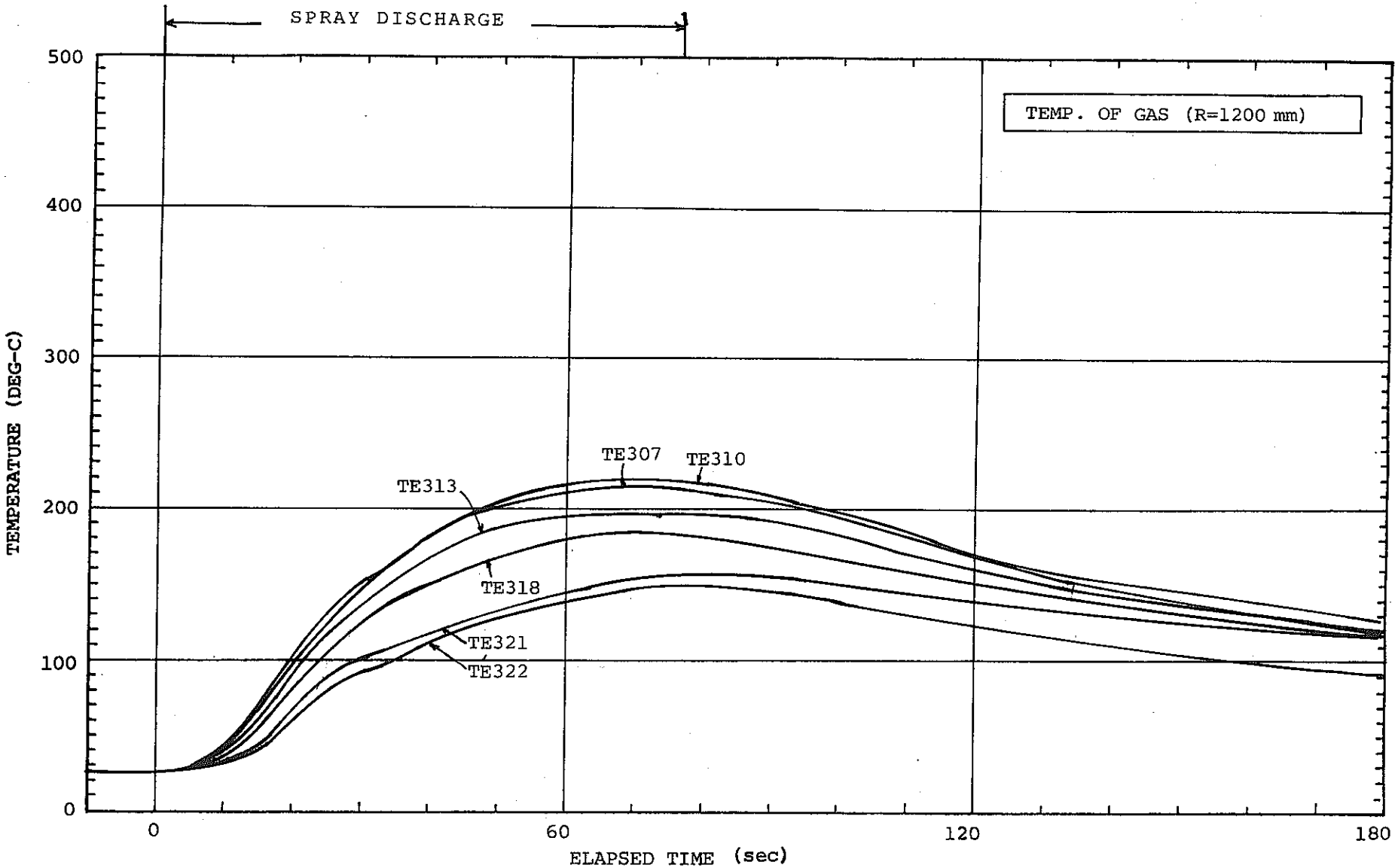

Fig.5.2(5) TASP-N2 Data ; Gas Temperature

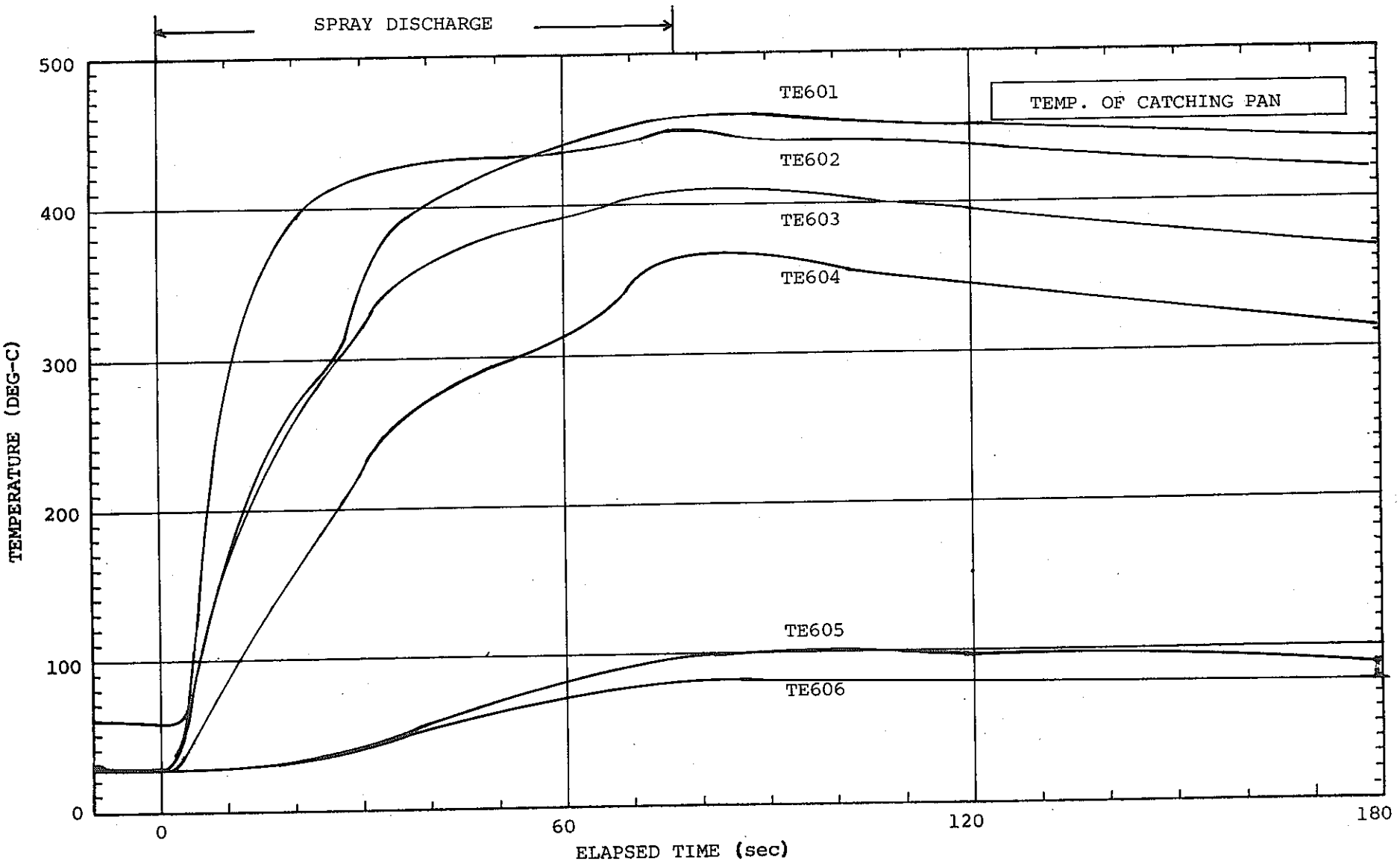

Fig.5.2(6) TASP-N2 Data ; Temperature of Catching Pan

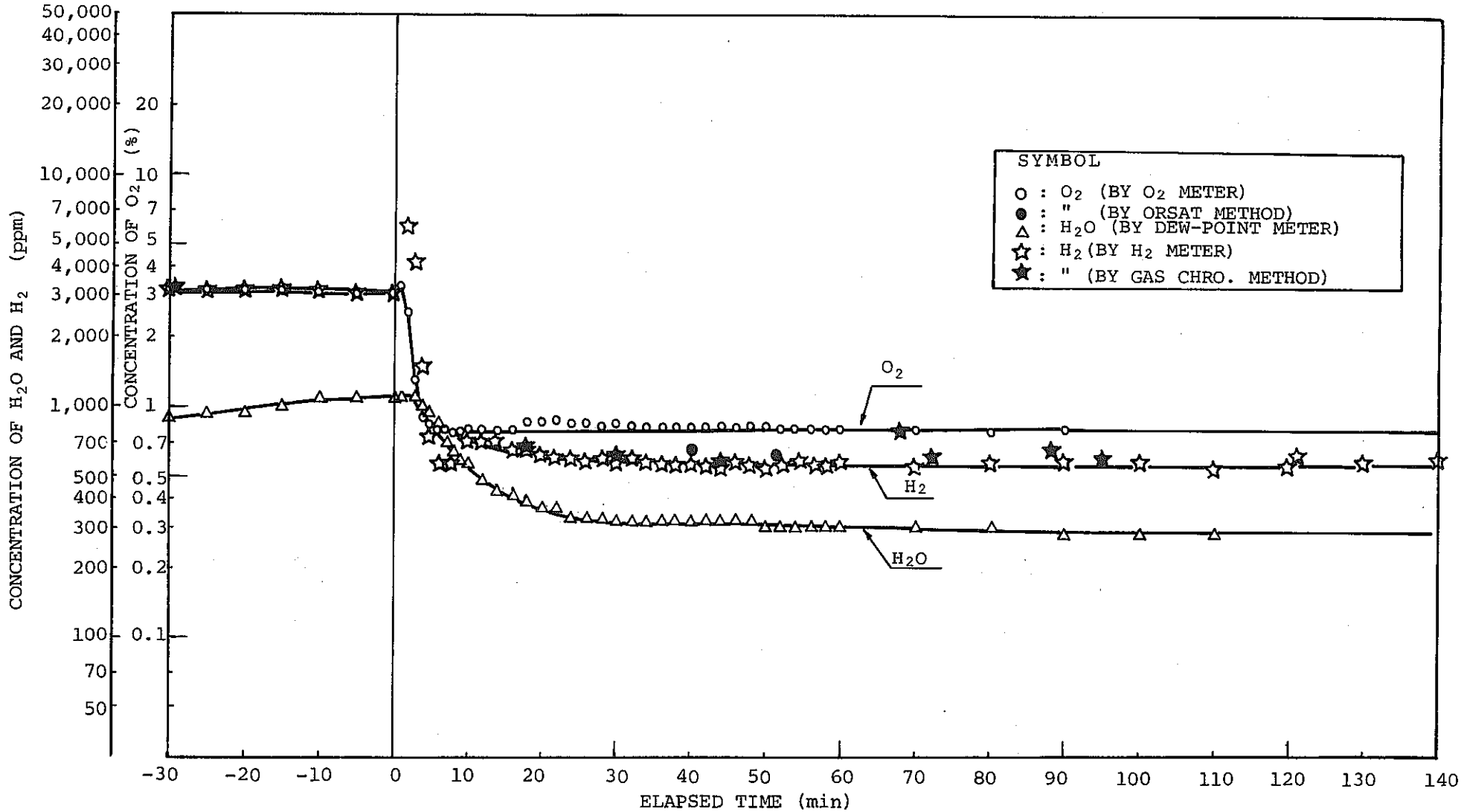

Fig.5.2(7) TASP-N2 Data ; Gas Concentration

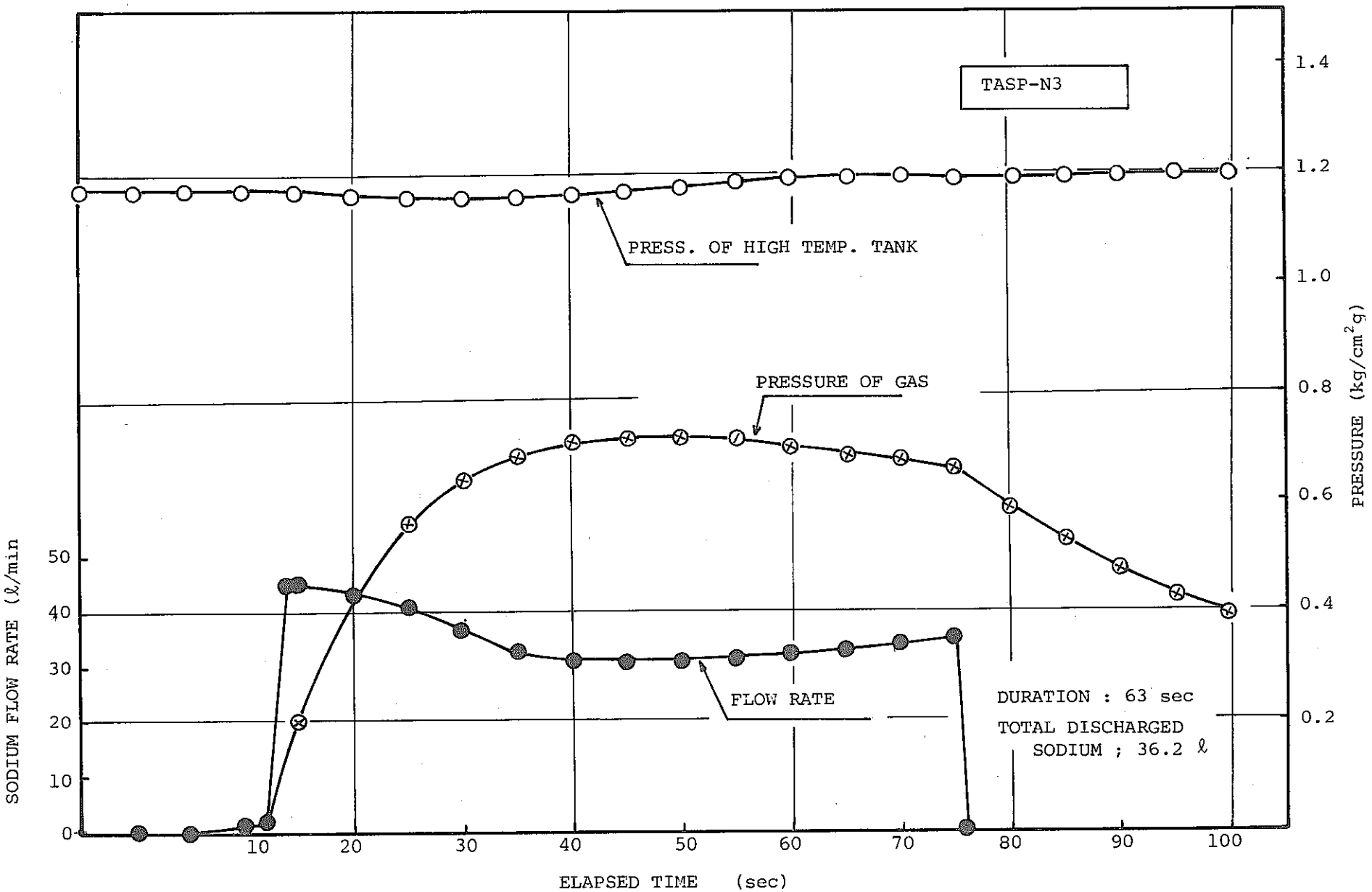

Fig.5.3(1) TASP-N3 Data ; Sodium Discharge Flow Rate

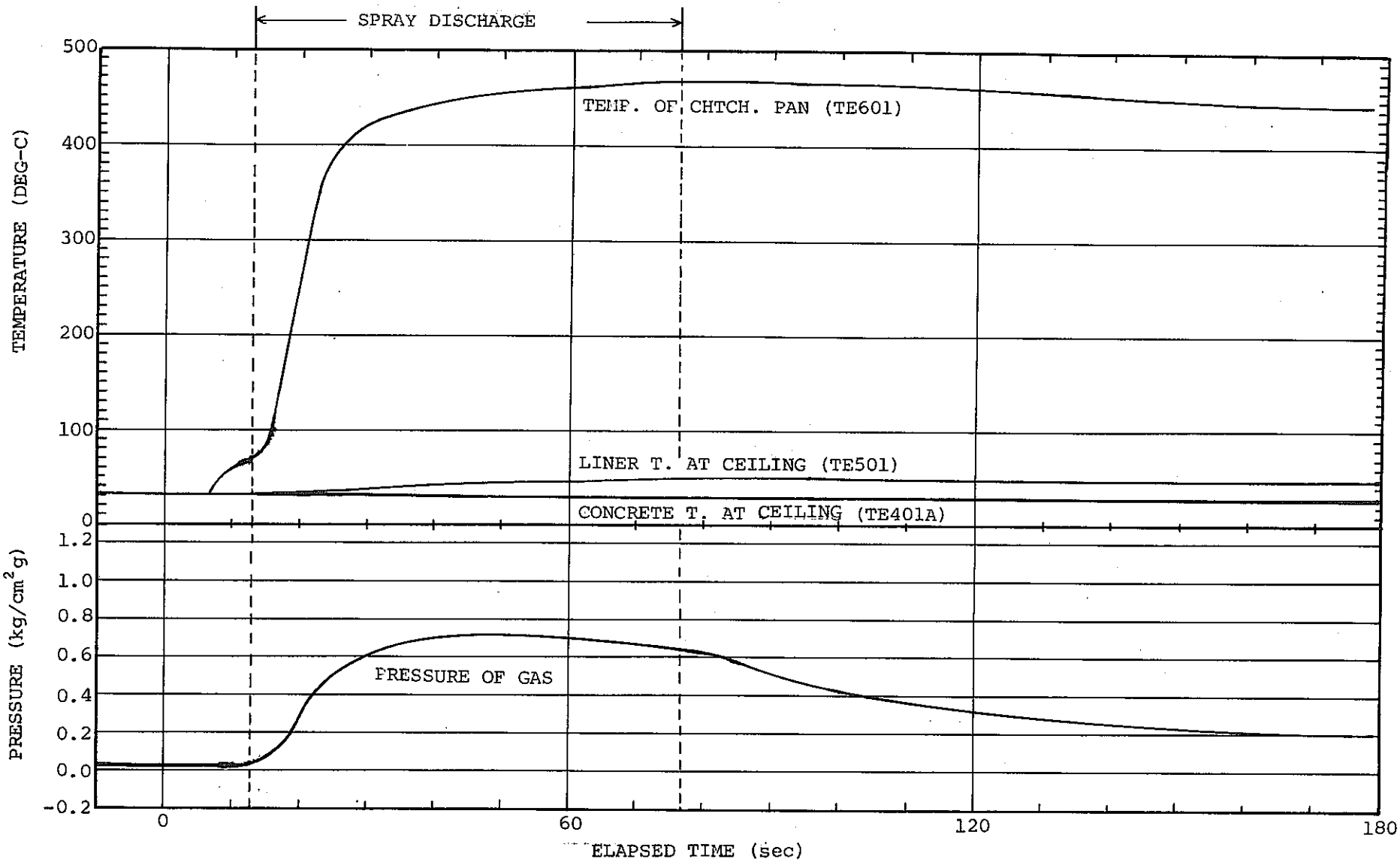

Fig.5.3(2) TASP-N3 Data ; Pressure and Temperature Response

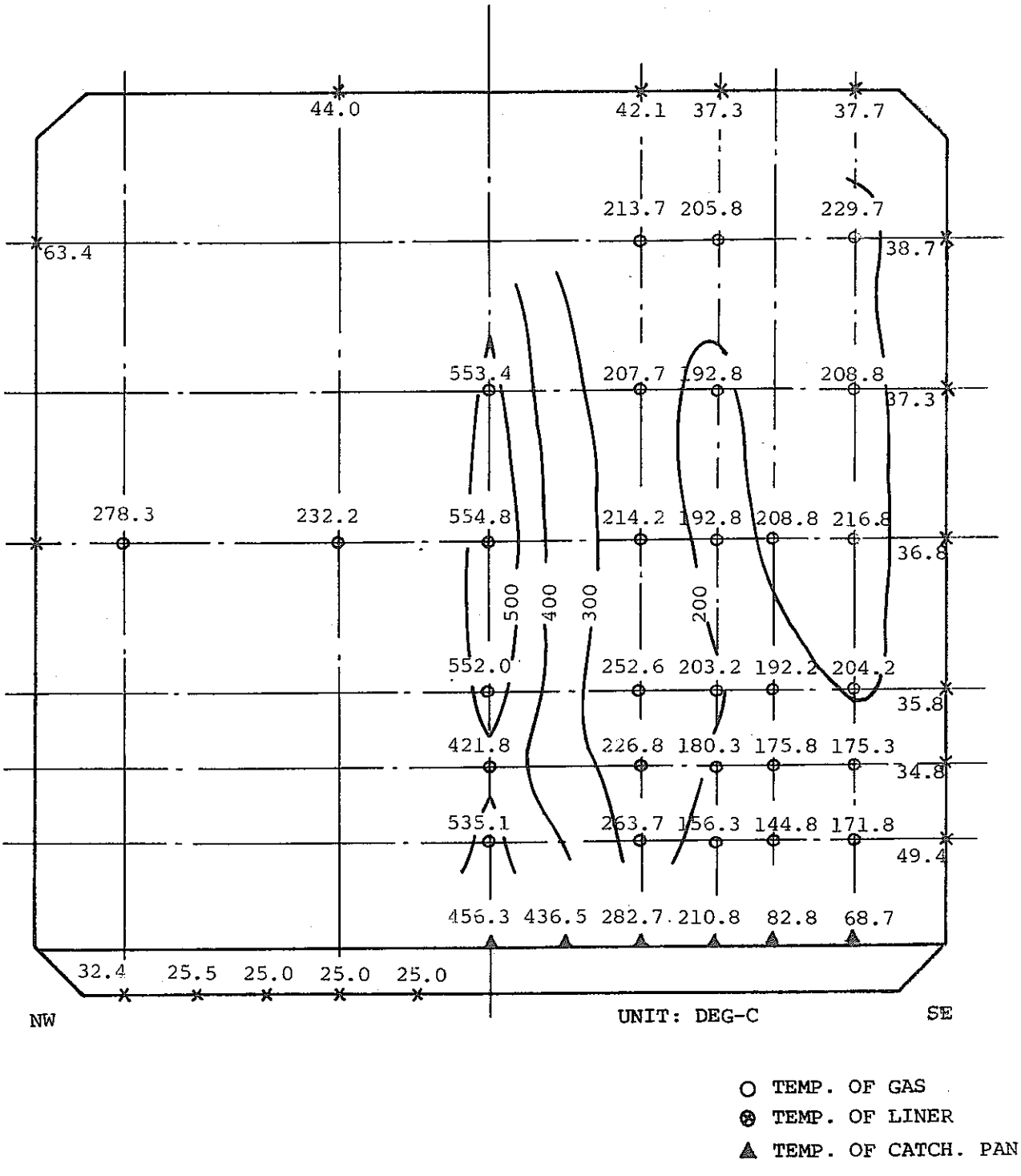

Fig.5.3(3) TASP-N3 Data ; Temperature Distribution

(Elapsed Time = 50 sec)

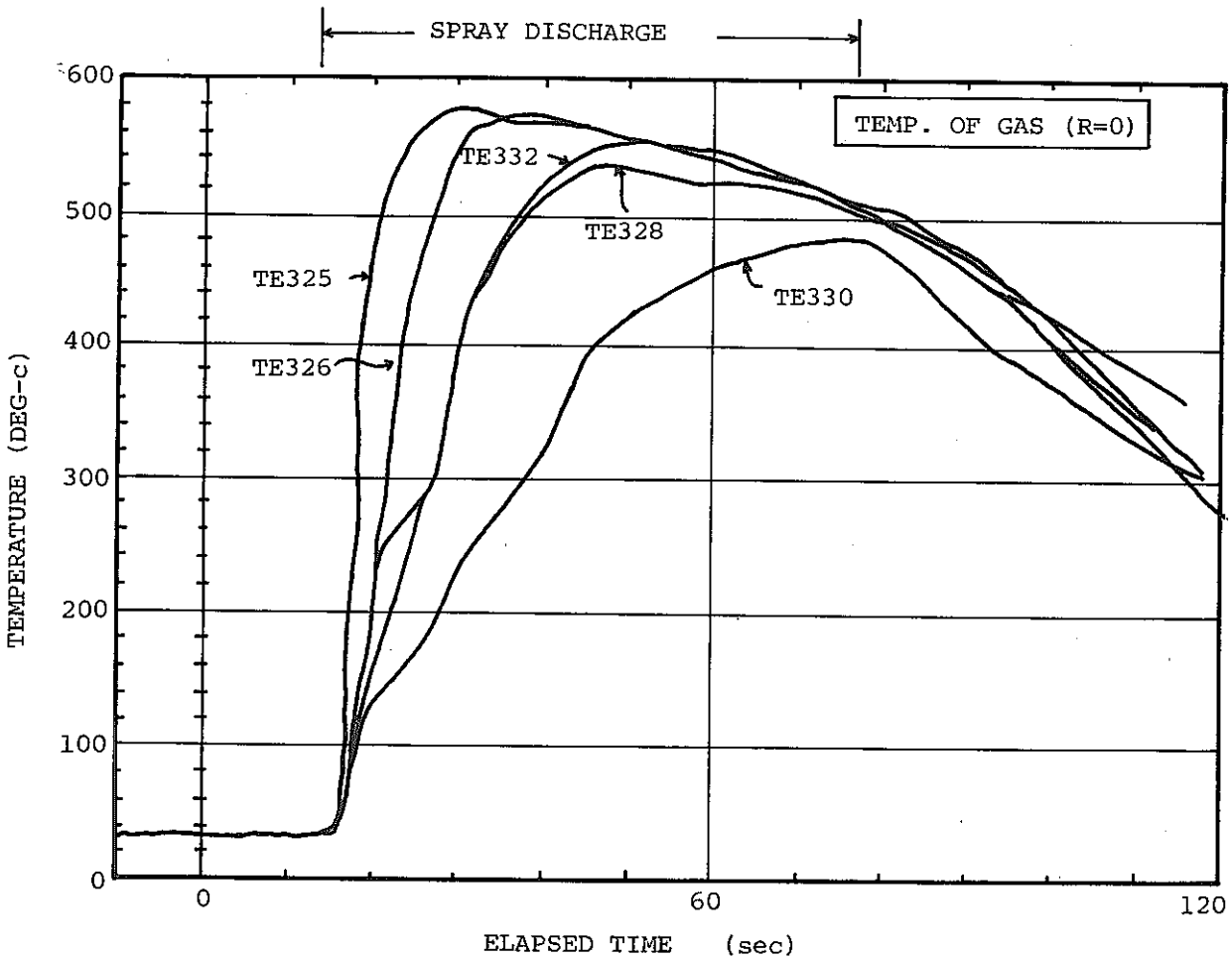

Fig.5.3(4) : TASP-N3 Data : Gas Temperature

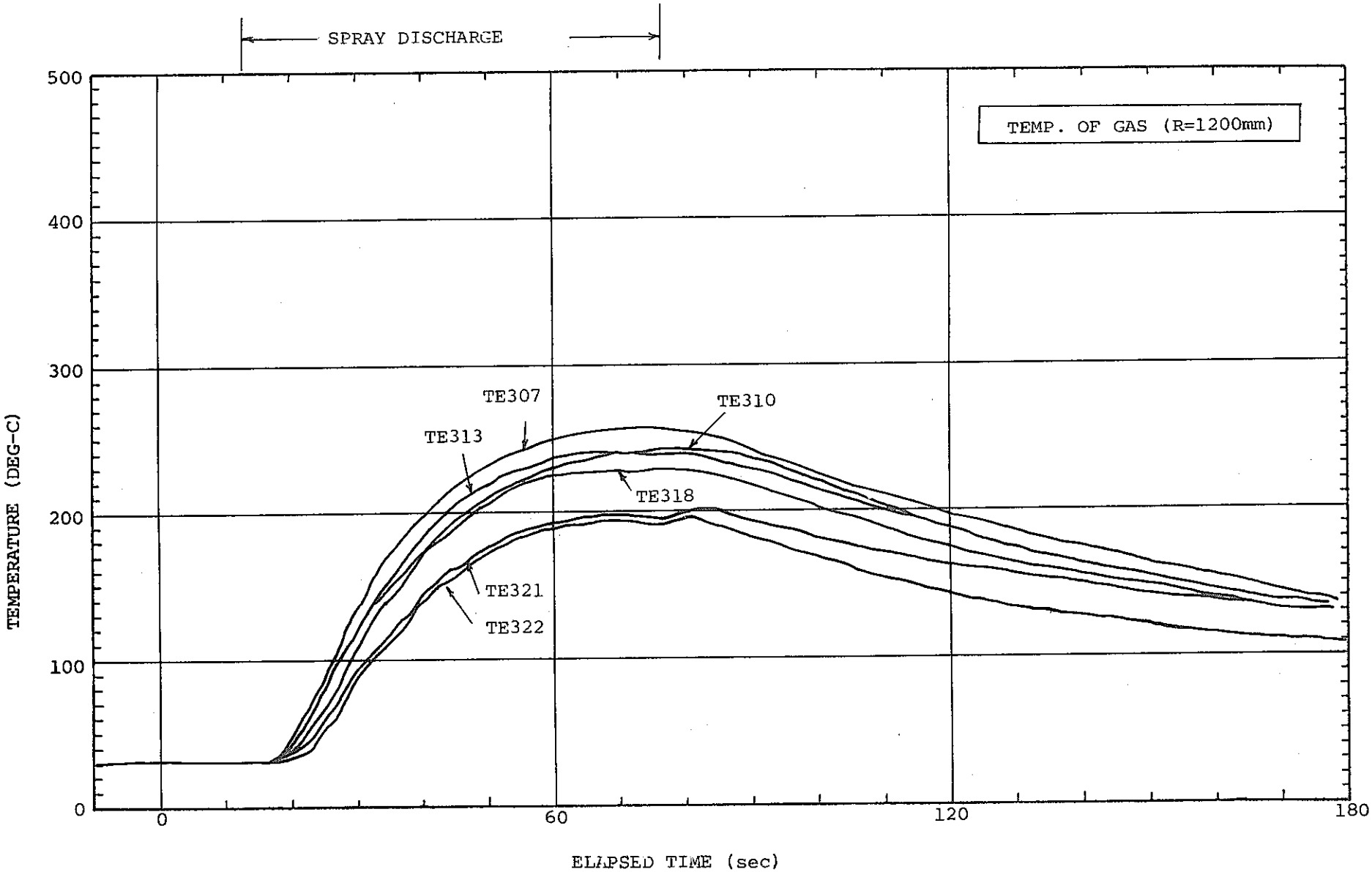

Fig.5.3(5) TASP-N3 Data ; Gas Temperature

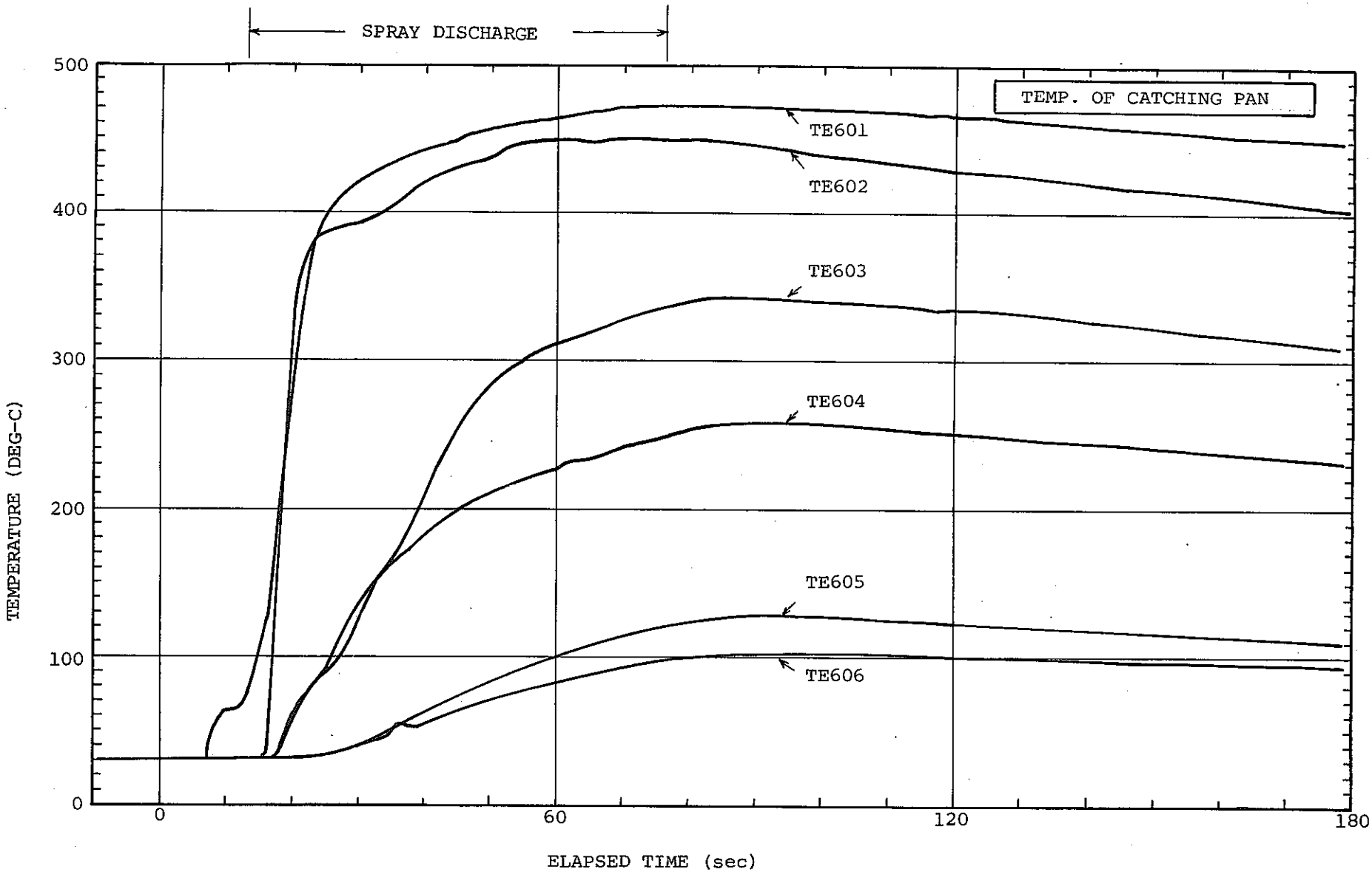

Fig.5.3(6) TASP-N3 Data ; Gas Temperature of Catching Pan

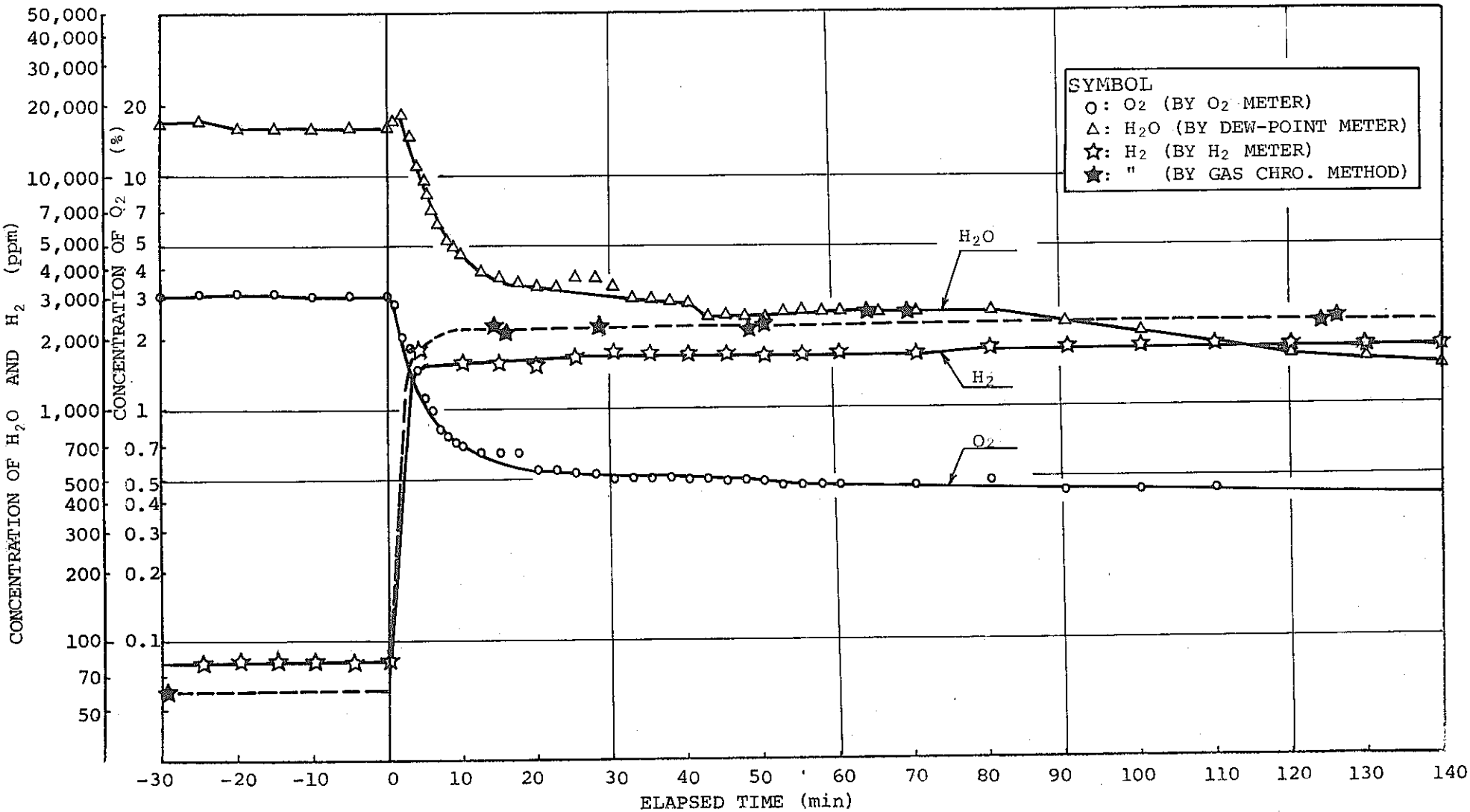

Fig.5.3(7) TASP-N3 Data ; Gas Concentration

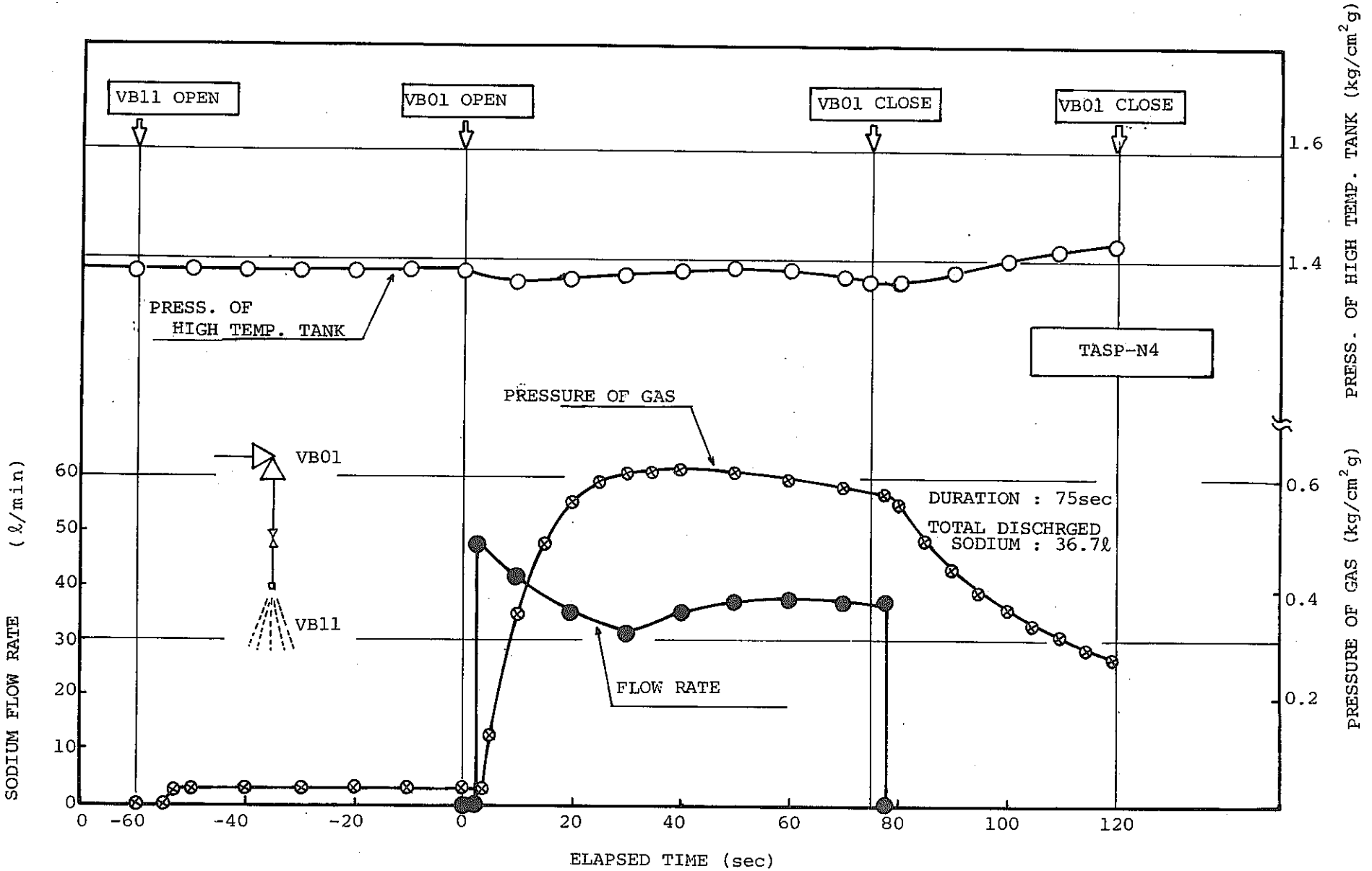

Fig.5.4(1) TASP-N4 Data ; Sodium Discharge Flow Rate

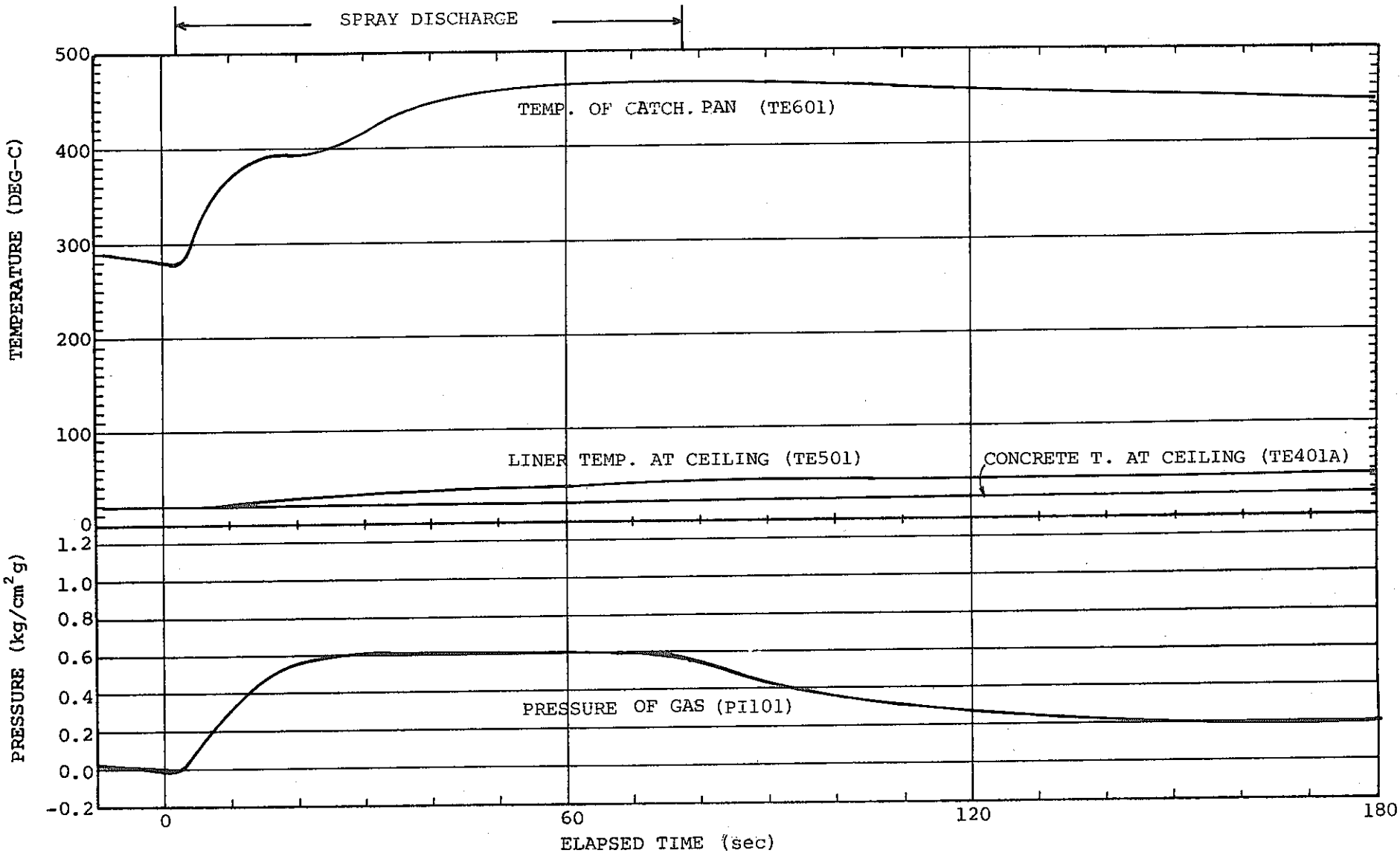

Fig.5.4(2) TASP-N4 Data : Pressure and Temperature Response

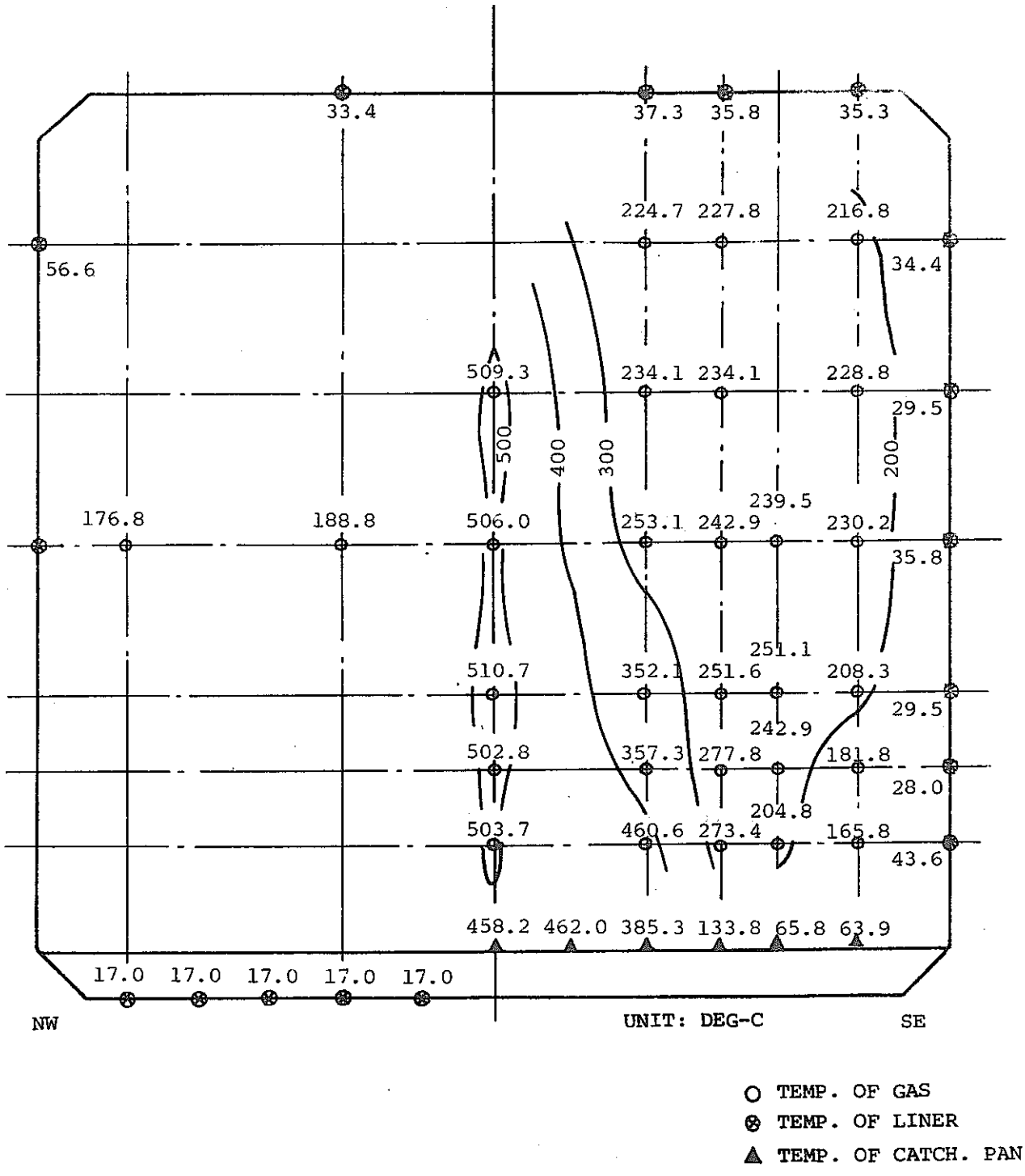

Fig.5.4(3) TASP-N4 Data ; Temperature Distribution

(Elapsed Time = 50 sec)

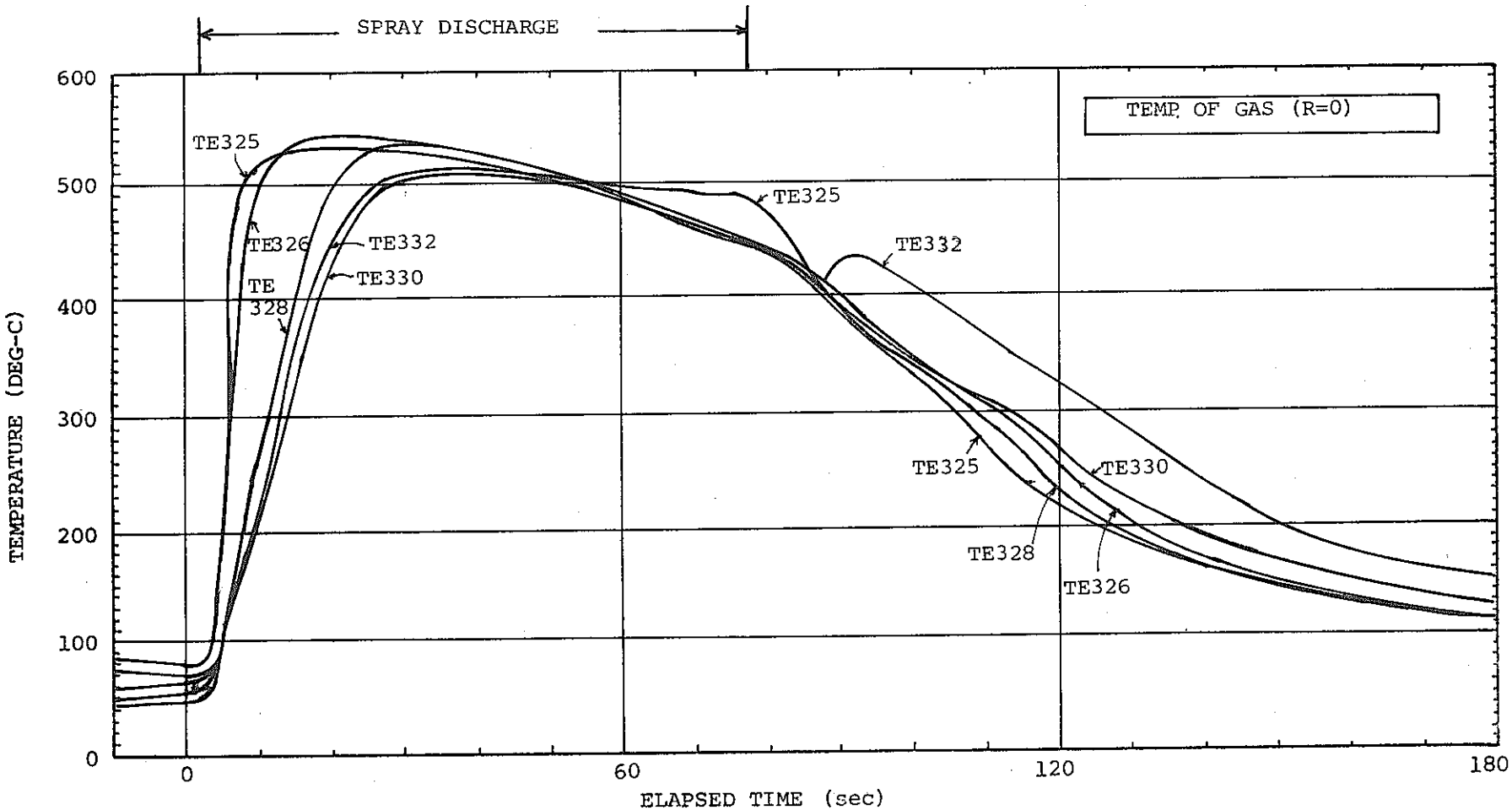

Fig.5.4(4) TASP-N4 Data ; Gas Temperature

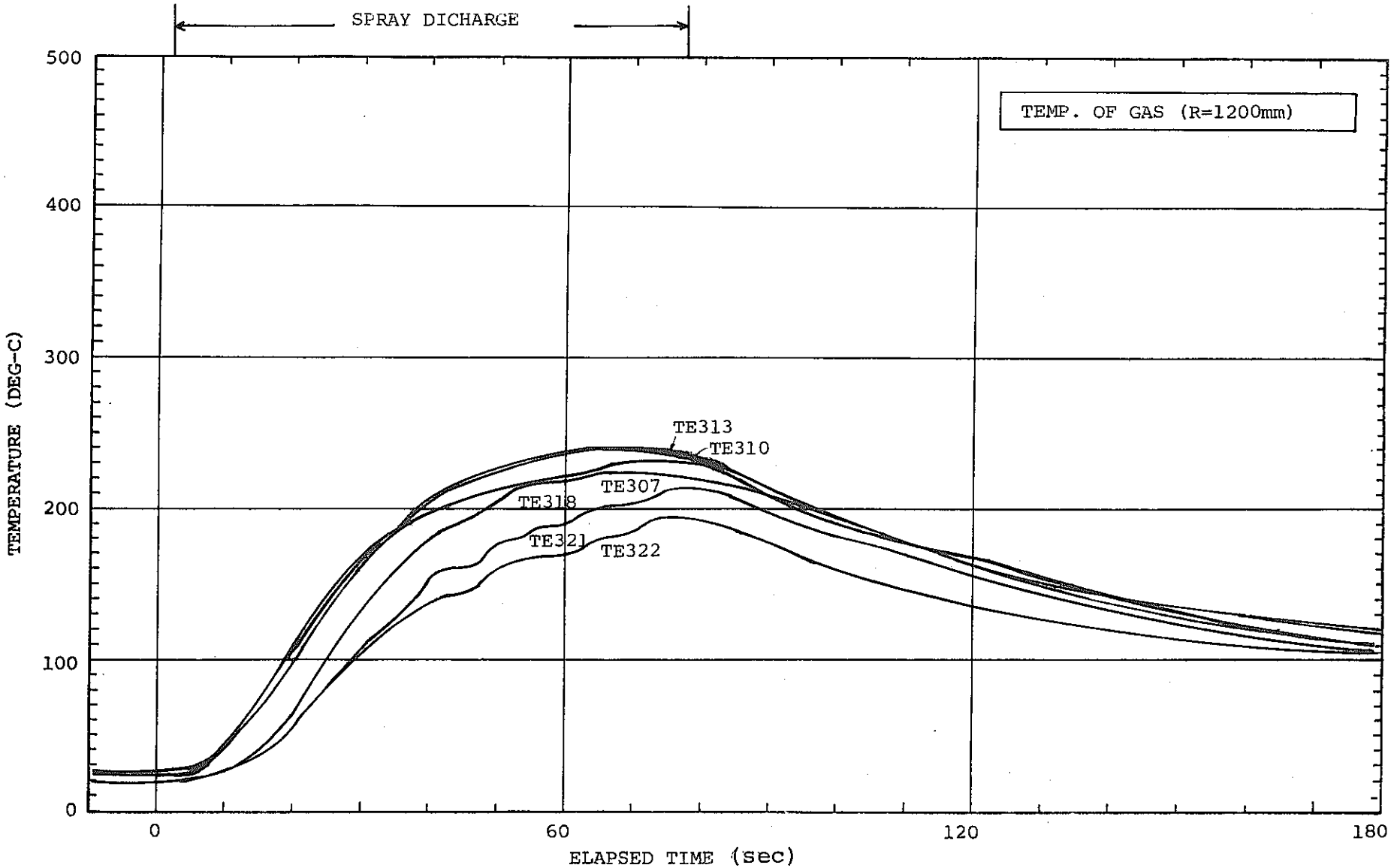

Fig.5.4(5) TASP-N4 Data ; Gas Temperature

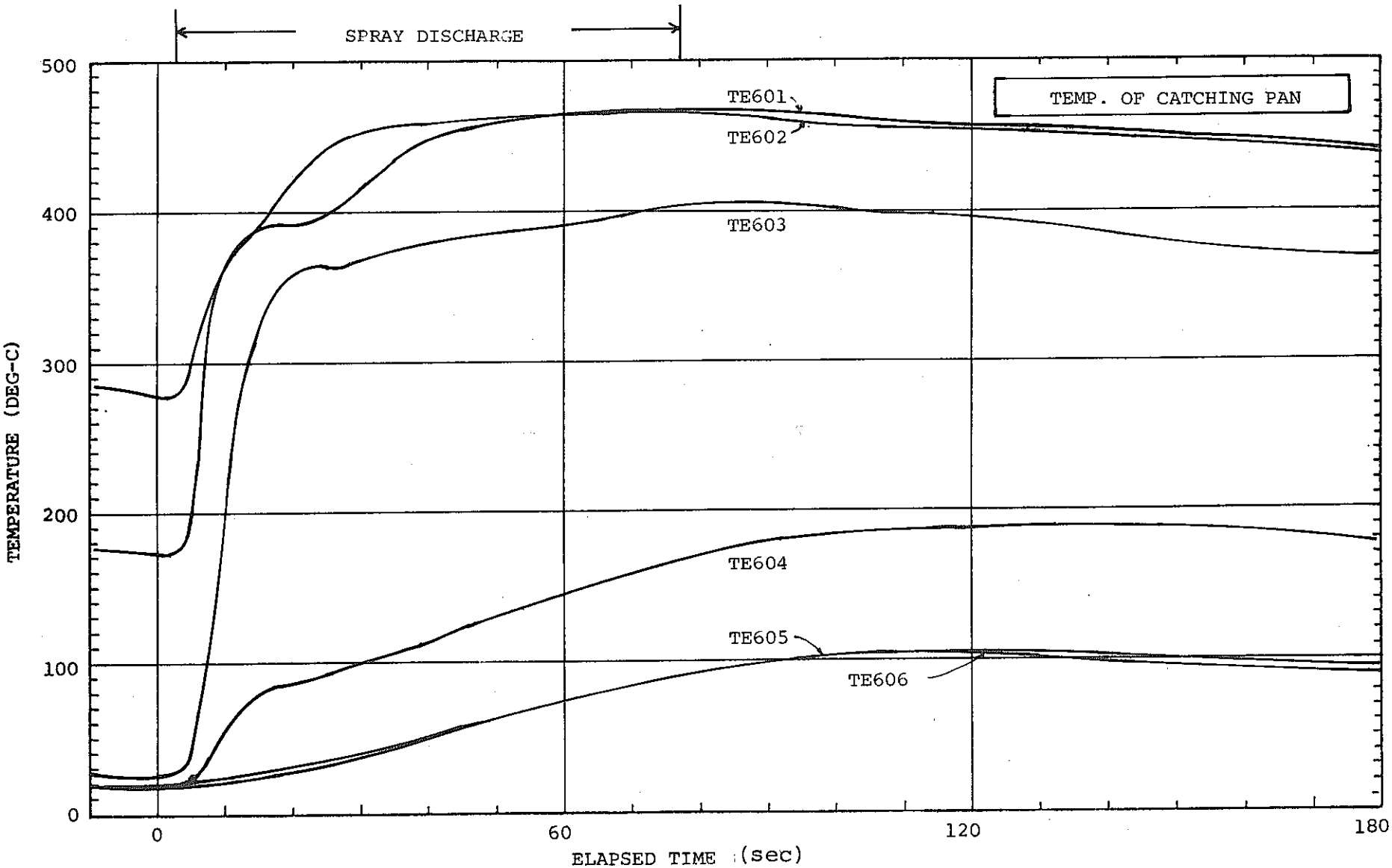

Fig.5.4(6) TASP-N4 Data : Temperature of CVtching Pan

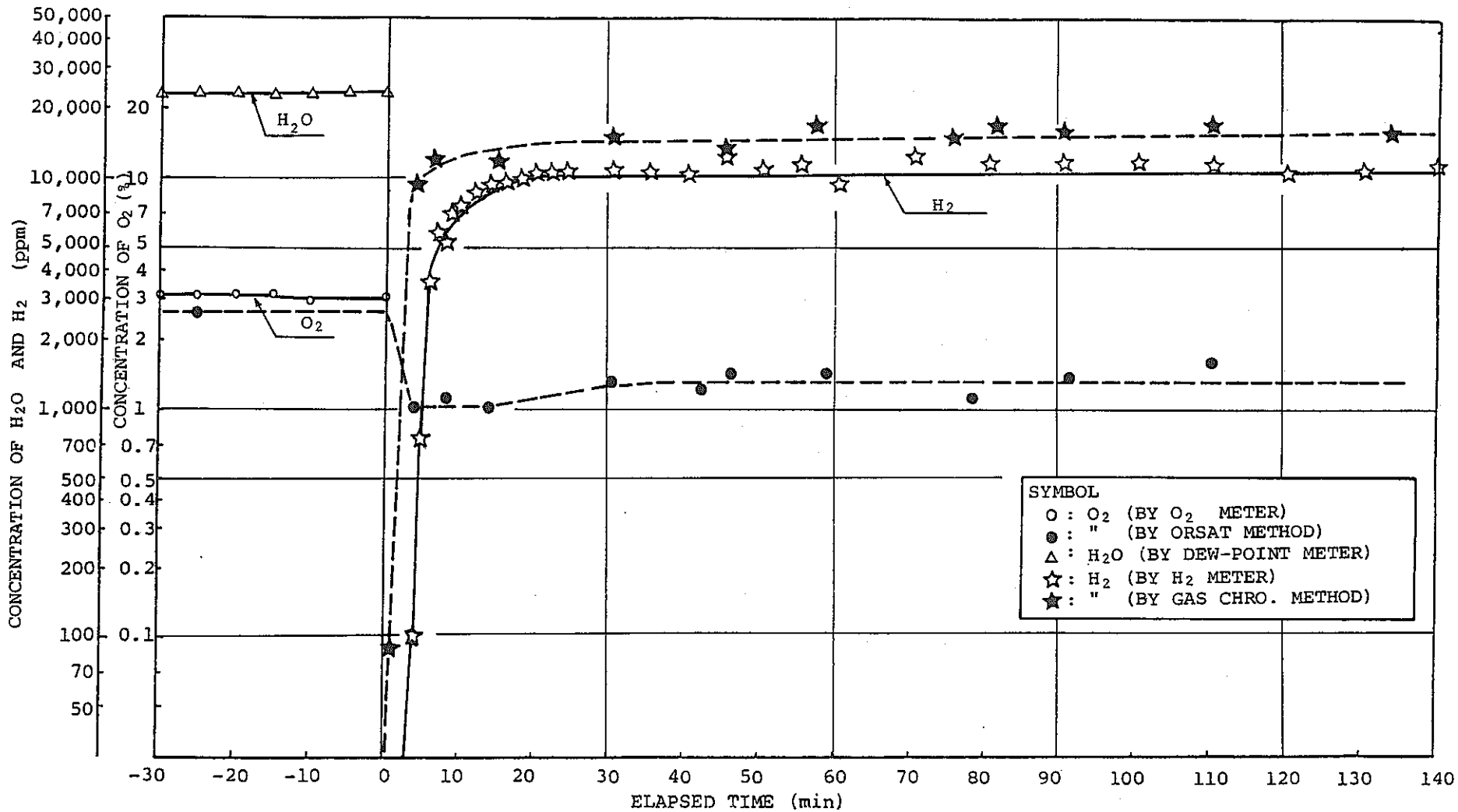

Fig.5.4(7) TASP-N4 Data ; Gas Concentration

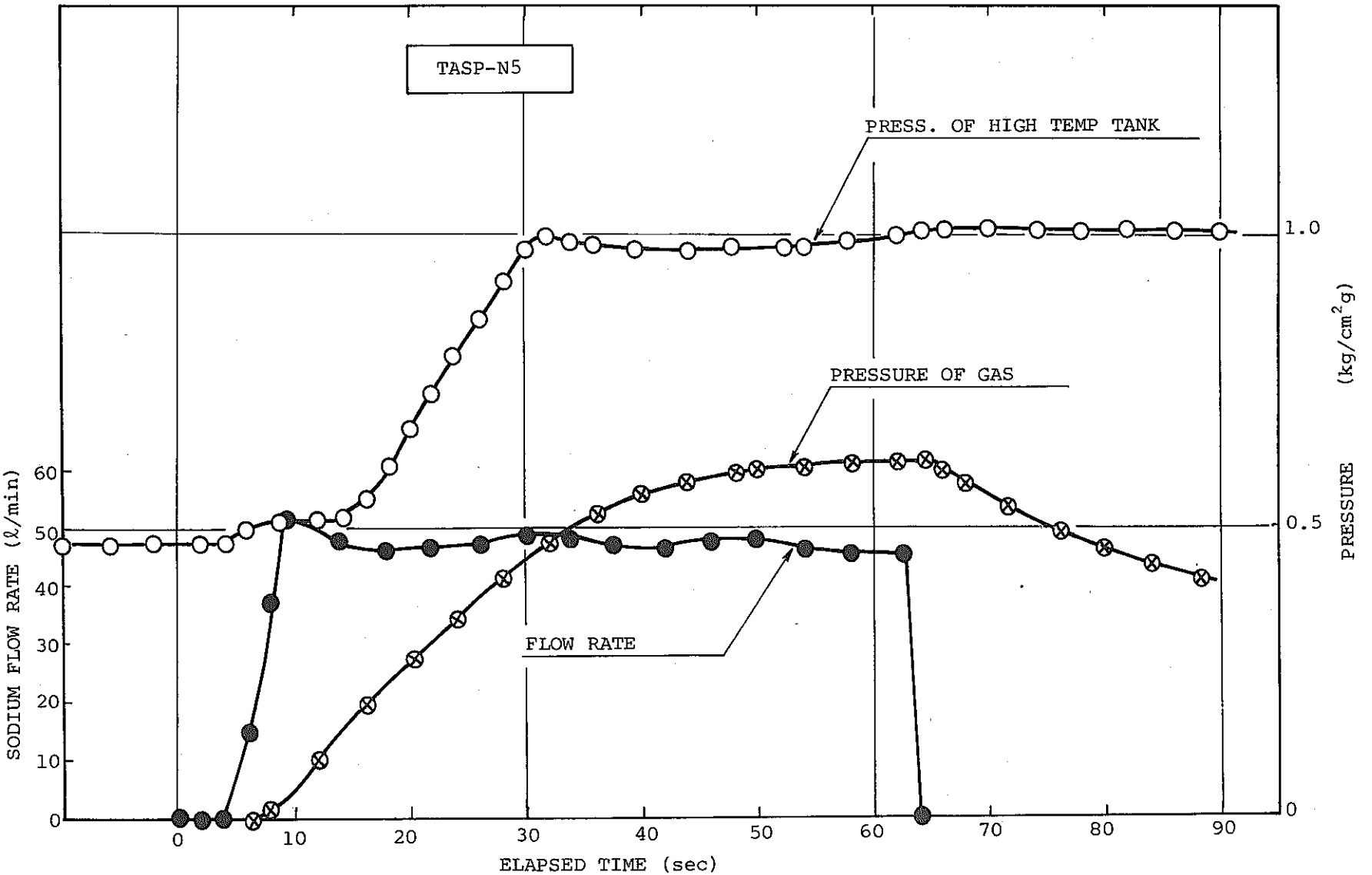

Fig.5.5(1) TASP-N5 Data ; Sodium Discharge Flow Rate

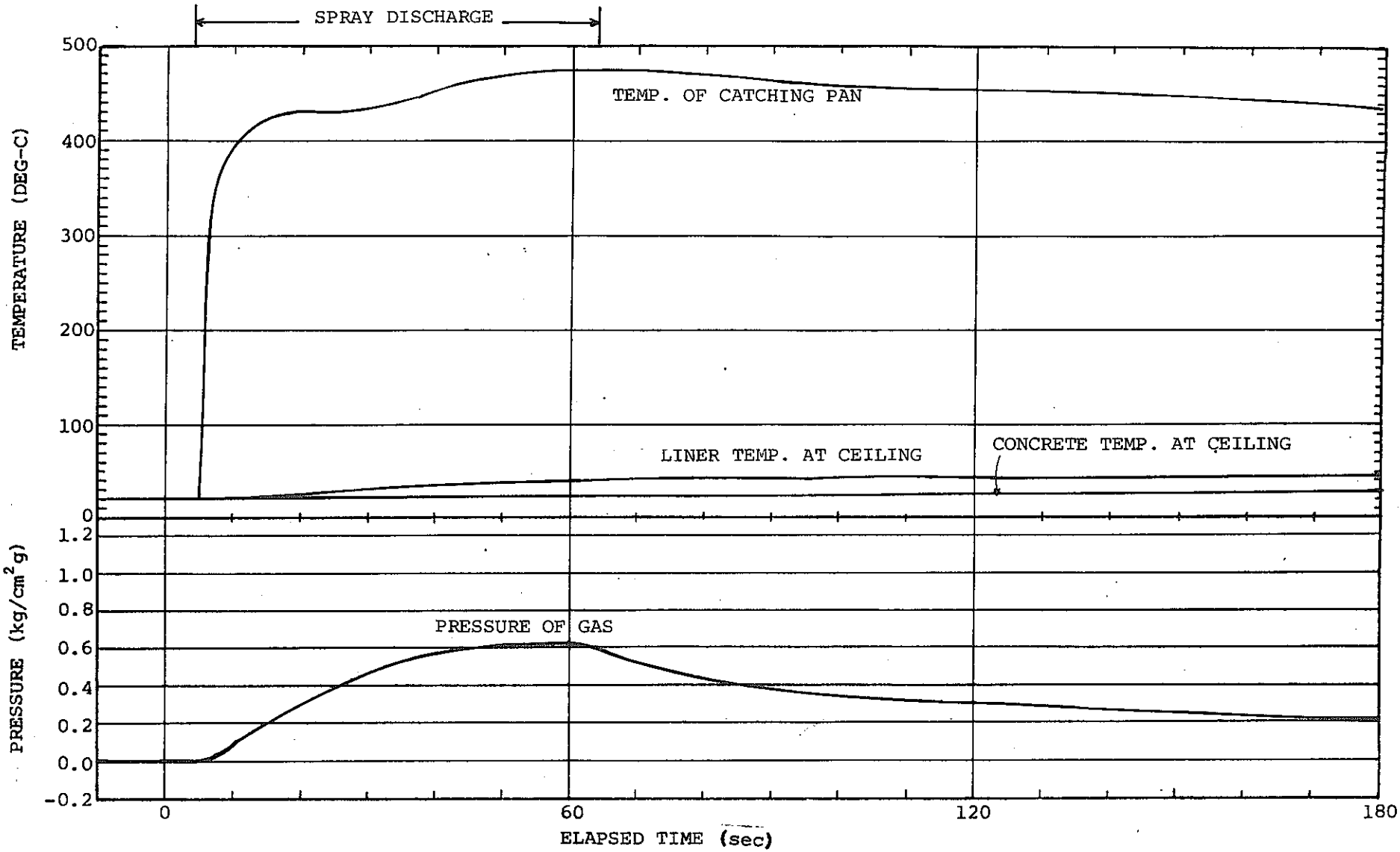

Fig.5.5(2) TASP-N4 Data ; Pressure and Temperature Response

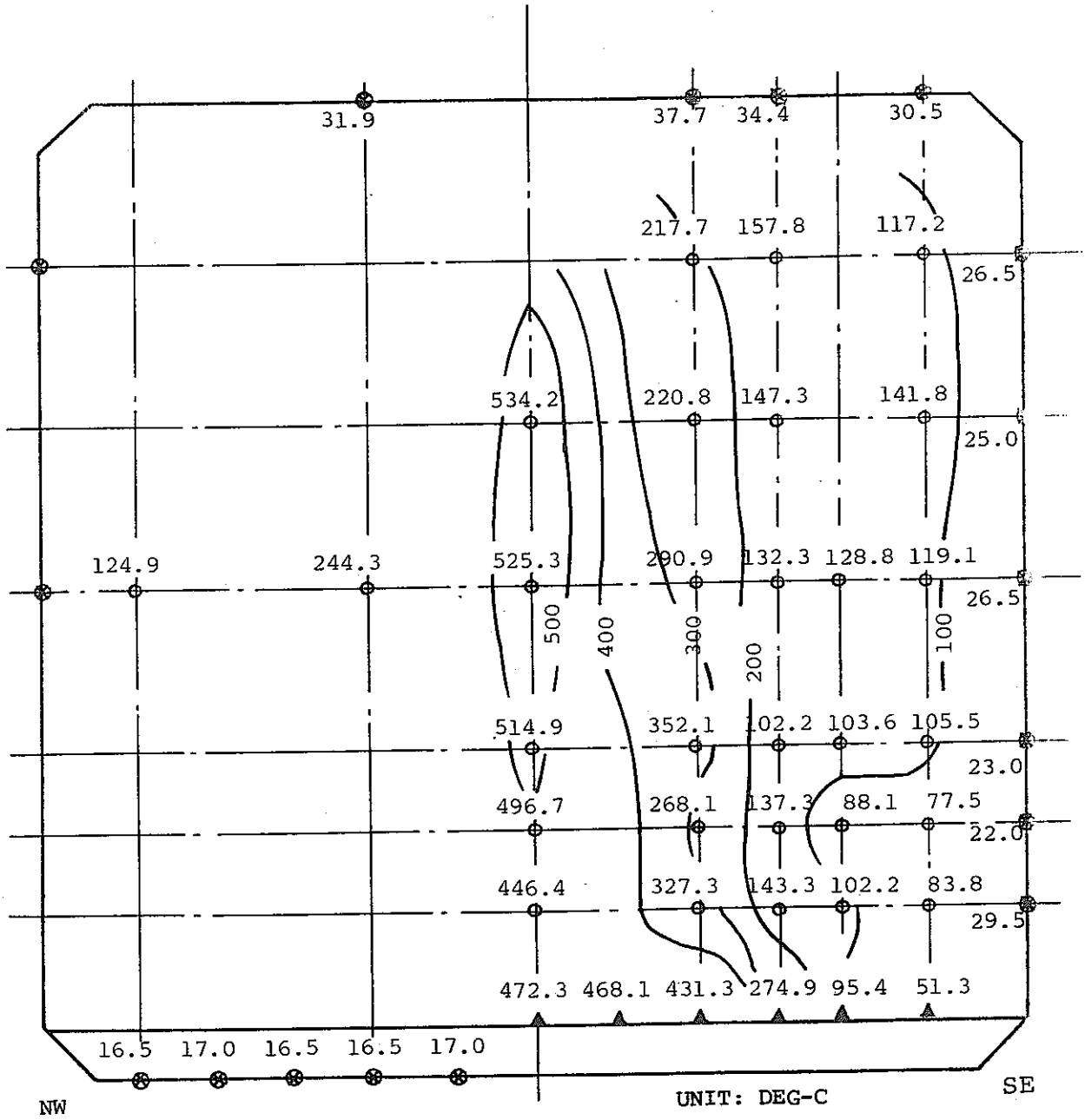

Fig.5.5(3) TASP-N5 Data ; Temperature Distribution

(Elapsed Time = 50 sec)

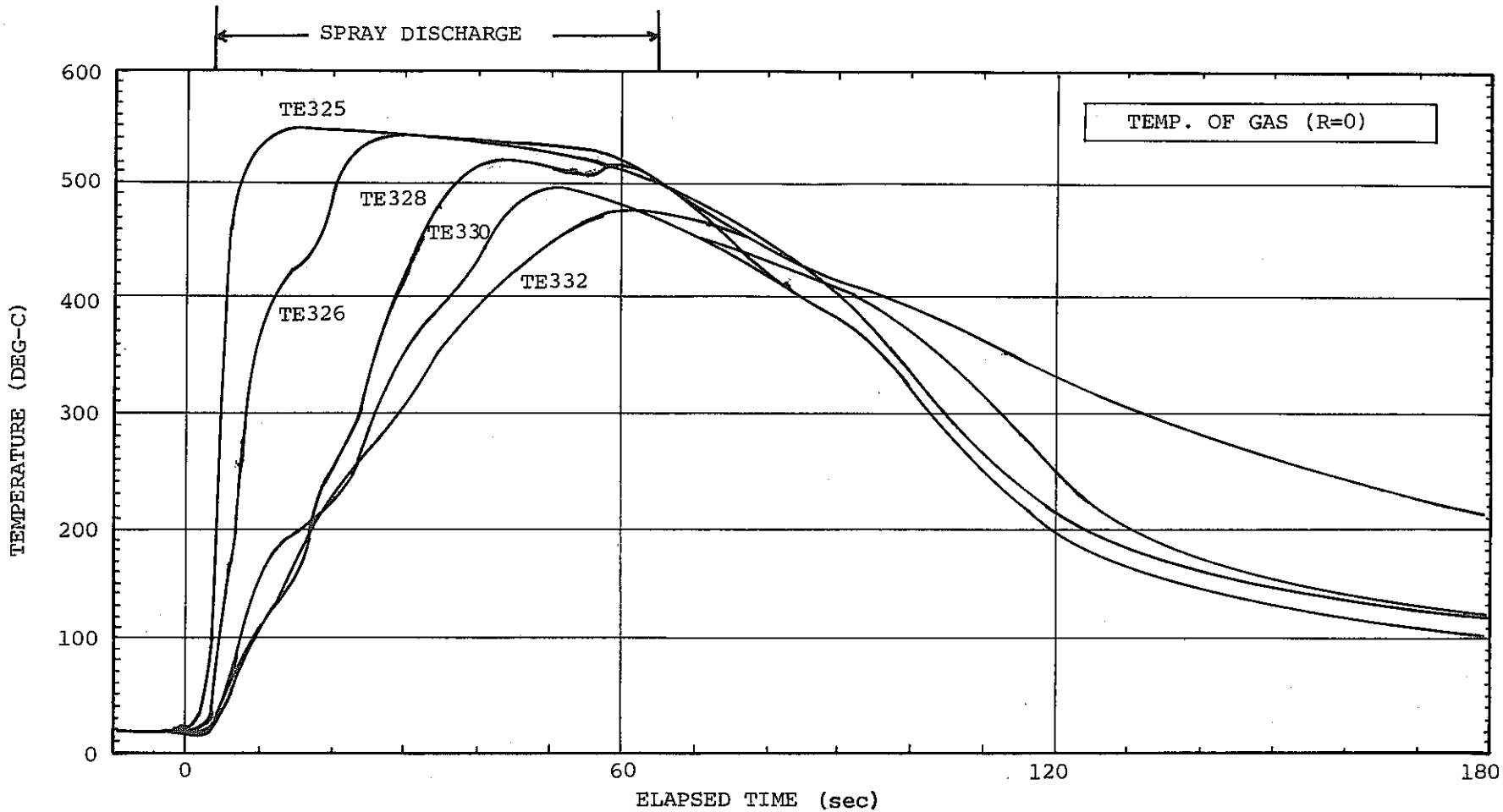

Fig.5.5(4) TASP-N5 Data ; Gas Temperature

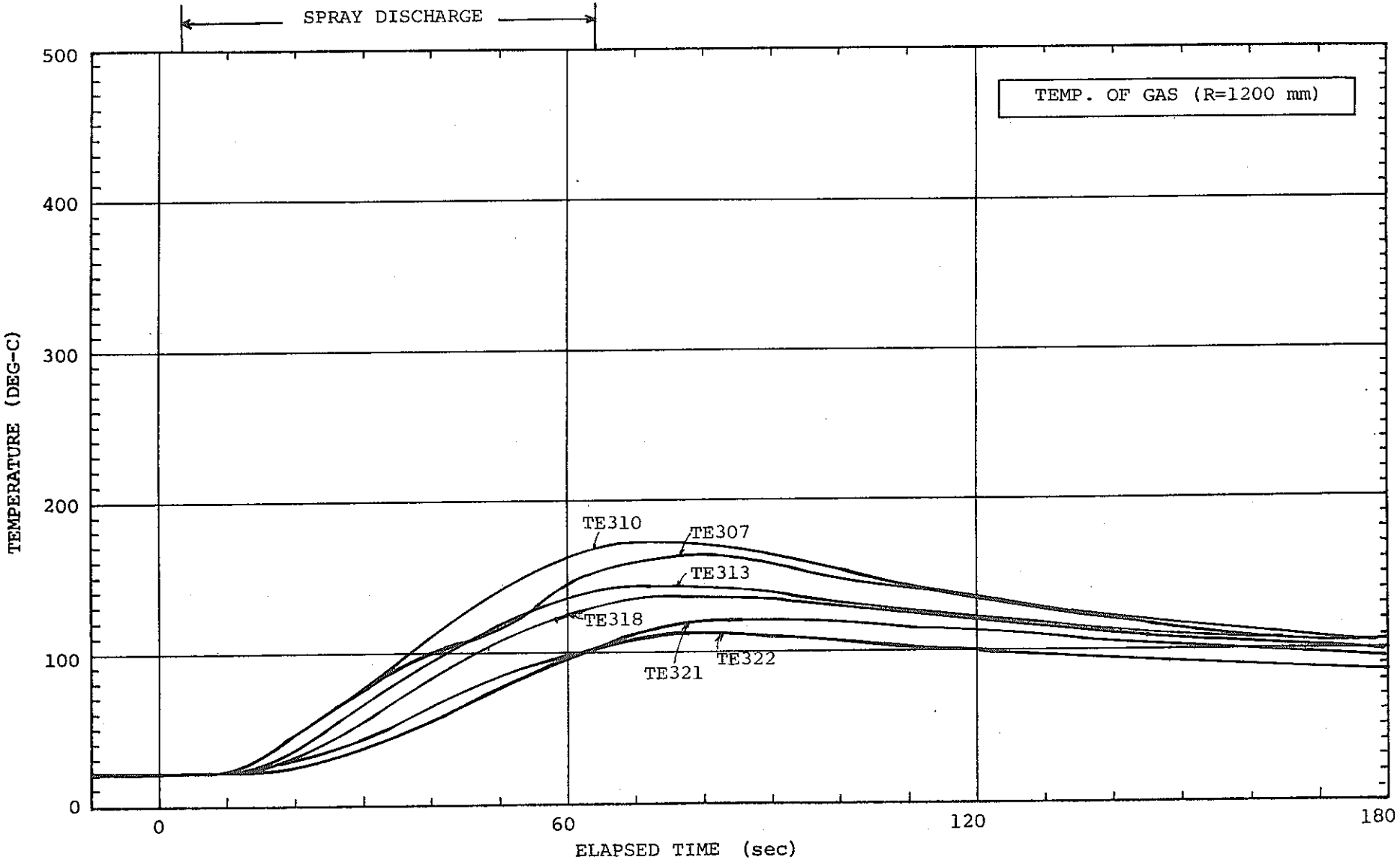

Fig.5.5(5) TASP-N5 Data ; Gas Temperature

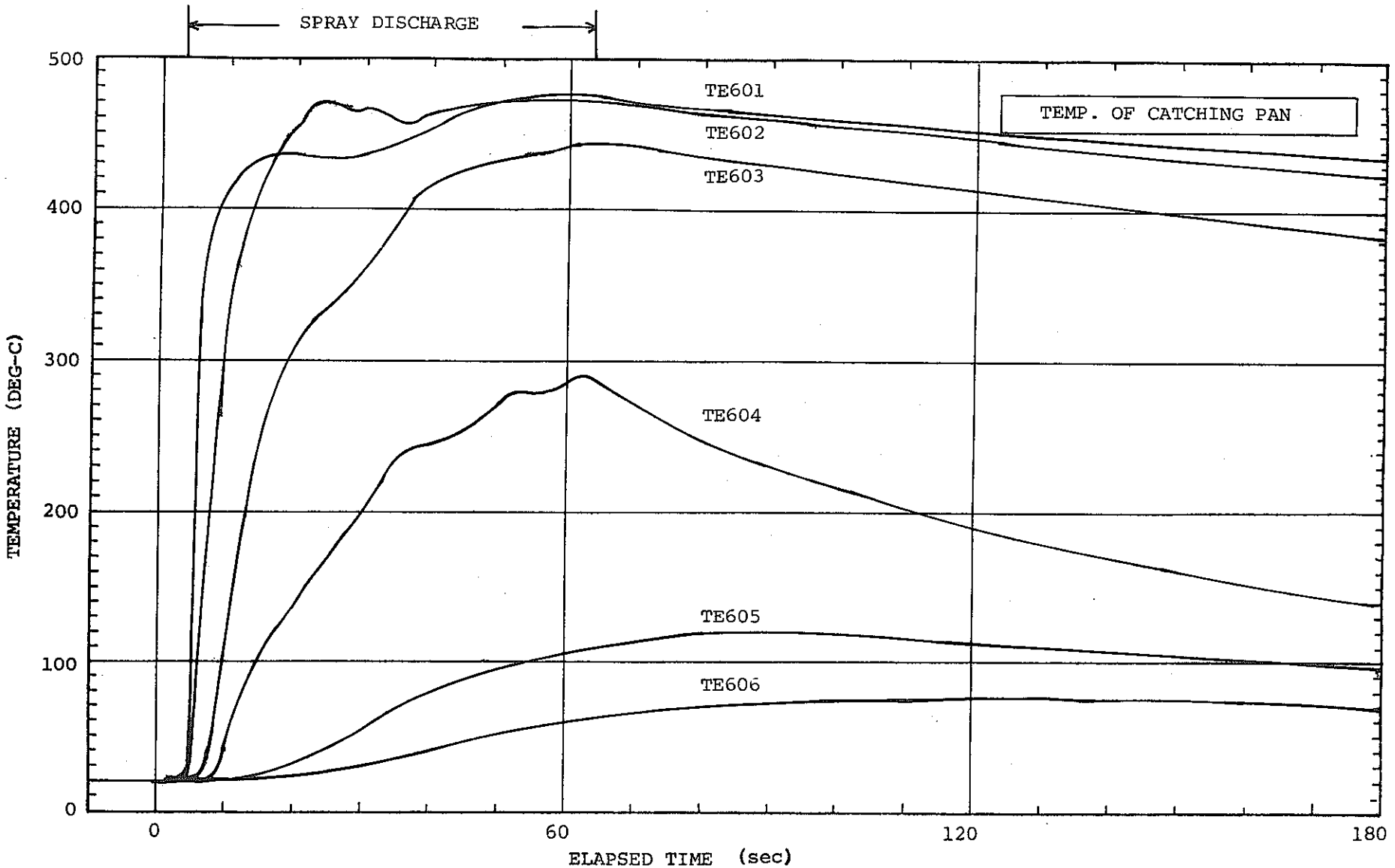

Fig.5.5(6) TASP-N5 Data ; Temperature of Catching Pan

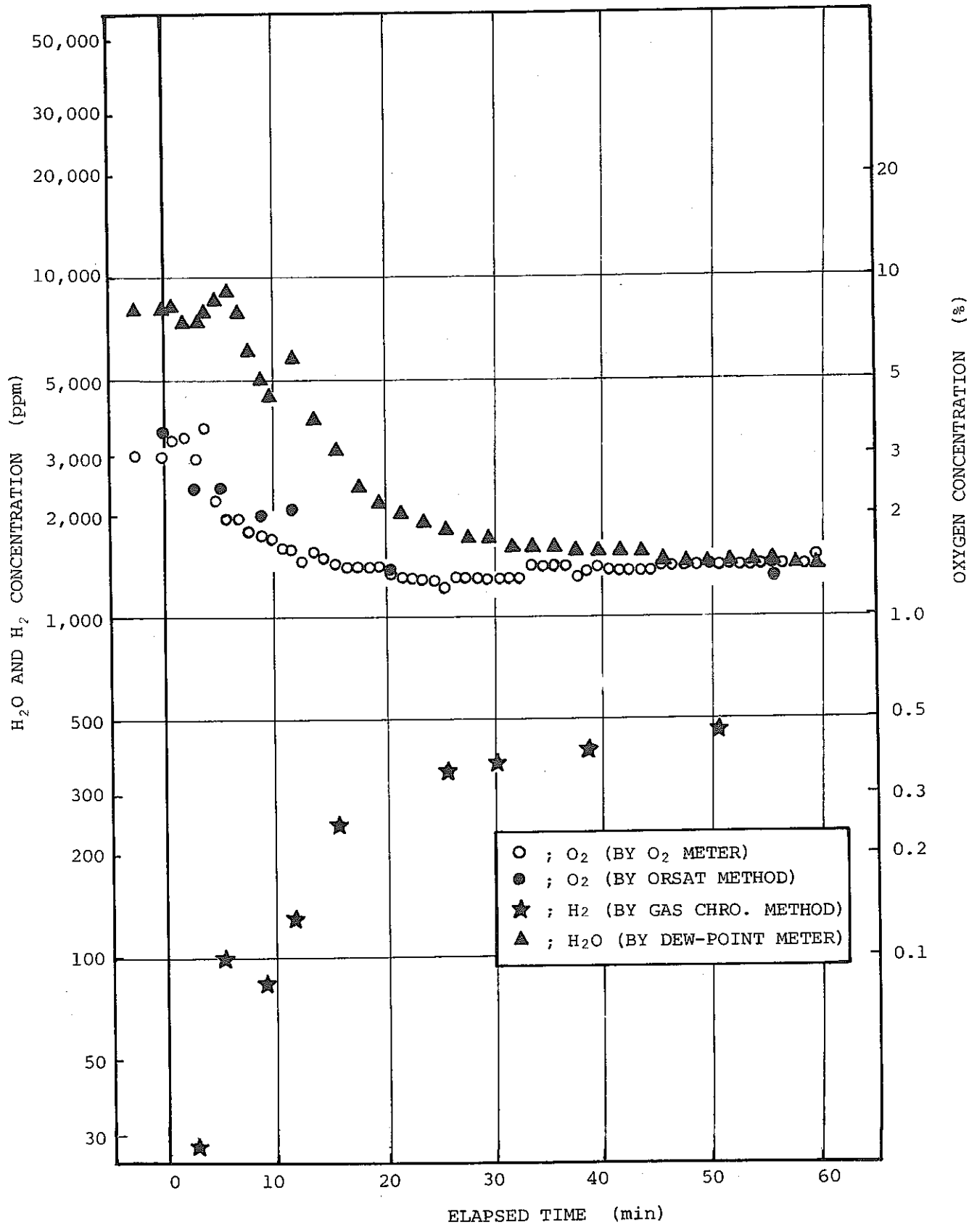

Fig.5.5(7) TASP-N5 Data ; Gas Concentration

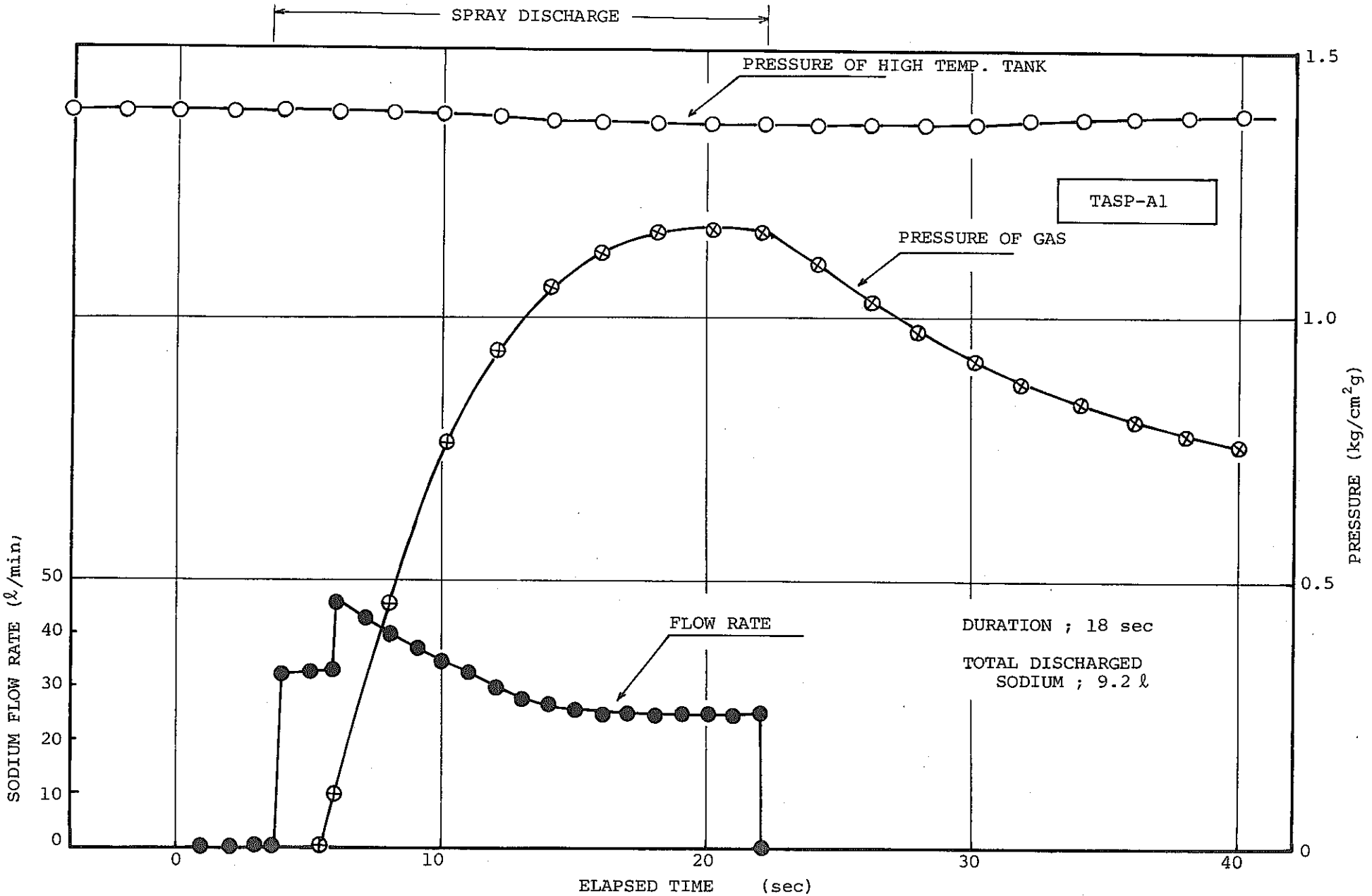

Fig.5.6(1) TASP-A1 Data ; Sodium Discharge Flow Rate

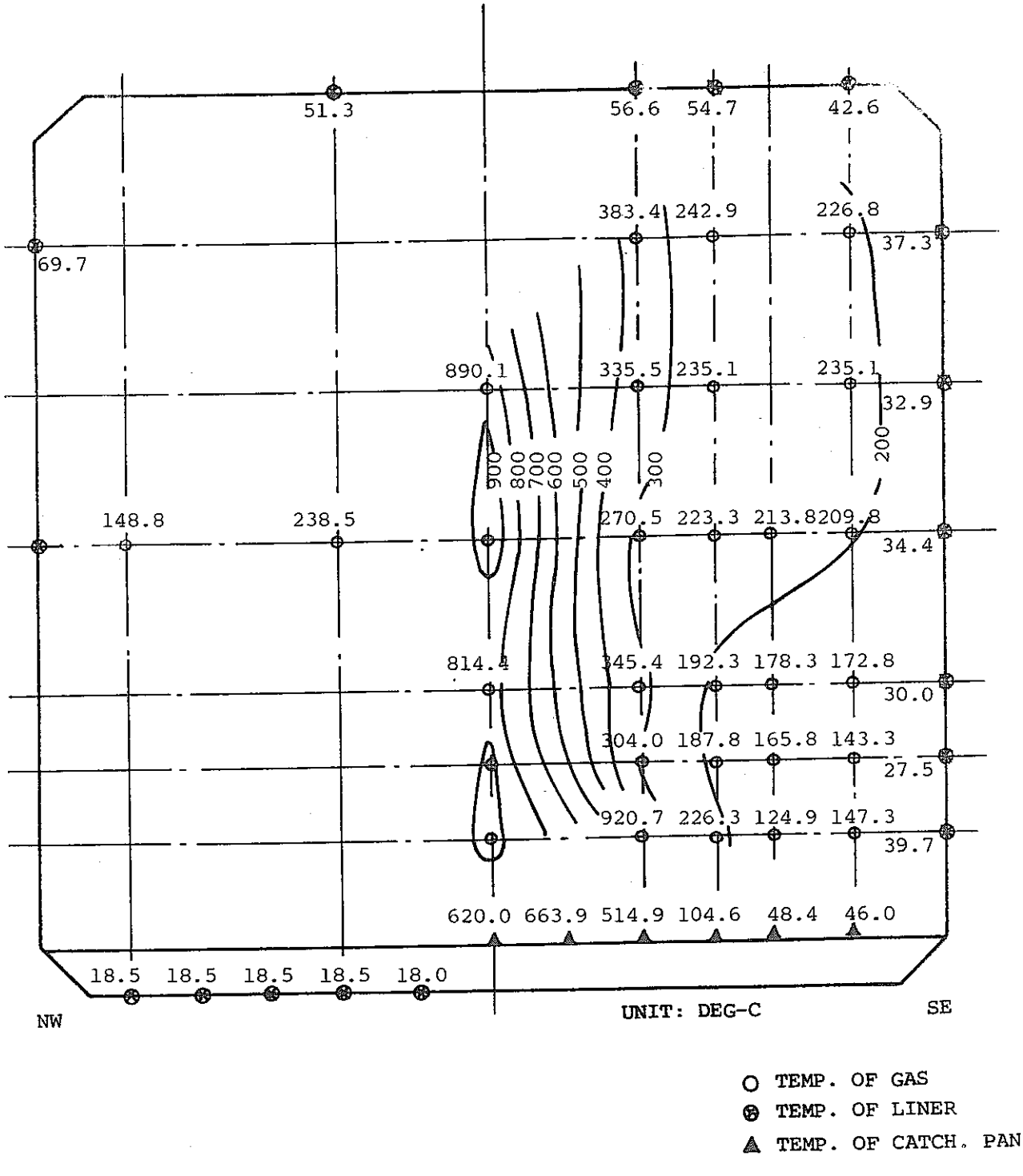

Fig.5.6(2) TASP¬A1 Data ; Temperature Distribution

(Elapsed Time = 20 sec)

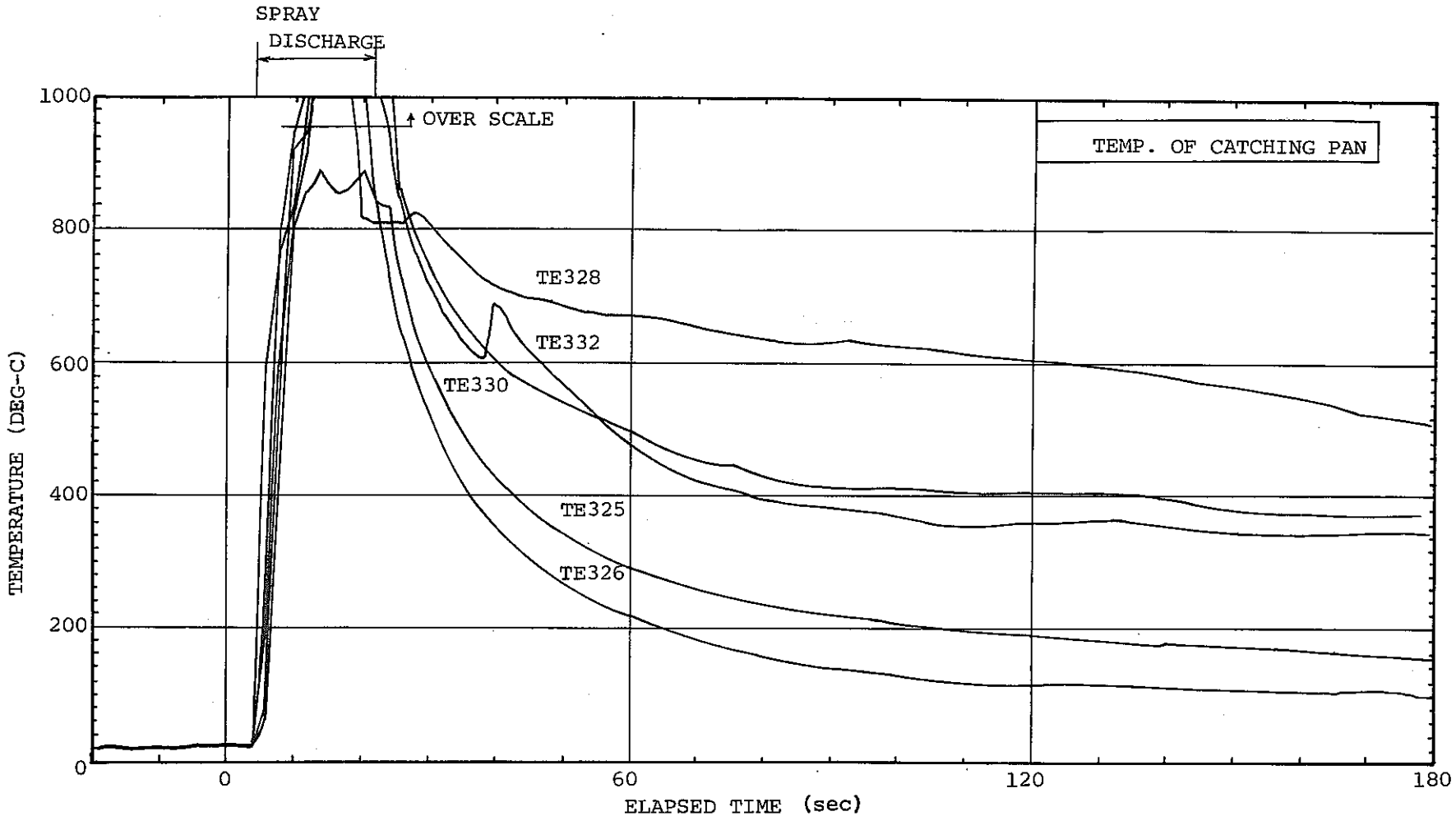

Fig.5.6(3) TASP-Al Data ; Gas Temperature

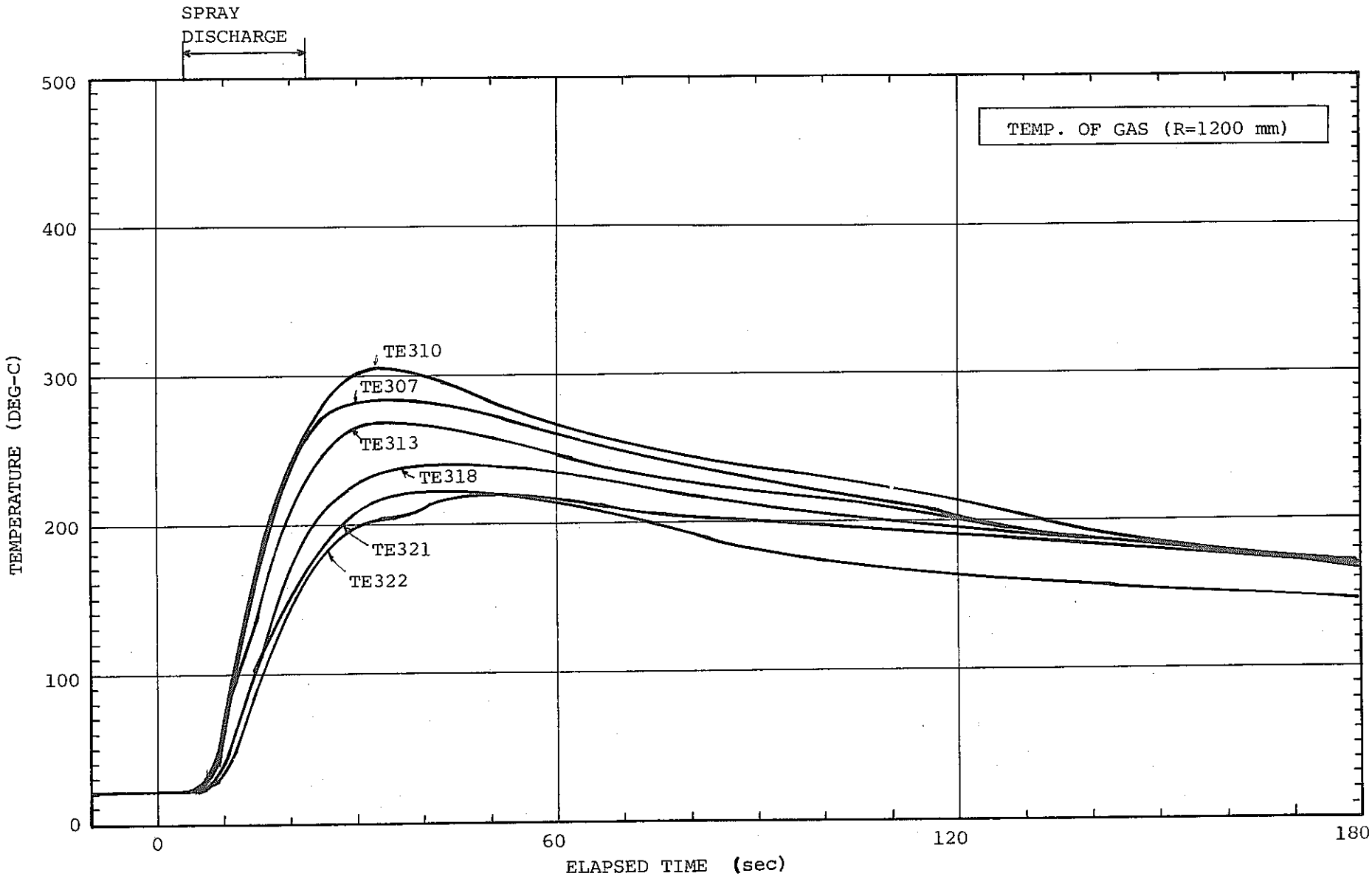

Fig.5.6(4) TASP-A1 Data ; Gas Temperature

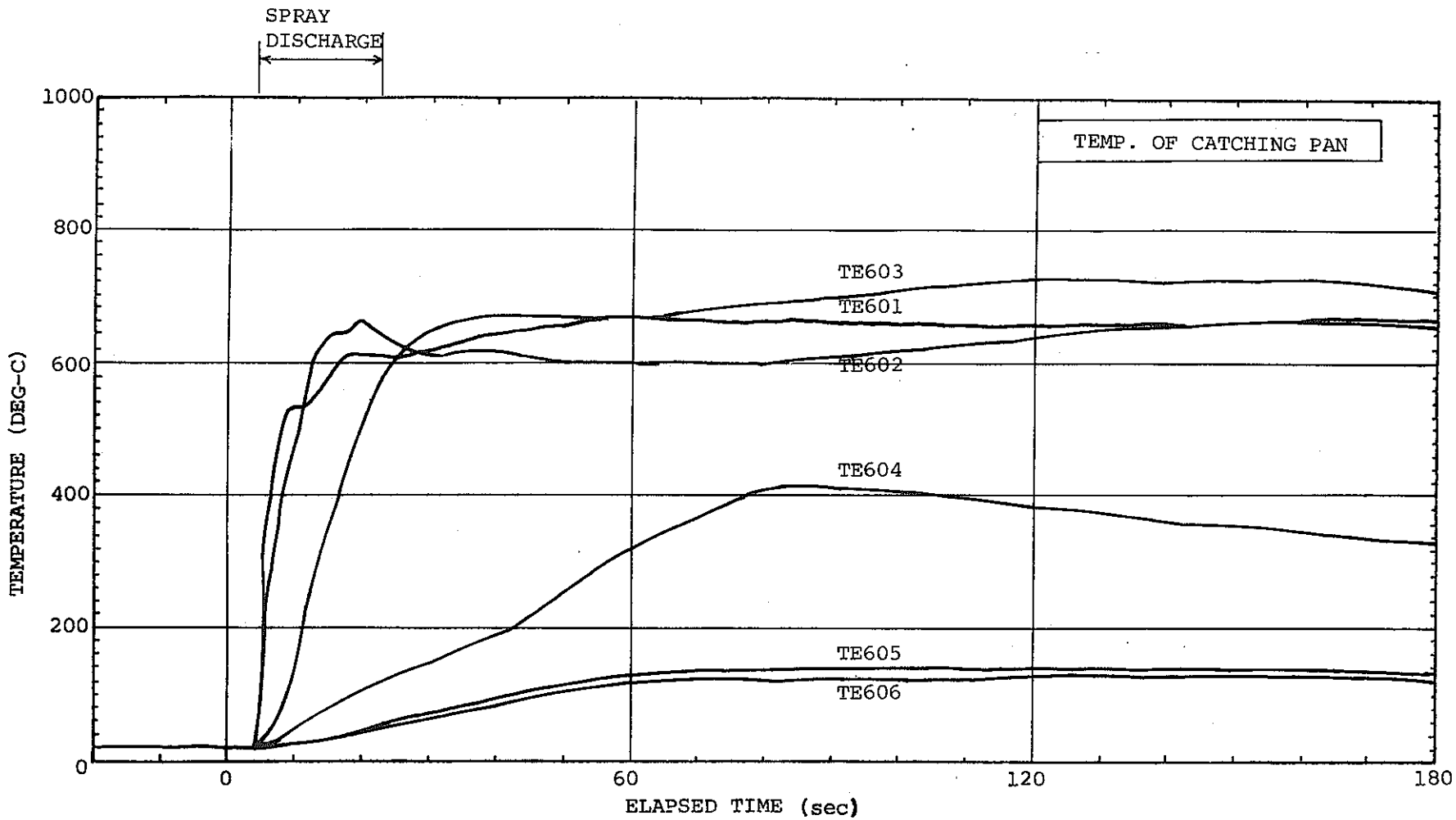

Fig.5.6(5) TASP-A1 Data ; Temperature of Catching Pan

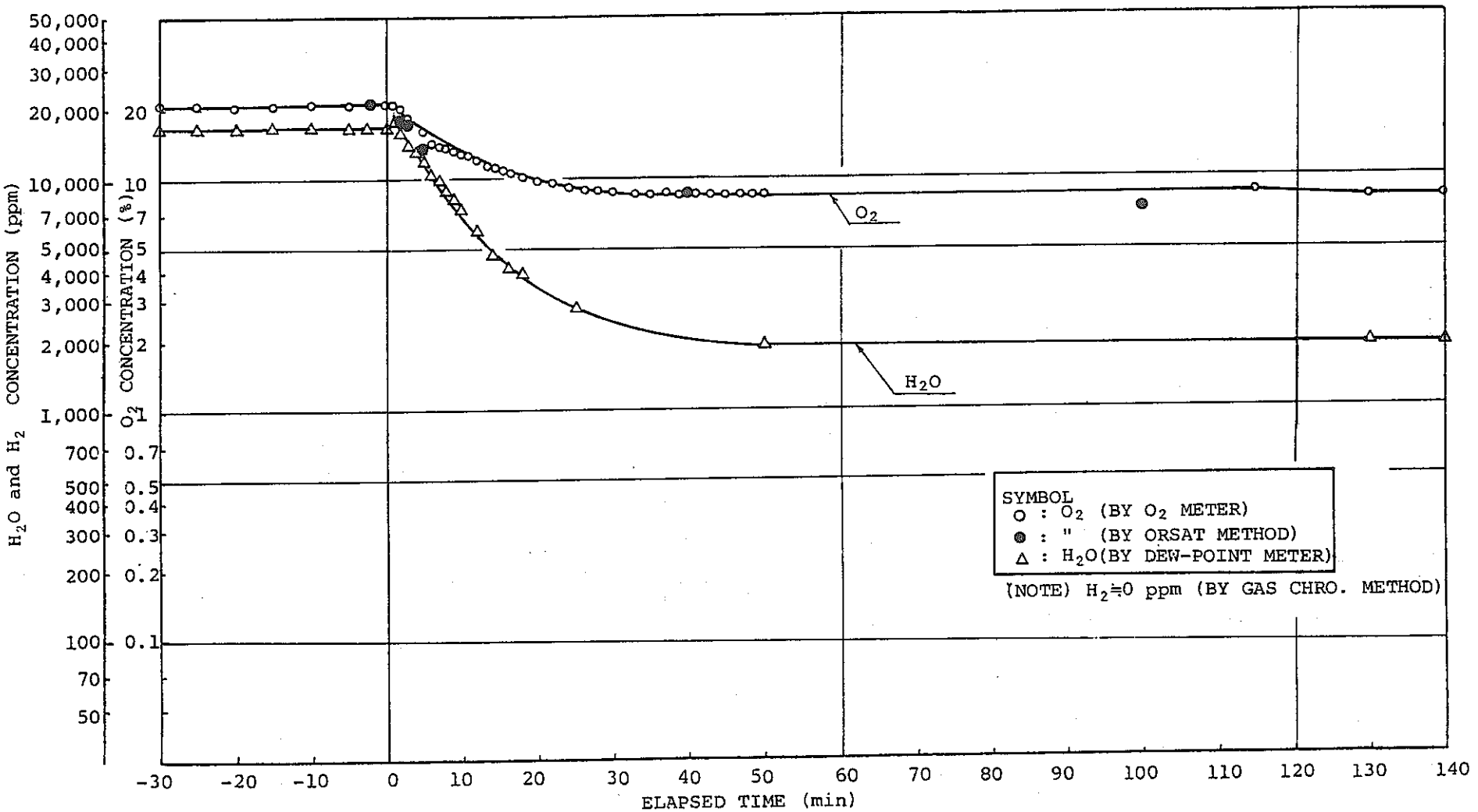

Fig.5.6(6) TASP-A1 Data ; Gas Concentration

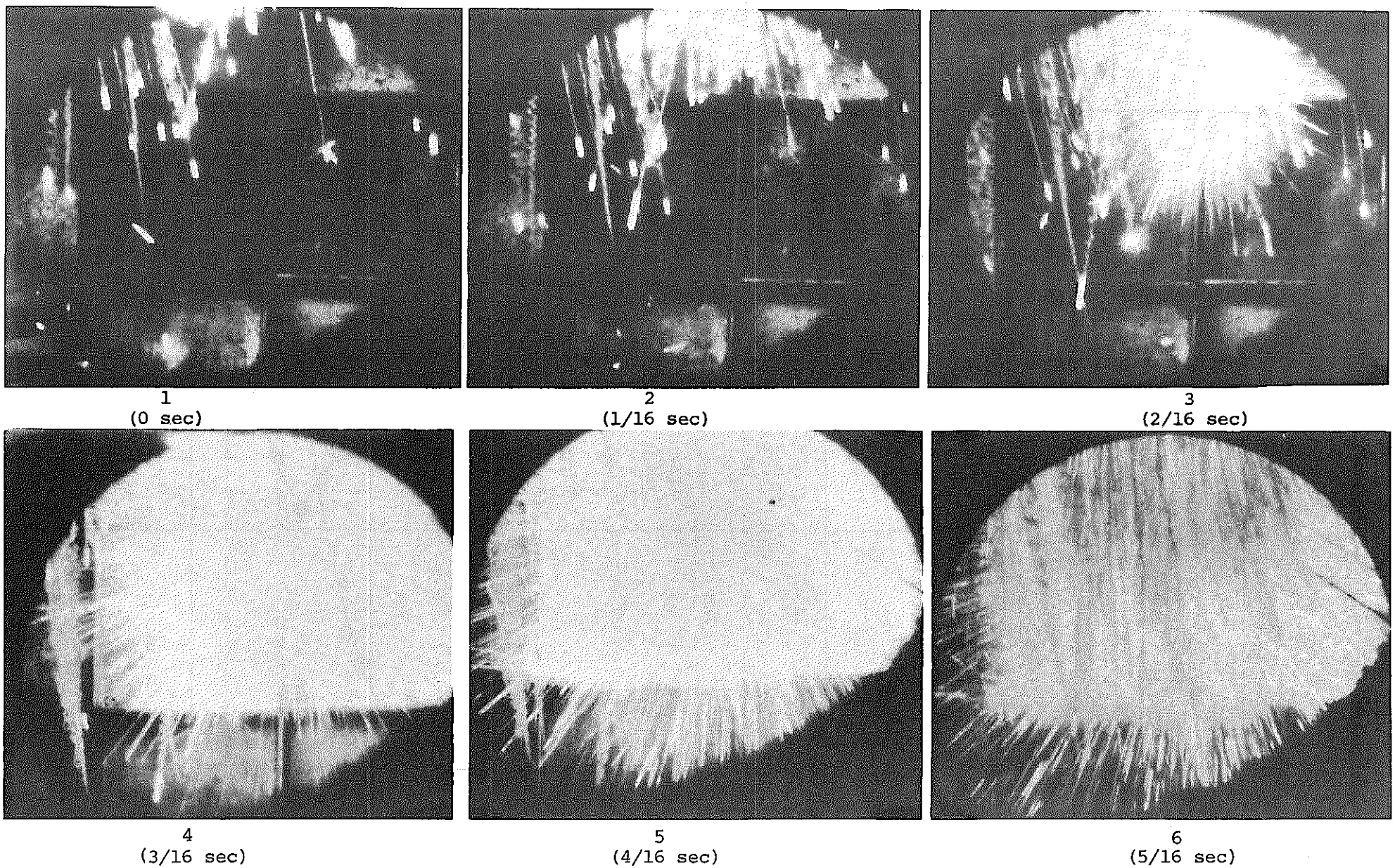

Fig. 5.6 (7) TASP-A1 Data ; Photograph of Spray Fire

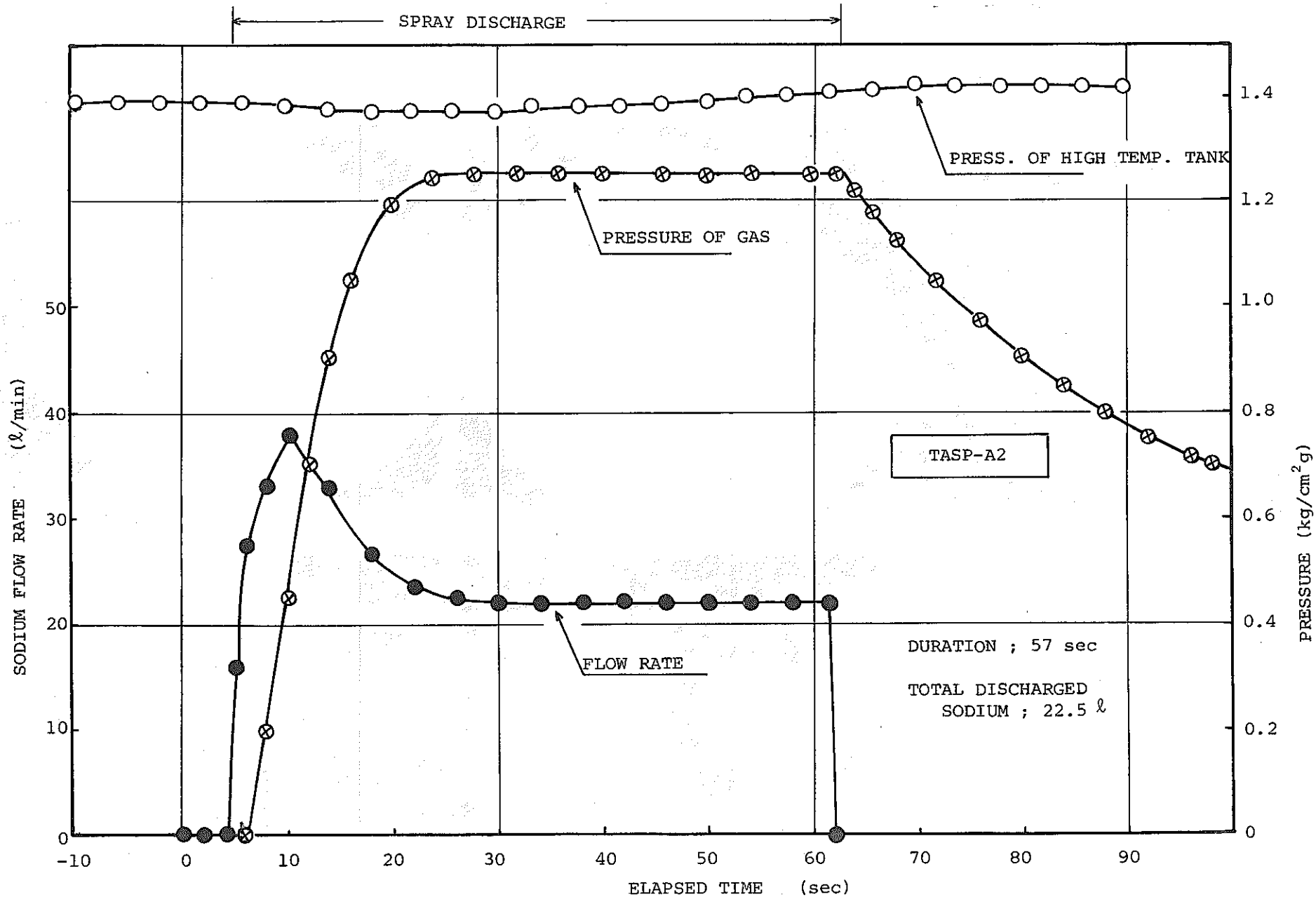

Fig.5.7(1) TASP-A2 Data ; Sodium Discharge Flow Rate

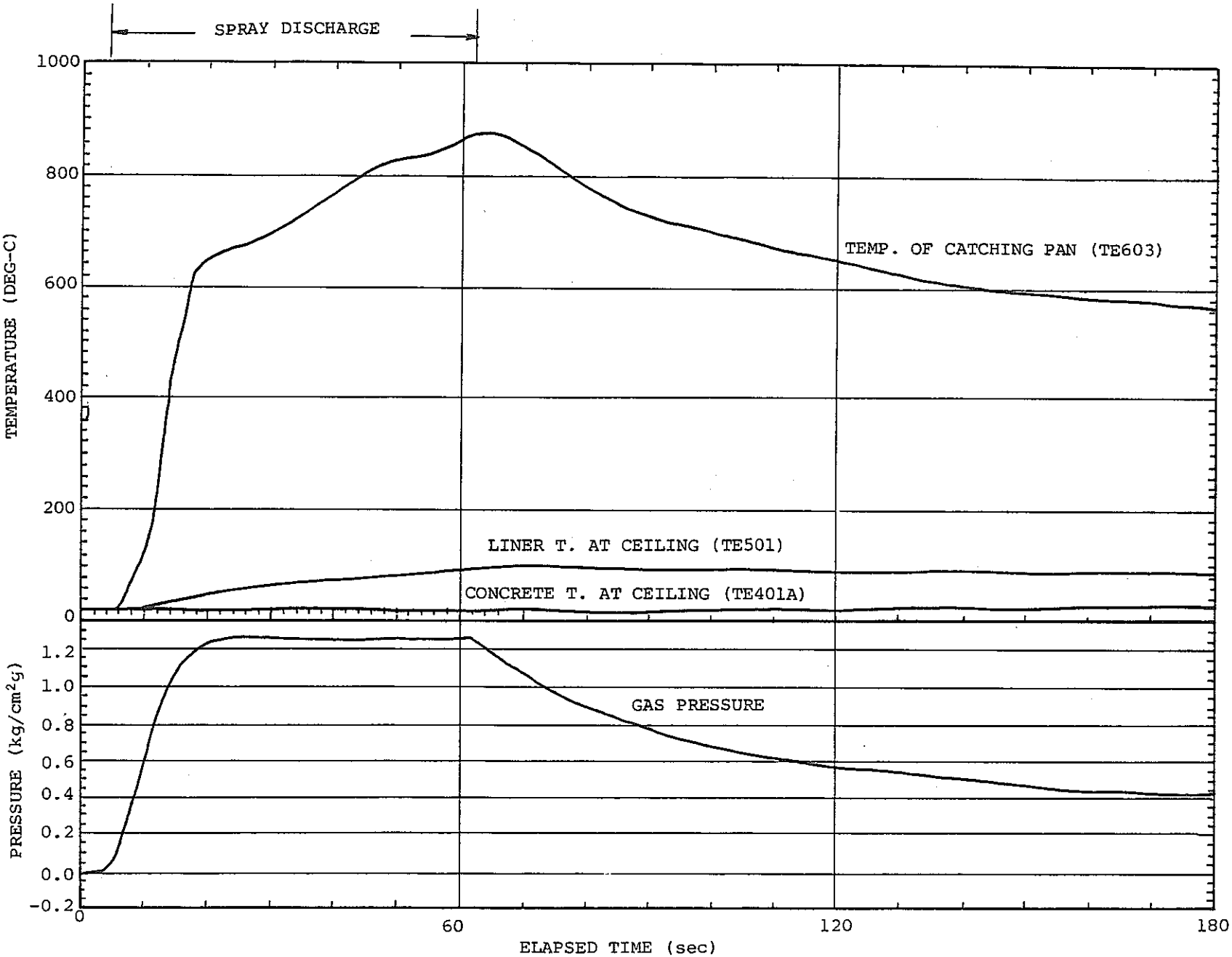

Fig.5.7(2) TASP-A2 Data ; Pressure and Temperature Distribution

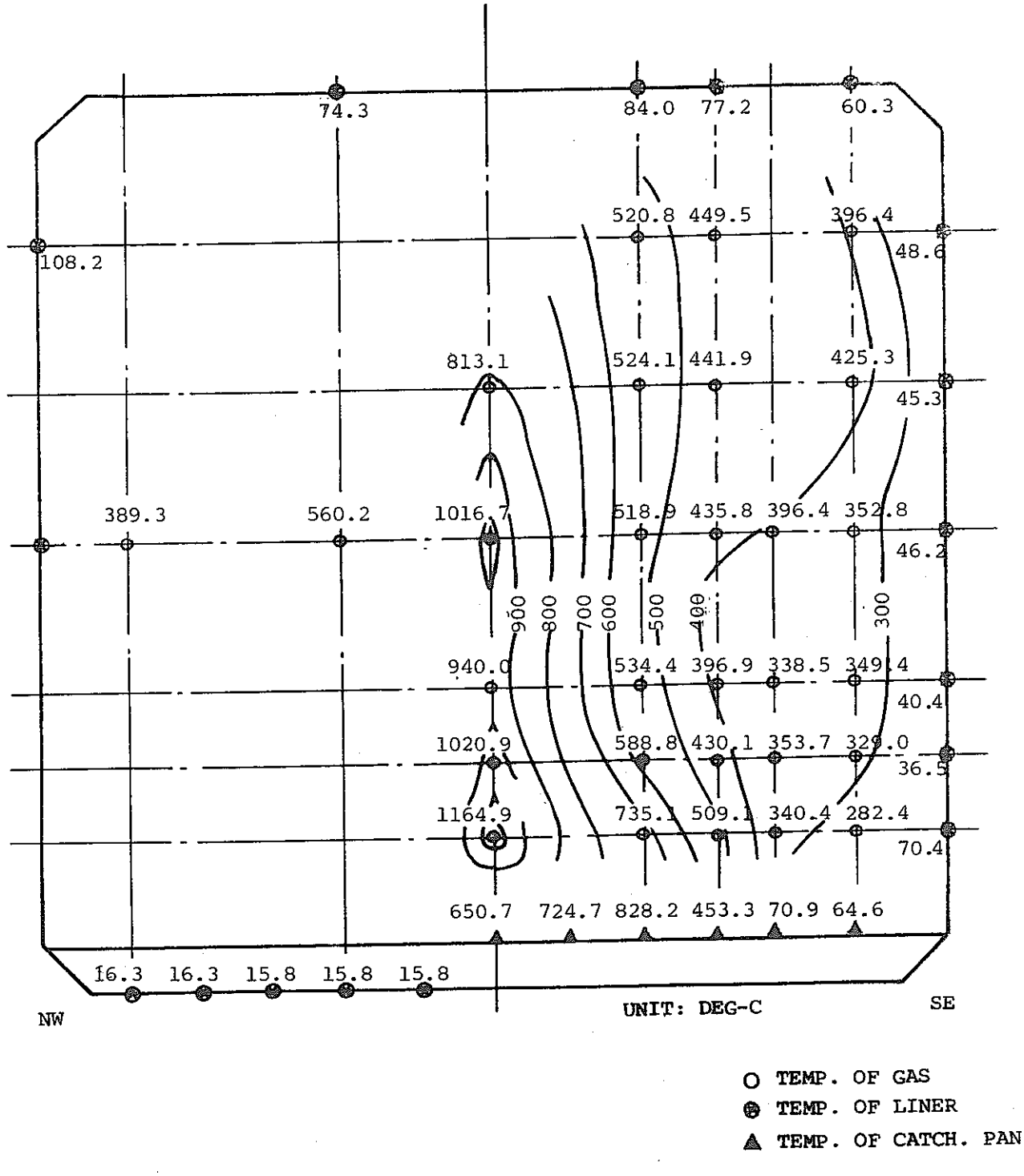

Fig.5.7(3) TASP-A2 Data ; Temperature Distribution

(Elapsed Time = 50 sec)

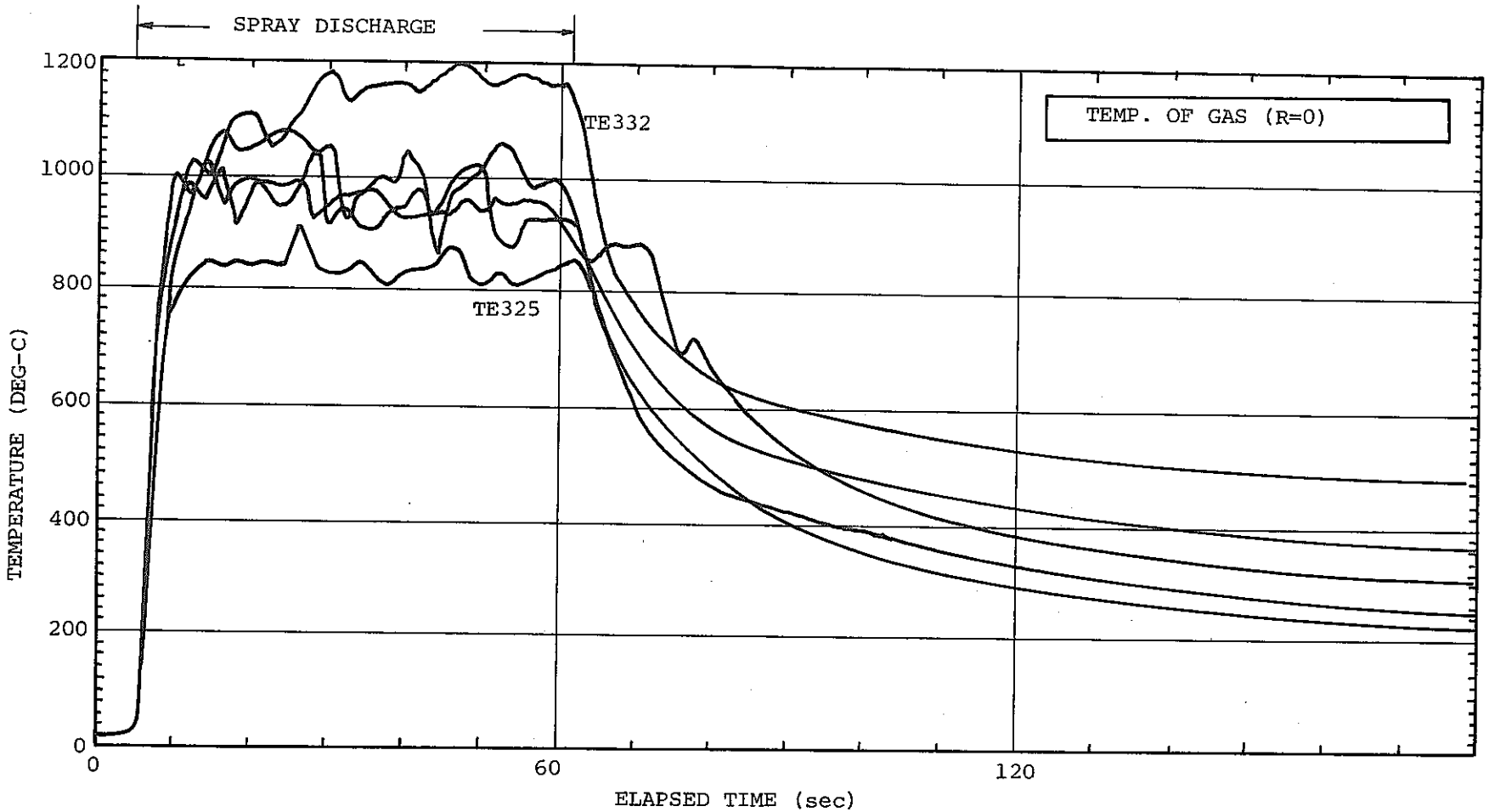

Fig. 5.7(4) TASP-A2 Data ; Gas Temperature

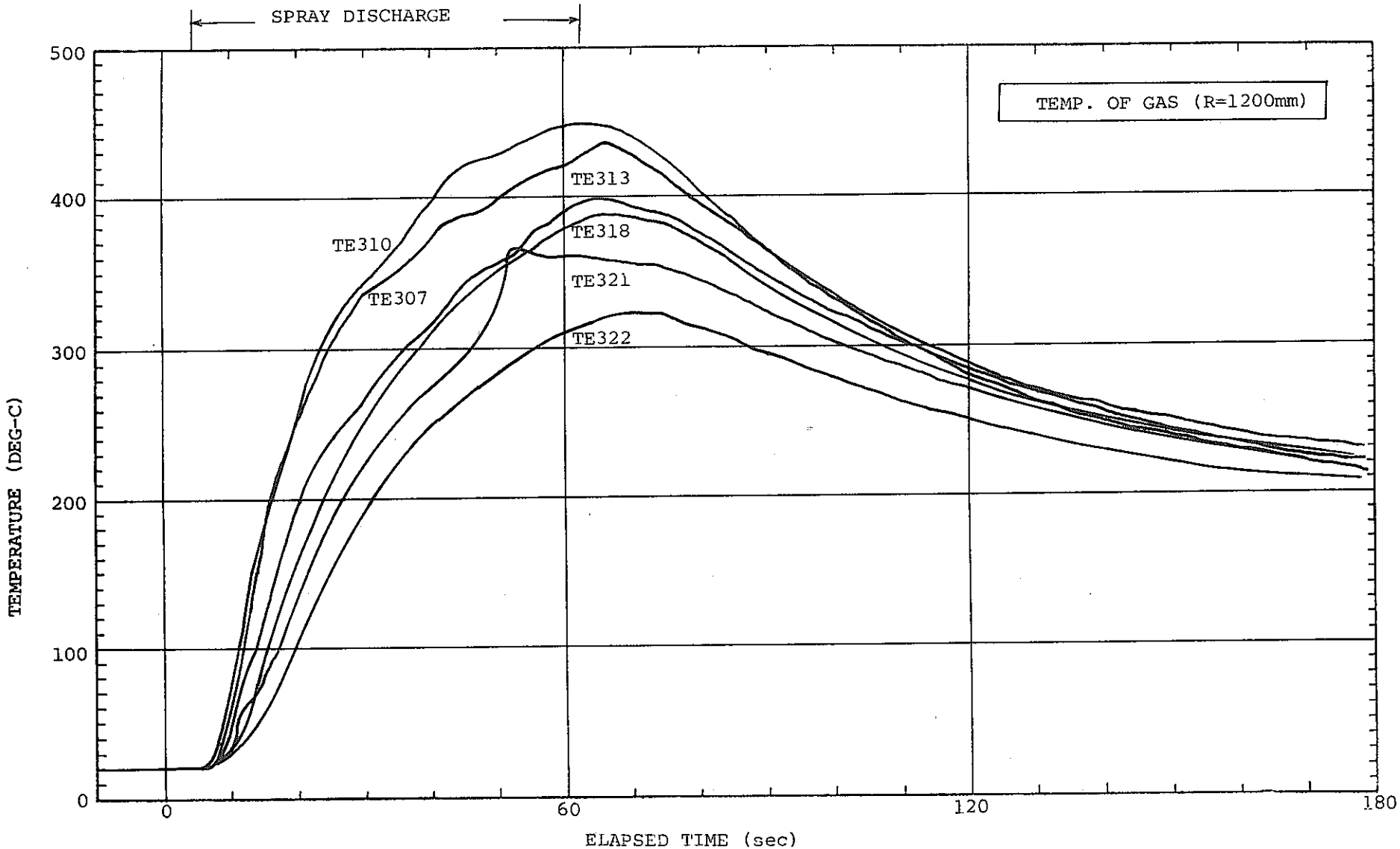

Fig.5.7(5) TASP-A2 Data ; Gas Temperature

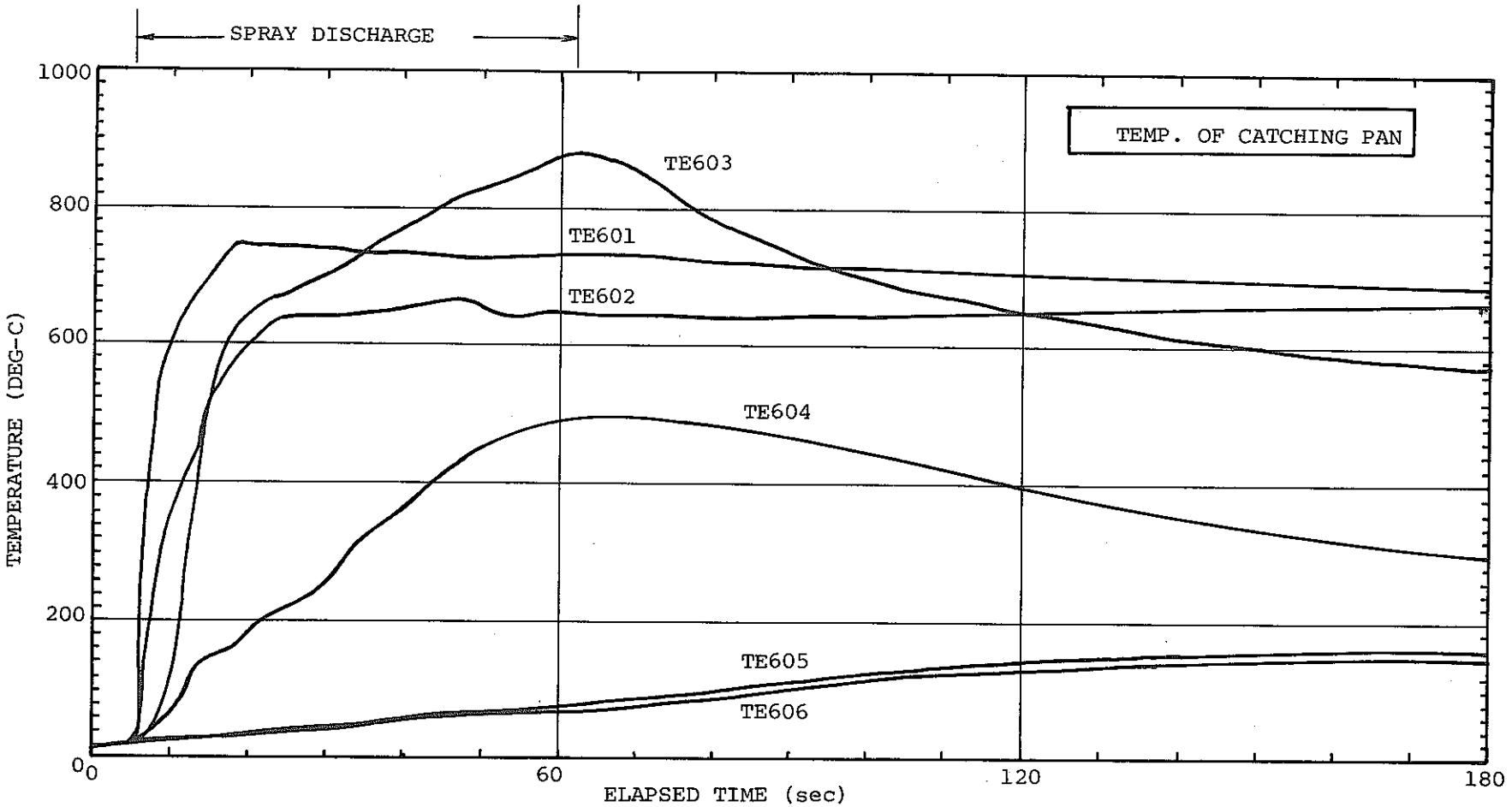

Fig.5.7(6) TASP-A2 Däta ; Temperature of Catching Pan

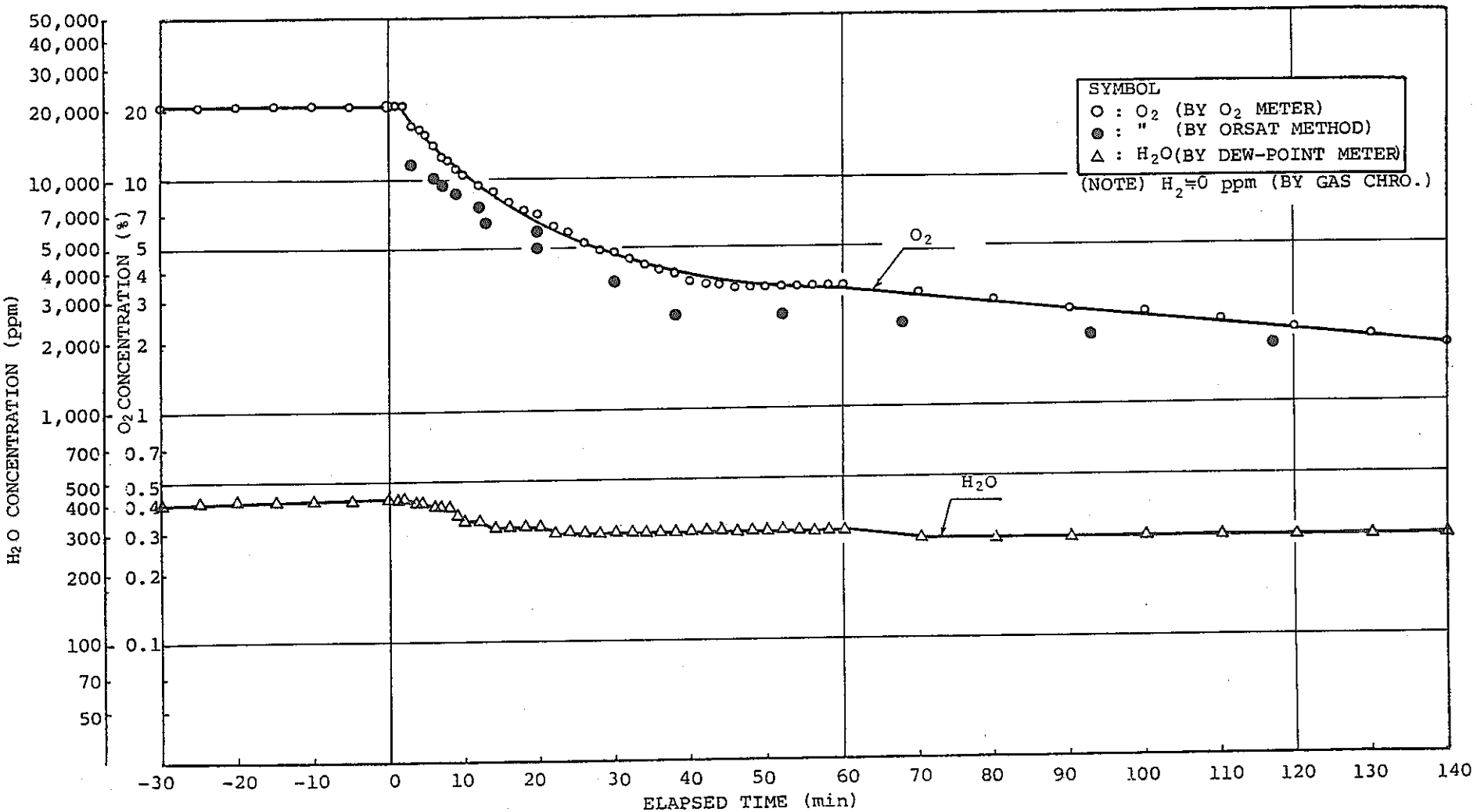

Fig.5.7(7) TASP-A2 Data ; Gas Concentration

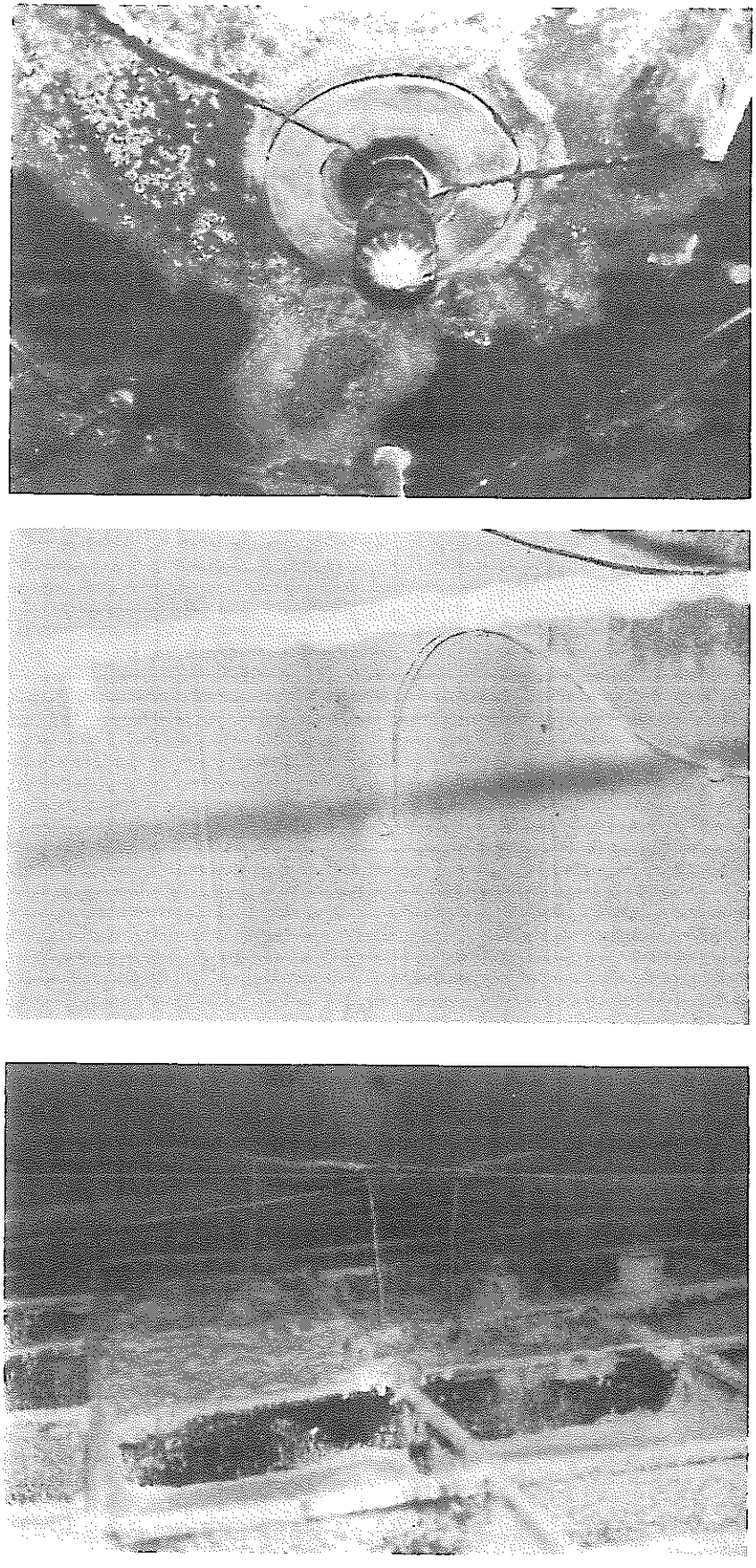

Fig. 5.7(8) TASP-A2 Data ; Photograph of View After Test

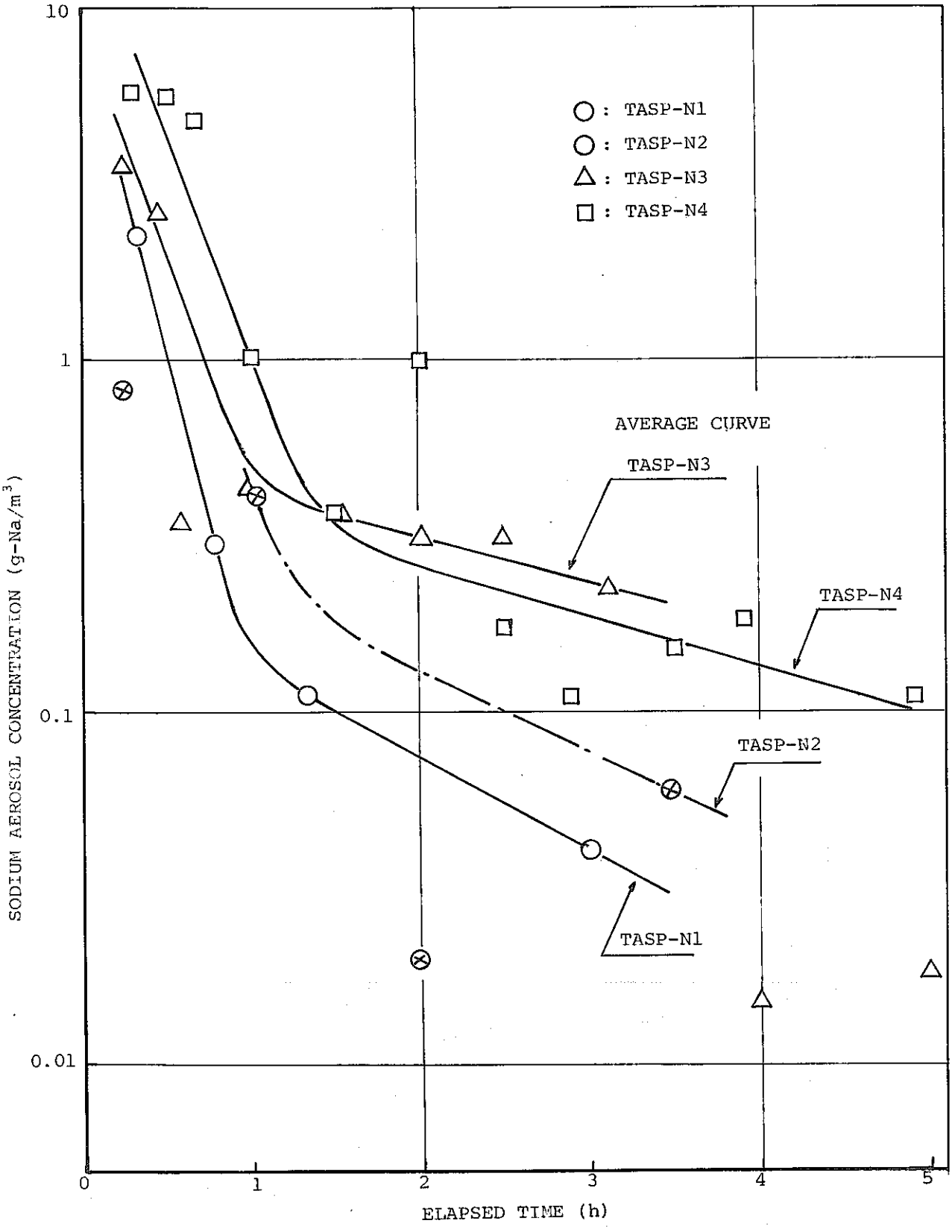

Fig.5.8(1) Sodium Aerosol Concentration (TASP-N1 ∿N4)

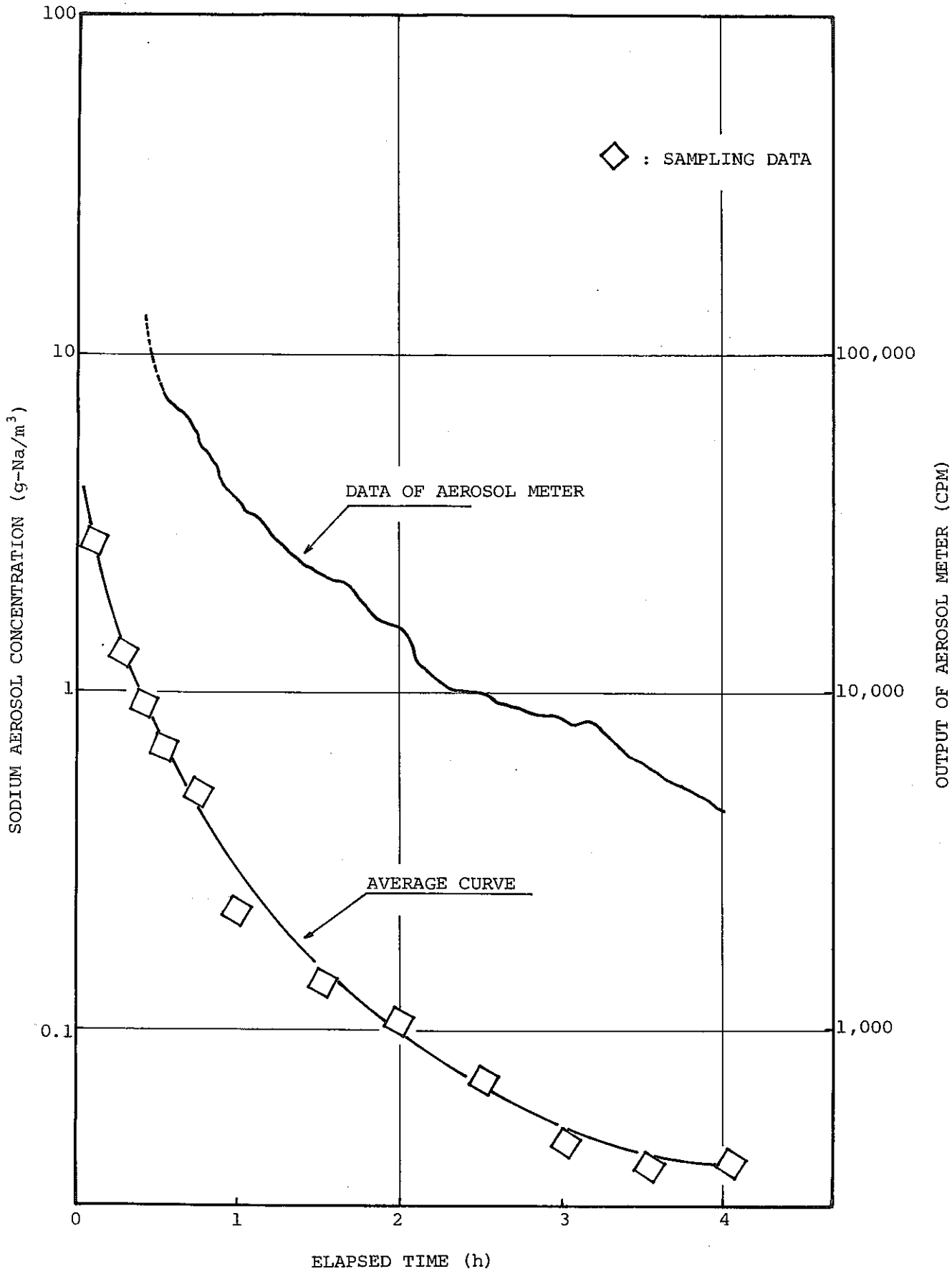

Fig.5.8(2) Sodium Aerosol Concentration (TASP-N5)

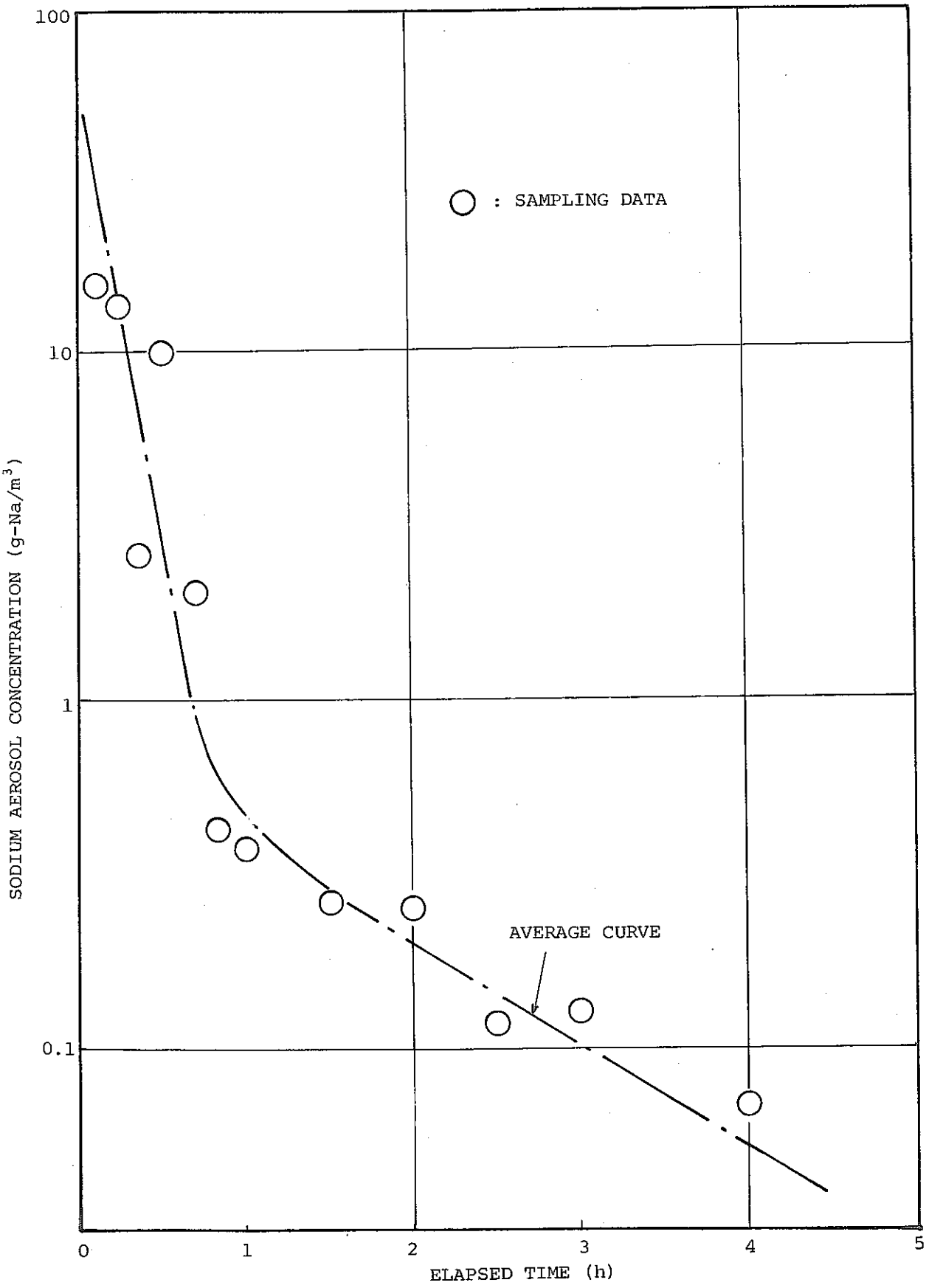

Fig.5.8(3) Sodium Aerosol Concentration (TASP-A2)

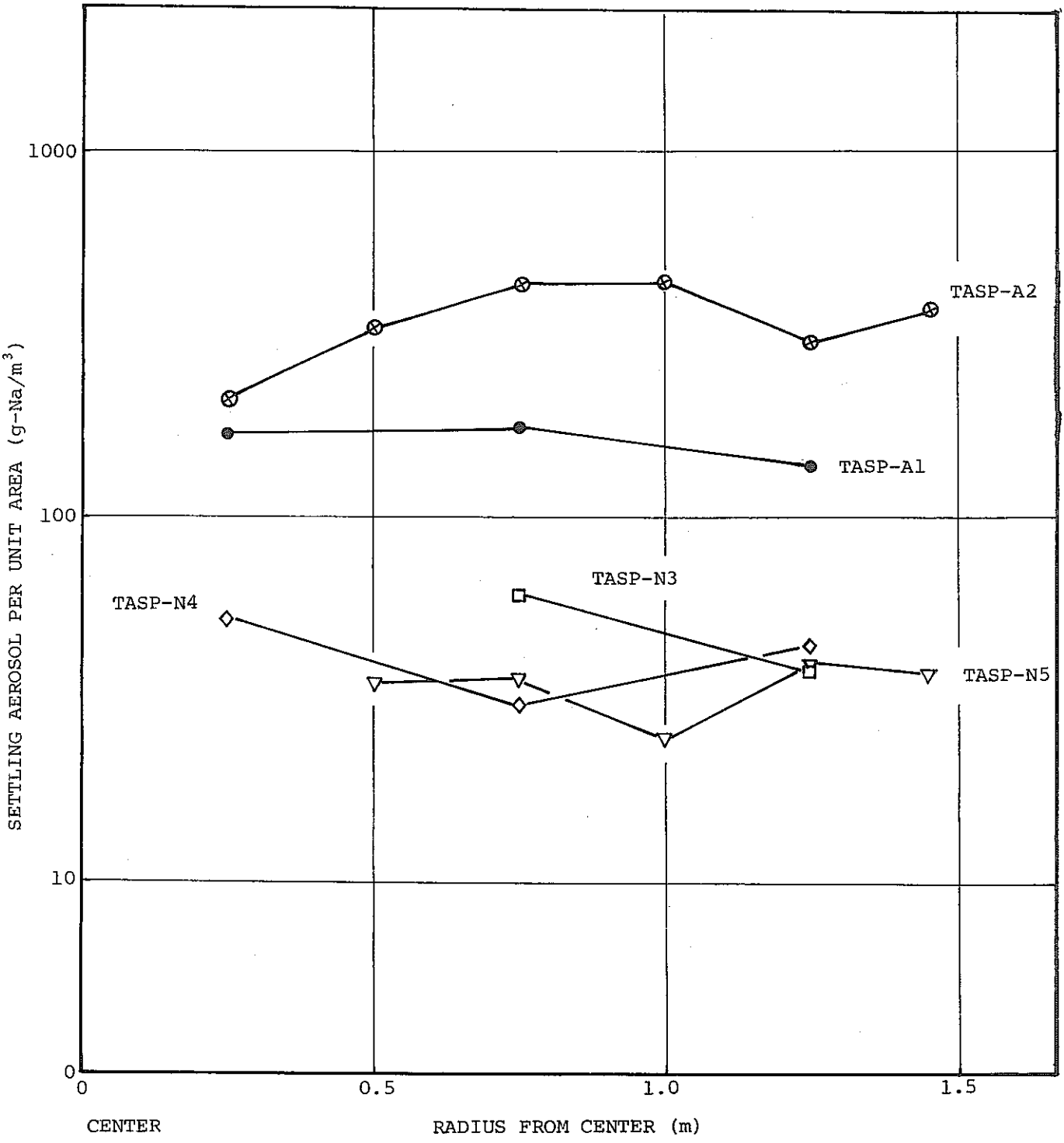

Fig.5.9 Total Amount of Settling Aerosol

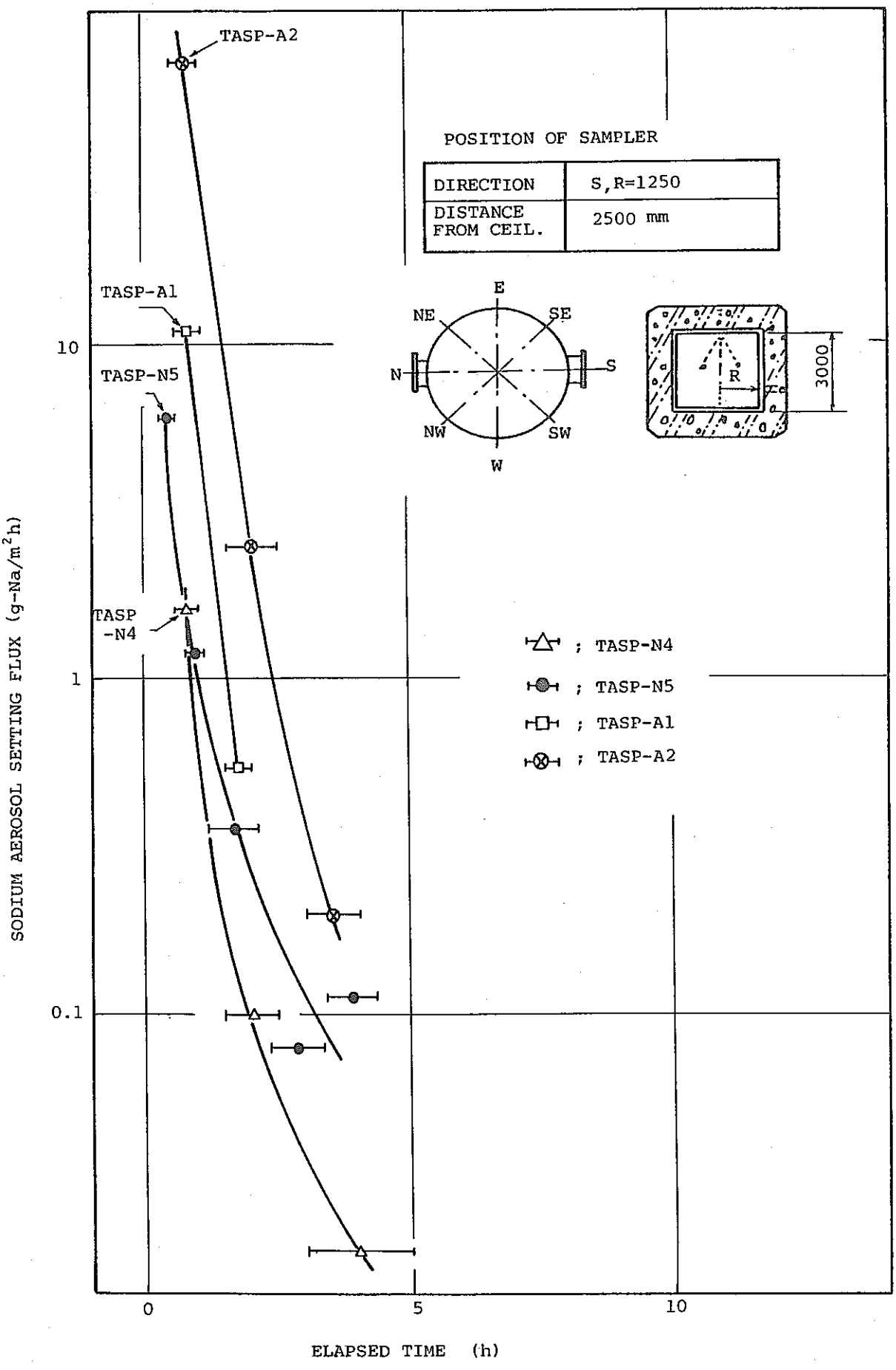

Fig.5.10 Transition of Aerosol Settling Flux

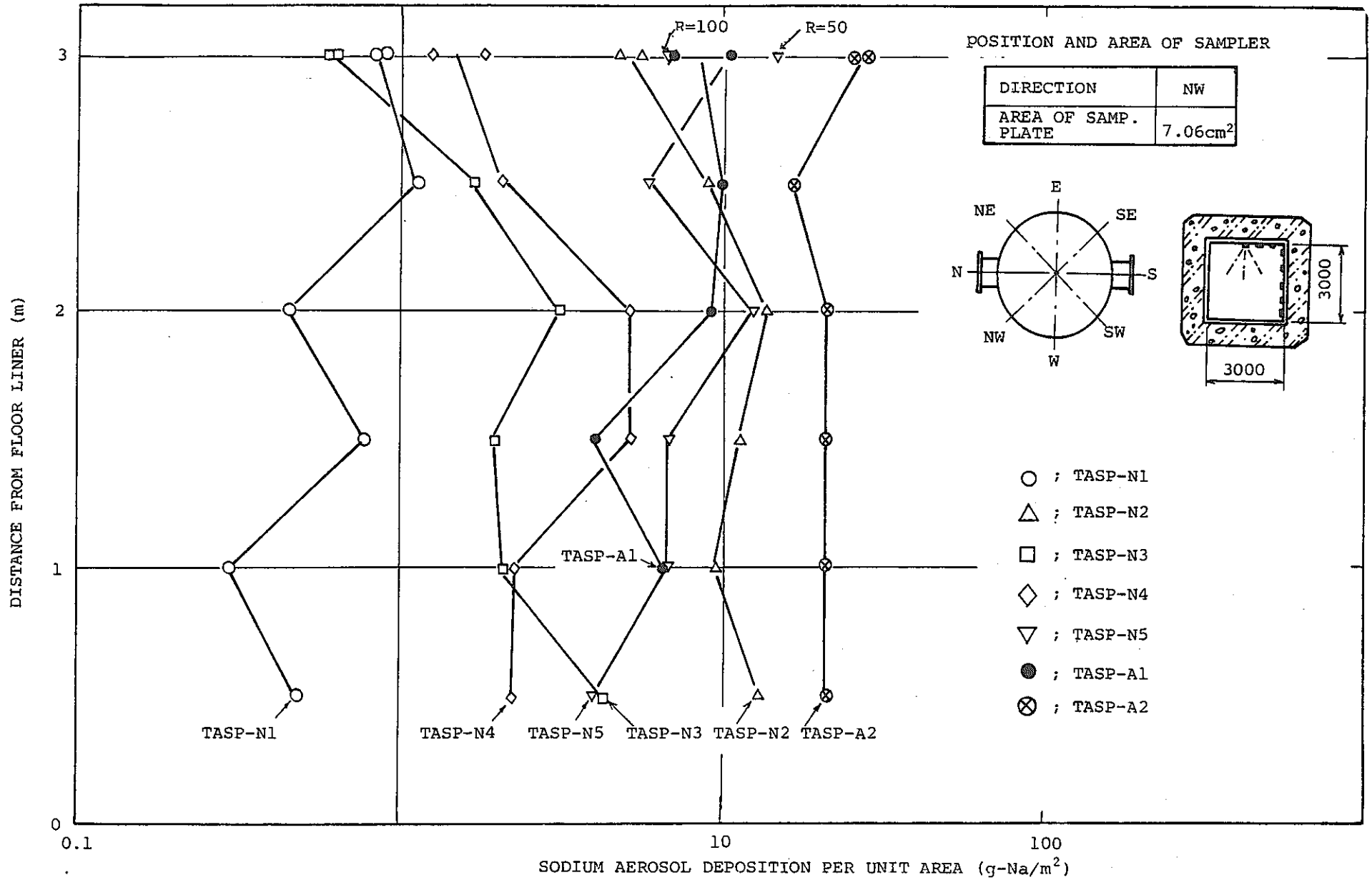

Fig.5.11(1) Total Amount of Aerosol Deposition

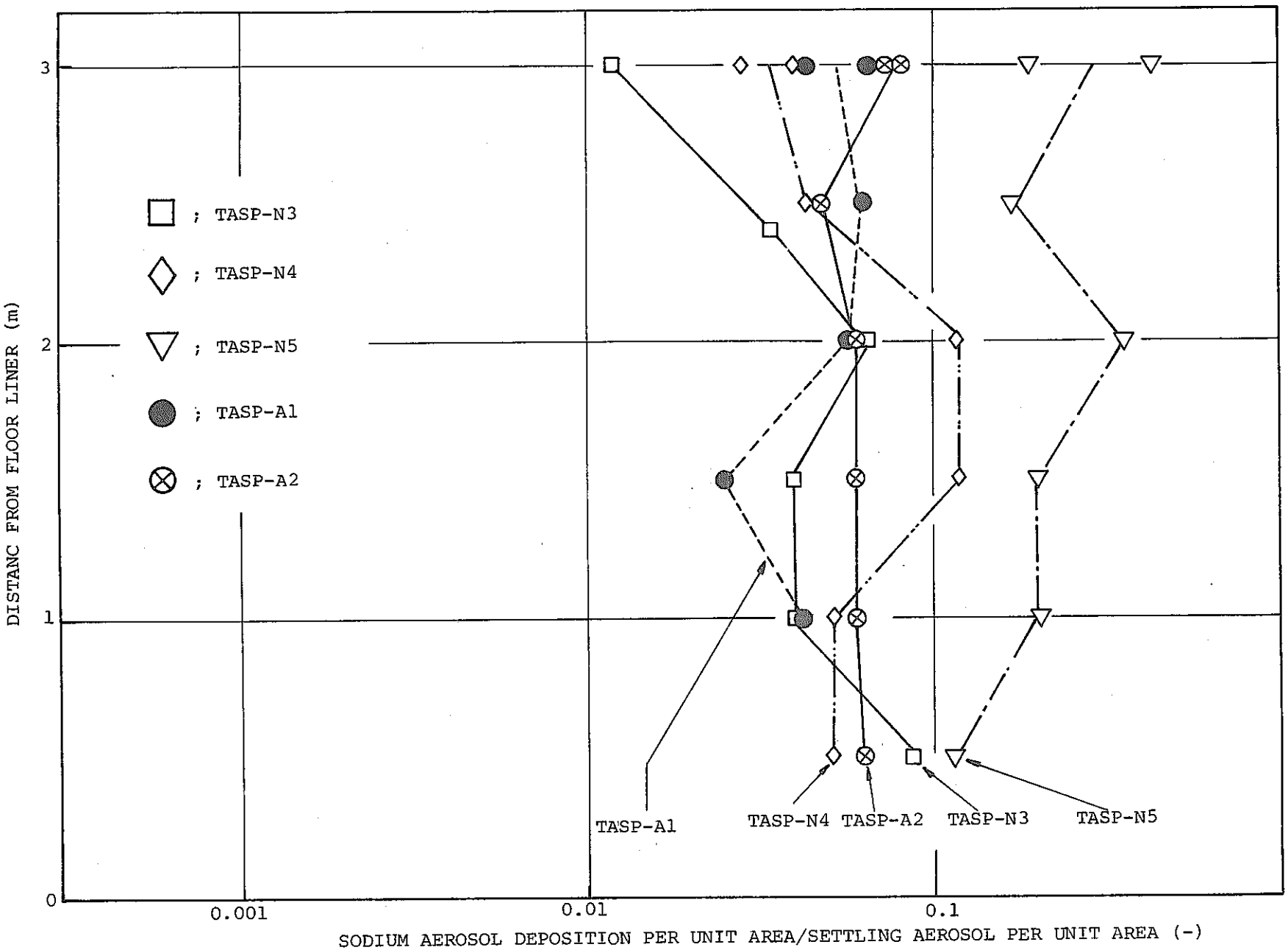

Fig.5.11(2) Total Amount of Aerosol Deposition

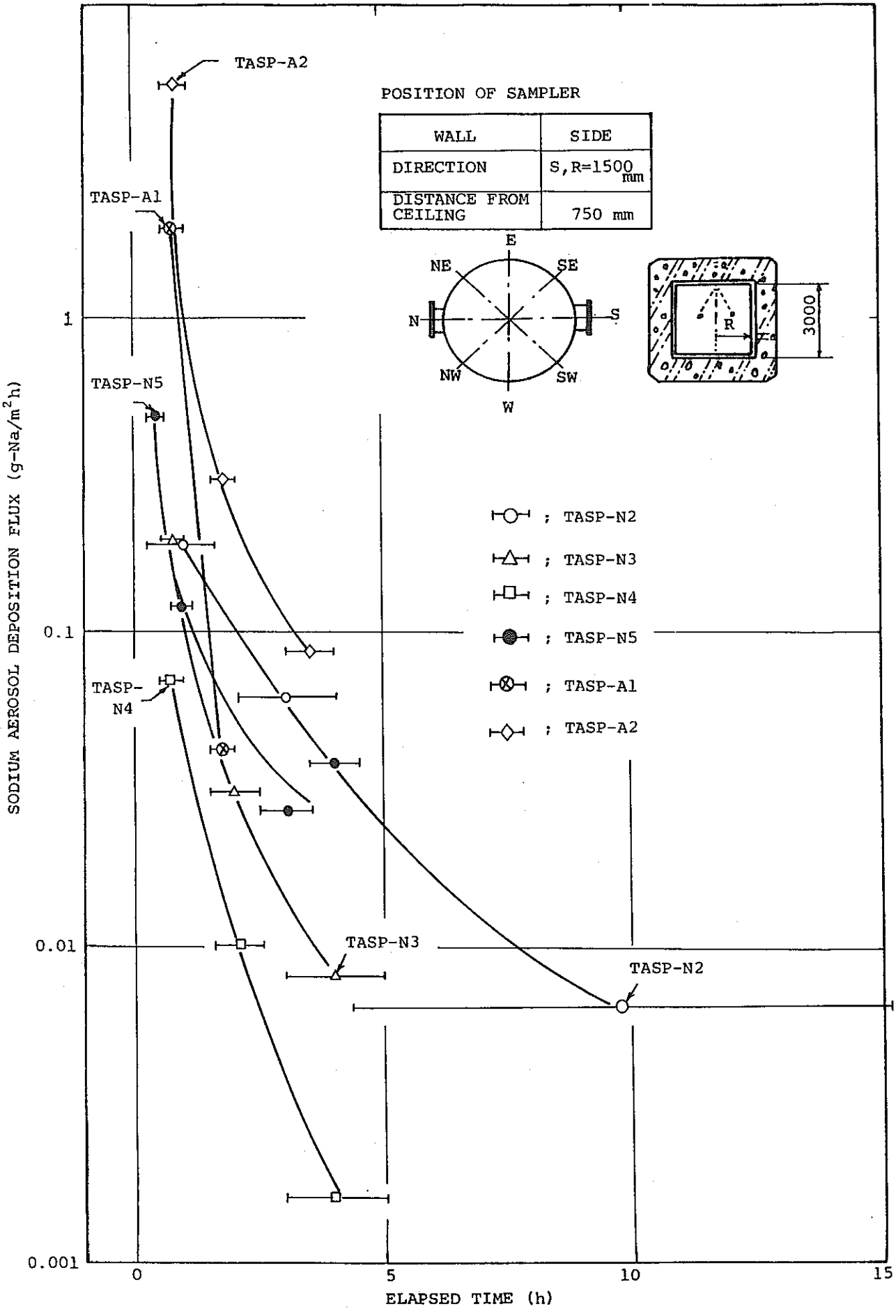

Fig.5.12 Transition of Aerosol Deposition Flux to Side Wall

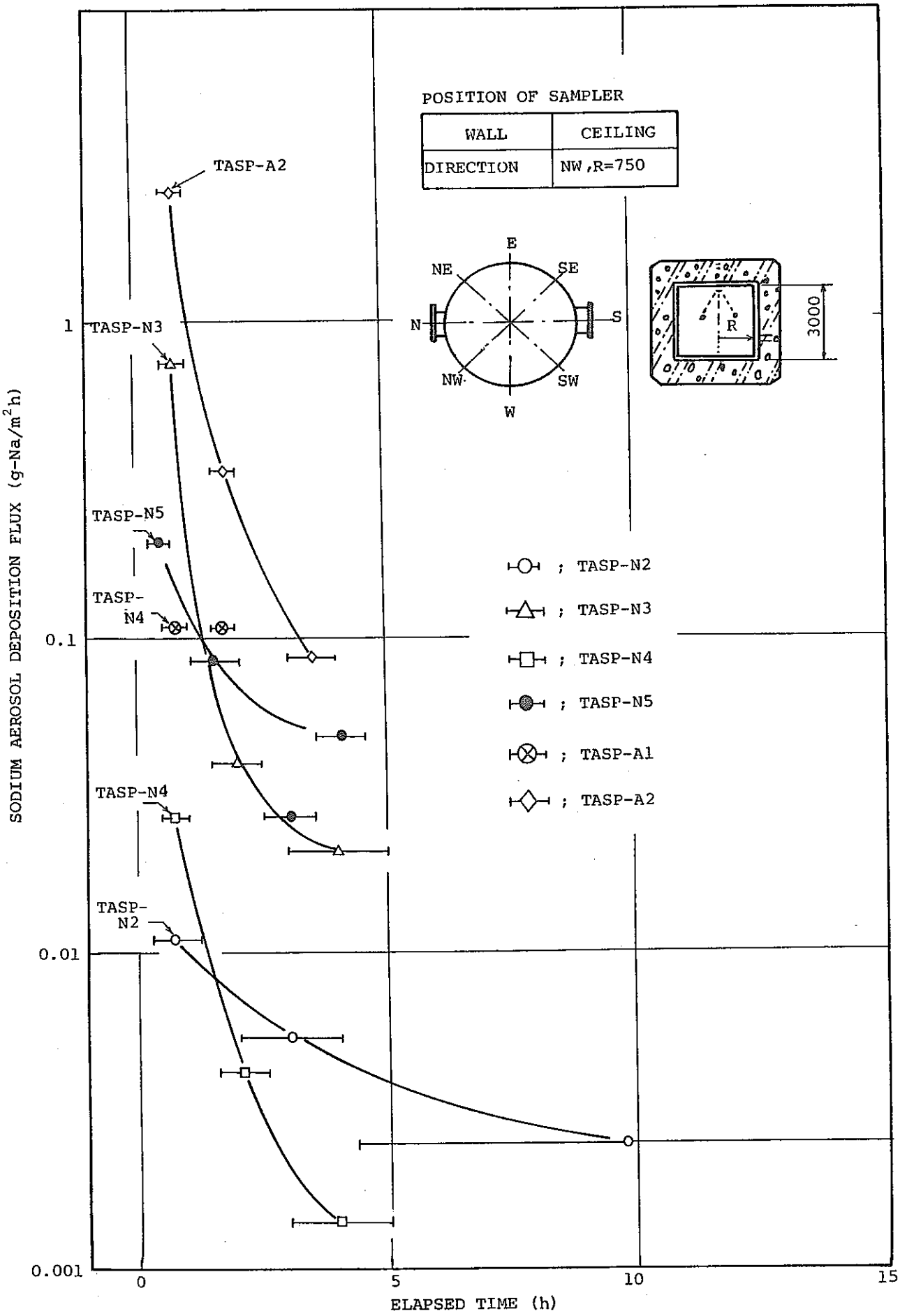

Fig.5.13 Transition of Aerosol Deposition Flux to Ceiling Wall

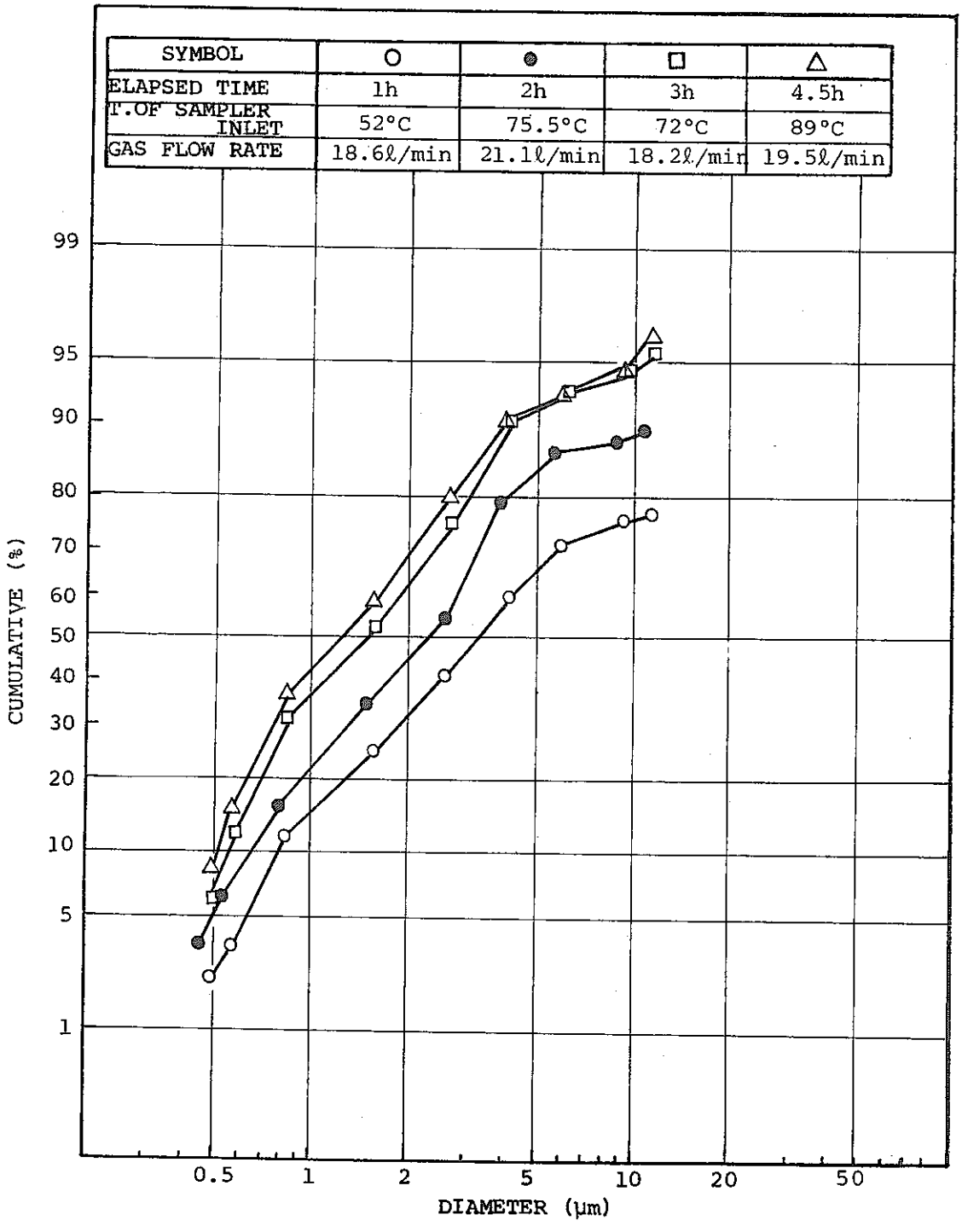

Fig.5.14(1) Aerosol Particle Diameter Distribution (TASP-N3)

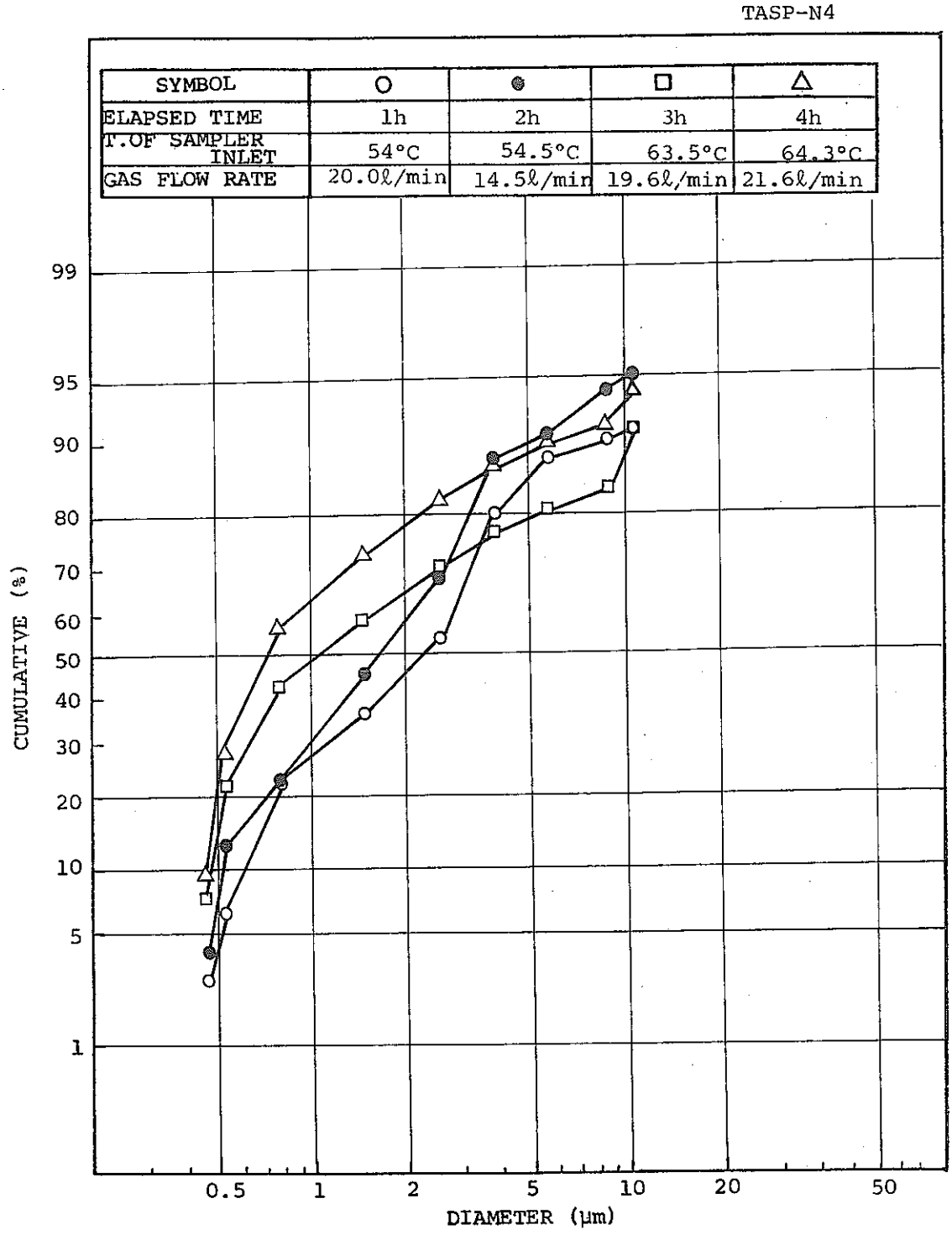

Fig.5.14(2) Aerosol Particle Diameter Distribution (TASP-N4)

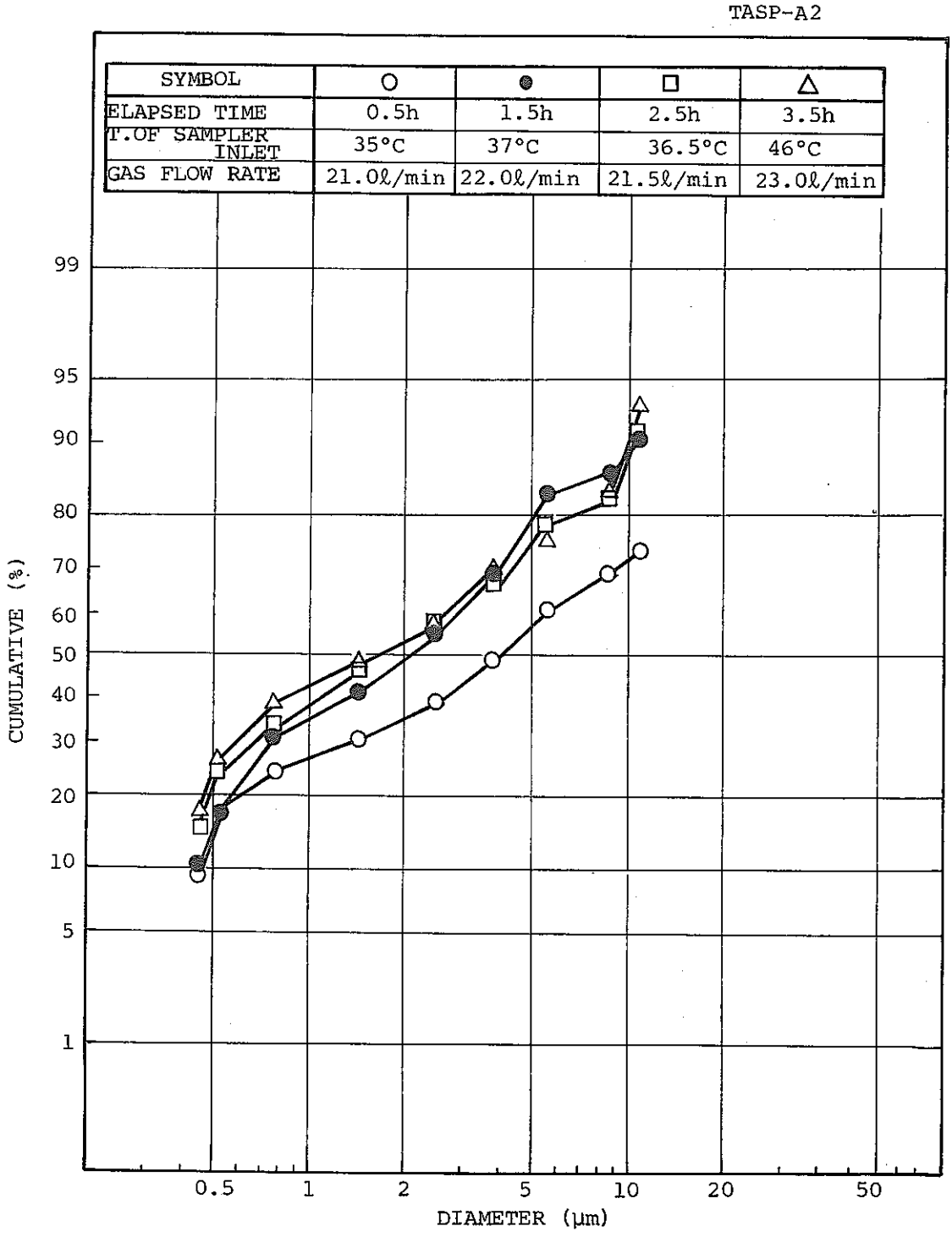

Fig.5.14(3) Aerosol Particle Diameter Distribution (TASP-A2)

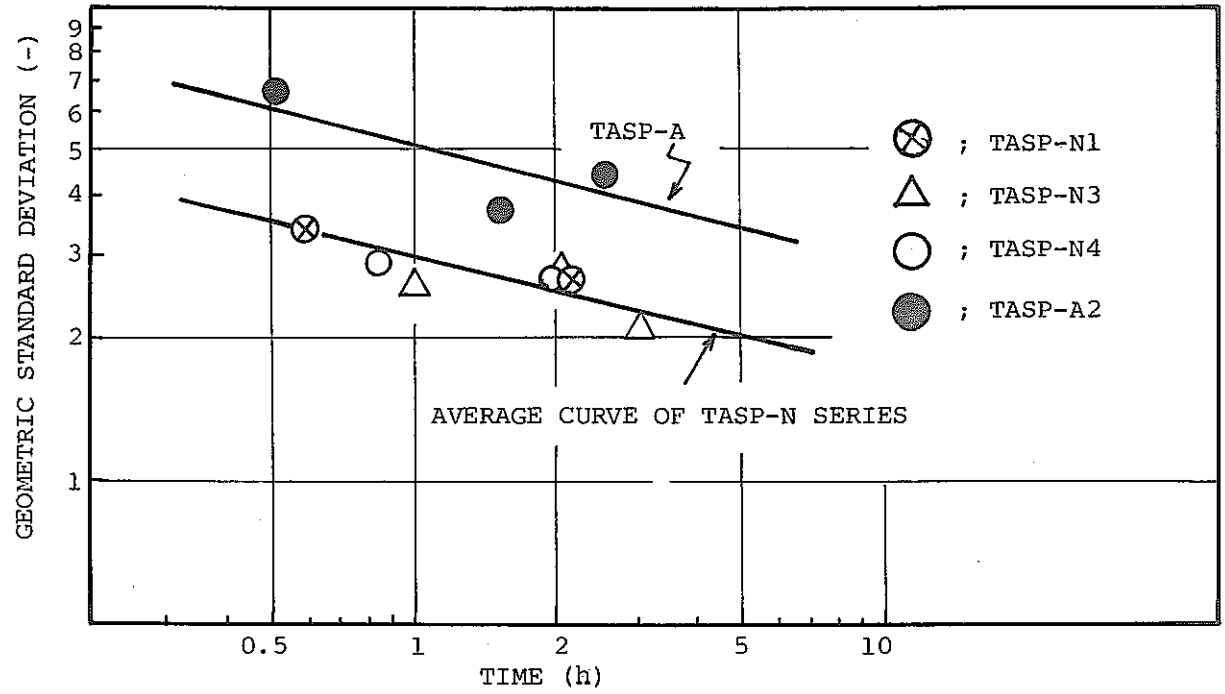

Fig.5.15 Standard Deviation for Aerosol Particle Diameter Distribution

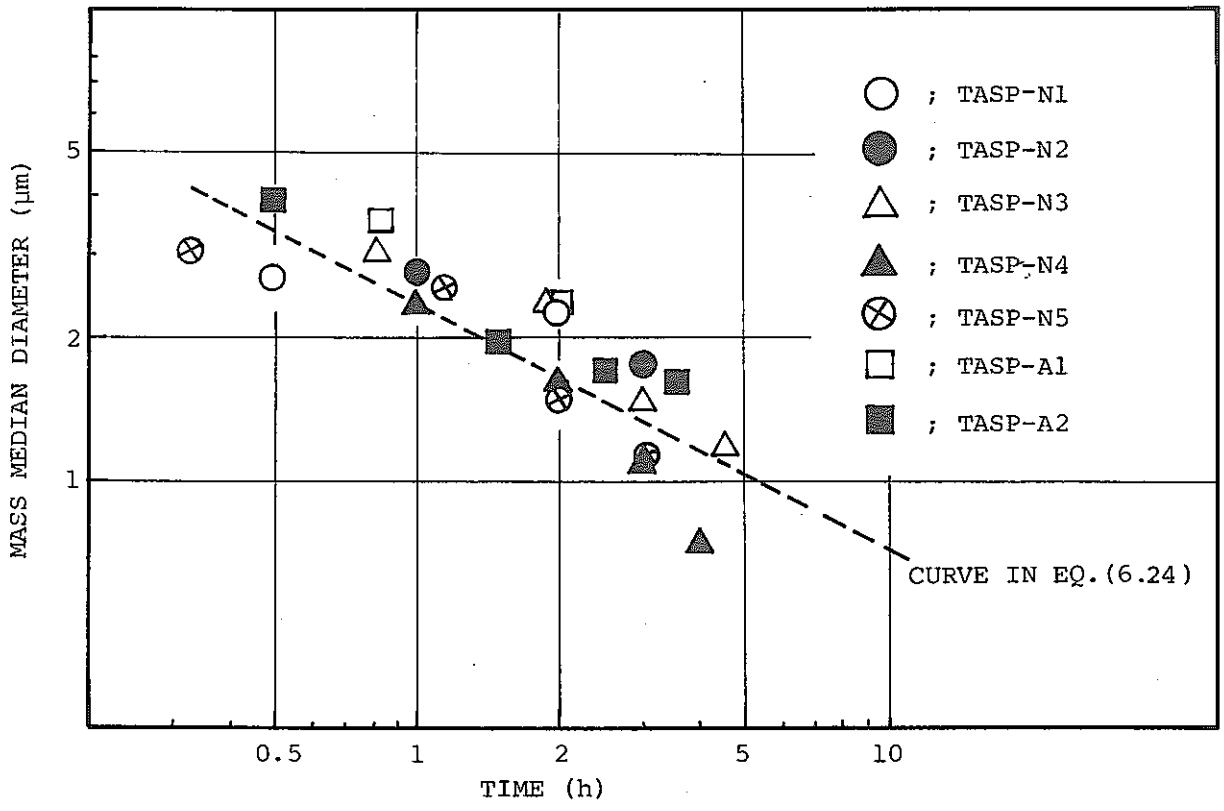

Fig.5.16 Transition of Aerosol Mass Median Diameter

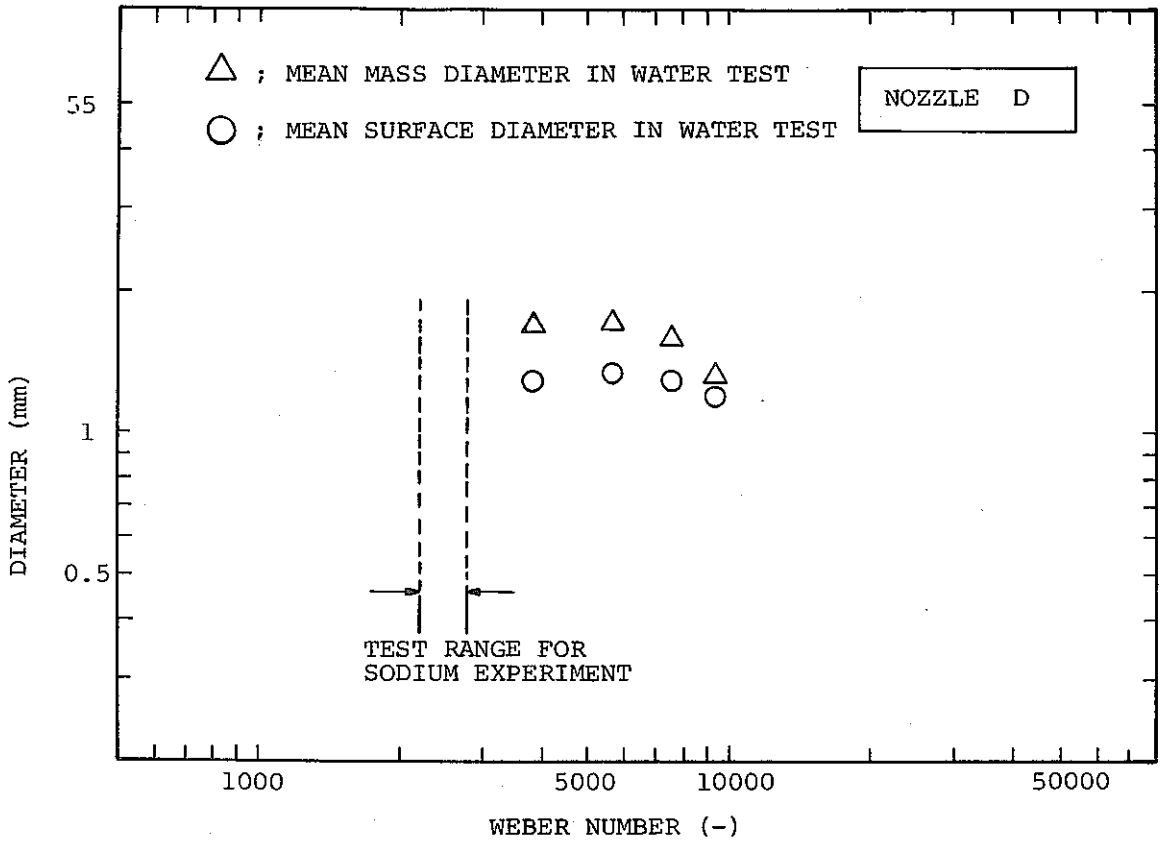

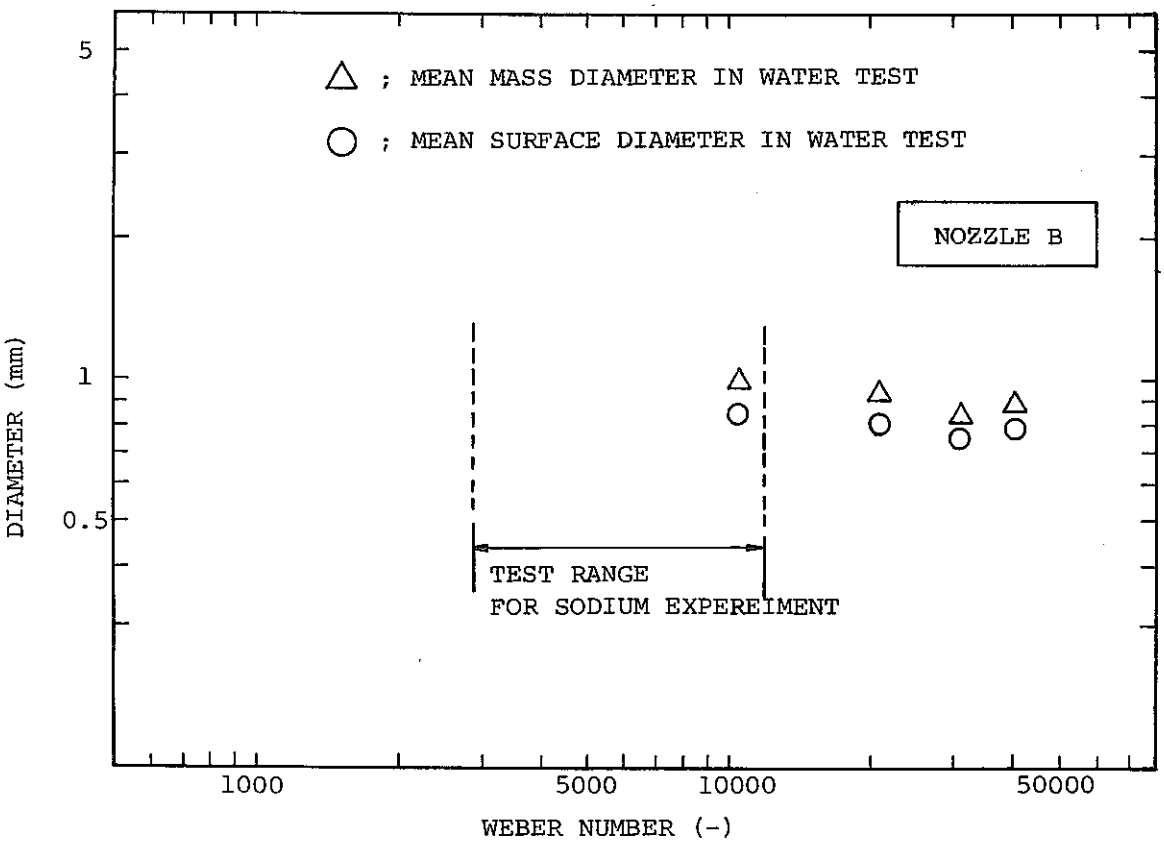

Fig.6.1 Mean Diameter Versus Weber Number

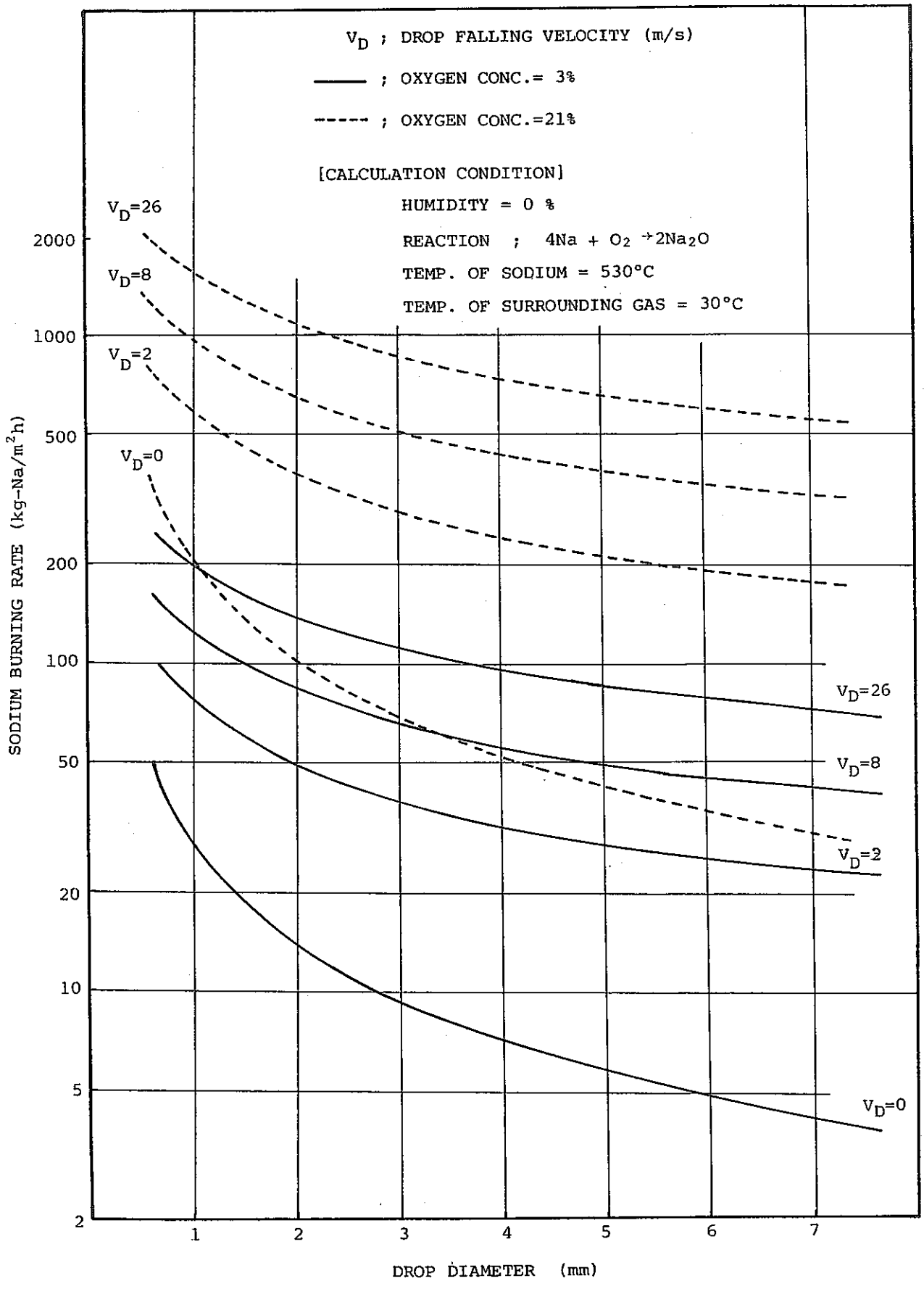

Fig.6.2(1) Parameter Search for Sodium Burning Rate

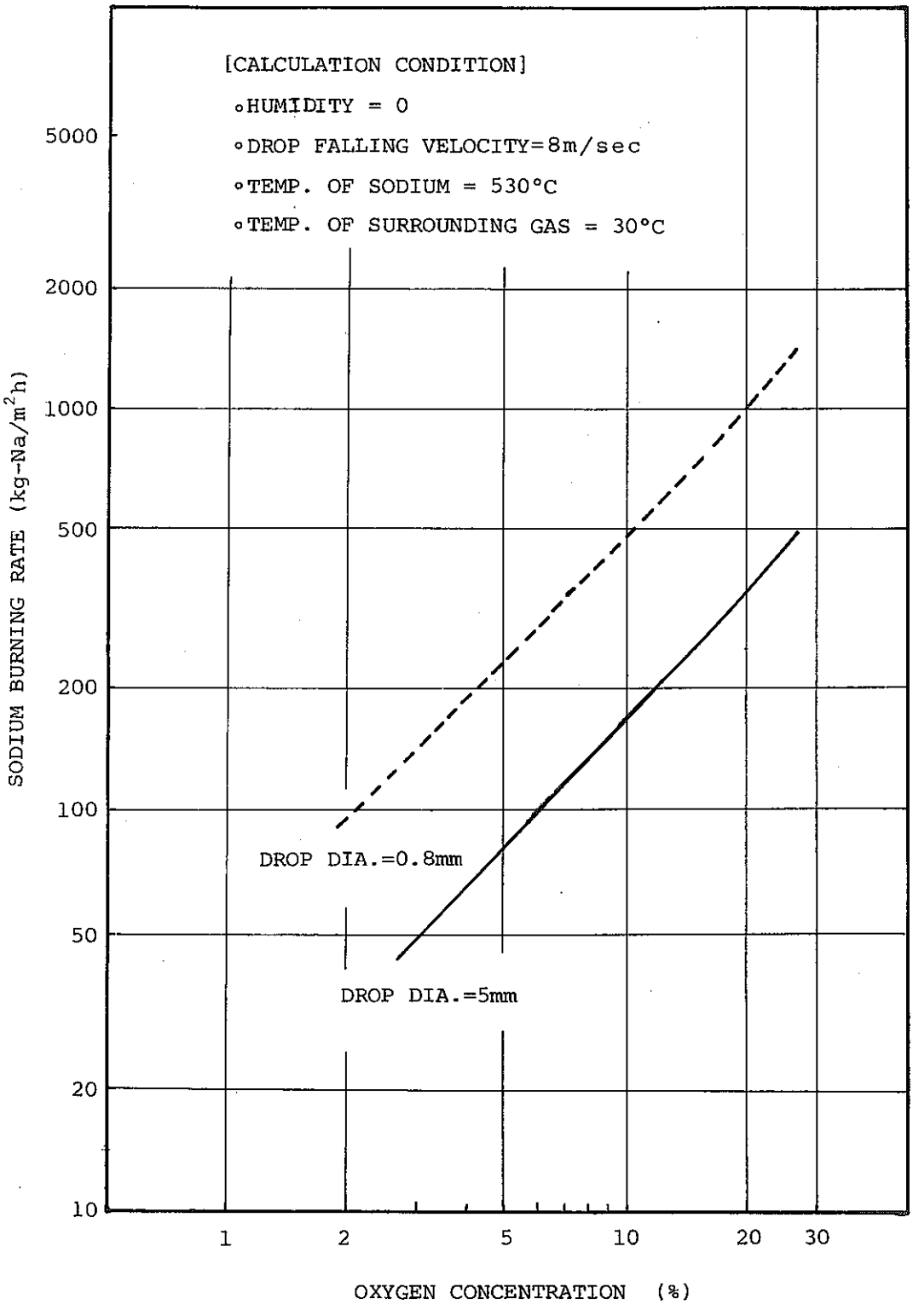

Fig.6.2 (2) Parameter Search for Sodium Burning Rate

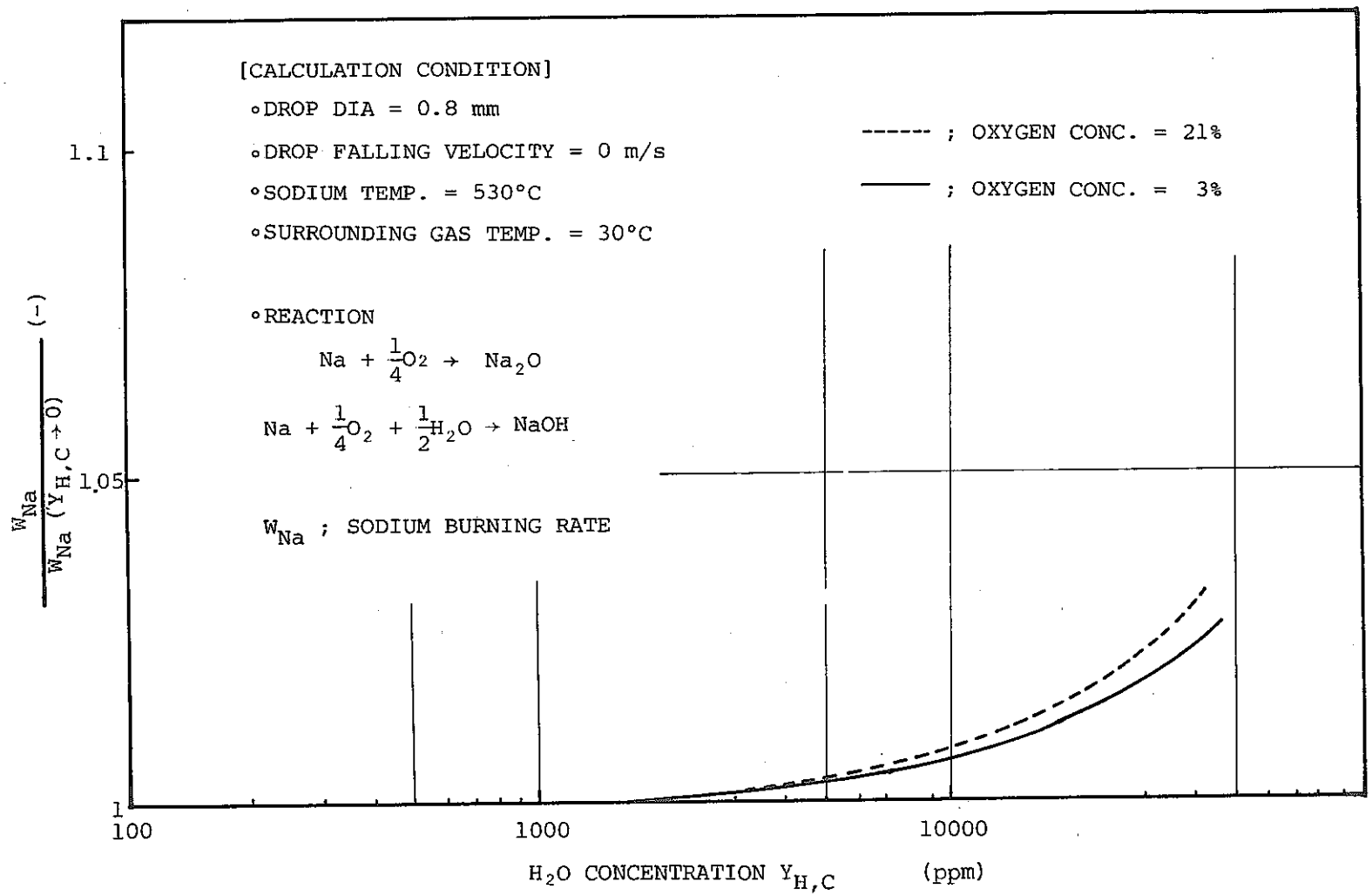

Fig.6.3(1) Effect of Humidity on Sodium Burning Rate

P ; PRESSURE

Tgas ; SURROUNDING GAS TEMPERATURE

Td ; DROP TEMPERATURE

Ya ; DROP RADIUS

Yo,c ; O_2 CONCENTRATION

Wna ; SODIUM BURNING RATE

Yn,c ; H_2O CONCENTRATION

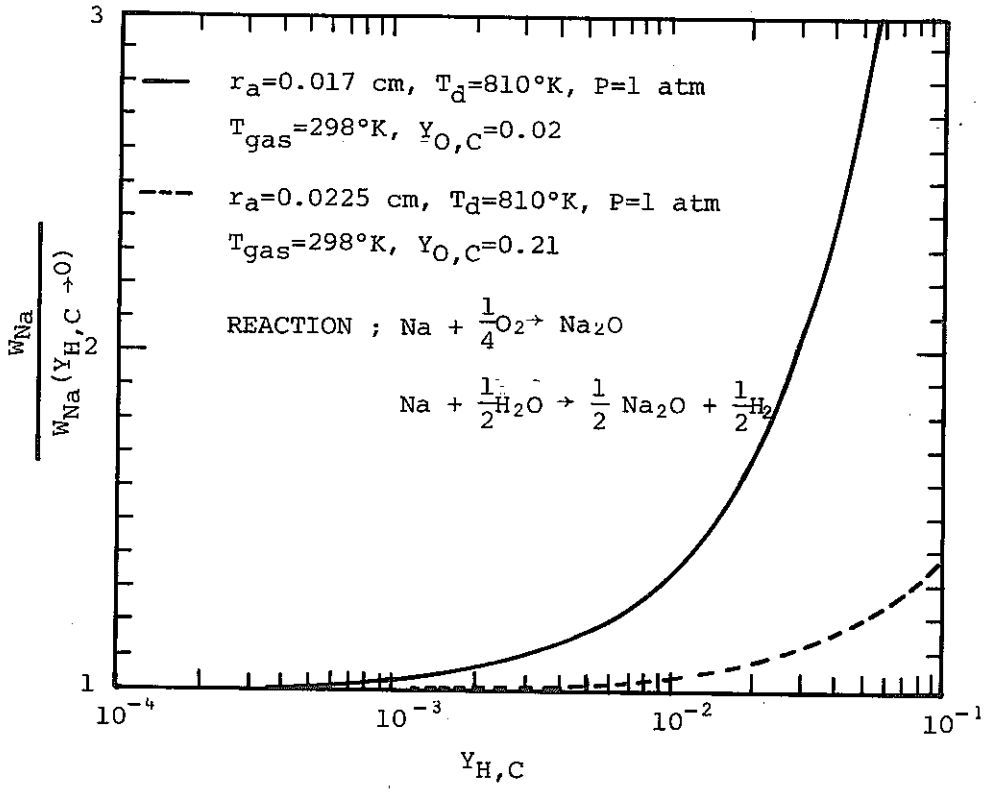

Fig.6.3(2) Effect of Humidity on Sodium Burning Rate

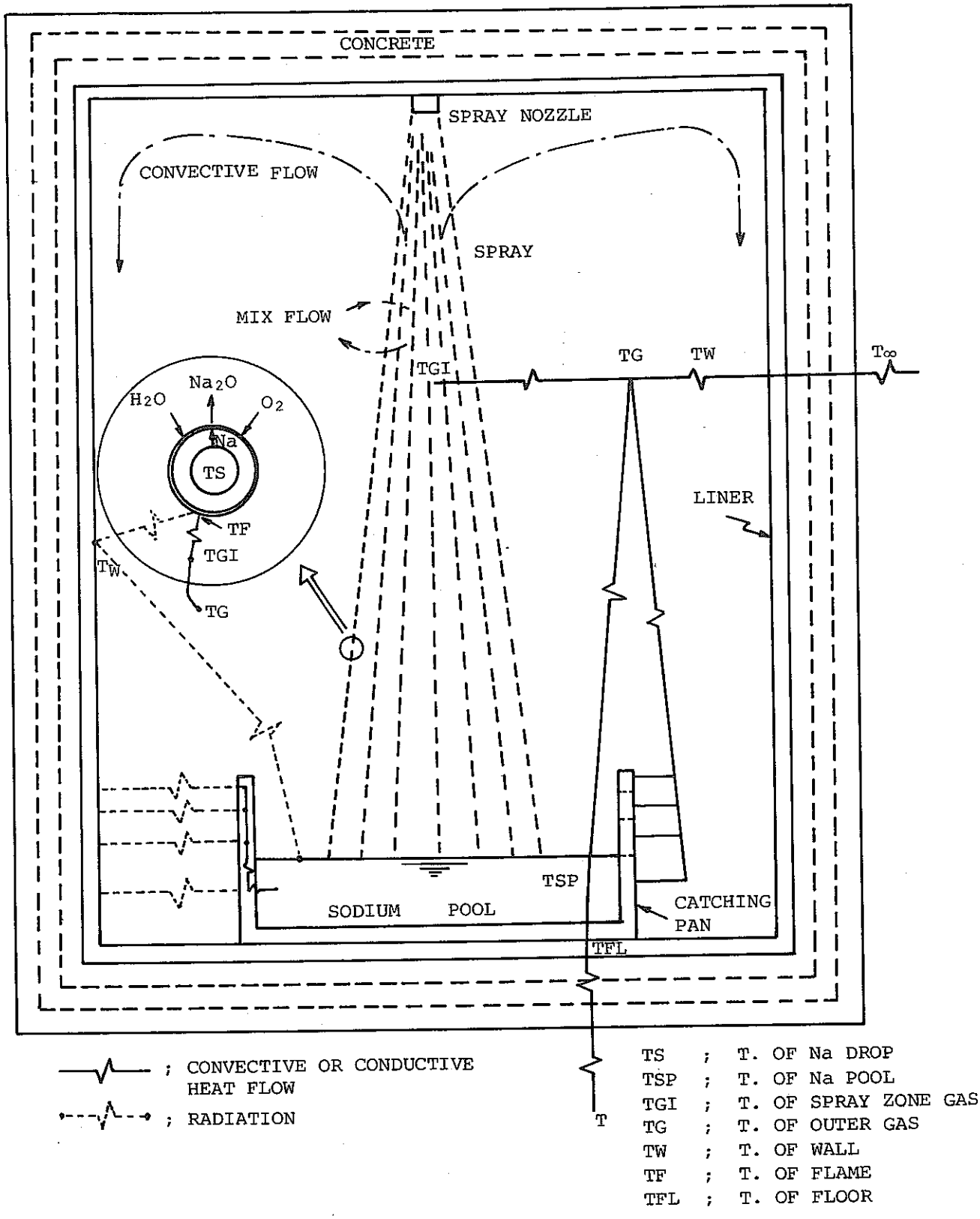

Fig.6.4 Heat and Mass Transfer Model of Spray Fire Calculation

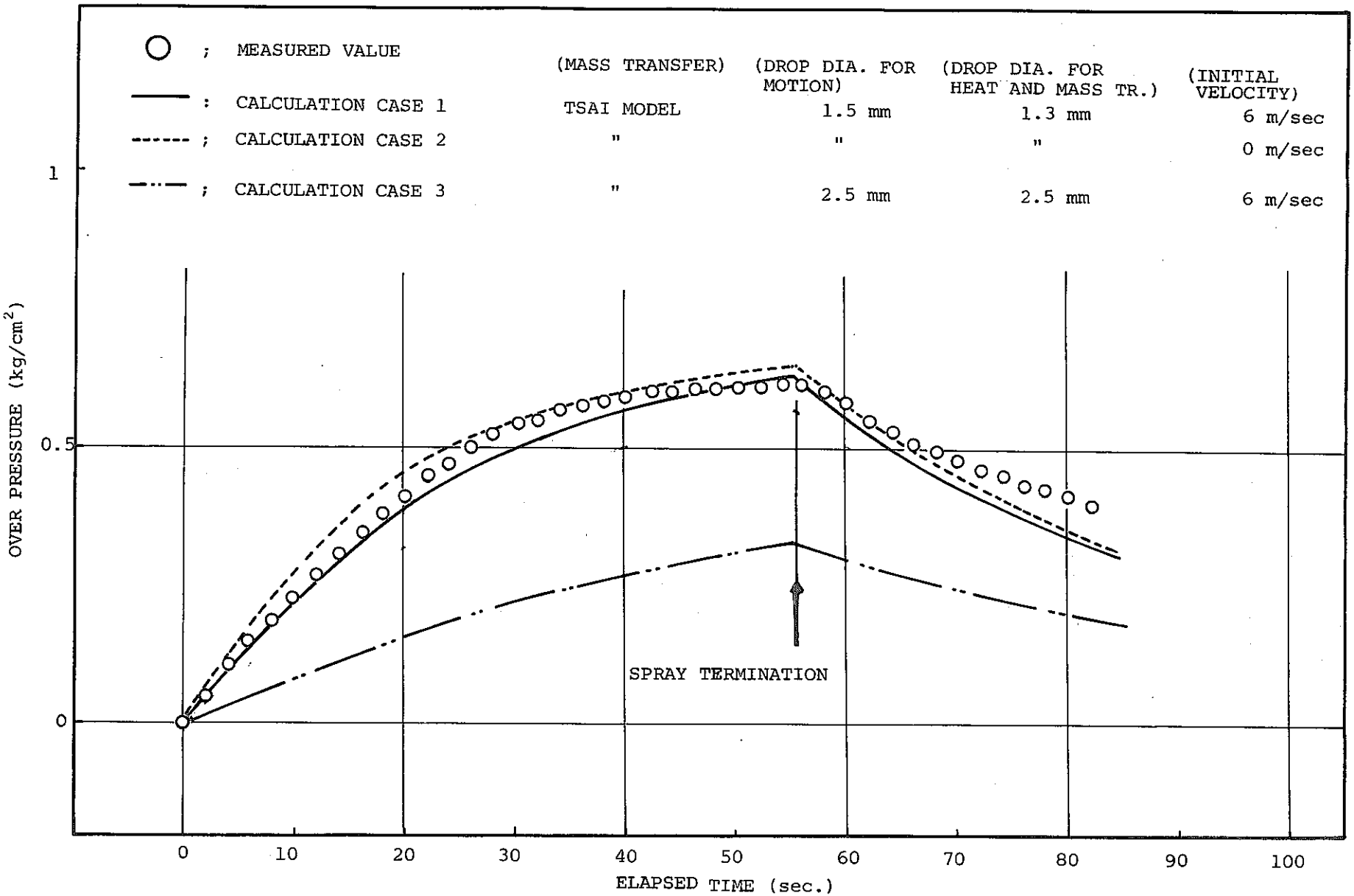

Fig.6.5 Comparison between Calculated and Experimental Value (TASP-N5)

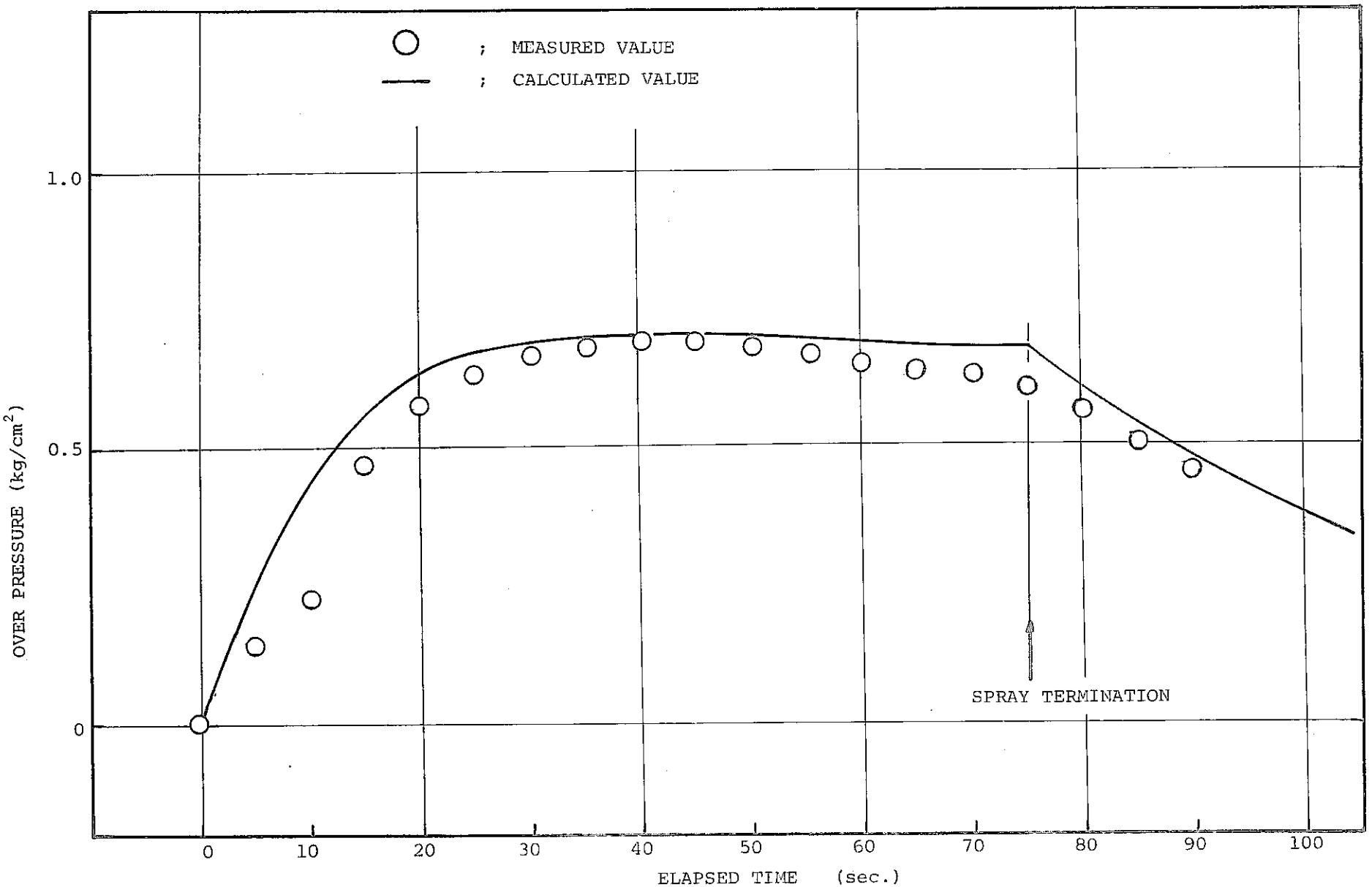

Fig.6.6 Comparison between Calculated and Experimental Value (TASP-N2)

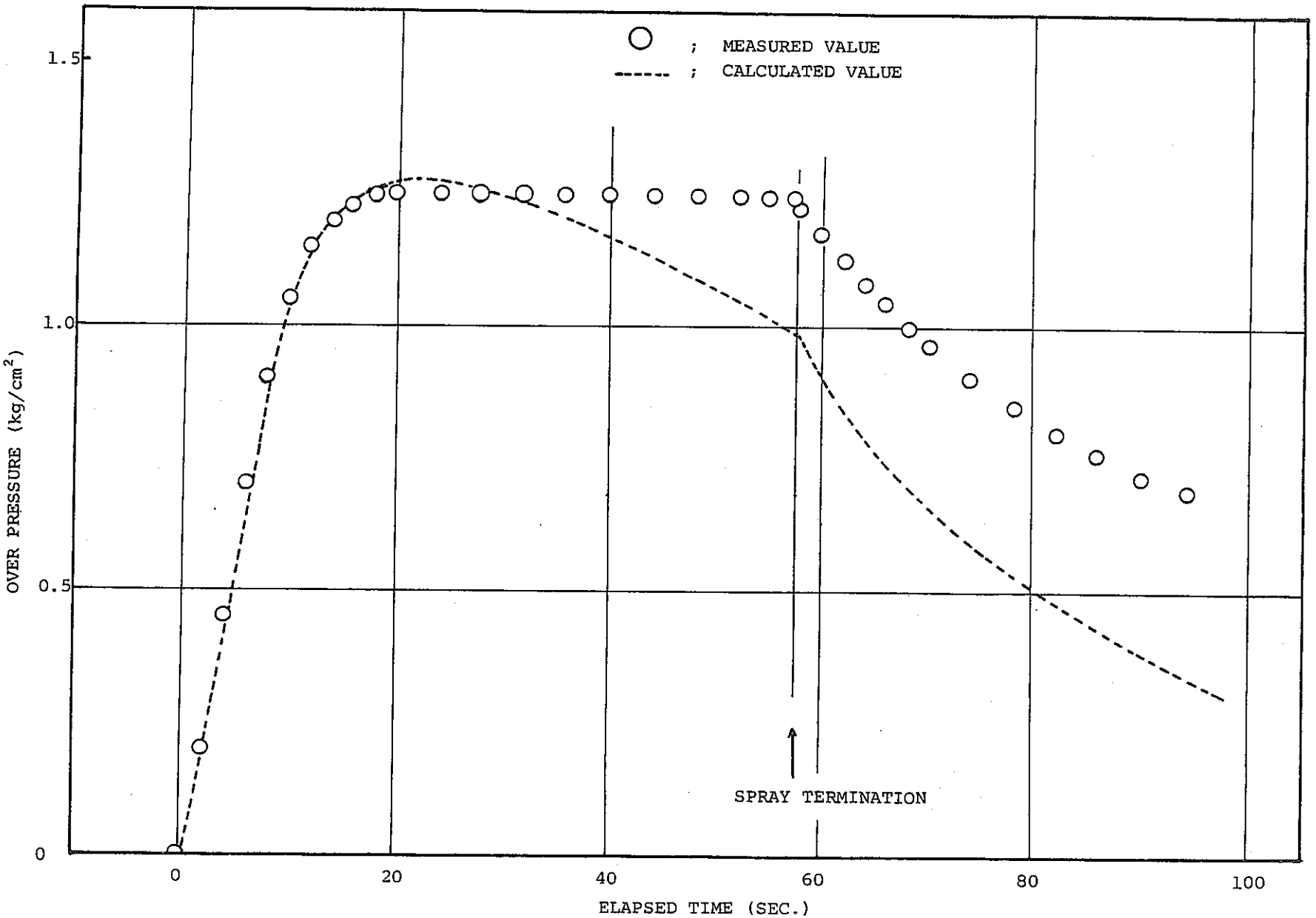

Fig.6.7 Comparison between Calculated and Experimental Value (TASP-A2)

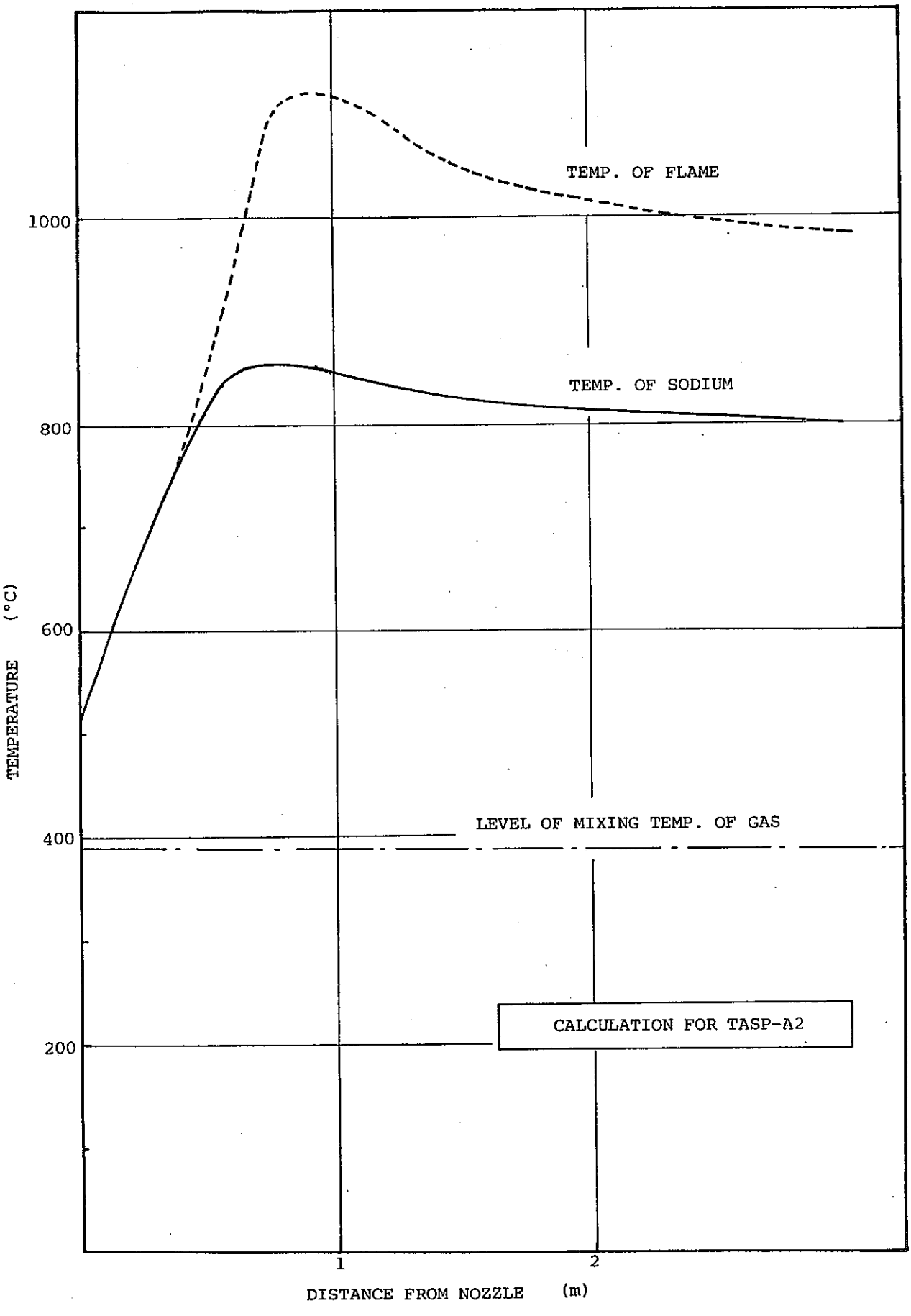

Fig.6.8 Temperature Distribution (Calculated Value)

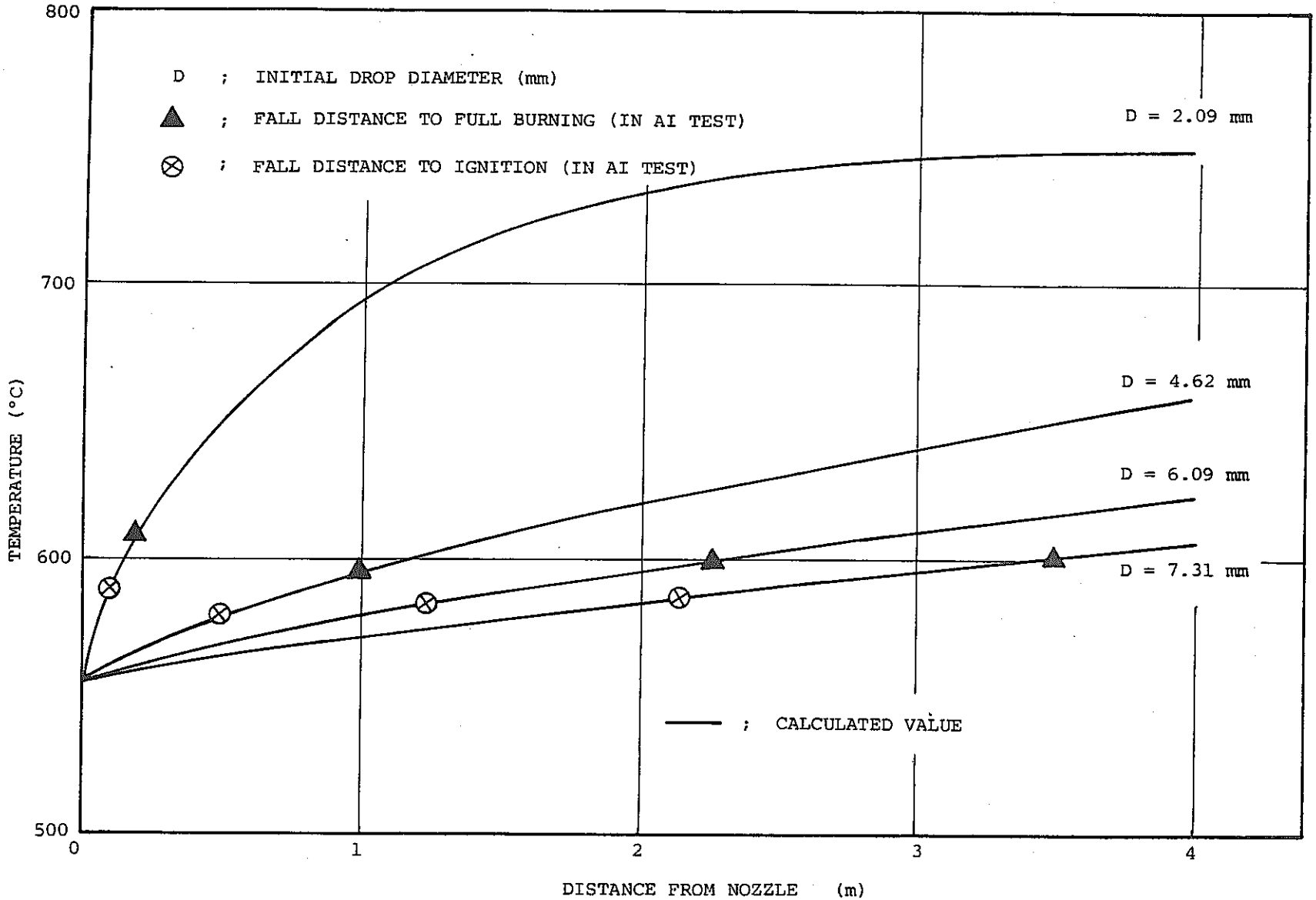

Fig.6.9 Comparison between Calculated Value and AI Single Drop Test

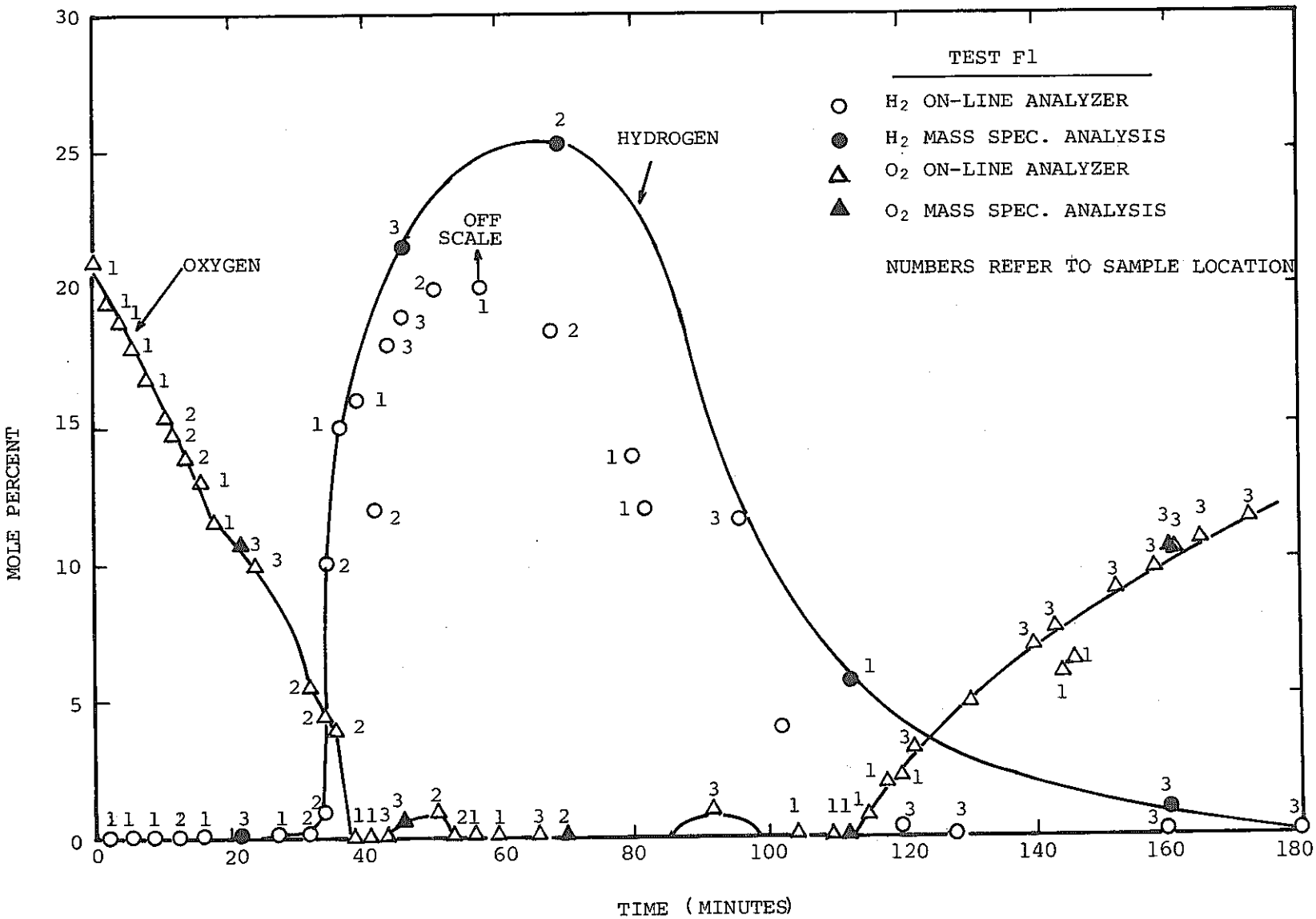

Fig.6.10 Hydrogen Formation in HEDL F-1 Test

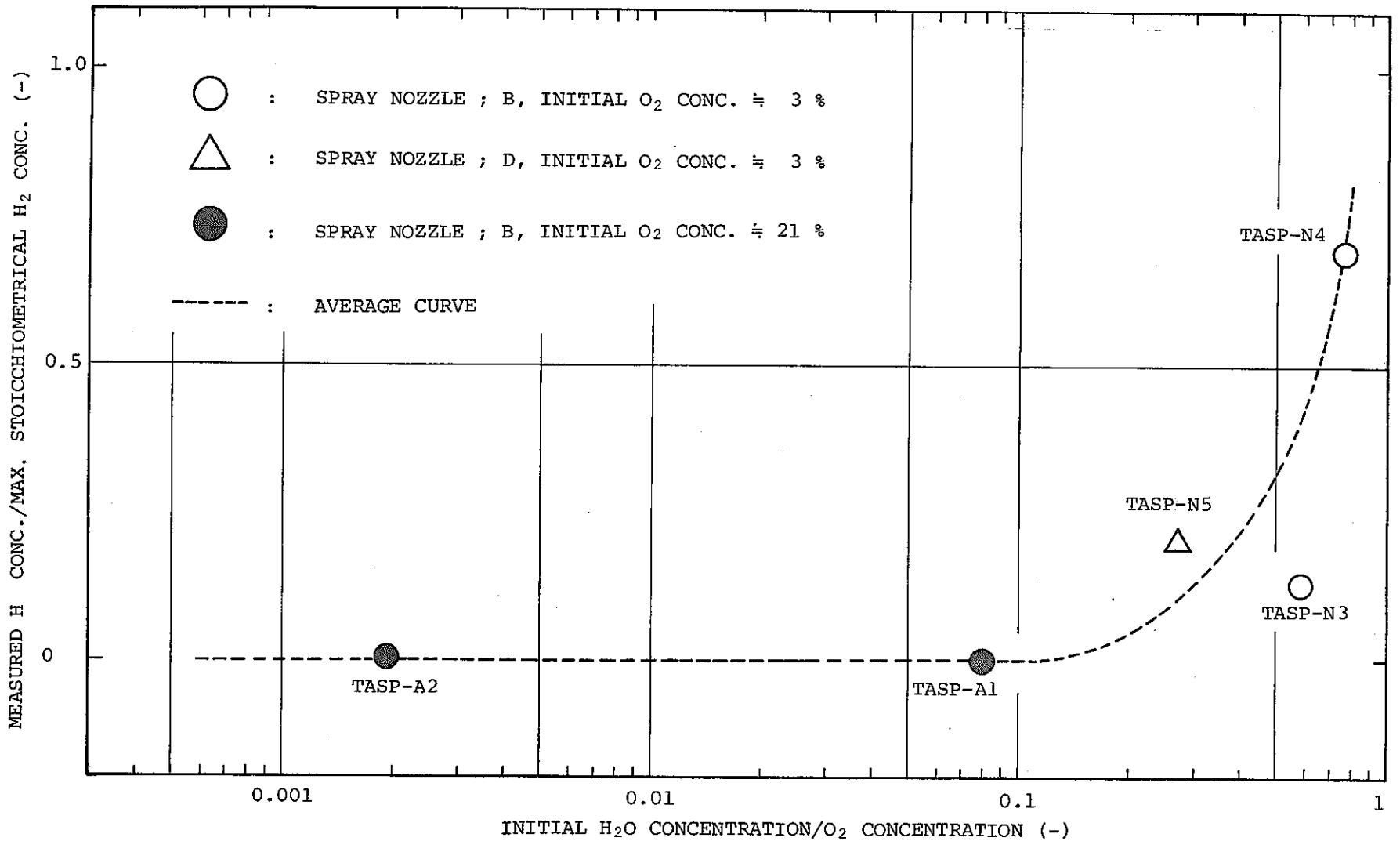

Fig.6.11 Hydrogen Generation Characteristics in TASP Experiment

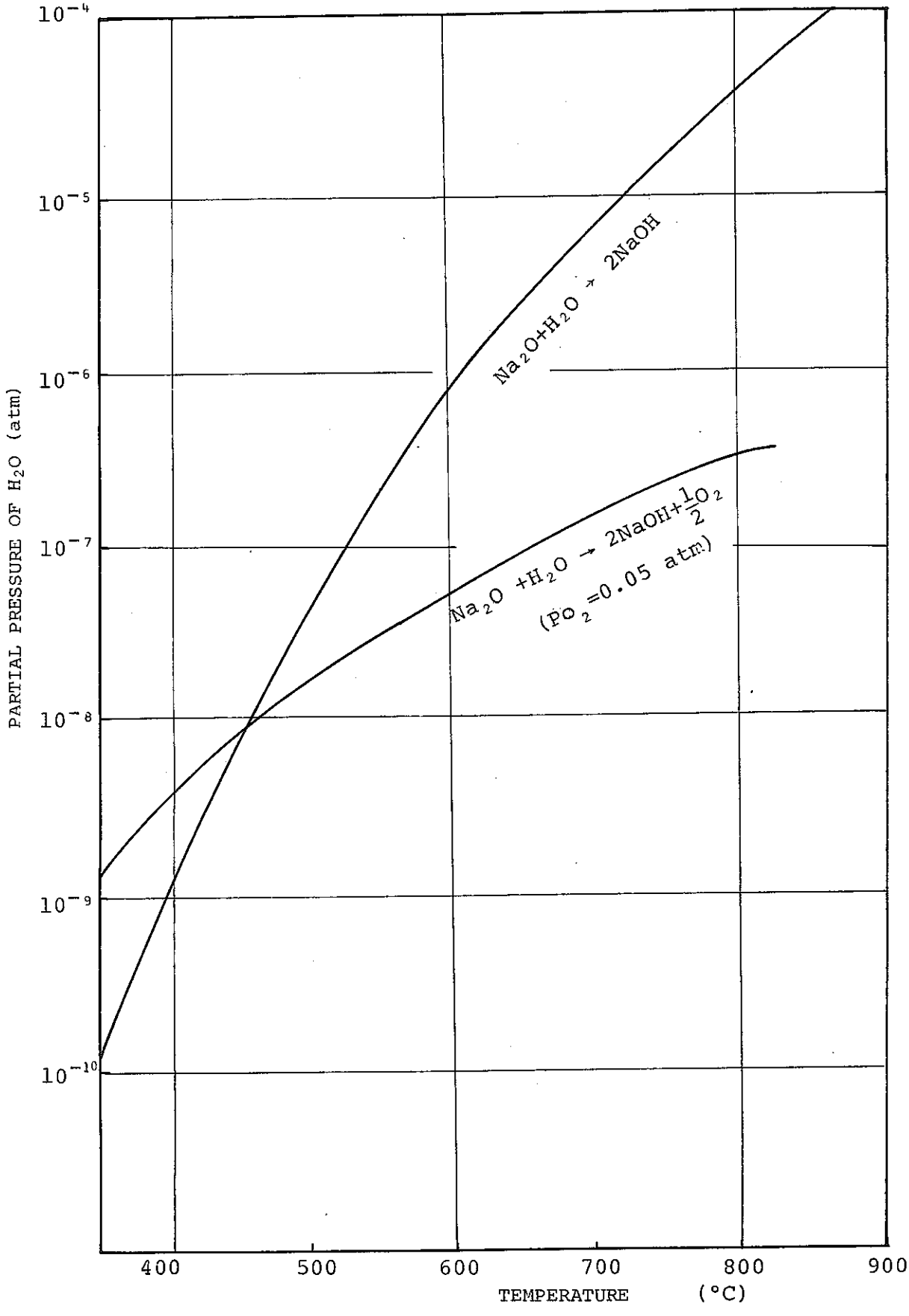

Fig.6.12 Equilibrium H_2O Pressure for the Reaction with Sodium Oxide

Table 3.1 Example of Spray Combustion Test

Research Institute	Test Conditions									Major Results	
	Test Equipment Dimensions	Run No.	Sprayed Sodium Mass	Sodium Spray Rate	Spray Duration	Sodium Temperature	Sodium Particle Size	Oxygen Concentration	Moisture	Gas Pressure Increase	Maximum Temperature
HEDL (US)	850 m^3	CSTF-AB3	48 kg	343 g/sec	140 sec	600°C	670 - MMD	21 %	-	0.4kg/cm^2	458 °C
	17m High	CSTF-NT1	82 kg	3.41 g/sec (1.05×10^2 sec)	4.8h	545°C	320-380 MMD	21 %	-	0.05kg/cm^2	97 °C
	(Spray downward)			6.84g/sec (6.72×10^4 sec)							Differs axially
CEA (FRANCE)	3.7m^3	FP 216 bis			-	550°C				1.8kg/cm^2	1600 °C
	(Spray upward)	209	0.387 kg		1 sec	550°C				0.5kg/cm^2	380 °C
		280	1.50 kg		3.5 sec	550°C				2.5kg/cm^2	1940 °C
		256	0.886 kg		3.5 sec	550°C				2.46kg/cm^2	1720 °C
		228	0.845 kg		1 sec	550°C				1.14kg/cm^2	1250 °C
		232	0.535 kg		2 sec	550°C				1.8kg/cm^2	1400 °C
		232P	0.429 kg		3.5 sec	550°C				1.6kg/cm^2	200 °C
		218	0.521 kg		2 sec	550°C				1.6kg/cm^2	760 °C
		245	1.02 kg		2 sec	550°C				2.4kg/cm^2	1700 °C

Table 3.1 Example of Spray Combustion Test (Continued)

Research Institute	Test Conditions									Major Results	
	Test Equipment Dimensions	Run No.	Sprayed Sodium Mass	Sodium Spray Rate	Spray Duration	Sodium Temperature	Sodium Particle Size	Oxygen Concentration	Moisture	Gas Pressure Increase	Maximum Temperature
PNC-HITACHI	$1.93m^3$ (Spray upward)	RUN-1	0.4 kg	43.5 g/sec	9.2 sec	300°C	50-60 MMD	21 %	∿ 0		
		2	0.4 kg	48.8 g/sec	8.2 sec	300°C		6 %	∿ 0	0.68kg/cm^2	
		3	0.4 kg	50.0 g/sec	8.0 sec	300°C		0 %	∿ 0	0.25kg/cm^2	
		4	0.4 kg	30.8 g/sec	13.0 sec	300°C		21 %	∿ 0	1.56kg/cm^2	
		5	0.4 kg	35.7 g/sec	11.2 sec	500°C		6 %	∿ 0	1.50kg/cm^2	
		TS-1	0.387 kg		19.5 sec	530°C		21 %		1.2 kg/cm^2	
		2	0.364 kg		7.7 sec	530°C		12.6 %		1.2 kg/cm^2	
		3	0.381 kg		7.6 sec	530°C		6.5 %		1.2 kg/cm^2	

Table 3.2 Measuring Items

Item	Name of data	Location	Instrumentation	No. of measure-ments	Remarks
Tempera-ture	Temperature in each section (Gas, concrete, liner)	See Fig. 3.7	CA thermo-couple	Approx. 100	
Pressure	Inner vessel pressure	Inside the cell	Strain gage type	2	
	Pressure behind liner	Liner gap	Strain gage type	2	
Flow rate	Sodium discharge rate	In front of the dis-charge valve	Electromag-netic flow meter	1	
Oxygen concen-tration	Oxygen concentra-tion in the gas	Inner cell gas	Orsat analyzer	1	Offline
			Magnetic oxygen motor	1	Response time: 5 sec (Specifica-tion)
Moisture concen-tration	Moisture concentra-tion in the gas	Inner cell gas	Dew indicator	1	Response time. approx. 20 min. (Actual measurement)
			Hygroscopic tube	1	Offline
Hydrogen concen-tration	Hydrogen concentra-tion in the gas	Inner cell gas	Catalic hydrogen moni-tor	1	Monitoring
			Gas chromatography	1	Offline

Table 3.2 Measuring Item(Continued)

Division	Name of data	Location	Instrumentation	No. of measure-ments	Remarks
Sodium aerosol	Aerosols floating in the gas	Inner cell gas	Airlock type sampler	1-2	Offline
			Optical densitometer	1	Offline
			Cascade im-pactor,	1	Offline
	Settled aerosol	Each section inner cell	Catch Pan	Sever-al	Total amount and change with time
	Deposed aerosol	Vertical and horizontal wall	Plate attach-ment method	Sever-al	Total amount and change with time

Table 3.3 Test Procedure

No.	Main Procedure	Guidelines
1	Preparation.	° Installation of nozzle, catch pans and thermocouples. ° Close the manhole .
2	Leak check	° Initial pressure is 0.2kg/cm^2g.
3	Filling with nitrogen gas	Replace air with nitrogen gas.
4	Adjustment of gas concentration	° Adjust the oxygen and moisture concentrations.
5	Filling with sodium	° Fill the high temperature tank with sodium.
6	Pre-check	° Temperature adjustment of high temperature tank and sodium supply system. ° Operation of each measuring instrument. ° Final check of ambient gas conditions.
7	Spray combustion test	° Spray the sodium for a specified period. ° Measurement of temperature, pressure, gas concentration and aerosol.
8	Post-test procedure	° Draining sodium from the high temperature tank. ° Other necessary procedures.
9	Leak check after test	° Leak check after the temperature decreases to normal.
10	Sodium stabilization	° Treatment of carbon dioxide.
11	Washing and cleaning	° Open the manhole and remove the sodium together with the catch pan. ° Wash and clean the liner, nozzle, termocouples, etc.

Table 3.4 Test Conditions of Sodium Spray Combustion

Test Number	Spray nozzle	Sprayed sodium temperature	Flow rate	Duration	Total amount of sprayed sodium	Initial oxygen concentration	Initial moisture concentration	Features	Test sequence
TASP-N1	Full-cone spray B nozzle	501 °C	43.6 ℓ/min	60 sec	43.6 ℓ	less than 0.1%	840 ppm	Sensible heat efficiency test	RUN 1
TSP-N2	Same as above	541 °C	34.3 ℓ/min	76 sec	43.4 ℓ	2.85%	1,200 ppm	Low moisture concentration (simulating primary cell)	2
TASP-N3	Same as above	538 °C	34.5 ℓ/min	63 sec	36.2 ℓ	2.8%	16,500 ppm	High moisture concentration	3
TASP-N4	Same as above	521 °C	36.7 ℓ/min	75 sec	45.9 ℓ	3.0%	23,000 ppm	Ultra-high moisture concentration	4
TASP-N5	Full-cone spray D nozzle	520 °C	45.5 ℓ/min	59 sec	44.7 ℓ	3.0%	8,000 ppm	Test of droplet size effect	7
TASP-A1	B nozzle	522 °C	30.7 ℓ/min	18 sec	9.2 ℓ	20.6%	16,500 ppm	High oxygen concentration (simulating secondary cell)	5
TASP-A2	B nozzle	512 °C	23.7 ℓ/min	57 sec	22.5 ℓ	20.4%	400 ppm	High oxygen and low moisture	6

(Note)
1. The initial gas pressure is the atmospheric pressure and initial gas temperature is the room temperature (18.7 ~ 31.1 C).
2. Mean volume radius of the B nozzle is approximately 1 mm, and that of the D nozzle is approximately 1.5mm.
3. The total amount of sprayed sodium is calculated by the area which consists of the sodium flow rate curve and spray period. The sodium spray flow rate is obtained by dividing the total sodium spray quantity by spray period. (Average flow rate).

Table 4.1 Summary of Water Spray Test

Nozzle	Distance from the nozzle (mm)	Pressure = 0.5kg/cm^{2}g	Pressure = 1.0kg/cm^{2}g	Pressure = 1.5kg/cm^{2}g	Pressure = 2.0kg/cm^{2}g
A	L = 0	Spray dispersion angle=67° Flow rate= 32 ℓ/min	Spray dispersion angle=73° Flow rate= 43 ℓ/min	Spray dispersion angle=73° Flow rate= 51 ℓ/min	Spray dispersion angle=70° Flow rate= 58 ℓ/min
	L = 1000	θ = 68°	θ = 70°	θ = 72°	θ = 74°
	L = 1750	-	-	-	-
	L = 2500	-	-	-	-
	L = 0	Spray dispersion angle=40° Flow rate= 32 ℓ/min	Spray dispersion angle=40° Flow rate= 43 ℓ/min	Spray dispersion angle=40° Flow rate= 52 ℓ/min	Spray dispersion angle=40° Flow rate= 60 ℓ/min
B	L = 1000	θ = 44°	θ = 44°	θ = 45°	θ = 46°
	L = 1750	θ = 38°	θ = 38°	θ ≒ 38°	θ = 38°
	L = 2500	θ = 35°	θ = 38°	θ = 36°	θ = 37°
	L = 0	Spray dispersion angle=25° Flow rate= 33 ℓ/min	Spray dispersion angle=28° Flow rate= 44 ℓ/min	Spray dispersion angle=30° Flow rate= 52 ℓ/min	Spray dispersion angle=30° Flow rate= 59 ℓ/min
C	L = 1000	θ = 38°	θ = 38°	θ = 38°	θ = 38°
	L = 1750	θ = 21°	θ = 30°	θ = 30°	θ = 32°
	L = 2500	θ = 23°	θ = 28°	θ = 30°	θ = 21°
D	Distance L	Pressure = 0.2kg/cm^{2}g	Pressure = 0.3kg/cm^{2}g	Pressure = 0.4kg/cm^{2}g	Pressure = 0.5kg/cm^{2}g
	L = 0	Average angle between L ≒ 1000 and 2000: θ = 24° flow rate = 37ℓ/min	Average angle θ = 29° flow rate = 45ℓ/min	Average angle θ = 0° flow rate = 52ℓ/min	Average angle θ = 34° flow rate = 58ℓ/min
	L = 1000	25°	31°	35°	36°
	L = 2000	23°	26°	29°	31°

(Note) Definition of spray dispersion angle θ at L is:

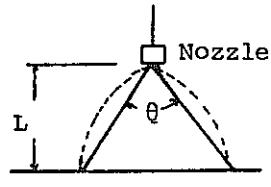

Table 5.1 Summary of Test Results

	Test number		TASP -N1	TASP -N2	TASP -N3	TASP -N4	TASP -N5	TASP -A1	TASP -A2
Test stipulations	Spray nozzle type	-	B	B	B	B	D	B	B
	Sprayed sodium temperature	°C	501	541	538	521	520	522	512
	Flow rate	ℓ/min	43.6	34.3	34.5	36.7	45.5	30.7	23.7
	Duration	sec	60	76	63	75	59	18	57
	Total amount of sprayed sodium	ℓ	43.6	43.4	36.2	45.9	44.7	9.2	22.5
	Initial oxygen concentration	%	Less than 0.1	2.85	2.8	3.0	3.0	20.6	20.4
	Initial moisture concentration	Vppm	840	1200	16500	23000	8000	16500	400
	Initial hydrogen concentration	ppm	80	3300	80	0	0	0	0
	Initial gas temperature	°C	26.3	30.1	31.1	21.1	20.4	22.4	18.7
	Initial gas pressure	mmHg	0	0	0	0	0	0	0
	Leak rate from cell	%/day	141	65	43	22.3	11.7	19.2	20.3
Pressure and temperature results	Peak gas pressure	kg/cm^2g	0.39	0.69	0.72	0.62	0.62	1.16	1.25
	Peak gas pressure duration	sec	60	40	38	40	59	16	20
	Pressure increase rate	$Kg/cm^2/sec$	0.018	0.048	0.08	0.07	0.03	0.22	0.156
	Local peak gas temperature	°C	317	580	580	543	547	over 955	1214
	Maximum sodium temperature in catch pan	°C	370	460	473	470	480	740	880
	Maximum temperature of ceiling liner	°C	36	60	52	44	42	70	98
	Maximum temperature of side wall	°C	34	53	63	53	50	66	90
	Maximum temperatur of concrete	°C	28	35	39	28	28	37	40
Ambient concentration	Attained oxygen concentration	%	Less than 0.1	0.8	0.45	1.0	1.3	8.0	1-3
	Attained moisture concentration	Vppm	-	300	2500	-	540	1800	Less than 300
	Attained hydrogen concentration	ppm	2300	700	2100	16000	1600	0	0

Table 5-1 Summary of Test Results (Continued)

	Test number		TASP -N1	TASP -N2	TASP -N3	TASP -N4	TASP -N5	TASP -A1	TASP -A2
Aerosol	Generated aerosol concentration (sampling value).	g-Na/m^2	5-10	5-10	5-10	5-10	5-10	30-80	50-100
	Generated aerosol concentration (estimated from settled amount)	g-Na/m^2	-	-	22	21	26.1	75.7	163.2
	Average particle size of aerosol	μm	2.5	2.8	3.0	2.4	2.	3.4	3.0
	Amount of aerosol settled on the floor surface	g-Na/m^2	-	-	50	44	35	160	350
	Amount of aerosol attached to the ceiling	g-Na/m^2	0.86	5.2	0.63	1.6	11	8.9	27
	Amount of aerosol attached to the side wall	g-Na/m^2	0.64	11.3	2.7	3.4	7.2	11.4	20.2
	Amount of aerosol attached to penetrate the piping	g-Na	-	-	7.1	5.2	3.7	10.0	49.2

Table 5.2 Description of Cascade Impactor

TITLE	CONTENTS	NOTE
(1) TYPE	Andersen-3371	
(2) MEASURABLE PARTICLE DIAMETER	0.41 μm 29.9 μm	FROM SPEC. TABLE
(3) NO. OF STAGE	8 STAGE	
(4) MAX. TEMP	815 °C	
(5) FLOW RATE	2.83 - 21.1 N/min.	
(6) DIAMETER OF FLOW HOLE AND NUMBER OF HOLES		
STAGE 1	Dc = 1.615 mm, N = 264	
STAGE 2	Dc = 1.181 mm, N = 264	
STAGE 3	Dc = 0.914 mm, N = 264	
STAGE 4	Dc = 0.711 mm, N = 264	
STAGE 5	Dc = 0.533 mm, N = 264	
STAGE 6	Dc = 0.343 mm, N = 264	
STAGE 7	Dc = 0.254 mm, N = 264	
STAGE 8	Dc = 0.254 mm, N = 156	

Table 5.3 Summary of Cell Leak Rate

RUN NO.	LEAK RATE BEFORE COMBUSTION	LEAK RATE AFTER COMBUSTION
TASP-N1	141 %/DAY	114 %/DAY
TASP-N2	65 %/DAY	37 %/DAY
TASP-N3	43 %/DAY	45 %/DAY
TASP-N4	22 %/DAY	41 %/DAY
TASP-N5	12 %/DAY	20 %/DAY
TASP-A1	19 %/DAY	10 %/DAY
TASP/A2	20 %/DAY	12 %/DAY

(NOTE) LEAK RATE WAS MEASURED AT 0.2 kg/cm^2g.

Table 6.1 Physical Properties of Sodium and Water

FLUID	SURFACE TENSION (kg/m)	SPECIFIC WEIGHT (kg/m^3)	VISCOSITY ($kg.sec/m^2$)
SODIUM (530°C)	0.00739	825.0	2.31×10^{-5}
WATER (20°C)	0.0157	998.2	1.022×10^{-4}

Table 6.2 Flow Chart of Spray Combustion Calculation

FLOW CHART	NOTE
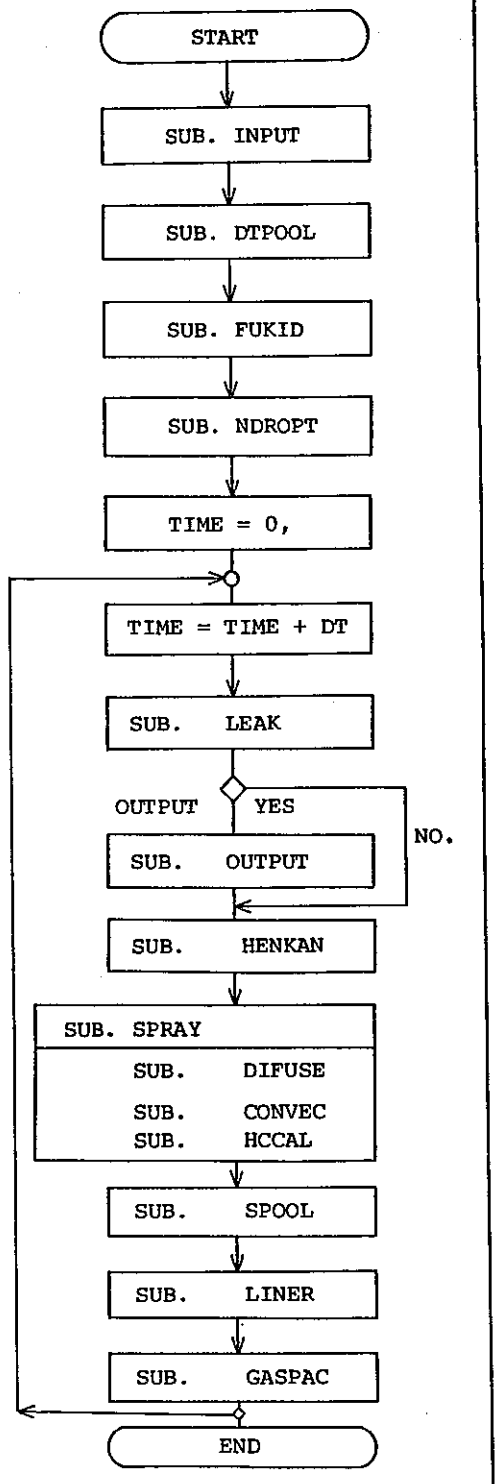	. Read in the input data . Determination of time step DT during pool combustion . Determination of time step DT during spray combustion and the spatial mesh size for the calculation of droplet settlement. . Calculation of droplet number. . Correction due to leak from the cell. . Output routine . Renewal of previous time step. . Calculation of spray combustion heat and mass transfer. . Calculation of natural circulation of gas. . Calculation of heat transfer coefficient to the wall. . Calculation of heat and mass transfer in the sodium pool. . Calculation of liner and concrete heat transfer. . Calculation of gas atmosphere.

Table 6.3 Maximum Aerosol Concentration

CATEGORY	RUN NO.	MAXIMUM AEROSOL CONCENTRATION	FRACTION OF AEROSOL RELEASE	SODIUM DISCHARGE DURATION
		($g\text{-}Na/m^3$)	(%)	(sec)
SPRAY COMBUSTION IN AIR-FILLED CONDITION	TASP-A1	76	9 - 18	18
	TASP-A2	163	20 - 40	57
SPRAY COMBUSTION UNDER LOW OXYGEN CONC.	TASP-N^3	22	19 - 38	63
	TASP-N^4	21	19 - 38	73
	TASP-N^5	26	22 - 44	59
COLUMNAR COMBUSTION UNDER LOW OXYGEN CONC.	RUN- 9	8	7 - 14	60
	RUN-10	9	22 - 45	220
	RUN-11	39	23 - 46	272
	RUN- 6	11	6 - 13	52
COLUMNAR COMBUSTION IN AIR-FILLED CONDITION	RUNII-1	84	10 - 21	30
	RUNII-2	87	10 - 21	38
	RUNII-3	81	10 - 19	58